

✓ **THEORETICAL AND EXPERIMENTAL STUDIES IN PULSED NUCLEAR
QUADRUPOLE RESONANCE SPECTROSCOPY : APPLICATION OF
TENSOR OPERATOR FORMALISM**

A Thesis Submitted
In Partial Fulfilment of the Requirements
for the Degree of

DOCTOR OF PHILOSOPHY

015001

by

RAVINDER REDDY

to the

**DEPARTMENT OF CHEMISTRY
INDIAN INSTITUTE OF TECHNOLOGY, KANPUR**

MAY, 1988

✓GHM-1988-2-RED-T

8 NOV 1989

LIBRARY

106246.

Th

543.0877

R246t

DEDICATED
TO
MY PARENTS

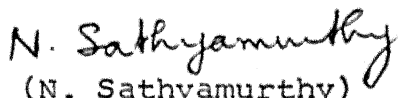
DEPARTMENT OF CHEMISTRY
INDIAN INSTITUTE OF TECHNOLOGY KANPUR, INDIA

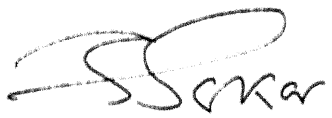
CERTIFICATE OF COURSE WORK

This is to certify that Mr. Ravinder Reddy has satisfactorily completed all the courses required for the Ph.D. degree programme. These courses include:

Chm 505 Principles of Organic Chemistry
Chm 521 Chemical Binding
Chm 524 Modern Physical Methods in Chemistry
Chm 525 Principles of Physical Chemistry
Chm 534 Electronics for Chemists
Chm 545 Principles of Inorganic Chemistry
Chm 634 Symmetry and Molecular Structure
Chm 800 General Seminar
Chm 801 Special Seminar
Chm 900 Ph.D. Thesis

Mr. Ravinder Reddy was admitted to the candidacy of the Ph.D. degree in August 1983 after he successfully completed the written and oral qualifying examinations.


(N. Sathyamurthy)
Professor and Acting Head,
Department of Chemistry,
I.I.T., KANPUR


(S. Sarkar)
Convener,
Departmental Post-
Graduate Committee,
Department of Chemistry,
I.I.T., KANPUR

CERTIFICATE II

Certified that the work contained in this thesis entitled: "Theoretical and Experimental Studies in Pulsed Nuclear Quadrupole Resonance Spectroscopy: Application of Tensor Operator Formalism" has been carried out by Mr. Ravinder Reddy under my supervision and the same has not been submitted elsewhere for a degree.



(P. T. Narasimhan)

Professor
Department of Chemistry,
I.I.T. Kanpur

Thesis Supervisor

Kanpur,

May 1988.

STATEMENT

I hereby declare that the matter embodied in this thesis is the result of investigations carried out by me in the Department of Chemistry, Indian Institute of Technology, Kanpur, India, under the supervision of Professor P.T. Narasimhan.

In keeping with the general practice of reporting scientific observations, due acknowledgements have been made wherever the work described is based on the findings of other investigators.

Ravinder Reddy
Ravinder Reddy

Kanpur
May 1988.

ACKNOWLEDGEMENTS

It is a great pleasure to express my gratitude to Professor P.T. Narasimhan who introduced me to the area of magnetic resonance in general and NQR in particular. The past several years of my association with him have helped shape my attitudes towards academic as well as non-academic matters. His inspiring guidance and constant encouragement have been the main factors responsible for the completion of this work.

I also thank,

Dr. (Mrs.) Amrita Sheikh, Messrs Arun L. Bhavsar, A.K. Dubey and A. Ramamoorthy for providing an ideal working atmosphere in the laboratory.

Dr. Narsimha Reddy for his invaluable help during the course of this work.

Professor P. Raghunathan for his encouragement and moral support.

Professor S. Chandrasekaran and N. Sathyamurthy for their help, in particular at the initial stages of my programme.

Dr. N. Chandrakumar for useful discussions on MQNQR.

All my friends who helped me in many ways and made my stay at IIT-K a pleasant one.

Mr. R.D. Singh for efficient typing of the manuscript.

Messrs Umesh and Ram Singh Chauhan for their help in the laboratory.

Ravinder Reddy

SYNOPSIS

The thesis deals with theoretical and experimental studies in pulsed nuclear quadrupole resonance (NQR) spectroscopy. Tensor operator formalism has been employed for the first time to analyse pulsed NQR experiments in a variety of situations.

The thesis consists of five chapters. Chapter I deals with the basic principles, methods of detection and applications of NQR spectroscopy. A description of the pulsed NQR spectrometer employed in the present investigations is also presented in this chapter. A brief outline of the various theoretical approaches available for the description of pulsed NQR is given. Scope of the present work is presented at the end of this chapter.

Chapter II is concerned with the application of tensor operator formalism for pure NQR. Since quadrupolar nuclei may be present in axially symmetric or non-axially symmetric electric field gradients (efg) the study of the responses of quadrupolar nuclei to radio frequency (r.f.) perturbations in these situations is of considerable importance. Of special interest is the study of response of spin $3/2$ nuclei to r.f. pulse excitations in the presence of a weak Zeeman field in order to obtain both the quadrupole coupling constant (e^2qQ) and the asymmetry parameter η .

Using the tensor operator formalism the response of non-interacting nuclear spin systems with $I = 1, 3/2, 5/2$ in single crystals to single- and two- r.f. pulse excitations have been evaluated. The following cases have been considered:

- i) Spin $I = 3/2, 5/2$ nuclei in axially symmetric efg's.
- ii) Spin $I = 1, 3/2$ nuclei in non-axially symmetric efg's.
- iii) Spin $I = 3/2$ in axially symmetric field gradients in the presence of a weak Zeeman field applied at an angle ' θ ' w.r.t. the principal Z-axis of the efg.
- iv) Spin $I = 3/2$ in non-axial field gradients, in the presence of Zeeman field applied along principal X-, Y-, or Z-axis of the efg.

In all these calculations relaxation effects are not considered. The time evolution of complete set of tensor operators for $I = 3/2$ under the action of r.f. Hamiltonian (including the phase of the r.f.) has been investigated in detail. For the purpose of illustration experimental recordings of the pulse responses in some cases are also presented.

Wherever possible the present results have been compared with available literature reports and agreement has been found. The present set of results are, however, more exhaustive than those given in previous literature reports.

Chapter III deals with the application of tensor operator formalism to the study of Zeeman-perturbed spin echo envelope modulations (ZSEEM) in spin $I = 3/2$ nuclei. In the first section of this chapter a brief discussion of the two-pulse ZSEEM experiment is given and illustrated using experimental recordings of ZSEEM patterns obtained from ^{35}Cl in polycrystalline specimen of AgClO_3 . In the second section tensor operator formalism has been

used for the calculation of the expression for the ZSEEM pattern. The present results agree with those of Ramachandran and Narasimhan who employed the matrix transformations approach.

Chapter IV is concerned with the experimental and theoretical investigations of responses of quadrupolar nuclei to multiple-pulse sequences. The nuclei investigated are: ^{35}Cl ($I = 3/2$) in (i) single crystal of NaClO_3 , (ii) polycrystalline samples of NaClO_3 , KClO_3 , SbCl_3 and ^{187}Re , ^{185}Re (both with $I = 5/2$) in polycrystalline sample of KReO_4 . The pulse sequences studied are: (a) spin-locking sequence (SLS): $(\pi/2)_x - (\tau - \theta_{(x+\phi)} - \tau)_n$, (b) phase-alternated pulse sequence (PAPS): $(\pi/2)_x - (\tau - (\theta)_{-x} - 2\tau - (\theta)_x - \tau)_n$ and (c) WAHUHA multiple pulse sequence: $(\pi/2)_x - \tau(\tau - (\pi/2)_{-x} - \tau - (\pi/2)_y - 2\tau - (\pi/2)_{-y} - \tau - (\pi/2)_x - \tau)_n$. Here, $(\theta)_\phi$ represents a pulse of flip angle θ and phase ϕ with τ corresponding to the pulse separation.

In Section IV.A a brief review of multiple-pulse studies in NQR is given. Section IV.B presents the experimental results with the aforesaid sequences. Under the influence of SLS and PAPS the establishment of a quasi-equilibrium state of the magnetization has been observed both in ^{35}Cl (in single crystal and powder samples) and ^{187}Re , ^{185}Re in KReO_4 . In all the cases studied the decay constant, T_{2e} of the quasi-equilibrium magnetization (QEM) has been found to be much larger than the spin-spin relaxation time T_2 . The dependence of the decay of the QEM on the parameters such as θ , ϕ , τ and resonance off-set, $\Delta\omega$

has been investigated. From these studies it is inferred that the spin-locking phenomenon can be observed in single crystals as well as in powder samples with arbitrary θ , ϕ values of the sequence pulses contrary to the theoretical predictions in the literature.

Section IV.C presents the results of a ^{23}Na - ^{35}Cl double resonance experiment carried out under the multiple pulse spin-locking condition in a polycrystalline sample of NaClO_3 . Section IV.D outlines the theoretical analysis of PAPS, WAHUHA and Mansfield-Rim-Elleman-Vaughan (MREV-8) sequences in the case of spin $I = 3/2$ nuclei. Using tensor operator formalism and average Hamiltonian theory it has been shown that in the case of single crystals under the action of PAPS the internal interactions due to (i) efg inhomogeneities ($\mathcal{H}_{\text{inhom}}$), (ii) torsional oscillations ($\mathcal{H}_{\text{tors}}$) and (iii) heteronuclear dipole-dipole interactions (\mathcal{H}_{het}) which contribute to the NQR line width are averaged out. In the case of polycrystalline samples it has been possible to show that under PAPS $\mathcal{H}_{\text{inhom}}$ and $\mathcal{H}_{\text{tors}}$ are averaged out. For both the WAHUHA and MREV-8 sequences it has been possible to show that in the case of single crystals $\mathcal{H}_{\text{inhom}}$ and $\mathcal{H}_{\text{tors}}$ are not averaged out.

Results of theoretical investigation of double quantum coherence in pure NQR of non-interacting nuclear spins with $I = 5/2$ for the case of axially symmetric efg in a single crystals are presented in Chapter V. Employing the tensor operator formalism

it has been shown that the creation and detection of double quantum coherence can be done by the application of a pulse scheme of the form $(\pi/2)_x(2\omega_Q)(\pi)_x(\omega_Q)-\tau-(\pi)_x(2\omega_Q)$. The effect of resonance off-set on the double quantum coherence has also been considered.

The thesis concludes with some critical comments on the merits and demerits of the tensor operator formalism as applied to pulsed NQR spectroscopy.

CONTENTS

	Page
CERTIFICATE OF COURSE WORK	i
CERTIFICATE II	ii
STATEMENT	iii
ACKNOWLEDGEMENTS	iv
SYNOPSIS	v
CHAPTER	
I - INTRODUCTION	1
I.A Introduction to NQR	2
I.B Some Applications of NQR	11
I.C Detection of Nuclear Quadrupole Resonance	17
I.C.1 Continuous Wave Techniques	17
I.C.2 Pulsed Techniques	19
I.C.3 Description of the Pulsed NQR Spectrometer Employed for the Experimental Investigations in the Present Thesis	22
I.D Theoretical Description of Pulsed NQR	29
I.D.1 Basic Theory	30
I.D.2 Theoretical Approaches for the Description of Pulse Responses in NQR. A Review	34
I.E Scope of the Present Work	36
Summary	39
II - PULSE RESPONSES IN NQR OF SINGLE CRYSTALS:	
APPLICATION OF TENSOR OPERATOR FORMALISM	52
II.A Tensor Operator Formalism	55
II.B Pulse Responses in the Absence of a Zeeman Field for the Case of Axially Symmetric Field Gradients	59
II.B.1 General	59
II.B.2 Spin $I = 3/2$	61

Contents (contd.)

Page

II.B.2(i)	Single-Pulse Response	62
II.B.2(ii)	Two-Pulse Response	69
II.B.3	Spin $I = 5/2$	71
II.B.3(i)	Irradiation Near ω_Q Frequency	71
	Single-Pulse Response	72
II.B.3(ii)	Irradiation Near $2\omega_Q$ Frequency	78
II.B.3(ii)a	Single-Pulse Response	79
II.B.3(ii)b	Two-Pulse Response	83
II.C	Pulse Responses in the Presence of a Weak Zeeman Field for Nuclear Spin $I = 3/2$ in Axially Symmetric Field Gradients	84
II.C.1	Transitions for a Nuclear Spin $I = 3/2$ in the Presence of a Weak Zeeman Field	84
II.C.2	Evaluation of Pulse Responses	86
II.C.2(i)	Single-Pulse Response	86
II.C.2(ii)	Two-Pulse Response	94
II.D	Pulse Responses in the Absence of a Zeeman Field for the Case of Non-axially Symmetric Field Gradients	98
II.D.1	Spin $I = 1$	98
II.D.1(i)	Irradiation Near f_3 Frequency	101
II.D.1(i)a	Single-Pulse Response	101
II.D.1(i)b	Two-Pulse Response	103
II.D.1(ii)	Irradiation Near f_2 Frequency	104
II.D.1(ii)a	Single-Pulse Response	104
II.D.1(ii)b	Two-Pulse Response	105
II.D.1(iii)	Irradiation Near F_1 Frequency	105
II.D.1(iii)a	Single-Pulse Response	106
II.D.1(iii)b	Two-Pulse Response	106
II.D.2	Spin $I = 3/2$	106
II.D.2(i)	Single-Pulse Response	111
II.D.2(ii)	Two-Pulse Response	111
II.D.3	Calculation in the Diagonal Frame	115

Contents (contd.)

Page

II.E	Pulse Responses in the Presence of a Weak Zeeman Field for Nuclear Spin $I = 3/2$ in Non-axially Symmetric Field Gradients	118
II.E.1	Zeeman Field Applied Along x-axis of the efg	118
II.E.1(i)	Single-Pulse Response	119
II.E.1(ii)	Two-Pulse Response	119
II.E.2	Zeeman Field Applied Along y-axis of the efg	119
II.E.2(i)	Single-Pulse Response	121
II.E.2(ii)	Two-Pulse Response	121
II.E.3	Zeeman Field Applied Along z-axis of the efg	123
II.E.3(i)	Single-Pulse Response	123
II.E.3(ii)	Two-Pulse Response	123
II.F	The Evolution of Tensor Operators Under the Action of r.f. Hamiltonian: Role of Phase of r.f.	125
	Summary	126
III -	APPLICATION OF TENSOR OPERATOR FORMALISM FOR THE STUDY OF ZEEMAN PERTURBED SPIN ECHO ENVELOPE MODULATIONS IN SPIN $I = 3/2$ NUCLEI	131
III.A	Zeeman Perturbed Spin Echo Envelope Modulations	132
III.B	Theoretical Investigation of ZSEEM Using Tensor Operator Formalism	140
III.B.1	Eigen Values of Spin $I = 3/2$ Nuclei with Non-axial Field Gradients in the Presence of a Weak Zeeman Field	140
III.B.2	Relevant Hamiltonians	142
III.B.2(i)	r.f. Hamiltonian	142
III.B.2(ii)	Total Hamiltonian in Terms of Tensor Operators	143
III.B.2(iii)	Total Hamiltonian in the Diagonal Frame	144
III.B.2(iv)	Total Hamiltonian $\mathcal{H}^d(t)$ in the Quadrupolar Interaction Representa- tion	145

III.B.3	The Evolution of Tensor Operators Under the Influence of Hamiltonian $\tilde{\mathcal{H}}_1^d$	148
III.B.4	The Evolution of Tensor Operators Under the Influence of the Hamil- tonian $\tilde{\mathcal{H}}_z^d$	151
III.B.5	Evolution of Two-Pulse Response: ZSEEM Pattern	163
III.B.5(i)	Powder Averaging	178
Summary		180

IV - EXPERIMENTAL AND THEORETICAL INVESTIGATIONS

	OF RESPONSES OF QUADRUPOLEAR NUCLEI TO SOME MULTIPLE-PULSE SEQUENCES	183
IV.A	Multiple Pulse Investigations in Pure NQR. A Review	185
IV.B	Experimental Investigations of Res- ponses of Quadrupolar Nuclei to Multiple-Pulse Sequences	189
IV.B.1	Experimental	190
IV.B.2	Results	192
IV.B.2(i)	Spin-Locking Sequence (SLS)	192
IV.B.2(i)a	Study of Flip Angle ' θ ' Depend- ence	200
IV.B.2(i)b	Study of θ and τ Dependence	216
IV.B.2(i)c	Study of Resonance off-set, $\Delta\omega$ Dependence	221
IV.B.2(ii)	Phase Alternated Pulse Sequence (PAPS)	223
IV.B.2(iii)	WAHUHA Sequence	230
IV.C	Double Resonance Under Multiple- Pulse Spin-Locking	237
IV.C.1	Experimental	237
IV.C.2	Results	238
IV.D	Theoretical Analysis of a few Multiple Pulse Experiments in NQR of Spin $I = 3/2$ Nuclei	243
IV.D.1	Hamiltonians of Internal Interactions	243
IV.D.1(i)	Hamiltonian of Inhomogeneous efg	243

Contents (contd.)

	Page
IV.D.1(ii) Hamiltonian Corresponding to Torsional Oscillations	244
IV.D.1(iii) Hamiltonian of Heteronuclear Dipole-Dipole Interactions	246
IV.D.2 Multiple Pulse NQR and the Average Hamiltonian	248
IV.D.3 Theoretical Analysis	252
IV.D.3(i) Zeroth Order Average Hamiltonian of Internal Interactions Under the Influence of PAPS and their Commutation with ρ_i : Case of Single Crystals	260
IV.D.3(ii) Influence of PAPS on Spin $I = 3/2$ Nuclei in Polycrystalline Samples ...	263
IV.D.3(ii)a Zeroth Order Average Hamiltonians of Internal Interactions and their Commutation with ρ_i	265
IV.D.3(iii) Influence of WAHUHA and MREV-8 Sequences on Spin $I = 3/2$ Nuclei in Single Crystals	266
IV.D.3(iii)a WAHUHA Sequence	267
IV.D.3(iii)b MREV-8 Sequence	268
Summary	269
 V - STUDY OF MULTIPLE QUANTUM COHERENCES IN PURE NQR	274
V.A Double Quantum Coherence for Spin $I = 5/2$ Case in Pure NQR	279
V.A.1 General Expressions for the Density Matrix at Various States of the Pulse Sequence	283
V.A.2 Results	288
Summary	293

CHAPTER I

INTRODUCTION

In this chapter a brief discussion on the principles, applications and detection of Nuclear Quadrupole Resonance (NQR) and some theoretical aspects of pulsed NQR are presented.

Section I.A outlines the basic principles of NQR while some applications of NQR are presented in Section I.B. A brief outline of the methods of detection of NQR and description of the pulsed NQR spectrometer employed in the present work is given in Section I.C. Section I.D presents the basic theoretical outlines concerning pulse responses in NQR. In Section I.E the scope of the present work is described.

I.A INTRODUCTION TO NQR

Nuclear quadrupole resonance spectroscopy deals with interactions between radio frequency (r.f.) field and nuclear spins with $I \gg 1$ in crystalline (solids) samples. I is the nuclear spin angular momentum measured in units of \hbar . A nucleus with spin $I \gg 1$ exhibits a non-spherical charge distribution and possess a magnetic dipole moment as well as an electric quadrupole moment and hence it can interact with surrounding magnetic fields and also with electric field gradients (efg). Such nuclei probe magnetic, electrostatic and electrodynamic properties of chemical systems and thus yield valuable information.

The scalar quadrupole moment (eQ) is a measure of the deviation of the nuclear charge distribution from spherical symmetry [1,2]*. When a nucleus with a quadrupole moment is placed in an inhomogeneous electric field arising from external charges, it orients itself in different directions with different energies. The observed NQR spectra correspond to the dipole transitions, between such energy levels induced by an oscillating r.f. field. Like in NMR these transitions are magnetic dipole transitions.

The theoretical treatment of the interaction of a quadrupolar nucleus with the surrounding electronic charge cloud in atoms was originally given by Casimir [3]. From a study of atomic spectra Schüller and Schmidt [4] have proved the existence of nuclear quadrupole moments. Nuclear quadrupole interaction in molecules was first observed by Kellogg et al. [5] in 1939 using the molecular beam technique. The first experimental observation of pure NQR was made by Dehmelt and Krüger [6].

In the principal axes system of efg, the Hamiltonian corresponding to the interaction between the electric quadrupole moment and electric field gradient at the nucleus can be written as [7]

*References appear at the end of each chapter.

$$\mathcal{H}_Q = \frac{e^2 q Q}{4I(2I-1)} [3I_z^2 - I^2 + \eta(I_x^2 - I_y^2)] \quad \dots (I.1)$$

where η the asymmetry parameter is defined as

$$\eta = \left| \frac{V_{XX} - V_{YY}}{V_{ZZ}} \right| \quad \dots (I.2)$$

η is a measure of the deviation of the efg from cylindrical symmetry. Conventionally, $e^2 q Q$ is referred to as the nuclear quadrupole coupling constant (QCC). The principal axes system of efg tensor has been chosen such that the diagonal components of the efg, V_{XX} , V_{YY} and V_{ZZ} satisfy the condition

$$|V_{ZZ}| > |V_{YY}| > |V_{XX}|$$

If we assume that the electric field at the nucleus is produced entirely by charges completely external to the nucleus then the Laplace equation $V_{XX} + V_{YY} + V_{ZZ} = 0$ is satisfied and we have only two independent parameters $V_{ZZ} = eq$ and η . The two conditions, viz., $|V_{ZZ}| > |V_{YY}| > |V_{XX}|$ and $V_{XX} + V_{YY} + V_{ZZ} = 0$ lead to the result that the value of η can vary between 0 and 1. η is zero for the axially asymmetric case.

In order to arrive at the energy levels of the quadrupolar nucleus, one needs to evaluate the matrix elements of the type $\mathcal{H}_Q^{mm'} = \langle I, m | \mathcal{H}_Q | I, m' \rangle$. For the case of axially symmetric field gradient ($\eta = 0$) the Hamiltonian matrix is

diagonal in the I_z representation and the energy levels are given by

$$E_m = \frac{e^2 q Q}{4I(2I-1)} [3 m^2 - I(I+1)] \quad \dots (I.3)$$

where m is the Z -component of the nuclear spin I . Since the energies of the states with $\pm m$ are the same the energy levels are degenerate in m .

The presence of asymmetry parameter η , mixes the states having $\Delta m = \pm 2$ and hence the Hamiltonian matrix is not diagonal in the ' m ' representation. In this case one has to construct linear combinations of spin functions $|I, m\rangle$, $|I, m'\rangle$ having $\Delta m = \pm 2$, and calculate the coefficients in these linear combinations from the energies obtained as the eigenvalues of the \mathcal{H}_Q matrix. For various values of nuclear spin I , the secular equations have been tabulated in the book by Das and Hahn [8].

For the case of spin $I = 1$ the energies of states with $m = 0, \pm 1$ are given respectively by

$$E_0 = - \frac{e^2 q Q}{2} \quad \dots (I.4)$$

$$E_{\pm} = (1 \pm \eta) \frac{e^2 q Q}{4} \quad \dots (I.5)$$

Hence the frequencies of transition are given by

$$\nu_{\pm} = \frac{3e^2qQ}{4} (1 \pm \eta/3) \quad \dots (I.6)$$

except for nuclear spin $I = 3/2$ in all other cases the nuclear spin energy levels will be established in such a way that more than one transition of $\Delta m = \pm 1$ between these levels is possible. Thus by observing these transitions the quadrupole coupling constant e^2qQ and η can be determined.

In the case of spin $I = 3/2$ we still get two doubly-degenerate levels which are given by [8,9]

$$E_{A_1, B_1} = - \frac{e^2qQ}{4} (1 + \eta^2/3)^{1/2} \quad \dots (I.7)$$

$$E_{A_3, B_3} = - \frac{e^2qQ}{4} (1 + \eta^2/3)^{1/2} \quad \dots (I.8)$$

where A_1, B_1, A_3, B_3 are appropriate linear combinations of pure m functions. As there are only two energy levels there is only one transition and it is not possible to obtain both e^2qQ and η by studying the pure NQR of spin $I = 3/2$ nuclei. In order to obtain both these parameters one has to do a Zeeman NQR study. Zeeman NQR studies have been reported both on single crystals [9] as well as on powder sample [10] to obtain these parameters.

Until recently the eigenvalues of \mathcal{H}_Q matrix in the case of spin $I > 3/2$ were not available in the analytical form. Bersohn [11] dealt with the secular equations for $I > 3/2$ by a perturbation procedure which is convergent for $\eta \leq 0.25$.

Cohen [12] has solved the secular equations for $I = 5/2, 7/2$ and $9/2$ numerically and tabulated eigenvalues for values of η ranging from 0.1 to 1.0. Recently, there have been reports where the exact analytical solutions of the secular equations for spin $I = 5/2, 7/2$ and $9/2$ are obtained [13]. Analytical expressions for eigenvalues in the case of spin $I \gg 3/2$ in the presence of a weak Zeeman field are also available in the literature [14,15]. Using a spherical tensor technique Krishnan and Sanctuary [16] have obtained secular equations in frequencies of spin $I = 1, 3/2$ and $5/2$ with non-axial field gradients, and solved exactly in terms of quadrupole coupling constant and asymmetry parameter.

Once the eigenvalues are known the eigenfunctions may be obtained by the usual procedure. The transitions between the doubly degenerate energy levels $E_{\pm m}$ and $E_{\pm m'}$ are induced by the application of a linearly polarized r.f. field which interacts with magnetic dipole moment of the nucleus. The frequency of the transition is given by

$$\omega_Q (m \rightarrow m') = \frac{E_m - E_{m'}}{\hbar} \quad \dots (I.9)$$

For the case of axial symmetry, transitions with $\Delta m = \pm 1$ are only allowed. But in the case of finite η , transitions corresponding to $\Delta m \gg \pm 1$ are also allowed but they are generally weak. In NQR only allowed transitions are studied in order to obtain

the field gradients at the nucleus.

The relative intensities W_{if} of NQR spectral lines arising from transitions between initial and final Quadrupole states Ψ_i and Ψ_f , are proportional to $|\langle i | \mathcal{H}_1 | f \rangle|^2$. Where \mathcal{H}_1 is the perturbing Hamiltonian due to the action of the r.f. field on the magnetic dipole moment of the nucleus. The intensities of the pure quadrupole lines for various values of I are discussed in the literature [9,12].

Like in other branches of magnetic resonance spectroscopy, in NQR also the relaxation behaviour of the nuclear spin ensemble is characterized by the spin-lattice relaxation time T_1 and the spin-spin relaxation time T_2 . These relaxation processes play an important role in determining NQR line widths. Experimentally observed NQR lines possess finite widths which can be related to the apparent spin-spin relaxation time T_2^* . The relative line widths, vary between 10^{-2} and 10^{-5} of the transition frequency. We now consider, briefly, the factors that contribute to the line widths in NQR.

In general, width, shape, and structure of NQR signals can have contributions from both 1) static and 2) dynamic effects [8]. Among static effects one has to consider both i) magnetic and ii) electrical effects.

i) Magnetic Effects:

Two types of magnetic interactions between the resonant nucleus and the other nuclei of the same or different species

are possible. These are, a) direct magnetic dipole-dipole interactions [17]. b) Indirect spin-spin interactions (J-interaction) [17].

(a) Direct dipole-dipole interaction between the resonant nucleus and close neighbouring nuclei leads to the fine splitting of quadrupolar spectra, whereas the magnetic dipole-dipole interaction between the resonant nucleus and other distant neighbouring nuclei, other than the very close neighbour, broadens the fine structure produced by the interaction of the close neighbour.

(b) The indirect spin-spin interaction between two nuclei, originates from the magnetic interactions of two nuclei with the electrons that form the chemical bond between them [17]. This interaction can lead to fine splitting of the quadrupole spectra if its short range effect is sufficiently strong to overcome the dipole-dipole interaction. Broadening [18] due to J-interaction can take place only if it occurs with equivalent strength between a resonant nucleus and a number of neighbours.

ii) Electrical Effects:

The main sources of electrical effects are dislocations and strains in the crystal or powder grains. These are found to broaden the NQR spectra [19-21]. Qualitatively, the broadening due to strains and dislocations can be understood as arising

from random distortions of intermolecular interactions, and a corresponding random distribution of field gradients at nuclear sites. Presence of impurities also causes a random distribution in environments around different nuclei and hence leads to a broadening of quadrupolar lines.

2) Dynamic Effects:

Among the dynamic effects the motions arising due to torsional oscillations of molecules are important. In NQR, torsional motions contribute most to the spin lattice relaxation. Since the spin lattice relaxation limits the life time of the excited state, it contributes to a line broadening known as the "life-time broadening". Hence the contribution to linewidths from dynamic effects are related to T_1 .

Thus, in general, a composite line shape $g(\omega)$ of the NQR line can be expressed as

$$g(\omega) = \int_{-\infty}^{\infty} \int_{-\infty}^{\infty} g_{\text{dyn}}(\omega, \omega') g_{\text{dip}}(\omega', \omega'') g_{\text{ele}}(\omega'', \omega_Q) d\omega' d\omega'' \quad \dots (I.10)$$

where g_{dyn} , g_{dip} and g_{ele} are the line shape functions corresponding to the dynamic effects, static magnetic dipolar interactions and static electric effects, respectively and ω_Q is the the NQR frequency. Now an approximation can be made that the net half width of the NQR signal $g(\omega)$ is given as a sum of the

half-widths of the individual line shape functions g_{dyn} , g_{dip} and g_{ele} . The net half-width $\delta\omega$ can be represented by

$$\delta\omega = \delta\omega_{\text{dyn}} + \delta\omega_{\text{dip}} + \delta\omega_{\text{ele}} \quad \dots (\text{I.11})$$

normally the net line shape in NQR can be described by a Gaussian. Hence T_2^* can be defined as

$$T_2^* = \frac{2(\pi \log_e 2)^{1/2}}{\delta\omega} \quad \dots (\text{I.12})$$

So far we have discussed the basic theoretical aspects of NQR. In the next section we present some of the applications of NQR spectroscopy.

I.B SOME APPLICATIONS OF NQR

NQR spectroscopic investigations yield information about the quadrupole coupling constant, e^2qQ , and asymmetry parameter, η , of the efg. These parameters can be used to get considerable information regarding the electronic environment around a quadrupolar nucleus which helps in understanding the chemical bond and other related properties of the molecules or ions in which the nucleus is present [8,22-24]. However, pure NQR study is possible only in the solid state. This is because of the fact that the efg tensor like the dipolar interaction

tensor is traceless and the rapid motion present in liquids and gases averages it out to zero. This does not imply that quadrupole interactions do not exist in liquids and gases. The information about quadrupole interactions in liquids and gases can be obtained by other spectroscopic methods like NMR, EPR, microwave and molecular beam techniques. Thus, the information from NQR complements the information from other techniques. The chemical applications of NQR have been reviewed extensively in the literature [8,23-30]. In what follows we present briefly typical applications of NQR spectroscopy. It must be emphasized here that no attempt for a thorough review of the literature is made.

The quadrupole coupling constant, e^2qQ , is a product of nuclear quadrupole moment (eQ), a nuclear property, and (eq), the principal Z-component of the efg tensor, which is a molecular property. Hence, if we know one of these, the other quantity can be determined using the experimental value of QCC. The quantity ' q ' could be estimated if the charge distribution over the molecule is known. This requires a knowledge of the wave functions for the electrons in the molecules.

Both ab initio and semi-empirical wave functions have been used in the theoretical calculation of the efg 's. Ab initio level calculations are expected to yield accurate efg 's. Results of ab initio calculations of efg 's for free molecules have been reviewed extensively [31-34]. Recently, Palmer [35]

and Brown et al. [36] have reported ab initio calculations of ^{14}N quadrupole coupling constants using different kinds of basis sets. However, in the case of efg calculations on large molecules, as the ab initio calculations become cumbersome and require large computer time, one has to resort to the approximation methods like empirical and semi-empirical methods. The two approximation methods, the Townes-Dailey method [37] and the Cotton-Harris method [38] are very commonly used for the calculation of efg's. Molecular orbital approach has been very popular in this regard. Bray et al. [39] have analyzed the results of ^{14}N NQR data in solids using Townes-Dailey approach. In the Townes-Dailey approach, Sternheimer effects [40-42] are not considered. These effects play an important role in the evaluation of efg's when deformation of electron core takes place either by efg due to outer orbitals or by nuclear quadrupole moment. Results of quadrupole coupling constants obtained using several semi-empirical methods have been reviewed [43].

In covalent molecules a knowledge of efg's can yield information on the ionic character of the chemical bond involving the quadrupolar nucleus and the hybridization of the atomic orbitals involved in the bond [8,22,23]. Asymmetry parameter η does not involve any properties of the nucleus and it can be interpreted directly in terms of the electron distribution in molecules. NQR spectral parameters can also be correlated with other chemical- and physicochemical constants such as Hammett-Toft σ parameters, electronegativities and dissociation constants [8,22,23].

NQR can be used to distinguish between "Chemically inequivalent" and "physically inequivalent" sites of the same quadrupolar nucleus in a crystal [8]. A lattice site is said to be chemically inequivalent to another lattice site if the components of principal efg tensor at the respective sites are different. The physically inequivalent lattice sites have at the respective sites the same magnitude for the principal efg components but they are oriented in different directions. Hence, chemically inequivalent sites have different NQR frequencies, whereas, physically inequivalent sites generally, have the same frequency.

As the efg is insensitive to isotopic substitution, the ratio of quadrupole moments of different isotopes can be obtained from the ratio of quadrupole coupling constants of the same compound with different isotopes [44-46].

The efg and hence the NQR frequencies are quite sensitive to temperature changes. Systematic studies of the temperature dependence of the NQR frequencies yield useful information regarding molecular motions in solids [8,28]. As precise frequency measurements are possible, temperature dependence of NQR frequency has been used for accurate measurement of temperature [47,48]. Normally the temperature dependence of the NQR frequency $d\nu_Q/dT$ is negative. Anomalous temperature dependence of NQR frequencies in coordinate compounds have been reviewed in the literature [49].

NQR studies of pressure dependence can reveal intermolecular interactions present in the crystal [50]. Several studies on the pressure dependence of NQR frequencies have been made in the literature [28,50-55].

Temperature and pressure changes on a crystal can induce phase transitions in solids. Since NQR frequencies and intensities undergo changes at these phase transition points, NQR can be used for the study of phase transitions [8,27,28,56-60].

As mentioned in the previous section relaxation processes play an important role in determining line widths. T_1 is found to be more sensitive to the dynamic structure of the solid than T_2 [61]. T_2^* can have contributions from both static and dynamic effects. In quadrupolar spin systems, T_1 can be quantitatively related to the nature and frequency of the molecular and lattice motions in the solid phase [61-63]. Since these relaxation times are temperature and pressure dependent, accurate measurements of NQR parameters as a function of temperature and pressure can yield information about structural and dynamical effects in solid state [64].

NQR frequency changes due to the transition from the conducting to superconducting state have been observed [65]. Careful investigation of NQR parameters is expected to lead to a better understanding of the superconducting state of the material. Recently, several workers have investigated the high temperature superconducting oxides by NQR spectroscopy [66,67].

Using NQR spectroscopy the existence of the quantum mechanically predicted Berry's phase has been demonstrated experimentally [68].

Nuclear spin with $I \geq 2$ possess, in addition to the quadrupole moments, electric hexadecapole moments [20]. Usually hexadecapole coupling constant values are small, which lie between few hundred Hz to few KHz, hence the direct detection of this interaction is rather difficult. Several workers have used accurate measurements of NQR frequencies to obtain hexadecapole coupling constant [20,69-74].

From the above discussion it is clear that NQR is one of the most important tools for the investigation of static and dynamic phenomena in solids. The research work in NQR is reflected in the nine bi-annual "International Symposia" that were held in the recent past. Proceedings of the first two symposia have been published in the form of books [75,76]. The papers presented in the subsequent symposia have been published in scientific journals namely, "Journal of Magnetic Resonance" "Journal of Molecular Structure" and "Zeitschrift für Naturforschung". The papers presented at the recent ninth symposium (Jan. 1988) will be published in the "Journal of molecular structure".

In the next section of this chapter we outline, briefly, the methods of detection of NQR and also present a brief description of the pulsed NQR spectrometer employed in the

experimental investigations in the present thesis.

I.C DETECTION OF NUCLEAR QUADRUPOLE RESONANCE

The information about nuclear quadrupole interactions can be obtained from a variety of the spectroscopic techniques. For example, to name a few, in the gaseous state, the quadrupole interactions can be measured by molecular microwave spectroscopy [77] and NMR spectroscopy can be used to measure the quadrupole interactions in liquid state [78]. Quadrupole interactions in excited molecular states in solids can be studied by a novel technique, known as optically detected magnetic resonance (o.d.m.r.) [79]. For a detailed discussion of various techniques for measuring quadrupole interactions the reader is referred to excellent articles by Smith [30,80]. In this section we deal only with the methods of pure nuclear quadrupole resonance in solid state.

Like in NMR, the direct detection of NQR can be made using continuous wave (c.w.) or pulsed and Fourier transform (FT) techniques. In what follows, we present a brief account of these methods and no attempt has been made for a rigorous survey of literature.

I.C.1 Continuous Wave Techniques:

In continuous wave spectrometers the sample is subjected to an r.f. field, by placing it in a coil which is part of an

r.f. oscillator. The same oscillator usually detects the NQR signal induced in the coil. The crossed-coil method [81] of detection which is commonly used in NMR spectroscopy is not possible in pure NQR as there is no net component of induced signal at right angles to the transmitter coil because of the opposite senses of quadrupole precession associated with the $\pm m_I$ degeneracies of the quadrupole state. However, if a small magnetic field is applied then this degeneracy is lifted, and the crossed-coil method can be used. Since a component of nuclear induction then appears normal to the axis of the r.f. coil. A few NQR studies have been done with crossed coil arrangements [82-84]. Since the magnitude of the splittings of nuclear energy levels by the interaction of a nuclear quadrupole with electric field gradients in solids can range from zero to several thousand MHz, NQR spectrometers are required to operate over a large range of frequencies. Because of this reason c.w. NQR spectrometers are based on frequency-swept oscillators, in which the frequency can be changed by slowly varying the tuning capacitor in the tank circuit of the oscillator.

Most of the c.w. NQR spectrometers are based on one or other of four main types of oscillators, namely,

- i) the marginal oscillator [85]
- ii) the regenerative oscillator [86]
- iii) the superregenerative oscillator (SRO) [87,88]
- and iv) Limited oscillator [89].

Among these, SRO's have the highest sensitivity and hence they have been used, extensively, for NQR studies. However, these oscillators are associated with frequency instabilities and it is very difficult to get pure absorption line shapes using simple SRO's. Injection- and phase-locking of an SRO to a stable external crystal oscillator can improve its frequency stability and line shape response [90-93]. In such spectrometers signal averaging can be used to improve signal-to-noise ratio of weak NQR signals [93]. For a detailed discussion of c.w. NQR spectrometers the reader is referred to [90-94].

I.C.2 Pulsed Techniques:

For the detection of NQR, pulse techniques, offer more flexibility over c.w. methods. In principle, a modern pulsed NMR spectrometer (with multinuclear capability) which is used for the study of NMR of solids can be employed for the study of NQR by simply removing the magnet.

There are distinct advantages in pulsed spin echo methods of detection of NQR over the c.w. methods; For example, in c.w. methods one often faces the problem of modulation broadening and inhomogeneous broadening of NQR line, whereas spin echo signals are free from these broadening effects. By following the spin echo envelope modulations it is possible to detect the small splittings in NQR lines due to dipolar or indirect spin-spin interactions [8]. Pulse techniques are better

suited for the measurement of various types of relaxation times. The fast signal averaging facilities in pulsed spectrometers can be used to improve the signal-to-noise ratio in the case of weak resonances. Multiple pulse techniques, which are commonly used in NMR of solids [95,96] can be used to remove the contributions of interactions which broaden the NQR line and thus achieve a narrowed line. The resolution enhancement in NQR is, in principle, facilitates the study of weak interactions. Using pulse techniques it should be possible to study the multiple quantum coherences in NQR also.

Like in NMR, in NQR also FT techniques have been implemented [97-99]. FT NQR method has been used for the study of spin-spin interactions [100] and for the study of fine structure in the NQR spectrum [99]. Details of pulsed and FT-NQR spectrometers are available in the literature [8,97-106].

In NQR spectroscopy the direct detection of quadrupolar nuclei with low abundance and/or low quadrupole coupling constant, (termed as rare nuclei) is rather difficult. This problem can be surmounted to some extent by using the signal averaging facilities available on pulsed NQR spectrometers. However, the double resonance techniques offer better sensitivity for the detection of the rare nuclei. All double resonance techniques take advantage of the large nuclear resonance signal characteristic of an abundant species of nuclei 'O' (observe nuclei) in the sample containing the rare nuclear species 'R' the two species being strongly coupled.

If the observe and the rare nuclear species are irradiated with suitable r.f. fields near their resonance frequencies, the dipole-dipole and exchange interactions between 'O' and 'R' spins can facilitate the observation of the resonance signal from 'O' with enhanced sensitivity. Different kinds of double resonance techniques have been developed and implemented in the literature [107-115].

Double resonance techniques can be classified as

- i) Pure quadrupole double resonance (PQDR) techniques,
- ii) NMR-NQR double resonance techniques.

In PQDR the observe nucleus 'O' and the nucleus to be detected 'R' are both quadrupolar. The NQR signal of 'R' spins can be detected by monitoring the NQR signal of 'O' spins. In NMR NQR double resonance experiments the NMR signal of observe nucleus 'O' (usually protons) is monitored while the 'R' spins are irradiated in the absence of magnetic field. Various double resonance techniques that are employed in the literature are reviewed [116-120]. Here we present a brief discussion of PQDR techniques only. There are three types of PQDR techniques that are employed in the literature. These are:

- i) spin-echo double resonance (SEDOR) [107, 108]
- ii) double resonance in the rotating frame (DRRF) [109, 110]
- iii) steady-state double resonance (SSDR) [111].

Recently, Ramachandran and Narasimhan [121] have developed a new DRRF technique based on Off-resonant pulse methods. The high sensitivity and low transmitter power requirements of this

technique have been demonstrated by detecting ^{23}Na in NaClO_3 .

Employing all the above mentioned double resonance techniques the resonances of rare nuclei such as, ^2H , ^{23}Na , ^{39}K , $^{85,87}\text{Rb}$, ^{133}Cs , ^{17}O , ^{27}Al and other nuclei have been detected with enhanced sensitivity in many chemically interesting compounds. In most of these cases the chlorine and bromine nuclei have been used as observe nuclei [113,121-124].

There have been several reports describing pulsed NQR double resonance spectrometer in the literature [106,110,117,125]. Computer and/or microprocessor-controlled pulsed spectrometers have been described in the literature [126,127]. Recently, Narsimha Reddy et al. [128,129] developed a microprocessor-controlled pulsed NQR spectrometer. The microprocessor, employed in this spectrometer, with proper software is not only capable of generating the various kinds of multiple-pulse sequences but also controls the entire spectrometer. This spectrometer can be effectively used for automatic acquisition, averaging and processing of NQR signal data.

In the next section we present the description of the pulsed NQR spectrometer system which has been employed for the experimental investigations in the present thesis.

I.C.3 Description of the Pulsed NQR Spectrometer Employed for the Experimental Investigations in the Present Thesis:

The block diagram of the home-made pulsed NQR spectrometer used in the present investigations is shown in Fig. I.1.

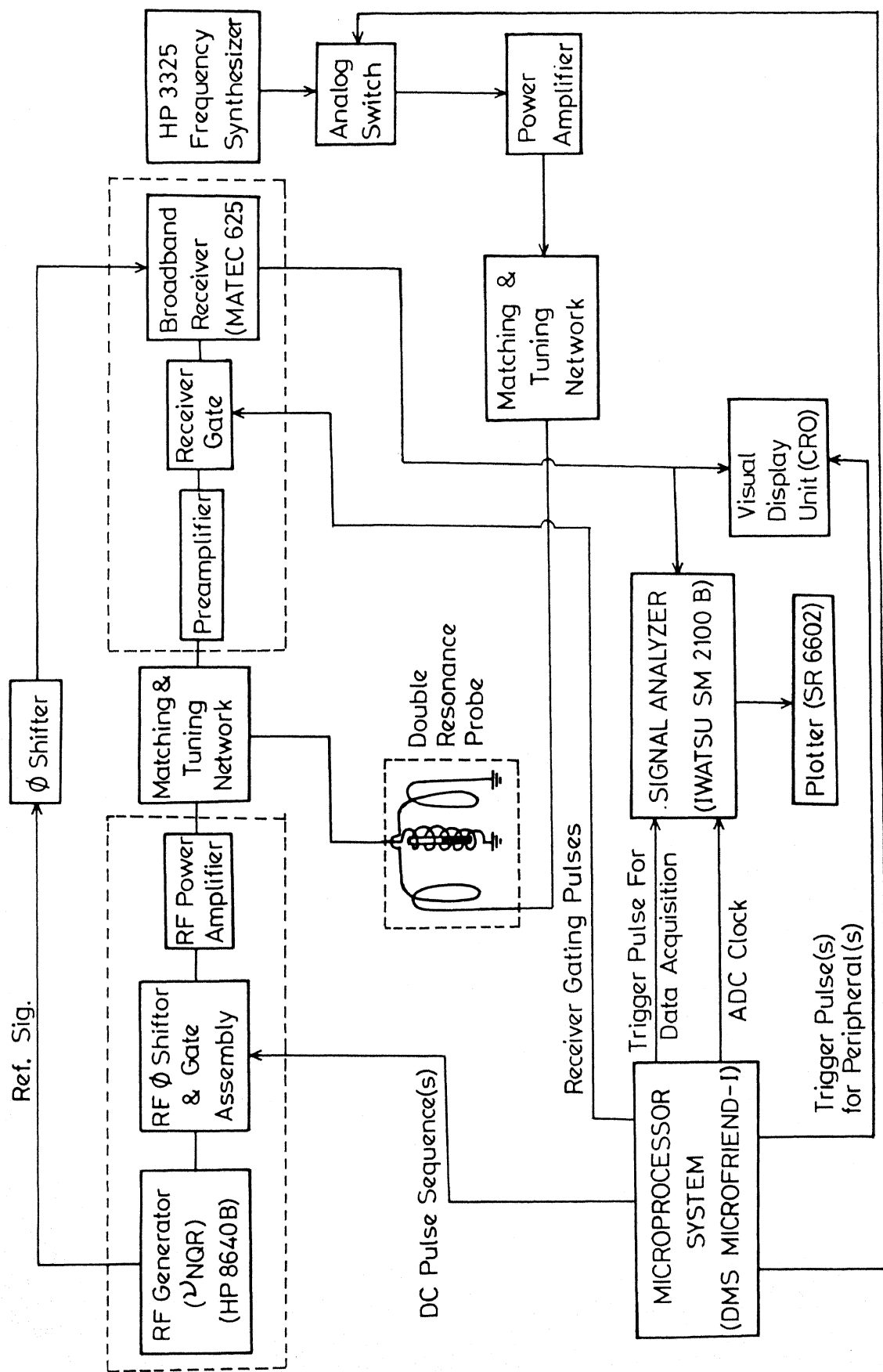


Fig.I.1 BLOCK DIAGRAM OF THE MICROPROCESSOR CONTROLLED PULSED NMR SPECTROMETER



Fig. I.2. A view of the pulsed NQR spectrometer

A photograph of the spectrometer system is given in Fig. I.2. Here we present a brief description of various modules of the spectrometer. For complete details of the spectrometer system the reader is referred to [106,128-130]. The spectrometer used in this work can be conveniently operated over a range of 15 MHz to 40 MHz. In this spectrometer the pulse sequence generation is done by an 8085-based eight-bit microprocessor system (Microfriend-I, Dynalog Microsystems, Bombay, India). The software required for the various kinds of pulse sequence generation (see ref. 129) can be stored in the EPROM and it can be called on to the on-board user RAM and executed for the pulse sequence generation. The pulse sequence is output through one of the I/O ports of the microprocessor system and are available at the BNC connectors on the side panel of the card cage of the microprocessor system. The pulses available at these BNC connectors can be used for r.f. gating and triggering of peripherals. Apart from the microprocessor system an hardware pulse programmer [130] capable of generating a maximum of three pulses is also available, in this spectrometer assembly.

The r.f. signal source is a signal generator (Model 8640B from Hewlett-Packard, USA). The r.f. is gated by an r.f. gate based on double balanced mixers. The gated r.f. pulses are amplified by a home-made low noise tuned power amplifier and coupled to the sample circuitry through an impedance matching and tuning network. This home-made power amplifier has considerable power droop and it has poor long-time power stability

especially in the experiments involving long train of r.f. pulses where large average power is drawn. Hence, in all the multiple pulse experiments a commercial broadband ENI (Model A-300, Electronic Navigation Industries, Inc., New York, USA) power amplifier is used to drive the final tuned stage of the home-made power amplifier. This power amplifier combination gives a better long time stability of the pulse power and it gives an approximate r.f. pulse power output of 800 W. Since the r.f. amplitude level, at the output of the r.f. gate is unable to drive the ENI power amplifier it is amplified by a broadband amplifier (Model Hp-461A from Hewlett Packard, USA). This power amplifier combination can be operated conveniently in the range 15 MHz to 35 MHz. A low power commercial broadband amplifier ENI (Model 440LA, Electronic Navigation Industries, Inc., New York, USA) is also available for the use at higher frequencies.

The NQR signal induced in the sample coil, by the application of r.f. pulse is coupled to a low noise tuned pre-amplifier based on 3N200 FET transistors. The cross diodes at the input of the preamplifier protect it from the high power r.f. pulses. The output signal at the preamplifier is further amplified and detected by a broadband (2-200 MHz) receiver (Model 625, from Matec, USA). Although this receiver has the provisions for both diode and phase sensitive detections we have used, in all the experiments, only the phase sensitive detection. In the phase sensitive detection the reference

signal is obtained by passing the output of HP 8640B signal generator through a delay line (Model 71-76, 0.4 sec, 10 turn, variable delay line of ESC, Electronic Corporation, U.S.A.). As the different delay line settings changes the level of the r.f. signal, the output of the delay line is passed through a tuned r.f. amplifier before connecting to the reference input of the receiver. The overall recovery time of the preamplifier and receiver combination is 10-15 μ s. In this spectrometer system receiver is also gated by a DBM (Model HP 10534A) to avoid the overload of the receiver from the r.f. pulse feed-through during the 'on' time of the transmitter.

The detected signal at the output of the receiver can either be monitored on an oscilloscope or it can be acquired into a signal analyzer (Model SM 2100B, from Iwatsu Electric Company Ltd., Tokyo, Japan). The signal analyzer has two input channels through which time domain signals can be acquired. It has a 12 bit ADC whose maximum clock frequency is 400 KHz. It can be operated in "Auto", "Program" and "BASIC" modes. The acquired time domain signals can be stored in any one of the eight blocks of the memory and these can be processed using the inbuilt routines of the system. The inbuilt routines like average, FFT, IFFT, auto-power spectrum, cross power spectrum, autocorrelation and cross correlation etc. can be executed by the 'Function Keys' available on the frontpanel of the signal analyser. In BASIC mode of operation, the BASIC Key board is used to write the software

program for processing the signals stored in the block memory of the signal analyzer. In the Basic program one can use the systems routines whenever necessary. The signals stored in the block memory can be displayed on the CRT display available in the signal analyzer. This CRT display is also useful for BASIC programming. The processed signals stored in the memory blocks can be transferred to a mini floppy disk for the permanent storage. These signals can be read into the block memory of the signal analyzer and can be recorded on to a plotter (Model SR 6602, from Iwatsu Electric Company Ltd., Tokyo, Japan) which has been interfaced to the signal analyzer through the GPIB interface facility available on the signal analyzer. In this spectrometer boxcar averager (Model CW-1, from Princeton Applied Research, USA) facility also available for experiments where single point averaging is required.

Facility for performing double resonance experiments also exists in this spectrometer. In the double resonance channel a frequency synthesizer (Model HP 3325A from Hewlett Packard, USA) is used as the signal source. The output of the synthesizer is gated by an analog switch (NS-AH001 4CD from National Semi-Conductor Corp., USA) for lower double resonance channel frequencies. The gated r.f. is amplified by a suitable r.f. amplifier depending upon the r.f. power requirements of the double resonance experiment, and coupled to the double resonance probe through a tuning and matching network.

So far we have discussed the principles, applications and methods of detection of NQR. In the previous section the advantages of the pulsed methods were brought out. In the present thesis we shall be mainly concerned with the theoretical and experimental studies of NQR signals of spin $I = 3/2$ and $5/2$ nuclei by pulse techniques.

In order to understand the various kinds of pulse experimental results one needs to have suitable theoretical tools for the description of such experiments. In the next section we present a brief outline of basic theoretical aspects for the description of pulse experiments.

I.D THEORETICAL DESCRIPTION OF PULSED NQR

The first experimental observation of pulse responses in pure NQR was made by Bloom and Norberg [131] and Hohn and Herzog [132]. Although the origins of NQR and NMR are entirely different the transient signals observed in NQR are similar to those in NMR. In NMR case, in thermal equilibrium there exists a net magnetization and the main interaction Hamiltonian is linear and proportional to a vector and hence it is possible to explain the transient signal formation in terms of simple vector models [133] in several cases. In the case of NQR in zero field there is no net magnetization [134] and the main interaction Hamiltonian is a bilinear operator which is proportional to a second

rank tensor. Hence, it is always not possible to visualize the formation of free induction and spin echo signals, in terms of simple models. Using a semiclassical model Bloom et al. [134] have attempted to give a geometrical explanation for free induction and spin echo signal formation in the special case of axially symmetric quadrupole interaction in spin $I = 3/2$ in zero field. However, no simple geometrical picture is possible for explaining the transient signal formation in NQR in the case of asymmetric quadrupole interaction and in the presence of a weak Zeeman field. However, the formation of transient signals in NQR can be studied by considering the quantum mechanical description of the evolution of the spin system.

I.D.1 Basic Theory:

In this sub-section we present a brief discussion of the procedure involved in the description of pulse experiments in NQR, in general terms. For the sake of simplicity we consider an ensemble of non-interacting nuclear spins with $I = 3/2$ in the absence of a Zeeman field.

The total interaction Hamiltonian for this case can be written as

$$\begin{aligned} \mathcal{H}(t) &= \frac{e^2 q Q}{4I(2I-1)} [3\tilde{I}_Z^2 - \tilde{I}^2 + \eta (\tilde{I}_X^2 - \tilde{I}_Y^2)] + \mathcal{H}_1(t) \\ &= \frac{\omega_Q}{\sqrt{6}} \mathcal{H}'_Q + \mathcal{H}_1(t) \end{aligned} \quad \dots (I.13)$$

$$\text{where } \omega_Q = \frac{e^2 q Q}{2} \quad \dots (I.14)$$

$$\mathcal{H}'_Q = \frac{1}{\sqrt{6}} [3I_z^2 - I^2 + \eta (I_x^2 - I_y^2)] \quad \dots (I.15)$$

The first term is the quadrupolar Hamiltonian and the second terms $\mathcal{H}_1(t)$ defines the interaction between the spins and the applied radio frequency (r.f.) field. The response of nuclear spin system to r.f. pulse excitations can be calculated using the equation of motion of the density matrix. From the time-dependent Schrödinger equation, one can arrive at the equation of motion for the density matrix [135],

$$\frac{d\sigma(t)}{dt} = -i [\mathcal{H}(t), \sigma(t)] \quad \dots (I.16)$$

This equation is known as Liouville-von Neumann equation or density operator equation. Its formal solution can be written as

$$\sigma(t) = U(t) \sigma(0) U(t)^{-1} \quad \dots (I.17)$$

$$\text{where } U(t) = T \exp \left(-i \int_0^t \mathcal{H}(t') dt' \right) \quad \dots (I.18)$$

Dyson time-ordering operator T defines a prescription for evaluating the exponential functions in cases where the Hamiltonians at different times do not commute i.e. $[\mathcal{H}(t'), \mathcal{H}(t'')] \neq 0$.

In the high temperature approximation, the thermal equilibrium density matrix is given by [136]:

$$\begin{aligned}\sigma(t < 0) &= \{\text{Tr} [\exp (-\frac{\mathcal{H}_Q}{kT})]\}^{-1} \exp (-\frac{\mathcal{H}_Q}{kT}) \\ &\approx [\text{Tr}(\mathbb{1})]^{-1} (1 - \frac{\mathcal{H}_Q}{kT}) \\ &\approx [\text{Tr}(\mathbb{1})]^{-1} (1 - \frac{\omega_Q}{\sqrt{6} kT} \mathcal{H}'_Q) \quad \dots (I.19)\end{aligned}$$

where $\mathcal{H}_Q = \frac{\omega_Q}{\sqrt{6} kT} \mathcal{H}'_Q$ is the quadrupolar Hamiltonian. In the right hand side of this equation, the first term being a constant it is not affected by any evolution of the spin system. So we need to follow only the evolution of the second term, proportional to reduced density matrix ρ , which is defined by setting

$$\sigma(t < 0) \approx [\text{Tr}(\mathbb{1})]^{-1} (1 - \frac{\omega_Q}{\sqrt{6} kT} \rho(0)) \quad \dots (I.20)$$

$$\text{where } \rho(0) = \mathcal{H}'_Q \quad \dots (I.21)$$

In the quadrupolar interaction representation defined by the transformation operator

$$U = \exp (i \frac{\omega}{\sqrt{6}} \mathcal{H}'_Q t) \quad \dots (I.22)$$

the total Hamiltonian can be written as [136]:

$$\tilde{\mathcal{H}} = \frac{\Delta\omega}{\sqrt{6}} \mathcal{H}'_Q + \tilde{\mathcal{H}}'_1 \quad \dots (I.23)$$

where $\Delta\omega = (\omega_Q - \omega)$

$$\frac{\Delta\omega}{\sqrt{6}} \mathcal{H}'_Q = U \frac{\omega_Q}{\sqrt{6}} \mathcal{H}'_Q U^{-1} - i \frac{U \partial U^{-1}(t)}{\partial t}$$

and $\tilde{\mathcal{H}}'_1 \simeq U \mathcal{H}_1(t) U^{-1}$.. (I.24)

$\tilde{\mathcal{H}}'_1$ represents the r.f. Hamiltonian, in the interaction representation, obtained after truncating the high frequency terms.

In the interaction representation the reduced density matrix satisfies the equation of motion

$$\frac{d\tilde{\rho}(t)}{dt} = i [\tilde{\rho}(t), \tilde{\mathcal{H}}] \quad \text{.. (I.25)}$$

Since, now $\tilde{\mathcal{H}}$ being independent of time $\tilde{\rho}(t)$ is given by

$$\tilde{\rho}(t) = \exp(-i \tilde{\mathcal{H}} t) \tilde{\rho}(0) \exp(i \tilde{\mathcal{H}} t) \quad \text{.. (I.26)}$$

An intense r.f. pulse of width ' t_w ', which satisfies the condition $\gamma H_1 \gg \Delta\omega$, is referred to as a "hard" pulse. When such a pulse is applied then during the pulse the spin system evolves under the Hamiltonian $\tilde{\mathcal{H}}'_1$ only. Following the removal of the pulse the spin system evolves under the influence of the Hamiltonian $\frac{\Delta\omega}{\sqrt{6}} \mathcal{H}'_Q$. Thus, the Eqn. (I.24) can be used to obtain the density matrix of the spin system after a pulse or a sequence of pulses.

The expression for the signal induced in the coil after a pulse or a sequence of pulses can be obtained by taking the expectation value of the operator, M , corresponding to the magnetization, i.e.,

$$\langle M \rangle_{\text{lab}} = \text{Tr} [\tilde{\sigma} \tilde{M}] \quad \dots (I.27)$$

I.D.2 Theoretical Approaches for the Description of Pulse Responses in NQR. A review:

In this section we present a short review of various theoretical approaches available for describing the spin dynamics in NQR. The first quantum mechanical description of the formation of the transient signals in NQR was given by Bloom et al. [134]. They used the time-dependent perturbation theory. Their method of calculation essentially involves solution of the time-dependent Schrödinger equations for the spin system in the presence and absence of the r.f. pulses. Using this approach they have calculated the single and two pulse responses in the case of spin $I = 3/2$ with axial field gradients in zero field as well as in the presence of a weak Zeeman field making an angle ' θ ' with respect to the symmetry axis of the crystal. Following this, Das and Saha [137,138] developed the density matrix method for calculating the free induction decay (FID) and spin echo signals in NQR. This method involves the matrix transformations of the density matrix in the presence of r.f. pulses and during the evolution periods. Using this method

they have calculated the FID and spin echo signals amplitudes for nuclei of any general spin I in single crystals with axially symmetric field gradients. Pratt [139] used interaction representation approach for the description of various pulse experiments in the case of spin $I = 3/2$ nuclei. In this method the spin dynamics are followed by matrix transformations of density matrix, in the interaction representation, in the presence of r.f. pulses and during evolution periods. In the above mentioned approaches in obtaining the solution to the equation of motion of the density matrix the explicit matrix representations of the operators are used. However, in many cases, it is not necessary to consider the entire density matrix either because certain elements are irrelevant for the selected observable, or because the number of the actual degrees of freedom is smaller than the total number of matrix elements. In such cases, it is convenient to do the calculations by expanding the density operator in terms of a suitably chosen set of base operators and to derive equations for their time-dependent coefficients [140].

The fictitious spin-1/2 operator formalism due to Vega and Pines [141] has been extensively used in the description of pulse experiments in pure NQR of spin $I = 1$ systems. Since the fictitious spin-1/2 operators possess simple cyclic commutation relationships it is relatively easy to evaluate the time dependence of the density operator in the presence of r.f. pulses and during the evolution periods. Cantor and Waugh [142]

have employed this formalism for the analysis of pulsed spin locking experiments in the case of nuclei with spin $I = 1$. This formalism has also been employed by other workers in the analysis of spin-locking and multiple pulse experiments in pure NQR of spin $I = 1$ [143-146]. Although the fictitious spin-1/2 operator formalism was generalized to higher spins by Vega [147] and by Wokaun and Ernst [148] there is no report where this formalism is employed in pure NQR of spin $I > 1$. As mentioned in Section I, Krishnan and Sanctuary [16] have used the spherical tensor method to obtain the analytical expressions for the eigenvalues of spin 1, 3/2 and 5/2 in terms of quadrupole coupling constant and asymmetry parameter. In this method they solve the appropriate Liouville equation to obtain time dependent polarizations ρ_q^k . They have also given the time evolution of quadrupolar tensor analytically. Recently, Bowden et al. [149-153] extended the tensor operator formalism, earlier applied to electron paramagnetic resonance [154] for the study of multiple quantum NMR of spin $I \gg 1$. They have discussed the advantages of this formalism over the fictitious spin-1/2 operator formalism and also the differences between their approach and the approach used by Sanctuary in the description of multiple quantum NMR experiments.

I.E SCOPE OF THE PRESENT WORK

This thesis deals with theoretical and experimental investigations in pulsed NQR spectroscopy. The tensor operator

formalism due to Bowden et al. [149-153] which has been employed earlier in NMR has been adapted for the present theoretical studies in NQR. The responses of quadrupolar nuclear spin system, to single, double and to a variety of multiple-pulse sequences have been experimentally investigated. The tensor operator formalism has been employed to analyze these experimental results.

In Chapter II of this thesis, we have employed the tensor operator formalism due to Bowden et al. [149-153] in the calculation of pulse responses in NQR of single crystals. Using this formalism, calculation of single and double r.f. pulse responses in the case of nuclei with spin $I = 1, 3/2$ and $5/2$ in single crystals but in the absence of a magnetic field are presented. In the case of spin $I = 3/2$ nuclei, the pulse response calculations in the presence of a weak Zeeman field are also given. Although we have presented only single- and two-pulse responses, especially in the case of spin $I = 3/2$, the results for the evolution of tensor operators given in this chapter can be used to calculate the response of any kind of r.f. pulse sequence in the absence of relaxation effects.

Chapter III illustrates the application of tensor operator formalism in the calculation of single and two pulse responses in polycrystalline samples containing spin $I = 3/2$ nuclei in the presence of a weak Zeeman field. Assuming a configuration in which r.f. and Zeeman fields are oriented parallel to

each other and which in turn are oriented in a random direction with respect to the principal axes of the efg we have calculated single and two pulse responses and the results are presented. It is shown that the two-pulse response contains a term which is responsible for the spin echo envelope modulations in the presence of a weak Zeeman field, and yields information about the asymmetry parameter (η) of efg. Typical experimental spectra of Zeeman spin echo envelope modulations of ^{35}Cl in AgClO_3 are also given.

Chapter IV presents the studies on multiple-pulse experiments in pure NQR. The experimental results of various multiple pulse sequences in NQR of single crystal of spin $I = 3/2$ (^{35}Cl) nuclei are given and compared with those obtained from polycrystalline samples. Results of ^{23}Na - ^{35}Cl double resonance experiment in NaClO_3 powder carried out under the multiple pulse spin locking condition are also presented. The experimental results of various multiple pulse sequences studied on ^{187}Re (spin $I = 5/2$) nuclei in polycrystalline sample of KReO_4 are given. Finally, using tensor operator formalism, some of the multiple pulse sequences are analyzed in pure NQR of spin $I = 3/2$ nuclei and the results are presented.

Chapter V deals with the theoretical investigation of double quantum coherence in pure NQR of spin $I = 5/2$ nuclei. Using tensor operator formalism it has been shown that the creation and detection of double quantum coherence in the case of spin $I = 5/2$ nuclei in single crystal can be done by the

application of pulse scheme similar to the one employed by Hatanaka et al. [155,156] in NMR of three level system.

SUMMARY

In this chapter a discussion of basic principles, and some applications of NQR spectroscopy are given. A brief outline of NQR detection techniques and the description of pulsed NQR spectrometer system employed in the experimental investigations in the present thesis are also given. The basic theoretical background for spin dynamics calculations and a short review of various approaches available for the description of pulse experiments in NQR are also presented.

REFERENCES

- [1] N.F. Ramsey, "Nuclear Moments", Wiley, New York (1953).
- [2] H. Kopfermann, "Nuclear Moments", English version by E.E. Schneider, Academic Press, New York (1958).
- [3] H.B.G. Casimir, *Physica*, 2, 719 (1935); "On the Interaction Between Atomic Nuclei and Electrons", Teylens Tweeden Genootschap, E.F. Bohn, Holland (1936).
- [4] H. Schüler and T. Schmidt, *Z. Phys.*, 94, 457 (1935).
- [5] J.M.B. Kellogg, I.I. Rabi, N.F. Ramsey and J.R. Zacharias, *Phys. Rev.*, 55, 728 (1939); 57, 677 (1940).
- [6] H.G. Dehmelt and H. Krüger, *Naturwissenschaften*, 37, 111 (1950).
- [7] R.V. Pound, *Phys. Rev.*, 69, 785 (1950).
- [8] T.P. Das and E.L. Hahn, "Nuclear Quadrupole Resonance Spectroscopy", Academic Press, New York (1958).
- [9] C. Dean, *Phys. Rev.*, 96, 1053 (1954).
- [10] Y. Morino and M. Toyama, *J. Chem. Phys.*, 35, 1289 (1961).
- [11] R. Bersohn, *J. Chem. Phys.*, 20, 1505 (1952).
- [12] M.H. Cohen, *Phys. Rev.*, 96, 1278 (1954).
- [13] (a) R.B. Creel, H.R. Brooker and R.G. Barnes, *J. Magn. Reson.*, 41, 146 (1980).
(b) R.B. Creel, *J. Magn. Reson.*, 52, 515 (1983).
- [14] R.B. Creel and D.A. Drabold, *J. Molec. Struct.*, 111, 85 (1983).
- [15] G.M. Muha, *J. Magn. Reson.*, 53, 85 (1983).

- [16] M.S. Krishnan and B.C. Sanctuary, *Z. Naturforsch.*, 41a, 353 (1986).
- [17] G.E. Pake, "Nuclear Magnetic Resonance", *Solid State Phys.*, 2, 24 (1956).
- [18] N. Bloembergen and T.J. Rowland, *Phys. Rev.*, 97, 1679 (1955).
- [19] G.D. Watkins and R.V. Pound, *Phys. Rev.*, 85, 1062 (1952).
- [20] T.C. Wang, *Phys. Rev.*, 99, 566 (1955).
- [21] R. Livingston, *J. Phys. Chem.*, 57, 496 (1953).
- [22] E.A.C. Lucken, "Nuclear Quadrupole Coupling Constants", Academic Press, New York (1969).
- [23] G.K. Semin, T.A. Babushkina and G.G. Yakobson, "Nuclear Quadrupole Resonance in Chemistry", John Wiley, New York (1975).
- [24] J.A.S. Smith, *J. Chem. Edu.*, 48, 39 (1971); 48, A77 (1971); 48, A149 (1977) and 48, A243 (1977).
- [25] E.A.C. Lucken in "Advances in Nuclear Quadrupole Resonance", Vol. 1, Ed. J.A.S. Smith, Heyden and Son, London (1974), p. 235.
- [26] A. Weiss in "Advances in Nuclear Quadrupole Resonance", Vol. 1, Ed. J.A.S. Smith, Heyden and Son, London (1974), p. 1.
- [27] L. Ramakrishna, S. Soudararajan, V.S.S. Sastry and J. Ramakrishna, *Coord. Chem. Rev.*, 22, 123 (1977).
- [28] A.L. Porte in "Annual Reports on the Progress in Chemistry", Section C (Physical Chemistry), Vol. 50, Royal Society of Chemistry, Burlington House, London (1983), p. 162.

- [29] K.V.S. Rama Rao and S. Rama Prabhu, Phys. Stat. Sol.(a), 93, 17 (1986).
- [30] J.A.S. Smith, Chem. Soc. Rev., 15, 225 (1986).
- [31] R. Moccia and M. Zandomenegi, "Advances in Nuclear Quadrupole Resonance", Vol. 2, Ed. J.A.S. Smith, Heyden and Son, London (1975), p. 135 and references therein.
- [32] E.A.C. Lucken, "Topics in Current Chemistry," Vol. 30, Springer Verlag, Berlin (1972), p. 155.
- [33] E. Serocco, in "Advances in Chemical Physics", Vol. 5, Ed. I. Prigogine, Interscience, London (1963), p. 319.
- [34] J.W. Jost, and C.T. O'Konski, J. Molec. Struct., 111, 387 (1983).
- [35] M.H. Palmer, Z. Naturforsch., 41a, 147 (1986) and references therein.
- [36] R.D. Brown and M.P. Head-Gordon, Molec. Phys., 61, 1183 (1987).
- [37] C.H. Townes and B.P. Dailey, J. Chem. Phys., 17, 1782 (1949).
- [38] F.A. Cotton and C.B. Harris, Proc. Natl. Acad. Sci., USA, 56, 21 (1966).
- [39] P.J. Bray and S.G. Greenbaum, J. Molec. Struct., 83, 35 (1982).
- [40] R.M. Sternheimer, Phys. Rev., 80, 102 (1950); 95, 736 (1954).
- [41] R.M. Sternheimer, Z. Naturforsch., 41a, 24 (1986) and references therein.

- [42] K.D. Sen and P.T. Narasimhan, in "Advances in Nuclear Quadrupole Resonance", Vol.1, Ed. J.A.S. Smith, Heyden and Son, London (1974), p. 277.
- [43] M.A. Whitehead in "Proceedings of the Second International Symposium on NQR Spectroscopy (1973)", Ed. A. Colligiani, A. Vallereni Publishers, PISA, Italy (1975), p. 27.
- [44] R. Livingston, Phys. Rev., A82, 289 (1951).
- [45] R. Livingston and H. Zeldas, Phys. Rev., 90, 609 (1953).
- [46] M. Bloom, Phys. Rev., 94, 1996 (1954).
- [47] D.B. Utton and J.B. Vannier, Instrum. Technol., 23, 47 (1976).
- [48] A. Ohte and I. Iwakawa, IEEE Trans. Instrum. Measu., 1M25, 357 (1976).
- [49] D. Nakamura, R. Ikeda and M. Kubo, Coord. Chem. Rev., 17, 281 (1975).
- [50] G.C. Gillies and R.J.C. Brown, Can. J. Chem., 54, 2266 (1976).
- [51] J. Staukowski and M. Zdanowka-Fraczek, J. Molec. Struct., 111, 11 (1983).
- [52] C. Dimitropoulos, J. Molec. Struct., 111, 163 (1983).
- [53] M. Mackowiak, M.Z. Fraczek, P. Koziol, J. Staukowski and A. Weiss, Z. Naturforsch., 41a, 290 (1986).
- [54] M. Mackowiak, P. Koziol and J. Staukowski, Z. Naturforsch., 41a, 225 (1986).
- [55] V. Krishnan, T.V. Krishnamoorthy and J. Ramakrishna, Z. Naturforsch., 41a, 338 (1986).
- [56] R.L. Armstrong and Henry M. Van Driel in "Advances in Nuclear Quadrupole Resonance", Vol. 2, (1975), p. 179.

- [57] R. Blinc, Z. Naturforsch., 41a, 243 (1986).
- [58] N. Nakamura, Z. Naturforsch., 41a, 243 (1986).
- [59] I.A. Kjuntsel, V.A. Mokeeva, G.R. Soifer and I.G. Shaposhnikov, Z. Naturforsch., 41a, 275 (1986).
- [60] T.J. Bastow, Z. Naturforsch., 41a, 283 (1986).
- [61] D.E. Woessner and H.S. Gutowsky, J. Chem. Phys., 39, 440 (1963).
- [62] G.W. Leppelmeier and E.L. Hahn, Phys. Rev., 142, 179 (1966).
- [63] H. Bayer, Z. Physik, 130, 227 (1951).
- [64] H. Chihara and N. Nakamura in "Advances in Nuclear Quadrupole Resonance", Vol. 4 (1980), p. 1
- [65] D.E. MacLaughlin, Solid State Phys., 31, 1 (1976).
- [66] I. Furo, A. Janossy, L. Mihaly, P. Banki, Pocsik, I. Bakonyi, I. Heinmaa, E. Joon, and E. Lippmaa, Phys. Rev. B, 36, 5690 (1987).
- [67] R.E. Walstedt, W.W. Warren, Jr., R.F. Bell, G.E. Brennert, G.P. Espinosa, J.P. Remeika, R. J. Cava and E.A. Rietman, Phys. Rev. B, 36, 5727 (1987).
- [68] R. Tycko, Phys. Rev. Lett., 58, 2281 (1987).
- [69] R.R. Hewitt and B.F. Williams, Phys. Rev., 129, 1188 (1963).
- [70] Dinesh and J.A.S. Smith, "Proceedings of the Second International Symposium on NQR Spectroscopy (1973)", Ed. A. Colligiani, A. Vallerini Publishers, Pisa, Italy (1975).
- [71] S.C. Segal, J. Chem. Phys., 69, 2434 (1978).
- [72] H. Gotou, J. Magn. Reson., 54, 36 (1983).
- [73] T.J. Wang, J. Magn. Reson., 64, 194 (1985).

- [74] S.K. Semin, A.M. Raevsky and S.I. Gushin, Chem. Phys. Lett., 121, 214 (1985).
- [75] "Advances in Nuclear Quadrupole Resonance", Vol. 1, Ed. J.A.S. Smith, Heyden and Son, London (1974).
- [76] "Proceedings of the Second International Symposium on NQR Spectroscopy (1973)", Ed. A. Colligiani, A. Vallerini Publishers, Pisa, Italy (1975).
- [77] W. Gordy and R.L. Cook, "Microwave Molecular Spectra", Wiley, New York, 3rd edition (1984).
- [78] P.C.M. Van Zijl, B.H. Ruessink, J. Bulthuis, and C. Maclean, Acc. Chem. Res., 17, 172 (1984).
- [79] (a) C.B. Harris and M.J. Buckley in "Advances in Nuclear Quadrupole Resonance", Vol. 2, Ed. J.A.S. Smith, Heyden and Son, London (1975), p. 15.
- (b) K.P. Dinse and C.J. Winscom, J. Chem. Phys., 68, 1337 (1978).
- (c) K.P. Dinse and C.V. Borczyskowski, Chem. Phys., 44, 93 (1979).
- [80] J.A.S. Smith, Z. Naturforsch., 41a, 453 (1986).
- [81] F. Bloch, W. Hansen and M. Packard, Phys. Rev., 70, 474 (1946).
- [82] L.B. Robinson, Can. J. Phys., 35, 1344 (1957); 36, 1295 (1958).
- [83] H. Hartmann and H. Sillescu, Theor. Chim. Acta, 2, 63 (1964); 2, 271 (1964).
- [84] W.C. Proctor and K. Lu, Varian Technical Information Bulletin (1965).

- [85] (a) R.V. Pound and W.D. Knight, Rev. Sci. Instrum., 21, 219 (1950).
- (b) G.D. Watkins and R.V. Pound, Phys. Rev., 85, 1062 (1951):
- (c) F.N.H. Robinson, J. Sci. Instrum., 36, 481 (1959); Rev. Sci. Instrum., B4, 1260 (1963).
- [86] (a) R. Livingston, Annals of New York Academy of Sciences, 55, 800 (1952).
- (b) D.C. Douglass, Ph.D. Thesis, Cornell University, Ithaca, New York (1957).
- [87] C. Dean, Ph.D. Thesis, Harvard University (1952); Phys. Rev., 96, 1053 (1954).
- [88] C. Dean and M. Pollack, Rev. Sci. Instrum., 29, 630 (1958).
- [89] F.N.H. Robinson, J. Phys. E: Sci. Instrum., 15, 814 (1982); 15, 1093 (1982).
- [90] J.G. Graybeal and C.D. Cornevell, J. Phy. Chem., 62, 483 (1958).
- [91] D.A. Tong, J. Phys. E: Sci. Instrum., 1, 1153 (1968).
- [92] M. Read, in "Advances in Nuclear Quadrupole Resonance," Vol. 1, Ed. J.A.S. Smith, Heyden & Son, London (1974), p. 203.
- [93] V. Harihara Subramanian, P.T. Narasimhan and K.R. Srivatsan, J. Phys. E: Sci. Instrum., 14, 870 (1981).
- [94] T.L. Viswanathan, T.R. Viswanathan and K.V. Sane, Rev. Sci. Instrum., 41, 477 (1970).
- [95] U. Haeberlen, "High Resolution NMR in Solids", Academic Press, New York (1976).

- [96] M. Mehring, "High Resolution NMR Spectroscopy in Solids", 2nd edition, Springer-Verlag, Berlin (1983).
- [97] R. Lenk and E.A.C. Lucken, Chem. Phys. Lett., 21, 552 (1973).
- [98] R. Lenk and E.A.C. Lucken, Pure and Appl. Chem., 40, 199 (1974).
- [99] A.A.V. Gibson, J.R. Brookman and T.A. Scott, Phys. Lett., 50A, 31 (1974).
- [100] M. Mackowiak and J.R. Brookman, Acta Phys. Polonica, A52, 281 (1977).
- [101] D. Geizendanner, R. Leuk and G. Litzistorf, J. Phys. E: Sci. Instrum., 8, 8 (1975).
- [102] G.L. Petersen, Ph.D. Thesis, Brown University (1975).
- [103] G.L. Petersen and T. Oja, in "Advances in Nuclear Quadrupole Resonance", Vol. 1, Ed. J.A.S. Smith, Heyden & Son, London (1974), p. 179.
- [104] A. Colligiani and G. Ambrosetti, Gazz. Chim. Ital., 106, 439 (1976); J. Magn. Reson., 32, 93 (1978).
- [105] U. Henriksson, L. Odberg, J.C. Eriksson and L. Westmau, J. Phy. Chem., 81, 76 (1977).
- [106] R. Ramachandran and P.T. Narasimhan, J. Phys. E: Sci. Instrum., 16, 643 (1983).
- [107] B. Herzog and E.L. Hahn, Phys. Rev., 103, 148 (1956).
- [108] M. Emswiller, E.L. Hahn and D. Kaplan, Phys. Rev., 118 414 (1960).
- [109] S.R. Hartmann and E.L. Hahn, Phys. Rev., 128, 2042 (1962).

- [110] R.E. Slusher and E.L. Hahn, Phys. Rev., 166, 332 (1968).
- [111] E.R. Jones and S.R. Hartmann, Phys. Rev. Lett., 22, 867 (1969); Phys. Rev., 6B, 757 (1972).
- [112] D.T. Edmonds, M.J. Hunt, A.L. Mackay and C.P. Summens, in "Advances in Nuclear Quadrupole Resonance", Vol. 1, Ed. J.A.S. Smith, Heyden and Son, London (1974), p. 145.
- [113] P.S. Ireland and T.L. Brown, J. Magn. Reson., 20, 330 (1975).
- [114] D.T. Edmonds and J.P.G. Mailer, J. Magn. Reson., 26, 93 (1977).
- [115] S.G.P. Brosnan and D.T. Edmonds, J. Magn. Reson., 38, 47 (1980); 45, 490 (1981).
- [116] R. Blinc, in "Advances in Nuclear Quadrupole Resonance", Vol. 2, Ed. J.A.S. Smith, Heyden and Son, London (1975), p. 71.
- [117] D.T. Edmonds, Phys. Rep., 29c, 234 (1977).
- [118] D.T. Edmonds, Bull. Magn. Reson., 3, 53 (1981).
- [119] J.L. Ragle and G.L. Minott III, in "Advances in Nuclear Quadrupole Resonance", Vol. 3, Ed. J.A.S. Smith, Heyden and Son, London (1978), p. 205.
- [120] I.J.F. Poplett, in "Advances in Nuclear Quadrupole Resonance", Vol. 4, Ed. J.A.S. Smith, Heyden and Son, London (1980), p.115.
- [121] R. Ramachandran and P.T. Narasimhan, J. Magn. Reson., 51, 67 (1983).
- [122] N. Weiden, J.J. Breit and A. Weiss, J. Molec. Struct., 58, 43 (1980).

- [123] N. Weiden and A. Weiss, J. Magn. Reson., 30, 403 (1978).
- [124] N. Weiden and A. Weiss, Faraday Symp., 13, 93 (1979).
- [125] A.G. Redfield, W. File and H.E. Bleich, Rev. Sci. Instrum., 39, 710 (1968).
- [126] D. Giesendanner, S. Sengupta and G. Litzistcorf, J. Mole. Struct., 58, 519 (1980).
- [127] M. Gourdjji and A. Penear, J. Molec. Struct., 83, 361 (1982).
- [128] Narsimha Reddy, Arun Bhavsar and P.T. Narasimhan, Z. Naturforsch., 41a, 449 (1986).
- [129] Narsimha Reddy, Ph.D. Thesis, Indian Institute of Technology, Kanpur, India (1987).
- [130] R. Ramachandran, Ph.D. Thesis, Indian Institute of Technology, Kanpur, India (1982).
- [131] M. Bloom and R.E. Norberg, Phys. Rev., 93, 638 (1954).
- [132] E.L. Hahn and B. Herzog, Phys. Rev., 93, 639 (1954).
- [133] E.L. Hahn, Phys. Rev., 80, 580 (1950).
- [134] M. Bloom, E.L. Hahn and B. Herzog, Phys. Rev., 97, 1699 (1955).
- [135] C.P. Slichter, "Principles of Magnetic Resonance," 2nd edn., Springer-Verlag, Berlin (1978).
- [136] M. Goldman, "Spin Temperature and NMR in Solids Oxford University Press, Oxford (1970).
- [137] T.P. Das, A.K. Saha and D.K. Roy, Proc. Roy. Soc. (London), A227, 407 (1955).
- [138] T.P. Das and A.K. Saha, Phys. Rev., 98, 516 (1955).

- [139] J.C. Pratt, Molec. Phys., 34, 539 (1977).
- [140] R.R. Ernst, G. Bodenhausen and A. Wokaun, "Principles of Nuclear Magnetic Resonance in one and two Dimensions", Clarendon Press, Oxford (1987).
- [141] (a) S. Vega and A. Pines, J. Chem. Phys., 66, 5624 (1977).
(b) S. Vega, J. Chem. Phys., 63, 3769 (1975).
- [142] R.S. Cauton and J.S. Waugh, J. Chem. Phys., 73, 1054 (1980).
- [143] D. Ya. Osokin, J. Mol. Struct., 83, 243 (1982).
- [144] D. Ya. Osokin, Phys. Status Solid ., 109, K7 (1982).
- [145] D. Ya. Osokin, Phys. Status Solid ., 102, 681 (1980).
- [146] M. Matti Maricq, Phys. Rev., B33, 4501 (1986).
- [147] S. Vega, J. Chem. Phys., 68, 5518 (1978).
- [148] A. Wokaun and R.R. Ernst, J. Chem. Phys., 67, 1752 (1977).
- [149] G.J. Bowden and W.D. Hutchison, J. Magn. Reson., 67, 403 (1986).
- [150] G.J. Bowden, W.D. Hutchison and J. Khachan, J. Magn. Reson., 67, 415 (1986).
- [151] G.J. Bowden and W.D. Hutchison, J. Magn. Reson., 70, 361 (1986).
- [152] G.J. Bowden and W.D. Hutchison, J. Magn. Reson., 71, 61 (1987).
- [153] W.D. Hutchison, Ph.D. Thesis, University of New South Wales, NSW, Australia (1987).

- [154] H.A. Buckmaster, R. Chatterjee and Y.H. Shing, Phys. Status Solidi, 13, 9 (1972).
- [155] H. Hatanaka, T. Terao and T. Hashi, J. Phys. Soc. Japan, 39, 835 (1975).
- [156] H. Hatanaka and T. Hashi, J. Phys. Soc. Japan, 39, 1139 (1975).

Acc. No. **106246**

CHAPTER II

PULSE RESPONSES IN NQR OF SINGLE CRYSTALS: APPLICATION OF TENSOR OPERATOR FORMALISM

In pulsed NQR, one is concerned with the study of responses of quadrupolar nuclei ($I \geq 1$) to an r.f. pulse or to a sequence of r.f. pulses. In order to understand the origins of such responses of nuclear spins one needs to have a suitable theoretical tool. As pointed out in Chapter I, several theoretical approaches are available to describe pulse responses in NQR. However, the most convenient method for spin dynamic calculations in NMR or NQR is the one based on Liouville-von Neumann equation. In this method of calculation one often needs to evaluate the operator expression

$$\rho(t) = \exp(-i\mathcal{H}t) \rho(0) \exp(i\mathcal{H}t) \quad \dots (II.1)$$

for different initial conditions and for different Hamiltonians. One way of evaluating the above expression is by expressing the operators in their explicit matrix representations and carrying out the matrix multiplication, which may often lead to lengthy expressions. But this problem can be considerably simplified when the density matrix is represented in terms of a complete orthogonal basis set of operators [1]. Various sets of base operators have been used in the description of spin dynamics in NMR spectroscopy [1].

The fictitious spin-1/2 operator formalism [2], has been used extensively for the description of spin dynamics in NQR in the case of spin $I = 1$ [3-5]. Although these operators have

been generalized to higher spins [6,7], there is no report where these have been employed in the spin dynamics calculation in the NQR of spins $I \geq 3/2$.

Since the quadrupolar nuclei may be present in axial or non-axial efg's the study of pulse responses of various spins $I \geq 1$ in both these cases is of importance. Especially, in the case of spin $I = 3/2$, in order to obtain both the quadrupolar interaction parameters it is necessary to study the pulse responses in the presence of a small Zeeman field. Keeping this in view, in this chapter we have employed the tensor operator formalism [8-11] to calculate the pulse responses in NQR of nuclei with spin $I = 1, 3/2$ and $5/2$ in single crystals. Our emphasis will be mostly on spin $I = 3/2$ case. The results presented in this chapter will be used in the subsequent chapters of this thesis for the analysis of pulse responses in a variety of situations.

This chapter consists of four sections. In Section II.A a brief account of tensor operator formalism is given. Section II.B deals with the calculation of pulse responses of nuclei with spin $I = 3/2$ and $5/2$ with axially symmetric field gradients. Section II.C discusses the pulse response calculation for the case of spin $I = 3/2$ nuclei with axial field gradients but in the presence of a Zeeman field. Pulse response calculation for nuclear spins $I = 1, 3/2$ with non-axial field gradients is presented in Section II.D. The last section of this chapter

presents calculations for spin $I = 3/2$ case with non-axial field gradient in the presence of a weak Zeeman field. This chapter concludes with a summary.

II.A TENSOR OPERATOR FORMALISM

In this section we present a brief account of the tensor operator formalism as used by Bowden et al. [8]. Irreducible tensor operators T_q^n of rank n and order q have been defined in the literature [12]. Irreducible tensor operators for $n \leq 5$ are given in Table II.1.

Matrix elements:

From the Wigner-Eckart theorem the matrix elements of the tensor operator T_q^n , of rank n , order q , are given by [12]

$$\langle I m | T_q^n | I m' \rangle = (-1)^{I-m} \begin{pmatrix} I & n & I \\ -m & q & m' \end{pmatrix} \langle I || T^n || I \rangle \quad \dots (II.2)$$

where $\begin{pmatrix} I & n & I \\ -m & q & m' \end{pmatrix}$ is the 3j coefficient

and

$\langle I || T^n || I \rangle$ is the reduced matrix element and is given by

$$\langle I || T^n || I \rangle = \left[\frac{n! n! (2I+n+1)!}{2^n (2n)! (2I-n)!} \right]^{1/2} \quad \dots (II.3)$$

Table II.1. Tensor Operators for $n \leq 5$ after Buckmaster et al. (1972)

$$\begin{aligned}
 \tilde{T}_0^0 &= 1 & ; & \quad T_0^2 = \left(\frac{1}{6}\right)^{1/2} [3 I_z^2 - I(I+1)] ; \\
 \tilde{T}_0^1 &= I_z & ; & \quad T_{\pm 1}^2 = \mp \frac{1}{2} [I_z, I_{\pm}]_{+} ; \\
 \tilde{T}_{\pm 1}^1 &= \mp \left(\frac{1}{2}\right)^{1/2} I_{\pm} & ; & \quad T_{\pm 2}^2 = \frac{1}{2} I_{\pm}^2 \\
 \tilde{T}_0^3 &= \left(\frac{1}{10}\right)^{1/2} [5 I_z^3 - \{3 I(I+1) - 1\} I_z] \\
 \tilde{T}_{\pm 1}^3 &= \mp \frac{1}{2} \left(\frac{3}{10}\right)^{1/2} \frac{1}{2} [\{5 I_z^2 - I(I+1) - \frac{1}{2}\}, I_{\pm}]_{+} \\
 \tilde{T}_{\pm 2}^3 &= \left(\frac{3}{4}\right)^{1/2} \frac{1}{2} [I_z, I_{\pm}^2]_{+} \\
 \tilde{T}_{\pm 3}^3 &= \mp \frac{1}{2} \left(\frac{1}{2}\right)^{1/2} I_{\pm}^3 \\
 \tilde{T}_0^4 &= \frac{1}{2} \left(\frac{1}{70}\right)^{1/2} [35 I_z^4 - \{30 I(I+1) - 25\} I_z^2 + 3 I^2(I+1)^2 - 6 I(I+1)] \\
 \tilde{T}_{\pm 1}^4 &= \mp \left(\frac{1}{14}\right)^{1/2} [\{7 I_z^3 - [3 I(I+1) + 1] I_z\}, I_{\pm}]_{+} \\
 \tilde{T}_{\pm 2}^4 &= \frac{1}{4} \left(\frac{1}{7}\right)^{1/2} [\{7 I_z^2 - I(I+1) - 5\}, I_{\pm}^2]_{+} \\
 \tilde{T}_{\pm 3}^4 &= \mp \left(\frac{1}{2}\right)^{1/2} \frac{1}{2} [I_z, I_{\pm}^3]_{+} \\
 \tilde{T}_{\pm 4}^4 &= \frac{1}{4} I_{\pm}^4 \\
 \tilde{T}_0^5 &= \frac{1}{6} \left(\frac{1}{14}\right)^{1/2} [63 I_z^5 + 35\{3 - 5 I(I+1)\} I_z^3 + \{12 - 50 I(I+1) \\
 &\quad + 15 I^2(I+1)^2\} I_z] \\
 \tilde{T}_{\pm 1}^5 &= \mp \left(\frac{5}{21}\right)^{1/2} I_{\pm} [21 I_z^4 \pm 42 I_z^3 + 7\{9 - 2 I(I+1)\} I_z^2 \pm \\
 &\quad 14\{3 - I(I+1)\} I_z + \{12 - 8 I(I+1) + I^2(I+1)^2\}] \\
 \tilde{T}_{\pm 2}^5 &= \frac{1}{2} \left(\frac{5}{3}\right)^{1/2} I_{\pm}^2 [3 I_z^3 \pm 9 I_z^2 + \{12 - I(I+1)\} I_z \pm \{6 - I(I+1)\}] \\
 \tilde{T}_{\pm 3}^5 &= \mp \frac{1}{12} \left(\frac{5}{2}\right)^{1/2} I_{\pm}^3 [9 I_z^2 \pm 27 I_z + \{24 - I(I+1)\}] \\
 \tilde{T}_{\pm 4}^5 &= \frac{1}{4} \left(\frac{5}{1}\right)^{1/2} I_{\pm}^4 [I_z \pm 2] \\
 \tilde{T}_{\pm 5}^5 &= \mp \frac{1}{4} \left(\frac{1}{2}\right)^{1/2} I_{\pm}^5
 \end{aligned}$$

Unit irreducible tensor operators:

These are defined as

$$\langle \text{Im} | \hat{T}_{\sim q}^n | \text{Im}' \rangle = \left[\frac{(2n+1)}{(2I+1)} \right]^{1/2} \langle \text{Im}' n q | \text{Im} \rangle \quad \dots (\text{II.4})$$

Relationship between unit and non-unit tensor operators:

$$\hat{T}_{\sim q}^n = \frac{1}{n!} \left[\frac{(2n+1)(2I-n)! 2^n (2n)!}{(2I+n+1)!} \right]^{1/2} T_{\sim q}^n \quad \dots (\text{II.5})$$

Orthonormality:

The unit tensor operators obey the following orthonormality relationship:

$$\text{Tr}[(\hat{T}_{\sim q}^n)^\dagger (\hat{T}_{\sim q'}^{n'})] = \delta_{nn'} \delta_{qq'} \quad \dots (\text{II.6})$$

where the adjoint

$$(\hat{T}_{\sim q}^n)^\dagger = (-1)^q \hat{T}_{\sim -q}^n \quad \dots (\text{II.7})$$

Symmetric and antisymmetric combinations of the tensors:

These are defined as

$$\begin{aligned} T_{\sim q}^n(s) &= \frac{1}{\sqrt{2}} [T_{\sim q}^n + T_{\sim -q}^n] \\ T_{\sim q}^n(a) &= \frac{1}{\sqrt{2}} [T_{\sim q}^n - T_{\sim -q}^n] \end{aligned} \quad \dots (\text{II.8})$$

with $q \neq 0$

Commutation relationship:

The commutation relationship which exists between the tensor operators is given by [13]

$$[T_{\tilde{q}}^n, T_{\tilde{q}'}^{n'}] = \sum_{NQ} a(n, n', N, I) \{1 - (-1)^{n+n'-N}\} \\ \langle NQ | n, q, n', q' \rangle T_Q^N \quad \dots (II.9)$$

where

- i) $a(n, n', N, I) = (2N+1)^{1/2} (-1)^{N+2I} \left\{ \begin{matrix} n & n' & N \\ I & I & I \end{matrix} \right\} \frac{\langle I || T^n || I \rangle \langle I || T^{n'} || I \rangle}{\langle I || T^N || I \rangle}$
- ii) $\langle NQ | n, q, n', q' \rangle$ is Clebsch-Gordon coefficient.
- iii) $\left\{ \begin{matrix} n & n' & N \\ I & I & I \end{matrix} \right\}$ is a Wigner 6j coefficient.

Since the unit irreducible tensor operators form a 'basis set' any operator can be expressed in terms of irreducible tensor operators. For example, the density matrix ρ can be expressed in the form

$$\rho = \sum_{n,q} \rho_q^n \hat{T}_{\tilde{q}}^n \quad \dots (II.10)$$

where the coefficient ρ_q^n , is referred to as a Fano statistical tensor and it is given by

$$\rho_q^n = \text{Tr}[(T_{\tilde{q}}^n)^\dagger \rho] \quad \dots (II.11)$$

The tensor operators in non-unit form are orthogonal but not orthonormal.

The tensor operators in non-unit form hold for all I . In all the calculations in this thesis we use tensor operators in non-unit form.

II.B PULSE RESPONSES IN THE ABSENCE OF A ZEEMAN FIELD FOR THE CASE OF AXIALLY SYMMETRIC FIELD GRADIENTS

II.B.1 General

The total laboratory-frame Hamiltonian for an ensemble of non-interacting nuclear spins experiencing nuclear electric quadrupole couplings can be written as

$$\mathcal{H}(t) = \frac{e^2 q Q}{4I(2I-1)} [3\tilde{I}_z^2 - \tilde{I}^2] + \mathcal{H}_1(t) \quad \dots (II.12)$$

The first term is the quadrupolar Hamiltonian for the case of axially symmetric field gradients, where the symbols have their usual meaning [14] and the second term $\mathcal{H}_1(t)$ defines the interaction between the spins and the applied (r.f.) field. In all the calculations in this chapter we assume that relaxation effects are not significant. Also we set $\hbar = 1$, and express energy values in radians/sec. The r.f. pulses are assumed to be applied along the x-axis of the crystal (which coincides with the direction of the principal field gradient axis V_{xx}). If the

r.f. field is applied along the x-axis of the crystal with amplitude H_1 and frequency ω then

$$\mathcal{H}_1(t) = -2\gamma H_1 \cos(\omega t) \tilde{I}_x = -2\omega_1 \cos(\omega t) \tilde{I}_x \quad \dots (II.13)$$

where $\omega_1 = \gamma H_1$ and γ is the gyromagnetic ratio of the nucleus.

Now $\mathcal{H}(t)$ can be written as

$$\mathcal{H}(t) = \frac{\omega_Q}{\sqrt{6}} \mathcal{H}'_Q - 2\omega_1 \cos(\omega t) \tilde{I}_x \quad \dots (II.14)$$

$$\text{where } \mathcal{H}'_Q = \frac{1}{\sqrt{6}} [3\tilde{I}_z^2 - \tilde{I}^2] \quad \dots (II.15)$$

Following the convention of Bowden et al. [8], $\mathcal{H}(t)$ can be written in terms of tensor operators as:

$$\mathcal{H}(t) = \frac{\omega_Q}{\sqrt{6}} T_0^2 + 2\omega_1 \cos(\omega t) \tilde{T}_1^1(a) \quad \dots (II.16)$$

In the quadrupolar interaction representation defined by the transformation operator

$$U = \exp \left(+i \frac{\omega}{\sqrt{6}} \mathcal{H}'_Q t \right) \quad \dots (II.17)$$

The total Hamiltonian can be written as

$$\tilde{\mathcal{H}} = \frac{\Delta\omega}{\sqrt{6}} \mathcal{H}'_Q + \tilde{\mathcal{H}}_1 \quad \dots (II.18)$$

where $\Delta\omega = (\omega_Q - \omega)$

$$\frac{\Delta\omega}{\sqrt{6}} \mathcal{H}'_Q = U \frac{\omega_Q}{\sqrt{6}} \mathcal{H}_Q U^{-1} - i U \frac{\partial U^{-1}(t)}{\partial t} \quad \dots (II.19)$$

and

$$\tilde{\mathcal{H}}_1 = U \mathcal{H}_1(t) U^{-1} = 2\omega_1 \cos(\omega t) U T_1^1(a) U^{-1} \quad \dots (II.20)$$

$\tilde{\mathcal{H}}_1$ is referred to as the r.f. Hamiltonian in the interaction representation.

In the evaluation of the pulse responses we often need to know the time evolution of density matrix (thus the time evolution of tensor operators) under the quadrupolar, r.f. and Zeeman Hamiltonians in the interaction representation. We have employed the method of "nested commutation relationships" [8] to obtain time evolution of tensor operators under the influence of quadrupolar and r.f. interactions. In evaluating the time evolution of tensor operators under the influence of Zeeman Hamiltonian, as the method of "nested commutation relationships" becomes tedious, we have adopted the "harmonics of the motion method" [13].

II.B.2 Spin I = 3/2

For this case the total Hamiltonian in the interaction representation, defined by the transformation operator given in Eqn. (II.17) can be written as

$$\tilde{\mathcal{H}} = \frac{\Delta\omega}{\sqrt{6}} T_0^2 + \tilde{\mathcal{H}}_1 \quad \dots (II.21)$$

$$\text{where } \Delta\omega = \omega_Q - \omega, \text{ with } \omega_Q = \frac{e^2 q Q}{2}. \quad \dots (II.22)$$

$\tilde{\mathcal{H}}_1$ can be obtained as follows. Making use of the evolution of the tensor operators under quadrupolar interaction (see Table II.2), we get

$$\begin{aligned} \tilde{\mathcal{H}}_1(t) = 2\omega_1 \cos(\omega t) & \left[T_1^1(a) \left\{ \frac{3}{5} \cos(\omega t) + \frac{2}{5} \right\} + i T_1^2(s) \frac{1}{\sqrt{2}} \sin(\omega t) \right. \\ & \left. + T_1^3(a) \frac{2}{\sqrt{15}} (\cos(\omega t) - 1) \right] \quad \dots \text{(II.23)} \end{aligned}$$

$$\tilde{\mathcal{H}}_1 \approx \omega_1 \left[\frac{3}{5} T_1^1(a) + \frac{2}{\sqrt{15}} T_1^3(a) \right] \quad \dots \text{(II.24)}$$

where we have dropped the terms with coherent time dependence as non-secular terms. The evolution of the tensor operators under the influence of the Hamiltonian $\tilde{\mathcal{H}}_1$ is set out in Table II.3.

II.B.2(i) Single-pulse response:

Let us consider the effect of a single r.f. pulse (as shown in Fig. II.1) on an ensemble of non-interacting nuclear spins $I = 3/2$ with axial field gradients. The thermal equilibrium reduced density matrix is given by (see Chapter I, Sec. I.D.1):

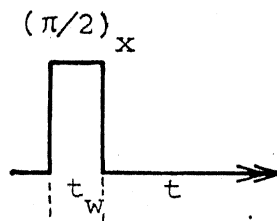


Fig.II.1. Single-Pulse Sequence

$$\rho(0) = T_0^2$$

Since it commutes with the quadrupolar Hamiltonian we have, the

Table II.2. The Evolution of the Tensor Operators $T_q^n(s, a)$ Under a Quadrupole Interaction $\mathcal{H}_Q = \frac{\omega_Q}{\sqrt{6}} T_0^2$ for $I = 3/2$ after Bowden et al. (1986)*

$$U T_1^1(s) U^{-1} = T_1^1(s) \left[\frac{3}{5} \cos(\omega_Q t) + \frac{2}{5} \right] - i T_1^2(a) \frac{1}{\sqrt{2}} \sin(\omega_Q t) \\ + T_1^3(s) \frac{2}{\sqrt{15}} [\cos(\omega_Q t) - 1]$$

$$U T_1^2(s) U^{-1} = -i T_1^1(a) \left[\frac{3\sqrt{2}}{5} \sin(\omega_Q t) \right] + T_1^2(s) \cos(\omega_Q t) \\ - i T_1^3(a) \frac{2\sqrt{2}}{\sqrt{15}} \sin(\omega_Q t)$$

$$U T_2^2(s) U^{-1} = T_2^2(s) \cos(\omega_Q t) - i T_2^3(a) \frac{2}{\sqrt{3}} \sin(\omega_Q t)$$

$$U T_1^3(s) U^{-1} = T_1^1(s) \frac{3}{5} \sqrt{\frac{3}{5}} [\cos(\omega_Q t) - 1] - i T_1^2(a) \sqrt{\frac{3}{10}} \sin(\omega_Q t) \\ + T_1^3(s) \left[\frac{2}{5} \cos(\omega_Q t) + \frac{3}{5} \right]$$

$$U T_2^3(s) U^{-1} = -i T_2^2(a) \frac{\sqrt{3}}{2} \sin(\omega_Q t) + T_2^3(s) \cos(\omega_Q t)$$

* $U = \exp(-i \mathcal{H}_Q t)$

For the antisymmetric combinations $T_q^n(a)$, replace s by a and a by s in the above equations. $\omega_Q = e^2 q Q / 2$. T_0^1 , T_0^2 , $T_3^3(s)$ and $T_3^3(a)$ all commute with the Hamiltonian.

able II.3. The Evolution of the Tensor Operators $T_q^n(s, a)$ Under the Influence of the Hamiltonian $\tilde{\mathcal{H}}_1 = +\omega_1 \left[\frac{3}{5} T_1^1(a) + \frac{2}{\sqrt{15}} T_1^3(a) \right]$ for $I = 3/2$

$$T_{\sim 0}^1 U^{-1} = T_{\sim 0}^1 \frac{1}{5} (\cos \xi + 4) + T_{\sim 0}^3 \frac{2}{3} \frac{\sqrt{2}}{\sqrt{5}} (\cos \xi - 1)$$

$$+ i T_{\sim 1}^1(s) \frac{\sqrt{3}}{5} \sin \xi + i T_{\sim 1}^3(s) \frac{2}{3\sqrt{5}} \sin \xi$$

$$T_{\sim 1}^1(s) U^{-1} = T_{\sim 1}^1(s) \frac{1}{5} [4 \cos \xi + 1] + T_{\sim 1}^3(s) \frac{1}{\sqrt{15}} (\cos \xi - 1)$$

$$- T_{\sim 3}^3(s) \frac{1}{3} (\cos \xi - 1) + i T_{\sim 0}^1 \frac{\sqrt{3}}{5} \sin \xi + i T_{\sim 0}^3 \frac{2\sqrt{2}}{\sqrt{15}} \sin \xi$$

$$- i T_{\sim 2}^3(s) \frac{\sqrt{2}}{3} \sin \xi$$

$$U T_{\sim 1}^1(a) U^{-1} = T_{\sim 1}^1(a) \frac{1}{5} (\cos \xi + 4) - T_{\sim 3}^3(a) \frac{1}{3} (\cos \xi - 1)$$

$$- T_{\sim 1}^3(a) \frac{1}{\sqrt{15}} (\cos \xi - 1) - i T_{\sim 2}^3(a) \frac{\sqrt{2}}{3} \sin \xi$$

$$U T_{\sim 0}^2 U^{-1} = T_{\sim 0}^2 \cos \xi + i T_{\sim 1}^2(s) \sin \xi$$

$$U T_{\sim 1}^2(s) U^{-1} = T_{\sim 1}^2(s) \cos \xi + i T_{\sim 0}^2 \sin \xi$$

$$U T_{\sim 1}^3(s) U^{-1} = T_{\sim 1}^3(s) \frac{1}{10} (7 \cos \xi + 3) + T_{\sim 1}^1(s) \frac{9}{10\sqrt{15}} (\cos \xi - 1)$$

$$+ T_{\sim 3}^3(s) \frac{\sqrt{3}}{2\sqrt{5}} (\cos \xi - 1) + i T_{\sim 0}^1 \frac{3}{5\sqrt{5}} \sin \xi$$

$$+ i T_{\sim 0}^3 \frac{2\sqrt{2}}{5} \sin \xi + i T_{\sim 2}^3(s) \frac{\sqrt{3}}{\sqrt{10}} \sin \xi$$

Table II.3 (contd.)

$$\begin{aligned}
 U\tilde{T}_1^3(a)U^{-1} &= \tilde{T}_1^3(a) \frac{1}{10} (3 \cos \xi + 7) + \tilde{T}_3^3(a) \frac{\sqrt{3}}{2\sqrt{5}} (\cos \xi - 1) \\
 &\quad - \tilde{T}_1^1(a) \frac{9}{10\sqrt{15}} (\cos \xi - 1) + i \tilde{T}_2^3(a) \frac{\sqrt{3}}{\sqrt{10}} \sin \xi
 \end{aligned}$$

$$\begin{aligned}
 U\tilde{T}_2^3(s)U^{-1} &= \tilde{T}_2^3(s) \cos \xi + i \tilde{T}_3^3(s) \frac{1}{\sqrt{2}} \sin \xi \\
 &\quad + i \tilde{T}_1^3(s) \frac{\sqrt{3}}{\sqrt{10}} \sin \xi - i \tilde{T}_1^1(s) \frac{3}{5\sqrt{2}} \sin \xi
 \end{aligned}$$

$$\begin{aligned}
 U\tilde{T}_2^3(a)U^{-1} &= \tilde{T}_2^3(a) \cos \xi + i \tilde{T}_3^3(a) \frac{1}{\sqrt{2}} \sin \xi \\
 &\quad + i \tilde{T}_1^3(a) \frac{\sqrt{3}}{\sqrt{10}} \sin \xi - i \tilde{T}_1^1(a) \frac{3}{5\sqrt{2}} \sin \xi
 \end{aligned}$$

$$\begin{aligned}
 U\tilde{T}_0^3U^{-1} &= \tilde{T}_0^3 \frac{1}{5} (1 + 4 \cos \xi) + \tilde{T}_0^1 \frac{6}{5\sqrt{10}} (\cos \xi - 1) \\
 &\quad + i \tilde{T}_1^3(s) \frac{2\sqrt{2}}{5} \sin \xi - i \tilde{T}_1^1(s) \frac{18}{5\sqrt{30}} \sin \xi
 \end{aligned}$$

$$\begin{aligned}
 U\tilde{T}_3^3(s)U^{-1} &= \tilde{T}_3^3(s) \frac{1}{2} (1 + \cos \xi) + \tilde{T}_1^3(s) \frac{3}{2\sqrt{15}} (\cos \xi - 1) \\
 &\quad - \tilde{T}_1^1(s) \frac{3}{10} (\cos \xi - 1) + i \tilde{T}_2^3(s) \frac{1}{\sqrt{2}} \sin \xi
 \end{aligned}$$

$$\begin{aligned}
 U\tilde{T}_3^3(a)U^{-1} &= \tilde{T}_3^3(a) \frac{1}{2} (1 + \cos \xi) + \tilde{T}_1^3(a) \frac{\sqrt{3}}{2\sqrt{5}} (\cos \xi - 1) \\
 &\quad - \tilde{T}_1^1(a) \frac{3}{10} (\cos \xi - 1) + i \tilde{T}_2^3(a) \frac{1}{\sqrt{2}} \sin \xi
 \end{aligned}$$

where $U = \exp (-i \tilde{\mathcal{H}}_1 t)$

$$\xi = \sqrt{3} \omega_1 t$$

$\tilde{T}_1^2(a)$, $\tilde{T}_2^2(s)$ and $\tilde{T}_2^2(a)$ all commute with the Hamiltonian

reduced density matrix in the interaction representation also, as

$$\tilde{\rho}(0) = T_0^2 \quad \dots (II.25)$$

Immediately following the application of an r.f. pulse of width 't_w' the density matrix of the spin system is given by (see Table II.3):

$$\tilde{\rho}(t_w) = T_0^2 \cos \xi + i \sin \xi T_1^2(s) \quad \dots (II.26)$$

$$\text{where } \xi = \sqrt{3} \omega_1 t_w \quad \dots (II.27)$$

Following the removal of the r.f. pulse the spin system evolves under the influence of $\frac{\Delta\omega}{\sqrt{6}} T_0^2$ and the density matrix is given by (refer to Table II.2):

$$\tilde{\rho}(t') = U_Q \tilde{\rho}(t_w) U_Q^{-1}$$

$$\text{where } U_Q = \exp(-i \frac{\Delta\omega}{\sqrt{6}} T_0^2)$$

$$\begin{aligned} \tilde{\rho}(t') = \cos \xi T_0^2 + i \sin \xi \left[-i T_1^1(a) \frac{3\sqrt{2}}{5} \sin(\Delta\omega t') \right. \\ \left. + T_1^2(s) \cos(\Delta\omega t') - i T_1^3(a) \cdot \frac{2\sqrt{2}}{\sqrt{15}} \sin(\Delta\omega t') \right] \end{aligned} \quad \dots (II.28)$$

$$\text{where } t' = t - t_w$$

The observed signal is proportional to the expectation value of the I_x operator, and it is given by

$$\langle I_x(t') \rangle \propto \text{Tr}[\tilde{\rho}(t') (T_1^1(a))^\dagger] \quad \dots \text{(II.29)}$$

Making use of Table II.2 and the orthogonality properties of tensor operators we have for the signal in the laboratory frame,

$$\begin{aligned} \langle I_x(t') \rangle &\propto \sin \varepsilon \left[\frac{3\sqrt{2}}{5} \sin(\Delta\omega t') \left[\frac{3}{2} \cos(\omega t') + \frac{2}{5} \right] \text{Tr}[(T_1^1(a))(T_1^1(a))^\dagger] \right. \\ &\quad + \frac{4\sqrt{2}}{15} \sin(\Delta\omega t') (\cos(\omega t') - 1) \text{Tr}[(T_1^3(a))(T_1^3(a))^\dagger] \\ &\quad \left. + \frac{1}{\sqrt{2}} \cos(\Delta\omega t') \sin(\omega t') \text{Tr}[(T_1^2(s))(T_1^2(s))^\dagger] \right] \\ &\quad \dots \text{(II.30)} \end{aligned}$$

which simplifies to give

$$\langle I_x(t') \rangle = \frac{\sqrt{3}}{4} \frac{\omega_Q}{kT} \sin \varepsilon [\sin(\Delta\omega + \omega)t'] \quad \dots \text{(II.31)}$$

Using Eqn. (II.28) and Table II.2 it can be easily shown that

$$\langle I_y \rangle = 0, \langle I_z \rangle = 0 \quad \dots \text{(II.32)}$$

These results are in agreement with those reported earlier in the literature [14-16].

Like in NMR, in NQR also one is generally interested in a phase-sensitive detected signal. This can be obtained by considering the expectation value of the magnetization operator in the interaction representation [3]. The magnetization operators (at the resonant frequency) in phase and 90° out of phase with

the applied r.f. pulses in the laboratory frame are given respectively by

$$M'_x = -\cos(\omega t) \tilde{T}_1^1(a) \text{ (in units of } \gamma \hbar) \quad \dots (II.33)$$

$$M_x = -\sin(\omega t) \tilde{T}_1^1(a) \text{ (in units of } \gamma \hbar) \quad \dots (II.34)$$

In the interaction representation these are given by

$$\begin{aligned} \tilde{M}'_x &= -\cos(\omega t) U \tilde{T}_1^1(a) U^{-1} \\ &\approx -\frac{1}{2} \left[\frac{3}{5} \tilde{T}_1^1(a) + \frac{2}{\sqrt{15}} \tilde{T}_1^3(a) \right] \quad \dots (II.35) \end{aligned}$$

$$\begin{aligned} \tilde{M}_x &= -\sin(\omega t) U \tilde{T}_1^1(a) U^{-1} \\ &\approx -i \frac{1}{2\sqrt{2}} \tilde{T}_1^2(s) \quad \dots (II.36) \end{aligned}$$

In obtaining Eqns. (II.35) and (II.36) we have made use of Table II.2 and dropped the high frequency terms.

Now using Eqns. II.28, II.35, II.36 and also making use of the orthogonality properties of the tensor operators, we have the expression for the in-phase signal as

$$\langle \tilde{M}'_x \rangle = \frac{\sqrt{3}\omega_Q}{4 kT} \frac{1}{2} \cdot \sin \xi [\sin(\Delta\omega t')] \quad \dots (II.37)$$

and the 90° out-of-phase signal as

$$\langle \tilde{M}_x \rangle = \frac{\sqrt{3}\omega_Q}{4 kT} \frac{1}{2} \cdot \sin \xi [\cos(\Delta\omega t')] \quad \dots (II.38)$$

where $t' = t - t_w$.

In all the subsequent calculations in this chapter we consider the expectation value of M_x only. Typical off-resonant FID's of ^{35}Cl obtained experimentally with our spectrometer from a single crystal of NaClO_3 are shown in Fig. II.3. The observed behaviour can be explained by Eqn. II.38. However, the decay of the signal is due to relaxation effects which are not included in the theoretical discussion.

II.B.2(ii) Two-pulse response:

Consider the response of an assemble of nuclear spins of $I = 3/2$ to the two-pulse sequence shown in Fig. II.2. Making use of Tables II.2 and II.3 it can be easily shown that the density matrix after the second r.f. pulse is given by

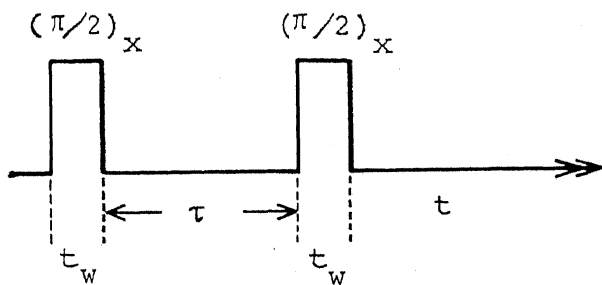


Fig.II.2. Two-Pulse Spin-Echo Sequence

$$\begin{aligned}
 \tilde{\rho}(t-\tau) = & \sin \epsilon \left[\sqrt{2} (T_1^1(a) \frac{3}{5} + \frac{2}{\sqrt{15}} T_1^3(a)) \{ \cos^2 \epsilon/2 \sin(\Delta \omega t) \right. \\
 & + \cos \epsilon \sin(\Delta \omega(t-\tau)) - \sin^2 \epsilon/2 \sin(\Delta \omega(t-\tau)) \} \\
 & + iT_1^2(s) \{ \cos^2 \epsilon/2 \cos(\Delta \omega t) + \cos \epsilon \cos(\Delta \omega(t-\tau)) \\
 & \left. - \sin^2 \epsilon/2 \cos(\Delta \omega(t-2\tau)) \} \right] \\
 & + T_0^2 (\cos^2 \epsilon - \sin^2 \epsilon \cos(\Delta \omega \tau)) \quad \dots \text{(II.39)}
 \end{aligned}$$

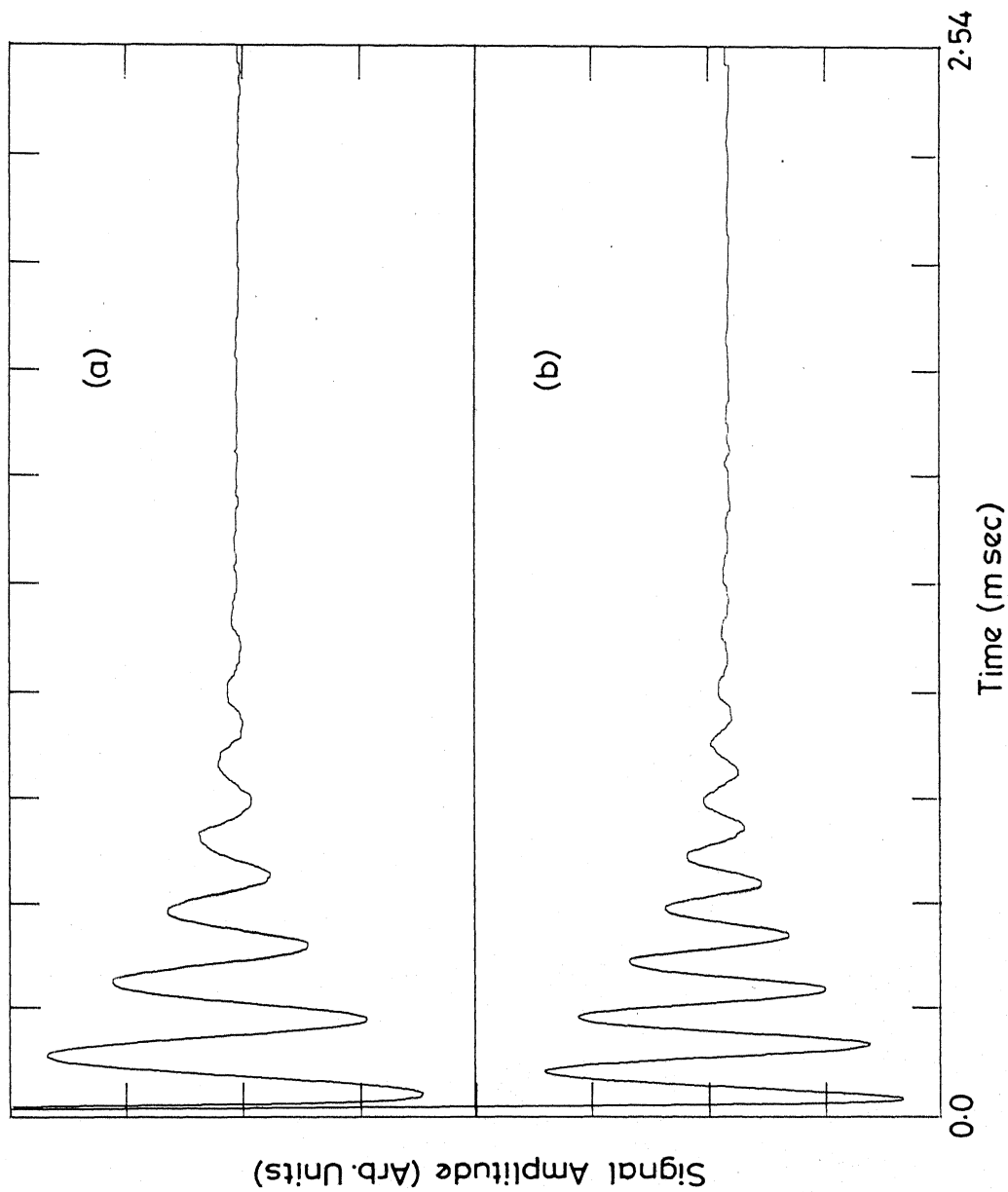


Fig.II.3 Off-resonant free induction signals of ^{35}Cl in a single crystal of NaClO_3 ($\nu = 29.9322$ MHz).

(a) with resonance off-set $\Delta\nu = -6$ KHz

(b) with resonance off-set $\Delta\nu = -8$ KHz

Now, the expectation value of \tilde{M}_x is given by

$$\begin{aligned} \langle \tilde{M}_x \rangle = \frac{\sqrt{3}}{4 kT} \frac{\omega_Q}{2} & [\sin \xi \cos^2 \xi / 2 \cos (\Delta \omega t) \\ & + \sin \xi \cos \xi \cos (\Delta \omega (t - \tau)) \\ & - \sin \xi \sin^2 \xi / 2 \cos (\Delta \omega (t - 2\tau))] \quad \dots (II.40) \end{aligned}$$

where $\tau \gg t_w$

$$t > (\tau + 2t_w)$$

In the above expression, the first term corresponds to the remnants of the FID due to the first pulse and the second term is due to the FID of the second pulse while the third term is responsible for the echo.

II.B.3 Spin I = 5/2

In the case of spin $I = 5/2$ nuclei, there are two possible transitions, one with the frequency ω_Q and other with a frequency $2\omega_Q$. First we consider the transition with ω_Q frequency:

II.B.3(i) Irradiation near ω_Q frequency:

The total Hamiltonian, in the interaction representation, for this case is given by

$$\tilde{\mathcal{H}} = \frac{\Delta \omega}{\sqrt{6}} T_0^2 + \tilde{\mathcal{H}}_1 \quad \dots (II.41)$$

where $\Delta\omega = \omega_Q - \omega$

$$\omega_Q = \frac{3}{20} e^2 q Q \quad \dots (II.42)$$

and $\tilde{\mathcal{H}}_1(t) = 2\omega_1 \cos(\omega t) U \tilde{T}_1^1(a) U^{-1}.$

The evolution of tensor operators under the influence of pure quadrupole Hamiltonian $\mathcal{H}_Q = \frac{\omega_Q}{\sqrt{6}} T_0^2$, is given in Table 12 of ref. [9]. Using Table 12 of [9], $\tilde{\mathcal{H}}_1$ can be written as

$$\begin{aligned} \tilde{\mathcal{H}}_1 = 2\omega_1 \cos(\omega t) & \left[\frac{1}{35} T_1^1(a) (9 + 16 \cos(\omega t) + 10 \cos(2\omega t)) \right. \\ & + i \frac{1}{14\sqrt{2}} T_1^2(s) (4 \sin(\omega t) + 5 \sin(2\omega t)) \\ & - \frac{1}{9\sqrt{15}} T_1^3(a) (3 + 2 \cos(\omega t) - 5 \cos(2\omega t)) \\ & - \frac{i}{6\sqrt{7}} T_1^4(s) (2 \sin(\omega t) - \sin(2\omega t)) \\ & \left. + \frac{1}{3\sqrt{210}} T_1^5(a) (3 - 4 \cos(\omega t) + \cos(2\omega t)) \right] \end{aligned} \quad \dots (II.43)$$

$$\tilde{\mathcal{H}}_1 \approx \omega_1 \left[-\frac{16}{35} T_1^1(a) + \frac{2}{9\sqrt{15}} T_1^3(a) + \frac{4}{3\sqrt{210}} T_1^5(a) \right] \quad \dots (II.44)$$

This equation is obtained after truncating the high frequency terms. A few selected commutation relations for spin $I = 5/2$ are set out in Table II.4. The evolution of a few selected tensor operators under the influence of the Hamiltonian $\tilde{\mathcal{H}}_1$ is given in Table II.5.

Single pulse response:

Now, the thermal equilibrium reduced density matrix in the interaction representation is given by

Table II.4. A Few Selected Commutation Relations for Spin
I = 5/2

$$[\tilde{T}_1^1(a), \tilde{T}_0^2] = -\sqrt{3} \tilde{T}_1^2(s)$$

$$[\tilde{T}_1^1(a), \tilde{T}_1^2(s)] = -\tilde{T}_2^2(s) - \sqrt{3} \tilde{T}_0^2$$

$$[\tilde{T}_1^1(a), \tilde{T}_2^2(s)] = -\tilde{T}_1^2(s)$$

$$[\tilde{T}_1^1(a), \tilde{T}_1^3(a)] = -\sqrt{\frac{5}{2}} \tilde{T}_2^3(a)$$

$$[\tilde{T}_1^1(a), \tilde{T}_2^3(a)] = -\sqrt{\frac{3}{2}} \tilde{T}_3^3(a) - \sqrt{\frac{5}{2}} \tilde{T}_1^3(a)$$

$$[\tilde{T}_1^1(a), \tilde{T}_3^3(a)] = -\sqrt{\frac{3}{2}} \tilde{T}_2^3(a)$$

$$[\tilde{T}_1^1(a), \tilde{T}_0^4] = -\sqrt{10} \tilde{T}_1^4(s)$$

$$[\tilde{T}_1^1(a), \tilde{T}_1^4(s)] = -\frac{3}{\sqrt{2}} \tilde{T}_2^4(s) - \sqrt{10} \tilde{T}_0^4$$

$$[\tilde{T}_1^1(a), \tilde{T}_2^4(s)] = -\sqrt{\frac{7}{2}} \tilde{T}_3^4(s) - \frac{3}{\sqrt{2}} \tilde{T}_1^4(s)$$

$$[\tilde{T}_1^1(a), \tilde{T}_1^5(a)] = -\sqrt{7} \tilde{T}_2^5(a)$$

$$[\tilde{T}_1^1(a), \tilde{T}_2^5(a)] = -2\sqrt{\frac{3}{2}} \tilde{T}_3^5(a) - \sqrt{7} \tilde{T}_1^5(a)$$

$$[\tilde{T}_1^1(a), \tilde{T}_3^5(a)] = -\frac{3}{\sqrt{2}} \tilde{T}_4^5(a) - \sqrt{6} \tilde{T}_2^5(a)$$

$$[\tilde{T}_1^3(a), \tilde{T}_0^2] = -\frac{81}{7\sqrt{5}} \tilde{T}_1^2(s) - 3\sqrt{\frac{5}{14}} \tilde{T}_1^4(s)$$

$$[\tilde{T}_1^3(a), \tilde{T}_1^2(s)] = \frac{81}{70} \sqrt{15} \tilde{T}_2^2(s) - \frac{81}{35} \sqrt{5} \tilde{T}_0^2 - 5\sqrt{\frac{3}{7}} \tilde{T}_0^4 + \frac{15}{2\sqrt{105}} \tilde{T}_2^4(s)$$

$$[\tilde{T}_1^3(a), \tilde{T}_2^2(s)] = \frac{\sqrt{30}}{2} \tilde{T}_3^4(s) + \frac{81}{70} \sqrt{15} \tilde{T}_1^2(s) - \sqrt{\frac{30}{7}} \tilde{T}_1^4(s)$$

...contd.

Table II.4 (contd.)

$$[\tilde{T}_1^3(a), \tilde{T}_2^3(a)] = \frac{17}{\sqrt{10}} \tilde{T}_3^3(a) + \frac{3}{\sqrt{2}} \tilde{T}_3^5(a) + \frac{324}{7\sqrt{10}} \tilde{T}_1^1(a) - \frac{27}{2\sqrt{21}} \tilde{T}_1^5(a)$$

$$[\tilde{T}_1^3(a), \tilde{T}_3^3(a)] = \frac{9}{\sqrt{6}} \tilde{T}_4^5(a) + \frac{17}{\sqrt{10}} \tilde{T}_2^3(a) - \frac{3}{\sqrt{2}} \tilde{T}_2^5(a)$$

$$[\tilde{T}_1^3(a), \tilde{T}_0^4] = -\frac{225}{7} \sqrt{\frac{3}{7}} \tilde{T}_1^2(s) - \frac{9}{7} \sqrt{\frac{3}{2}} \tilde{T}_1^4(s)$$

$$[\tilde{T}_1^3(a), \tilde{T}_1^4(s)] = -\frac{90}{7} \sqrt{\frac{15}{14}} \tilde{T}_2^2(s) - \frac{18}{7\sqrt{30}} \tilde{T}_2^4(s) - \frac{135}{7} \sqrt{\frac{5}{14}} \tilde{T}_0^2 - \frac{9}{7} \sqrt{\frac{3}{2}} \tilde{T}_0^4$$

$$[\tilde{T}_1^3(a), \tilde{T}_2^4(s)] = \frac{9}{7} \sqrt{\frac{7}{30}} \tilde{T}_3^4(s) + \frac{45}{14} \sqrt{\frac{15}{7}} \tilde{T}_1^2(s) - \frac{18}{7} \sqrt{\frac{1}{30}} \tilde{T}_1^4(s)$$

$$[\tilde{T}_1^3(a), \tilde{T}_1^5(a)] = -\frac{75}{2\sqrt{21}} \tilde{T}_2^3(a) + \frac{9}{2} \sqrt{\frac{7}{15}} \tilde{T}_2^5(a)$$

$$[\tilde{T}_1^3(a), \tilde{T}_2^5(a)] = -\frac{25}{3\sqrt{2}} \tilde{T}_3^3(a) - \frac{1}{\sqrt{10}} \tilde{T}_3^5(a) + \frac{9}{2} \sqrt{\frac{7}{15}} \tilde{T}_1^5(a)$$

$$[\tilde{T}_1^3(a), \tilde{T}_3^5(a)] = -\frac{24}{\sqrt{30}} \tilde{T}_4^5(a) + \frac{24}{3\sqrt{2}} \tilde{T}_2^3(a) - \frac{1}{\sqrt{10}} \tilde{T}_2^5(a)$$

$$[\tilde{T}_1^5(a), \tilde{T}_0^2] = -\sqrt{5} \tilde{T}_1^4(s)$$

$$[\tilde{T}_1^5(a), \tilde{T}_1^2(s)] = 4\sqrt{\frac{5}{6}} \tilde{T}_2^4(s) - 5\sqrt{\frac{2}{3}} \tilde{T}_0^4$$

$$[\tilde{T}_1^5(a), \tilde{T}_2^2(s)] = -\frac{5}{2} \sqrt{\frac{7}{15}} \tilde{T}_3^4(s) + \frac{5}{2} \sqrt{\frac{5}{3}} \tilde{T}_1^4(s)$$

$$[\tilde{T}_1^5(a), \tilde{T}_2^3(a)] = -\frac{25}{42} \sqrt{35} \tilde{T}_3^3(a) - 2\sqrt{7} \tilde{T}_3^5(a) + \frac{75}{14} \sqrt{\frac{7}{3}} \tilde{T}_1^3(a)$$

$$[\tilde{T}_1^5(a), \tilde{T}_3^3(a)] = 3\sqrt{\frac{7}{3}} \tilde{T}_4^5(a) - \frac{25}{42} \sqrt{35} \tilde{T}_2^3(a) - \frac{5}{2} \sqrt{7} \tilde{T}_2^5(a)$$

$$[\tilde{T}_1^5(a), \tilde{T}_0^4] = -\frac{75}{7} \sqrt{6} \tilde{T}_1^2(s) + 15 \sqrt{\frac{3}{7}} \tilde{T}_1^4(s)$$

$$[\tilde{T}_1^5(a), \tilde{T}_1^4(s)] = \frac{75}{7} \frac{\sqrt{15}}{2} \tilde{T}_2^2(s) - \frac{15}{2} \sqrt{\frac{5}{21}} \tilde{T}_2^4(s) - \tilde{T}_0^2 \frac{45}{7} \sqrt{5} + \tilde{T}_0^4 15 \sqrt{\frac{3}{7}}$$

...contd.

Table II.4 (contd.)

$$[\tilde{T}_1^5(a), \tilde{T}_2^4(s)] = -\frac{15}{2} \sqrt{\frac{5}{3}} \tilde{T}_3^4(s) + \frac{60}{7} \sqrt{\frac{15}{2}} \tilde{T}_1^2(s) - \tilde{T}_1^4(s) \frac{15}{2} \sqrt{\frac{5}{21}}$$

$$[\tilde{T}_1^5(a), \tilde{T}_2^5(a)] = -\frac{125}{18} \sqrt{7} \tilde{T}_3^3(a) + \frac{10}{3} \sqrt{\frac{5}{7}} \tilde{T}_3^5(a) + \frac{180}{\sqrt{7}} \tilde{T}_1^1(a) \\ - \frac{25}{2} \sqrt{\frac{7}{15}} \tilde{T}_1^3(a)$$

$$[\tilde{T}_1^5(a), \tilde{T}_3^5(a)] = 5 \sqrt{\frac{5}{21}} \tilde{T}_4^5(a) - \frac{50}{9} \sqrt{7} \tilde{T}_2^3(a) + \frac{10}{3} \sqrt{\frac{5}{7}} \tilde{T}_2^5(a)$$

Table II.5. The Evolution of a few Selected Tensor Operators
Under the Influence of the Hamiltonian $\tilde{\mathcal{H}}_1$

$$U \tilde{T}_0^2 U^{-1} = \frac{1}{28} \tilde{T}_0^2 (25 + 3 \cos(\xi)) + \tilde{T}_0^4 \frac{5}{4\sqrt{105}} (\cos(\xi) - 1) \\ + i \sin(\xi) \left(\frac{3}{7\sqrt{2}} \tilde{T}_2^2(s) - \frac{1}{2\sqrt{21}} \tilde{T}_1^4(s) \right)$$

$$U \tilde{T}_1^2(s) U^{-1} = \tilde{T}_1^2(s) \frac{1}{7} (2 \cos(\xi) + 5 \cos(\xi/2)) \\ - \tilde{T}_1^4(s) \frac{2}{3\sqrt{14}} (\cos(\xi) - \cos(\xi/2)) \\ + i \sin(\xi) \left(\frac{\sqrt{3}}{7\sqrt{2}} \tilde{T}_0^2 - \frac{5}{3\sqrt{70}} \tilde{T}_0^4 \right) \\ + i \sin(\xi/2) \left(\frac{5}{7\sqrt{2}} \tilde{T}_2^2(s) + \frac{1}{\sqrt{14}} \tilde{T}_2^4(s) \right)$$

$$U \tilde{T}_0^4 U^{-1} = \tilde{T}_0^4 \frac{1}{28} (3 + 25 \cos(\xi)) - \tilde{T}_0^2 \frac{15}{28} \frac{\sqrt{15}}{\sqrt{7}} (\cos(\xi) - 1) \\ + i \sin(\xi) \left(-\frac{75}{7\sqrt{70}} \tilde{T}_1^2(s) + \frac{5\sqrt{5}}{14} \tilde{T}_1^4(s) \right)$$

$$U \tilde{T}_1^4(s) U^{-1} = -\tilde{T}_1^2(s) \frac{30}{7\sqrt{14}} (\cos(\xi) - \cos(\xi/2)) + \tilde{T}_1^4(s) \frac{1}{7} (5 \cos(\xi) \\ + 2 \cos(\xi/2)) + i \sin(\xi) \left(-\frac{15\sqrt{3}}{14\sqrt{7}} \tilde{T}_0^2 + \frac{25}{14\sqrt{5}} \tilde{T}_0^4 \right) \\ + i \sin(\xi/2) \left(\frac{15}{7\sqrt{7}} \tilde{T}_2^2(s) + \frac{3}{7} \tilde{T}_2^4(s) \right)$$

$$\tilde{\mathcal{H}}_1 = \omega_1 \left(\frac{16}{35} \tilde{T}_1^1(a) - \frac{2}{9\sqrt{15}} \tilde{T}_1^3(a) - \frac{4}{3\sqrt{210}} \tilde{T}_1^5(a) \right)$$

$$U = \exp(-i \tilde{\mathcal{H}}_1 t_w), \quad \xi = \sqrt{8} \omega_1 t_w$$

$$\tilde{\rho}(0) = T_0^2$$

Immediately following the application of an r.f. pulse of width 't_w', the density matrix is given by (see Table II.5):

$$\begin{aligned} \tilde{\rho}(t_w) = & \frac{1}{28} T_0^2 (25 + 3 \cos \xi) + \frac{5}{4\sqrt{105}} (\cos \xi - 1) T_0^4 \\ & - i \frac{2\sqrt{3}}{7\sqrt{8}} T_1^2(s) \sin \xi + i \frac{1}{2\sqrt{21}} T_1^4(s) \sin \xi \quad \dots \text{(II.45)} \end{aligned}$$

$$\text{where } \xi = \sqrt{8} \omega_1 t_w$$

Following the removal of the pulse the spin system evolves under the influence of $\frac{\Delta\omega}{\sqrt{6}} T_0^2$ and the density matrix is given by

$$\begin{aligned} \tilde{\rho}(t') = & \frac{1}{28} [25 + 3 \cos \xi] T_0^2 + \frac{5}{4\sqrt{105}} (\cos \xi - 1) T_0^4 \\ & + T_1^1(a) \left[-\sin \xi \frac{8\sqrt{3}}{35} \sin(\Delta\omega t') \right] \\ & + T_1^3(a) \left[\sin \xi \frac{1}{6\sqrt{5}} \sin(\Delta\omega t') \right] \\ & + T_1^5(a) \left[\sin \xi \frac{\sqrt{2}}{7\sqrt{35}} \sin(\Delta\omega t') \right] \\ & + T_1^2(s) \left[-i \sin \xi \left(\frac{\sqrt{6}}{14} \cos(\Delta\omega t') \right) \right] \\ & + T_1^4(s) \left[i \sin \xi \left(\frac{1}{2\sqrt{21}} \cos(\Delta\omega t') \right) \right] \quad \dots \text{(II.46)} \end{aligned}$$

The magnetization operator (in units of $\gamma \hbar$) (90° out of phase with the applied r.f. pulse) in the interaction representation,

for this case, is given by

$$\tilde{M}_x = -\sin(\omega t) U T_1^1(a) U^{-1} \approx \frac{i}{2} \left[-\frac{1}{7\sqrt{2}} T_1^2(s) + \frac{1}{6\sqrt{7}} T_1^4(s) \right] \quad \dots (II.47)$$

Making use of the orthogonality relationship of tensor operator, from Eqns. II.46 and II.47 we have for the expectation value of the magnetization operator \tilde{M}_x

$$\langle \tilde{M}_x \rangle = \frac{\omega_Q}{6 kT} \frac{\sqrt{8}}{2} \sin \epsilon \cos(\Delta \omega t') \quad \dots (II.48)$$

where $t' = t - t_w$

II.B.3(ii) Irradiation near $2 \omega_Q$ frequency:

The r.f. Hamiltonian for this case is given by

$$\mathcal{H}_1(t) = 2\omega_1 \cos(2\omega t) T_1^1(a) \quad \dots (II.49)$$

In the interaction representation it is given by

$$\begin{aligned} \tilde{\mathcal{H}}_1(t) = 2\omega_1 \cos(2\omega t) & \left[\frac{1}{35} T_1^1(a) \{9 + 16 \cos(\omega t) + 10 \cos(2\omega t)\} \right. \\ & + \frac{i}{14\sqrt{2}} T_1^2(s) \{4 \sin(\omega t) + 5 \sin(2\omega t)\} \\ & - \frac{1}{9\sqrt{15}} T_1^3(a) \{3 + 2 \cos(\omega t) - 5 \cos(2\omega t)\} \\ & - \frac{i}{6\sqrt{7}} T_1^4(s) \{2 \sin(\omega t) - \sin(2\omega t)\} \\ & \left. + \frac{1}{3\sqrt{210}} T_1^5(a) \{3 - 4 \cos(\omega t) + \cos(2\omega t)\} \right] \quad \dots (II.50) \end{aligned}$$

After dropping the high frequency terms we have

$$\tilde{\mathcal{H}}_1 \approx \omega_1 \left[-\frac{2}{7} \mathcal{T}_1^1(a) - \frac{5}{9\sqrt{15}} \mathcal{T}_1^3(a) - \frac{1}{3\sqrt{210}} \mathcal{T}_1^5(a) \right] \quad \text{.. (II.51)}$$

The evolution of a few selected tensor operators under the influence of $\tilde{\mathcal{H}}_1$ is given in Table II.6.

II.B.3(ii)a Single pulse response:

The thermal equilibrium reduced density matrix in the interaction representation is given by

$$\tilde{\rho}(0) = \mathcal{T}_0^2 \quad \text{.. (II.52)}$$

Immediately following the application of an r.f. pulse of duration ' t_w ' the density matrix is given by (see Table II.6):

$$\begin{aligned} \tilde{\rho}(t_w) = & \frac{1}{7} \mathcal{T}_0^2 (4+3 \cos \xi) + \frac{2}{\sqrt{105}} \mathcal{T}_0^4 (\cos \xi - 1) \\ & - i \frac{\sqrt{15}}{7} \mathcal{T}_1^2(s) \sin \xi - i \frac{2}{\sqrt{210}} \mathcal{T}_1^4(s) \sin \xi \quad \text{.. (II.53)} \end{aligned}$$

$$\text{where } \xi = \sqrt{5} \omega_1 t_w$$

Following the removal of the pulse, the spin system evolves under $\frac{\Delta\omega}{\sqrt{6}} \mathcal{T}_0^2$ (see Table 12 of ref. [9]) and the density matrix is given by

Table II.6. The Evolution of a few Selected Tensor Operators
Under the Influence of the Hamiltonian $\tilde{\mathcal{H}}_1$

$$\begin{aligned} U T_1^1(a) U^{-1} &= T_1^1(a) \frac{1}{35} (19 + 16 \cos(\xi/2)) \\ &\quad - T_1^3(a) \frac{2}{9\sqrt{15}} (\cos(\xi/2) - 1) \\ &\quad - T_1^5(a) \frac{4}{3\sqrt{210}} (\cos(\xi/2) - 1) \\ &\quad - i \sin(\xi/2) \left(\frac{2\sqrt{5}}{9\sqrt{6}} T_2^3(a) + \frac{2}{15\sqrt{6}} T_2^5(a) \right) \end{aligned}$$

$$\begin{aligned} U T_1^3(a) U^{-1} &= T_1^1(a) \frac{72}{35\sqrt{15}} (1 - \cos(\xi/2)) + \\ &\quad + T_1^3(a) \frac{1}{15} (14 + \cos(\xi/2)) \\ &\quad + T_1^5(a) \frac{2}{5\sqrt{14}} (\cos(\xi/2) - 1) \\ &\quad + i \sin(\xi/2) \left(T_2^3(a) \frac{1}{3\sqrt{2}} + \frac{1}{5\sqrt{10}} T_2^5(a) \right) \end{aligned}$$

$$\begin{aligned} U T_1^5(a) U^{-1} &= - T_1^1(a) \frac{240}{7\sqrt{210}} (\cos(\xi/2) - 1) \\ &\quad + T_1^3(a) \frac{10}{9\sqrt{14}} (\cos(\xi/2) - 1) \\ &\quad + T_1^5(a) \frac{1}{21} (11 + 10 \cos(\xi/2)) \\ &\quad + i \sin(\xi/2) \left(\frac{25}{9\sqrt{7}} T_2^3(a) + \frac{5}{3\sqrt{35}} T_2^5(a) \right) \end{aligned}$$

$$\begin{aligned} U T_0^2 U^{-1} &= \frac{1}{7} T_0^2 (4 + 3 \cos(\xi)) + \frac{2}{\sqrt{105}} T_0^4 (\cos(\xi) - 1) \\ &\quad + i \sin(\xi) \left(\frac{\sqrt{15}}{7} T_1^2(s) + \frac{2}{\sqrt{210}} T_1^4(s) \right) \end{aligned}$$

$$\begin{aligned} U T_1^2(s) U^{-1} &= T_1^2(s) \frac{1}{7} (2 \cos(\xi/2) + 5 \cos(\xi)) + \\ &\quad + T_1^4(s) \frac{2}{3\sqrt{14}} (\cos(\xi) - \cos(\xi/2)) \\ &\quad + i \sin(\xi) \left(\frac{\sqrt{15}}{7} T_0^2 + \frac{2}{3\sqrt{7}} T_0^4 \right) \\ &\quad - i \sin(\xi/2) \left(\frac{\sqrt{5}}{7} T_2^2(s) + \frac{1}{\sqrt{35}} T_2^4(s) \right) \end{aligned}$$

...contd

Table II.6 (contd.)

$$U T_0^4 U^{-1} = T_0^2 \frac{90}{7\sqrt{105}} (\cos(\xi) - 1) + T_0^4 \frac{1}{7} (3 + 4 \cos(\xi)) \\ + i \sin(\xi) \left(\frac{30}{7\sqrt{7}} T_1^2(s) + \frac{2\sqrt{2}}{7} T_1^4(s) \right)$$

$$U T_1^4(s) U^{-1} = T_1^2(s) \frac{90}{21\sqrt{14}} (\cos(\xi) - \cos(\xi/2)) \\ + T_1^4(s) \frac{1}{7} (5 \cos(\xi/2) + 2 \cos(\xi)) \\ + i \sin(\xi) \left(\frac{180}{7\sqrt{210}} T_0^2 + \frac{4\sqrt{2}}{7} T_0^4 \right) \\ + i \sin(\xi/2) \left(\frac{75}{7\sqrt{70}} T_2^2(s) + \frac{15}{7\sqrt{10}} T_2^4(s) \right)$$

$$U T_2^2(s) U^{-1} = T_2^2(s) \cos(\xi/2) \\ + i \sin(\xi/2) \left(-\frac{\sqrt{5}}{7} T_1^2(s) + \frac{\sqrt{5}}{3\sqrt{14}} T_1^4(s) - \frac{1}{\sqrt{10}} T_3^4(s) \right)$$

$$U T_2^3(a) U^{-1} = T_2^3(a) \cos(\xi/2) \\ + i \sin(\xi/2) \left(-\frac{72}{7\sqrt{30}} T_1^1(a) + \frac{1}{3\sqrt{2}} T_1^3(a) - \frac{\sqrt{5}}{3\sqrt{6}} T_3^3(a) \right. \\ \left. + \frac{1}{\sqrt{7}} T_1^5(a) - \frac{2}{5\sqrt{6}} T_3^5(a) \right)$$

$$U T_2^4(s) U^{-1} = T_2^4(s) \cos(\xi/2) \\ + i \sin(\xi/2) \left(-\frac{45}{7\sqrt{35}} T_1^2(s) + \frac{15}{7\sqrt{10}} T_1^4(s) + \frac{\sqrt{5}}{\sqrt{14}} T_3^4(s) \right)$$

$$U T_2^5(a) U^{-1} = T_2^5(a) \cos(\xi/2) \\ + i \sin(\xi/2) \left(-\frac{24}{7\sqrt{6}} T_1^1(a) + \frac{\sqrt{5}}{9\sqrt{2}} T_1^3(a) + \frac{\sqrt{5}}{3\sqrt{7}} T_1^5(a) \right. \\ \left. + \frac{25}{9\sqrt{6}} T_3^3(a) + \frac{2\sqrt{5}}{3\sqrt{6}} T_3^5(a) \right)$$

$$\tilde{\mathcal{H}}_1 = \omega_1 \left(\frac{2}{7} T_1^1(a) + \frac{5}{9\sqrt{15}} T_1^3(a) + \frac{1}{3\sqrt{210}} T_1^5(a) \right)$$

$$U = \exp(-i \tilde{\mathcal{H}}_1 t_w)$$

$$\xi = \sqrt{5} \omega_1 t_w$$

$$\begin{aligned}
\tilde{\rho}(t') = & [\sin\xi \sin(2\Delta\omega t') \{ -\frac{4\sqrt{30}}{35} T_1^1(a) - \frac{2\sqrt{2}}{9} T_1^3(a) \\
& - \frac{2}{15\sqrt{7}} T_1^5(a) \} \\
& + i \sin\xi \cos(2\Delta\omega t') \{ -\frac{\sqrt{15}}{7} T_1^2(s) - \frac{\sqrt{30}}{15\sqrt{7}} T_1^4(s) \}] \\
& \dots \text{ (II.54)}
\end{aligned}$$

where $t' = t - t_w$.

The laboratory frame magnetization operator for this case is given by

$$M_x = -\sin(2\omega t) T_1^1(a) \text{ (in units of } \gamma\hbar \text{)}$$

In the interaction representation it is given by

$$\begin{aligned}
\tilde{M}_x &= -\sin(2\omega t) \tilde{T}_1^1(a) \\
&\approx -\frac{i}{2} [T_1^2(s) \frac{5}{28\sqrt{2}} + \frac{1}{12\sqrt{7}} T_1^4(s)] \dots \text{ (II.55)}
\end{aligned}$$

The signal in the interaction representation is given by the expectation value of the magnetization operator \tilde{M}_x

$$\langle \tilde{M}_x \rangle = \text{Tr} [\tilde{\rho}(t') \cdot \tilde{M}_x]$$

Making use of the orthogonality property of the tensor operators we have

$$\langle \tilde{M}_x \rangle = \frac{2\omega_0}{6 kT} \frac{\sqrt{5}}{2} \sin\xi \cos(2\Delta\omega t') \dots \text{ (II.56)}$$

II.B.3(ii)b Two-pulse response:

We consider here the response of nuclear spins with spin $I = 5/2$ to the two-pulse sequence shown in the Fig. II.2. Making use of Tables II.6 and II.12 of [9] and proceeding as in the single pulse case we obtain for the signal following the second pulse as

$$\begin{aligned} \langle \tilde{M}_x \rangle = \frac{2\omega_Q}{6 kT} \frac{\sqrt{5}}{2} & [\sin \xi \cos^2 \xi/2 \cos(2\Delta\omega t) \\ & + \sin \xi \cos \xi \cos(2\Delta\omega(t-\tau)) \\ & - \sin \xi \sin^2 \xi/2 \cos(2\Delta\omega(t-2\tau))] \quad \dots (II.57) \end{aligned}$$

where $\xi = \sqrt{5} \omega_1 t_w$

$\tau \gg t_w$

$t > (\tau + 2 t_w)$

In Eqn. II.57 the first term corresponds to the remnants of the FID due to the first pulse and the second term is due to the FID of the second pulse while the third term is responsible for the echo. These results are in agreement with those available in the literature [14].

II.C PULSE RESPONSES IN THE PRESENCE OF A WEAK ZEEMAN FIELD FOR NUCLEI WITH SPIN $I = 3/2$ IN AXIALLY SYMMETRIC FIELD GRADIENTS

II.C.1 Transitions for a Nuclear Spin $I = 3/2$ in the Presence of a Weak Zeeman Field

If we apply a constant magnetic field H_0 in a direction with polar coordinates θ, ϕ in the 'efg' principal axes system then the Hamiltonian corresponding to the interaction of Zeeman field with nuclear spin system is given by

$$\mathcal{H}_Z = -\gamma H_0 (\tilde{I}_X \cos\theta \sin\phi + \tilde{I}_Y \sin\theta \sin\phi + \tilde{I}_Z \cos\theta) \quad \dots (II.58)$$

The presence of the magnetic field (for $\omega_0 \ll e^2 q Q$) removes the degeneracy between states $m = \pm 3/2$ and first order perturbation theory gives [15]

$$E_{\pm m} = A [3 m^2 - I(I+1)] \pm m \omega_0 \cos\theta \quad \dots (II.59)$$

corresponding to the states Ψ_{+m} and Ψ_{-m} , respectively, with

$$A = \frac{e^2 q Q}{4I(2I-1)} \quad \dots (II.60)$$

The states with $m = \pm 1/2$ have non-zero off-diagonal elements

$\langle 1/2 | \mathcal{H}_m | -1/2 \rangle$ for \mathcal{H}_m . Hence, diagonalization of \mathcal{H}_m sub-matrix for $m = \pm 1/2$ leads to the zero order mixing of the states $\Psi_{+1/2}$ and $\Psi_{-1/2}$ and yields two new states

$$\Psi_+ = \Psi_{+1/2} \sin \alpha + \Psi_{-1/2} \cos \alpha$$

$$\Psi_- = \Psi_{-1/2} \sin \alpha - \Psi_{+1/2} \cos \alpha \quad \dots (II.61)$$

where $\tan \alpha = \left[\frac{(f+1)}{(f-1)} \right]^{1/2}$

$$f = [1 + 4 \tan^2 \theta]^{1/2} \quad \dots (II.62)$$

The energies of these states E_{\pm} are given by

$$E_{\pm} = A [3/4 - I(I+1)] \mp f/2 \omega_0 \cos \theta \quad \dots (II.63)$$

where $\omega_0 = \gamma H_0$.. (II.64)

Now, four transitions with $\Delta m = \pm 1$ are possible between the mixed states Ψ_{\pm} and with states $\Psi_{\pm 3/2}$ with the frequencies:

$$\omega_{\alpha} = 6A - \frac{3-f}{2} \omega_0 \cos \theta$$

$$\omega_{\beta} = 6A - \frac{3+f}{2} \omega_0 \cos \theta$$

$$\omega_{\alpha'} = 6A + \frac{3-f}{2} \omega_0 \cos \theta$$

$$\omega_{\beta'} = 6A + \frac{3+f}{2} \omega_0 \cos \theta \quad \dots (II.65)$$

Thus, the original line is split into a symmetrical quadruplet, the outer pair of lines is referred to as the α doublet and the inner pair as the β doublet. It should be noted from Eqns.

II.63 and II.65 that the Zeeman pattern is independent of azimuthal angle θ . The energy level diagram for the above situation

is given in the Fig. II.4.

II.C.2 Evaluation of Pulse Responses

In this section, we assume in our analysis that a weak Zeeman field is applied in a general (θ, ϕ) direction in the principal axis system, and that the r.f. field is applied parallel to the principal x-axis. Since, for the case of axially symmetric field gradients ($\eta=0$) the Zeeman pattern is independent of ϕ (see Eqns. II.63 and II.65) we may set the azimuthal angle ϕ equal to zero without loss of generality.

Now, the Zeeman Hamiltonian, in the laboratory frame, corresponding to this situation is given by

$$\mathcal{H}_Z = - \omega_0 [\tilde{I}_x \sin\theta + \tilde{I}_z \cos\theta] \quad \dots (II.66)$$

where $\omega_0 = \gamma H_0$, H_0 being the strength of the magnetic field. In the interaction representation it is given by

$$\begin{aligned} \tilde{\mathcal{H}}_Z &= U \mathcal{H}_Z U^{-1} \\ &\approx \omega_0 \left[\sin\theta \left\{ \frac{2}{5} T_1^1(a) - \frac{2}{\sqrt{15}} T_1^3(a) \right\} - \cos\theta T_0^1 \right] \quad \dots (II.67) \end{aligned}$$

In arriving at Eqn. II.67 we have made use of Table II.2 and truncated the high frequency terms.

In the presence of weak magnetic field we consider the response of nuclear spin system to resonant r.f. pulses (i.e.,

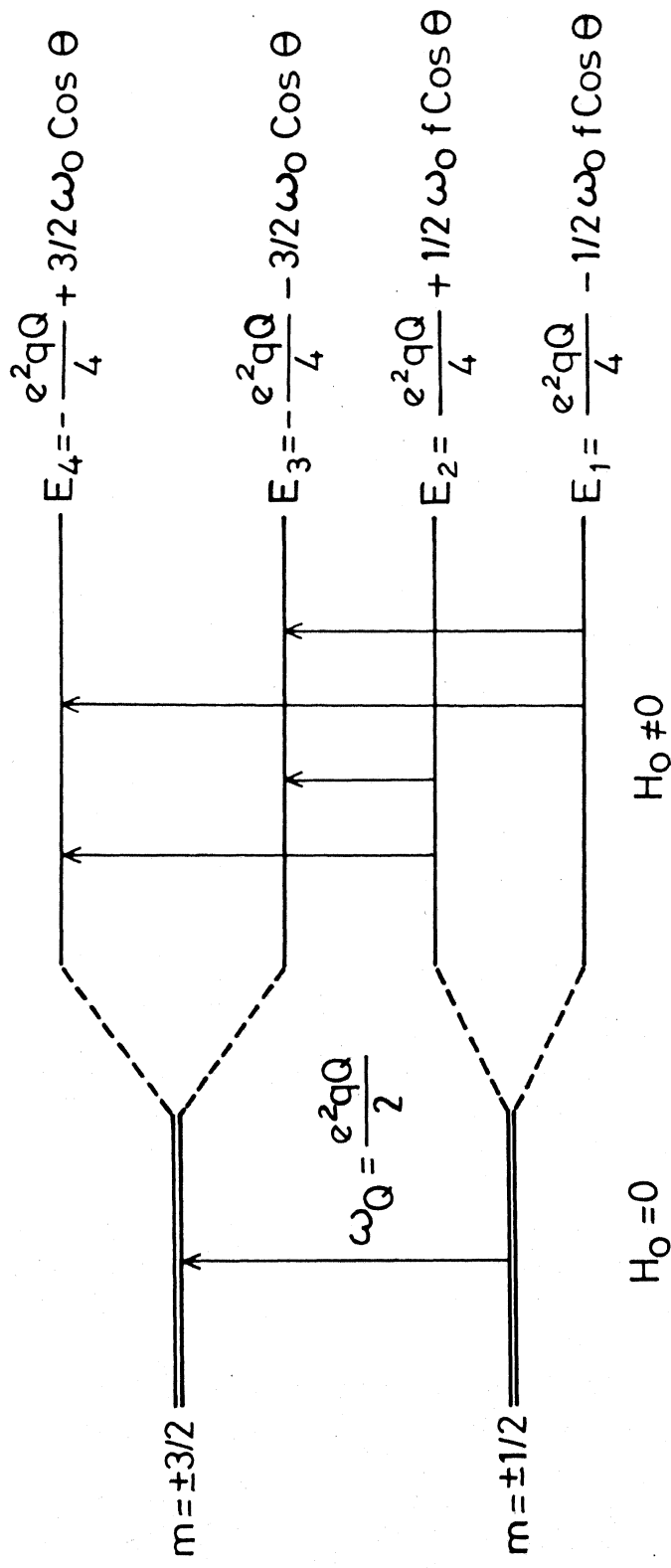


Fig.II.4 Energy level diagram for nuclear spin $I = 3/2$ in the presence of a weak Zeeman Field H_0 .

$\Delta\omega = 0$). So in the interaction representation the total Hamiltonian for this case can be written as,

$$\tilde{\mathcal{H}} = \tilde{\mathcal{H}}_1 + \tilde{\mathcal{H}}_z \quad \dots \text{ (II.68)}$$

The evolution of a few selected tensor operators under the influence of the Zeeman Hamiltonian is set out in Table II.7. Table II.8 gives the commutation relationships of the Hamiltonian with the tensor operators. In all the calculations, we neglect the effect of the Zeeman field in the time interval ($0 \leq t \leq t_w$) during which the pulse is on, assuming that the magnetic field causes negligible precession of the spin system during application of r.f. pulse.

II.C.2(i) Single pulse response:

The thermal equilibrium reduced density matrix, in the laboratory frame for this case is given by (see I.D.1),

$$\rho(0) = T_0^2 + \frac{\omega_0}{(\omega_Q/\sqrt{6})} [T_1^1(a) \sin\theta - T_0^1 \cos\theta] \quad \dots \text{ (II.69)}$$

However, if the magnetic field satisfies the condition $\omega_0 \ll \omega_Q$, then, to a good approximation, the initial density matrix can be taken as:

$$\rho(0) = T_0^2$$

Table II.7. The Evolution of a few Selected Tensor Operators
Under the Influence of the Hamiltonian $\tilde{\mathcal{H}}_Z$ for $I = 3/2$

$$\begin{aligned}
 U_Z T_1^2(s) U_Z^{-1} &= T_1^2(s) \left[\left(\frac{f-1}{2f} \right) \cos A + \left(\frac{f+1}{2f} \right) \cos B \right] \\
 &+ i T_1^2(a) \left[\left(\frac{f-1}{2f} \right) \sin A + \left(\frac{f+1}{2f} \right) \sin B \right] \\
 &+ T_2^2(a) \frac{(f^2-1)^{1/2}}{2f} [\cos A - \cos B] \\
 &+ i T_2^2(s) \left[\frac{(f^2-1)^{1/2}}{2f} (\sin A - \sin B) \right]
 \end{aligned}$$

$$\begin{aligned}
 U_Z T_1^2(a) U_Z^{-1} &= T_1^2(a) \left[\left(\frac{f-1}{2f} \right) \cos A + \left(\frac{f+1}{2f} \right) \cos B \right] \\
 &+ i T_1^2(s) \left[\left(\frac{f-1}{2f} \right) \sin A + \left(\frac{f+1}{2f} \right) \sin B \right] \\
 &+ T_2^2(s) \left[\frac{(f^2-1)^{1/2}}{2f} (\cos A - \cos B) \right] \\
 &+ i T_2^2(a) \frac{(f^2-1)^{1/2}}{2f} (\sin A - \sin B)
 \end{aligned}$$

$$\begin{aligned}
 U_Z T_2^2(a) U_Z^{-1} &= T_1^2(s) \frac{(f^2-1)^{1/2}}{2f} [\cos A - \cos B] \\
 &+ i T_1^2(a) \frac{(f^2-1)^{1/2}}{2f} (\sin A - \sin B) \\
 &+ T_2^2(a) \left[\left(\frac{f+1}{2f} \right) \cos A + \left(\frac{f-1}{2f} \right) \cos B \right] \\
 &+ i T_2^2(s) \left[\left(\frac{f+1}{2f} \right) \sin A + \left(\frac{f-1}{2f} \right) \sin B \right]
 \end{aligned}$$

...contd.

Table II.7 (contd.)

$$\begin{aligned}
U_Z T_2^2(s) U_Z^{-1} &= T_1^2(a) \frac{(f^2-1)^{1/2}}{2f} [\cos A - \cos B] \\
&+ i T_1^2(s) \frac{(f^2-1)^{1/2}}{2f} (\sin A - \sin B) \\
&+ T_2^2(s) \left[\left(\frac{f+1}{2f} \right) \cos A + \left(\frac{f-1}{2f} \right) \cos B \right] \\
&+ i T_2^2(a) \left[\left(\frac{f+1}{2f} \right) \sin A + \left(\frac{f-1}{2f} \right) \sin B \right]
\end{aligned}$$

$$U_Z T_0^2 U_Z^{-1} = T_0^2$$

where

$$U_Z = \exp(-i \tilde{\mathcal{H}}_Z t)$$

$$\tilde{\mathcal{H}}_Z = \omega_0 \left[\sin \theta \left\{ \frac{2}{5} T_1^1(a) - T_1^3(a) \frac{2}{\sqrt{15}} \right\} - \cos \theta T_0^1 \right]$$

$$f = [1 + 4 \tan^2 \theta]^{1/2}, \quad A = \left(\frac{3+f}{2} \right) \cos \theta \omega_0 t$$

$$B = \left(\frac{3-f}{2} \right) \cos \theta \omega_0 t, \quad \omega_0 = \gamma H_0$$

Table II.8. Commutation Relationships of Irreducible Tensor

Operators $T_q^n(s, a)$ for $I = 3/2$, with the Hamiltonian

$$\tilde{\mathcal{H}}_Z = \omega_0 \left[\beta \left\{ \frac{2}{5} T_1^1(a) - T_1^3(a) \frac{2}{\sqrt{15}} \right\} - \alpha T_0^1 \right] = \omega_0 F$$

$$[F, T_0^1] = \beta \left[-\frac{2}{5} T_1^1(s) + \frac{2}{\sqrt{15}} T_1^3(s) \right]$$

$$[F, T_1^1(s)] = -\alpha T_1^1(a) + \beta \left[-\frac{2}{5} T_0^1 - \sqrt{\frac{2}{3}} T_2^3(s) + \frac{2\sqrt{2}}{\sqrt{5}} T_0^3 \right]$$

$$[F, T_1^1(a)] = -\alpha T_1^1(s) - \sqrt{\frac{2}{3}} \beta T_2^3(a)$$

$$[F, T_1^3(s)] = -\alpha T_1^3(a) + \beta \left[-\sqrt{\frac{2}{5}} T_2^3(s) + \frac{9}{5\sqrt{15}} T_0^1 - \frac{3\sqrt{6}}{5} T_0^3 \right]$$

$$[F, T_1^3(a)] = -\alpha T_1^3(s) - \beta \sqrt{\frac{2}{5}} T_2^3(a)$$

$$[F, T_2^3(s)] = -2\alpha T_2^3(a) - \sqrt{\frac{2}{5}} \beta T_1^3(s) - \frac{9}{5\sqrt{6}} \beta T_1^1(s)$$

$$[F, T_2^3(a)] = -2\alpha T_2^3(s) - \sqrt{\frac{2}{5}} \beta T_1^3(a) - \frac{9}{5\sqrt{6}} \beta T_1^1(a)$$

$$[F, T_3^3(s)] = -3\alpha T_3^3(a)$$

$$[F, T_3^3(a)] = -3\alpha T_3^3(s)$$

$$[F, T_0^3] = \beta \left[-\frac{3\sqrt{6}}{5} T_1^3(s) + \frac{9}{5} \sqrt{\frac{2}{5}} T_1^1(s) \right]$$

$$[F, T_1^2(s)] = -\alpha T_1^2(a) - \beta T_2^2(s)$$

$$[F, T_1^2(a)] = -\alpha T_1^2(s) - \beta T_2^2(a)$$

$$[F, T_2^2(s)] = -2\alpha T_2^2(a) - \beta T_1^2(s)$$

$$[F, T_2^2(a)] = -2\alpha T_2^2(s) - \beta T_1^2(a) ; \quad [F, T_0^2] = 0$$

where $\omega_0 = \gamma H_0$, $\alpha = \cos\theta$, $\beta = \sin\theta$

$$F = \beta \left\{ \frac{2}{5} T_1^1(a) - \frac{2}{\sqrt{15}} T_1^3(a) \right\} - \alpha T_0^1$$

Immediately following the application of an r.f. pulse of width 't_w' the density matrix is given by the Eqn. II.26. Since we are considering the pulse response, on resonance ($\Delta\omega = 0$), the density matrix following the removal of the pulse evolves under the influence of the Zeeman Hamiltonian $\tilde{\mathcal{H}}_Z$, and it is given by (see Table II.7):

$$\begin{aligned}\tilde{\rho}(t') = & T_0^2 \cos\xi + i \sin\xi [T_1^2(s) \{(\frac{f-1}{2f}) \cos A + (\frac{f+1}{2f}) \cos B\} \\ & + i T_1^2(a) \{(\frac{f-1}{2f}) \sin A + (\frac{f+1}{2f}) \sin B\} \\ & + T_2^2(a) \{ \frac{(f^2-1)^{1/2}}{2f} (\cos A - \cos B) \} \\ & + i T_2^2(s) \{ \frac{(f^2-1)^{1/2}}{2f} (\sin A - \sin B) \}] \\ & \dots \text{.. (II.70)}\end{aligned}$$

$$\text{where } A = 3+f/2 \cos\theta \omega_0 t'$$

$$B = 3-f/2 \cos\theta \omega_0 t' \quad \dots \text{.. (II.71)}$$

Now the signal in the interaction representation is given by

$$\begin{aligned}\langle \tilde{M}_x \rangle & \propto \text{Tr}[\tilde{\rho} \cdot \tilde{M}_x] \\ & = \frac{\sqrt{3} \omega_Q}{4 kT} \frac{1}{2} \sin\xi [(\frac{f-1}{2f}) \cos A + (\frac{f+1}{2f}) \cos B] \quad \dots \text{.. (II.72)}\end{aligned}$$

Similarly, in the laboratory frame the operator corresponding to the Y-component of the magnetization (in quadrature with the applied r.f. pulses) is given by

$$M_Y = \sin(\omega t) I_Y = i \sin(\omega t) T_1^1(s) \text{ (in units of } \gamma \hbar) \quad \dots \text{.. (II.73)}$$

In the interaction representation it is given by

$$\tilde{M}_Y = \frac{1}{2\sqrt{2}} T_1^2(a) \quad \dots (II.74)$$

$$\langle \tilde{M}_Y \rangle = \frac{\sqrt{3} \omega_Q}{4 kT} \frac{1}{2} \sin \epsilon \left[\left(\frac{f-1}{2f} \right) \sin A + \left(\frac{f+1}{2f} \right) \sin B \right] \quad \dots (II.75)$$

These results agree with those presented earlier in the literature [15,16]. Also, it can be easily shown that

$$\langle \tilde{M}_Z \rangle = 0$$

These results indicate that in the presence of a weak Zeeman field, a crossed-coil experiment is possible in NQR. Now, the FID signal is modulated with the frequencies which correspond to the splitting of the steady-state pure quadrupole line due to the magnetic field. For example, at a particular orientation of magnetic field i.e., with $\theta = 54^\circ 44'$, the steady-state splittings of the $\alpha\alpha'$ lines coalesce into a single pair at the original pure quadrupole frequency [14]. For this orientation of the magnetic field we have

$$f = (1 + 4 \tan^2 \theta)^{1/2} = 3$$

From the Eqn. II.72, for this orientation of magnetic field it can be seen that the FID gets modulated by only one frequency corresponding to $\beta\beta'$ and is given by

$$3 \omega_Q \cos(54^\circ 44')$$

The experimental results of the modulation of ^{35}Cl FID signal in the single crystal of NaClO_3 when the Zeeman field orientation corresponds to $\theta = 54^\circ 44'$ are shown in Fig. II.5. From this figure it is clear that the FID is being modulated by only one frequency, which is equal to $3 \omega_0 \cos(54^\circ 44')$.

II.C.2(ii) Two pulse response:

Again considering the two-pulse sequence given in Fig. II.2, the density matrix after the second pulse can be written as

$$\tilde{\rho}(t-\tau) = U_Z(t-\tau) U_R(t_w) U_Z(\tau) U_R(t_w) \tilde{\rho}(0) U_R^{-1}(t_w) U_Z^{-1}(\tau) U_R^{-1}(t_w) U_Z^{-1}(t-\tau)$$

$$\text{where } U_R(t) = \exp(-i \tilde{\mathcal{H}}_1 t_w) \quad \dots (\text{II.76})$$

$$\dots (\text{II.77})$$

$$U_Z(\tau) = \exp(-i \tilde{\mathcal{H}}_Z \tau) \quad \dots (\text{II.78})$$

$\tilde{\mathcal{H}}_1$ and $\tilde{\mathcal{H}}_Z$ are given respectively by Eqns. II.24 and II.67.

Now, making use of Tables II.3 and II.7 we obtain, after some trigonometric manipulations, for the expectation value of the magnetization operator

$$\langle \tilde{M}_x \rangle = \frac{\sqrt{3}}{4} \frac{\omega_0}{kT} \frac{1}{2} \left[\sin \xi \cos^2 \xi / 2 \left\{ \left(\frac{f-1}{2f} \right) \cos \left(\frac{3+f}{2} \cos \theta \omega_0 t \right) + \left(\frac{f+1}{2f} \right) \cos \left(\frac{3-f}{2} \cos \theta \omega_0 t \right) \right\} \right] \dots (i)$$

....contd..

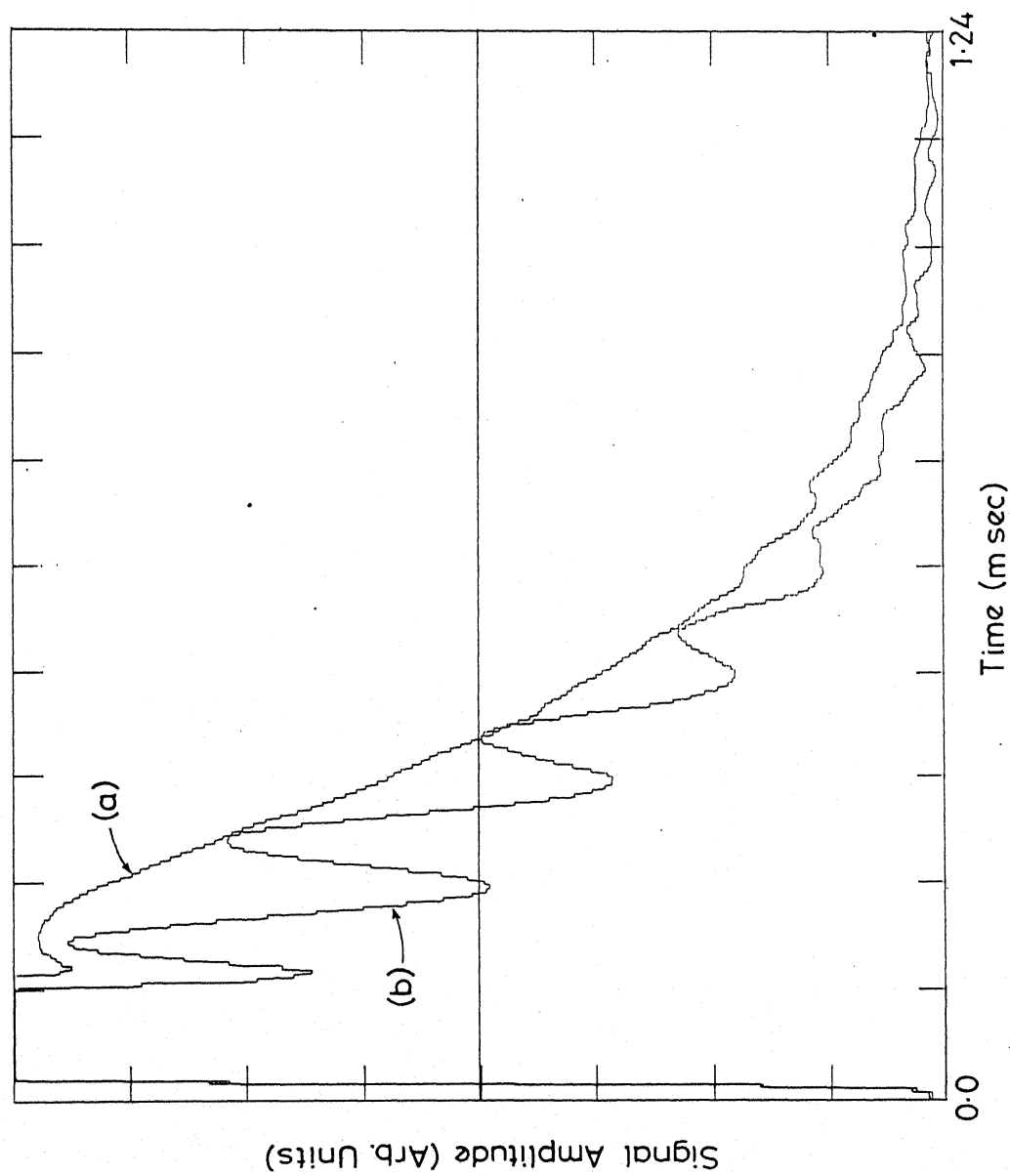


Fig.II.5 On-resonant free induction signal of ^{35}Cl in a single crystal of NaClO_3 ($\nu = 29.9322 \text{ MHz}$).

(a) In the absence of a Zeeman Field

(b) In the presence of a Zeeman Field. $H_0 \approx 15.9 \text{ Gauss}$.

$$\begin{aligned}
& + \sin \xi \cos \xi \left\{ \left(\frac{f-1}{2f} \right) \cos \left(\frac{3+f}{2} \cos \theta \omega_0 (t-\tau) \right) \right. \\
& \quad \left. + \left(\frac{f+1}{2f} \right) \cos \xi \left(\frac{3-f}{2} \cos \theta \omega_0 (t-\tau) \right) \right\} \dots (ii)
\end{aligned}$$

$$\begin{aligned}
& - \sin \xi \sin^2 \xi / 2 \left\{ \left(\frac{f-1}{2f} \right)^2 \cos \left(\frac{3+f}{2} \cos \theta \omega_0 (t-2\tau) \right) \right. \\
& \quad \left. + \left(\frac{f+1}{2f} \right)^2 \cos \left(\frac{3-f}{2} \cos \theta \omega_0 (t-2\tau) \right) \right\} \dots (iii)
\end{aligned}$$

$$\begin{aligned}
& - \sin \xi \sin^2 \xi / 2 \left[\left(\frac{f^2-1}{2f^2} \right) \left\{ \cos \left(\frac{3}{2} \cos \theta \omega_0 (t-2\tau) \right) \right. \right. \\
& \quad \cos \left(\frac{f}{2} \cos \theta \omega_0 t \right) \\
& \quad + \cos \left(\frac{f}{2} \cos \theta \omega_0 (t-2\tau) \right) \cos \left(\frac{3}{2} \cos \theta \omega_0 t \right) \\
& \quad \left. \left. - \cos \left(\frac{3}{2} \cos \theta \omega_0 t \right) \cos \left(\frac{f}{2} \cos \theta \omega_0 t \right) \right\} \right] \dots (iv) \\
& \dots (II.79)
\end{aligned}$$

Our results are in agreement with those reported earlier in the literature [15,16]. The first term corresponds to the remnants of FID due to the first pulse, the second term gives the FID due to the second pulse while the third term contributes to the echo at 2τ and the fourth term is responsible for the echo envelope modulation as a function of τ .

Experimental recording of two-pulse response, in the presence of a weak Zeeman field, obtained from ^{35}Cl in single crystal of NaClO_3 is shown in Fig. II.6.

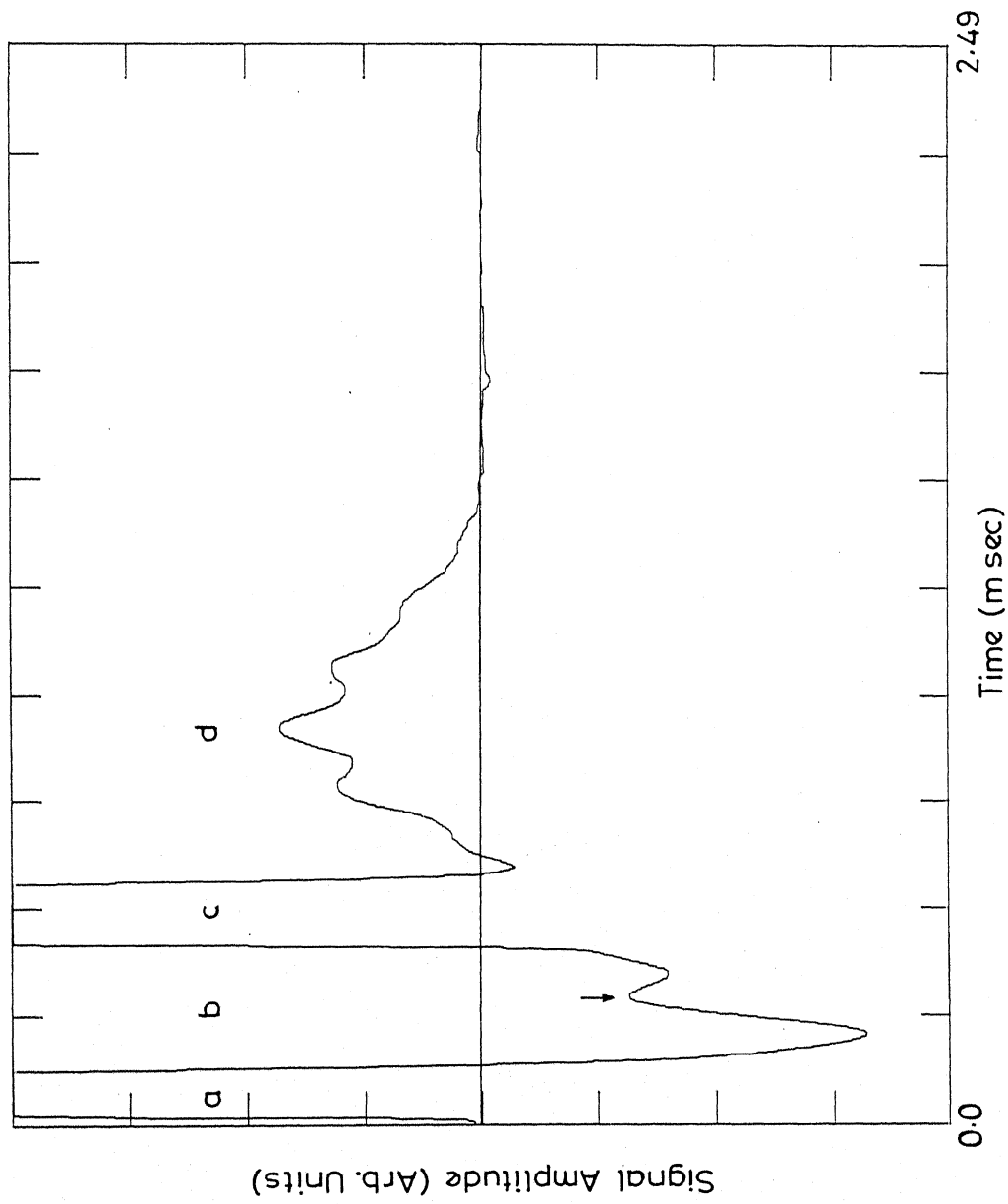


Fig.II-6 Free induction and spin-echo signals of ^{35}Cl in a single crystal of NaClO_3 ($\nu = 29.9322 \text{ MHz}$) in the presence of a Zeeman field ($H_0 \approx 13 \text{ Gauss}$) applied along the crystalline $(1,0,0)$ direction. (a) first pulse, (b) FID due to first pulse, (c) second pulse applied at $t = \tau$, (d) spin-echo at $t = 2\tau$.

II.D PULSE RESPONSES IN THE ABSENCE OF A ZEEMAN FIELD FOR THE CASE OF NON-AXIALLY SYMMETRIC FIELD GRADIENTS

This section deals with the calculation of single- and two-pulse responses of nuclear spins $I = 1$ and $3/2$ with non-axial field gradients. We first consider the $I = 1$ case.

II.D.1 Spin $I = 1$

Since the asymmetry parameter (η) mixes the basis functions whose m_I values differ by ± 2 , the eigen functions of \mathcal{H}_Q are linear combinations of these basis functions [15]. The eigenfunctions, energy levels and the transition frequencies for spin $I = 1$, nucleus with non-axial field gradients are given in Fig. II.7. Now, as there are three transitions possible we discuss the observation of signals corresponding to each of these transitions separately.

The evolution of tensor operators under the quadrupolar Hamiltonian $\mathcal{H}_Q = \frac{\sqrt{2}}{\sqrt{3}} \omega_Q [T_{20}^2 + \eta/\sqrt{3} T_{22}^2(s)]$ are given in Table II.9. In the interaction representation defined by the transformation operator

$$U = \exp \left(+ i \frac{\sqrt{2}\omega}{\sqrt{3}} (T_{20}^2 + \eta/\sqrt{3} T_{22}^2(s)) \right) \quad \dots (II.80)$$

the total Hamiltonian is given by

$$\tilde{\mathcal{H}} = \frac{\sqrt{2}\Delta\omega}{\sqrt{3}} (T_{20}^2 + \eta/\sqrt{3} T_{22}^2(s)) + \tilde{\mathcal{H}}_1 \quad \dots (II.81)$$

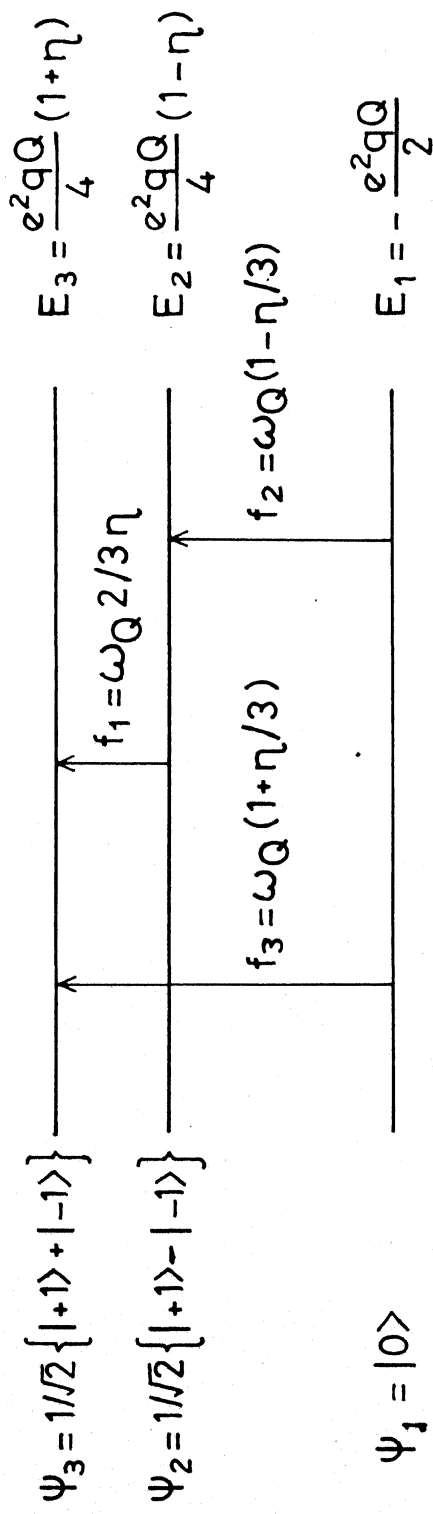


Fig.II.7 Eigenvalues, Eigenfunctions and transition frequencies for nuclear spin $I=1$, in nonaxial field gradients $\omega_Q = 3/4 e^2 q Q$.

Table II.9. The Evolution of Irreducible Tensor Operators Under the Influence of Quadrupolar Hamiltonian

$$\mathcal{H}_Q = \frac{\sqrt{2}}{\sqrt{3}} \omega_Q [\mathcal{T}_0^2 + \eta/\sqrt{3} \mathcal{T}_2^2(s)] \text{ for spin } I = 1^*$$

$$U \mathcal{T}_0^1 U^{-1} = \mathcal{T}_0^1 \cos(f_1 t) + i \mathcal{T}_2^2(a) \sqrt{2} \sin(f_1 t)$$

$$U \mathcal{T}_1^1(s) U^{-1} = \mathcal{T}_1^1(s) \cos(f_2 t) - i \mathcal{T}_1^2(a) \sqrt{2} \sin(f_2 t)$$

$$U \mathcal{T}_1^1(a) U^{-1} = \mathcal{T}_1^1(a) \cos(f_3 t) - i \mathcal{T}_1^2(s) \sqrt{2} \sin(f_3 t)$$

$$U \mathcal{T}_1^2(s) U^{-1} = \mathcal{T}_1^2(s) \cos(f_3 t) - i \mathcal{T}_1^1(a) \frac{1}{\sqrt{2}} \sin(f_3 t)$$

$$U \mathcal{T}_1^2(a) U^{-1} = \mathcal{T}_1^2(a) \cos(f_2 t) - i \mathcal{T}_1^1(s) \frac{1}{\sqrt{2}} \sin(f_2 t)$$

$$U \mathcal{T}_2^2(a) U^{-1} = \mathcal{T}_2^2(a) \cos(f_1 t) + i \mathcal{T}_0^1 \frac{1}{\sqrt{2}} \sin(f_1 t)$$

where $U = \exp(-i \mathcal{H}_Q t)$

\mathcal{T}_0^2 and $\mathcal{T}_2^2(s)$ commute with the Hamiltonian

$$f_1 = \frac{2}{3} \eta \omega_Q, \quad f_2 = \omega_Q (1 - \eta/3), \quad f_3 = \omega_Q (1 + \eta/3)$$

$$\omega_Q = \frac{3}{4} e^2 q Q$$

*These results can also be obtained from Table 1 of ref. [10] by setting $\hbar = 1$, & $\omega_0 = 0$.

where $\Delta\omega = \omega_Q - \omega$;

$$\omega_Q = \frac{3}{4} e^2 q Q \quad \dots (II.82)$$

II.D.1(i) Irradiation near f_3 frequency:

The r.f. Hamiltonian for this case can be written as

$$\tilde{\mathcal{H}}_1 = 2\omega_1 \cos(f_3 t) U T_1^1(a) U^{-1} \quad \dots (II.83)$$

Using Table II.9 and dropping the high frequency terms we get

$$\tilde{\mathcal{H}}_1 \approx \omega_1 T_1^1(a) \quad \dots (II.84)$$

The evolution of tensor operators under $\tilde{\mathcal{H}}_1 = \omega_1 T_1^1(a)$ can be obtained from Table 3 of ref. [8].

II.D.1(i)a Single-pulse response:

The thermal equilibrium reduced density matrix is given by

$$\tilde{\rho}(0) = (T_0^2 + \eta/\sqrt{3} T_2^2(s)) \quad \dots (II.85)$$

Immediately following the application of an r.f. pulse of width ' t_w ' the density matrix is given by

$$\begin{aligned}
\tilde{\rho}(t_w) = & \tilde{T}_0^2 \left[\frac{1}{4} (1-\eta) + \frac{3}{4} (1 + \eta/3) \cos \xi \right] \\
& - i \tilde{T}_1^2(s) \sin \xi \frac{\sqrt{3}}{2} (1 + \eta/3) \\
& + \tilde{T}_2^2(s) \left[-\frac{\sqrt{3}}{4} (1-\eta) + \frac{\sqrt{3}}{4} (1 + \eta/3) \cos \xi \right] \\
& \dots \text{.. (II.86)}
\end{aligned}$$

where $\xi = 2\omega_1 t_w$

Following the removal of the r.f. pulse the spin system evolves under the influence of $\frac{\sqrt{2}\Delta\omega}{\sqrt{3}} (\tilde{T}_0^2 + \eta/\sqrt{3} \tilde{T}_2^2(s))$ and the density matrix is given by

$$\begin{aligned}
\tilde{\rho}(t') = & \tilde{T}_0^2 \left(\frac{1}{4} (1-\eta) + \frac{3}{4} (1 + \eta/3) \cos \xi \right) \\
& + \tilde{T}_2^2(s) \left[-\frac{\sqrt{3}}{4} (1-\eta) + \frac{\sqrt{3}}{4} (1 + \eta/3) \cos \xi \right] \\
& + \tilde{T}_1^2(s) \left[-i \frac{\sqrt{3}}{2} (1 + \eta/3) \sin \xi \cos (\Delta f_3 t') \right] \\
& + \tilde{T}_1^1(a) \left[-\frac{\sqrt{3}}{2\sqrt{2}} (1 + \eta/3) \sin \xi \sin (\Delta f_3 t') \right] \\
& \dots \text{.. (II.87)}
\end{aligned}$$

with $t' = t - t_w$

The magnetization operator for this case is given by

$$\begin{aligned}
M_x &= -\sin(f_3 t) \tilde{T}_1^1(a) \text{ (in units of } \gamma \hbar) \\
\tilde{M}_x &= -\sin(f_3 t) U \tilde{T}_1^1(a) U^{-1} \\
&\approx -i \frac{1}{\sqrt{2}} \tilde{T}_1^2(s) \\
&\dots \text{.. (II.88)}
\end{aligned}$$

Now, the expectation value of the magnetization operator is given by

$$\begin{aligned}
\langle \tilde{M}_x \rangle & \propto \text{Tr} [\tilde{\rho} \cdot \tilde{M}_x] \\
& = \frac{2}{3} \frac{\omega_Q (1 + \eta/3)}{kT} \sin \xi \cos (\Delta f_3 t') \quad \dots \text{(II.89)}
\end{aligned}$$

Also, making use of the orthogonality property of the tensor operators, from Eqn. II.87 it can be easily shown that

$$\begin{aligned}
\langle \tilde{M}_y \rangle & = -\frac{i}{\sqrt{2}} \langle \tilde{T}_1^2(a) \rangle = 0 \\
\langle \tilde{M}_z \rangle & = \frac{i}{\sqrt{2}} \langle \tilde{T}_2^2(a) \rangle = 0 \quad \dots \text{(II.90)}
\end{aligned}$$

II.D.1(i)b Two-pulse response:

Let us consider the effect of two pulse sequence shown in Fig. II.2 on the nuclear spin $I = 1$ system. The density matrix after the second pulse can be written as

$$\begin{aligned}
\tilde{\rho}(t-\tau) & = U_Q(t-\tau) U_R(t_w) U_Q(\tau) U_R(t_w) \tilde{\rho}(0) U_R^{-1}(t_w) U_Q^{-1}(\tau) \\
& \quad U_R^{-1}(t_w) U_Q^{-1}(t-\tau) \quad \dots \text{(II.91)}
\end{aligned}$$

$$\text{where } U_R(t_w) = \exp(-i \tilde{\mathcal{H}}_1 t_w)$$

$$U_Q(\tau) = \exp\left(-i \frac{\sqrt{2}}{\sqrt{3}} \Delta \omega \mathcal{H}'_Q\right) \quad \dots \text{(II.92)}$$

$\tilde{\mathcal{H}}_1$ is given in Eqn. II.84.

Making use of Table II.9 of this thesis and Table 3 of ref. [8] we obtain for the expectation value of the magnetization operator,

$$\begin{aligned}
\langle \tilde{M}_x \rangle = & \frac{2}{3} \frac{\omega_Q (1 + \eta/3)}{kT} \frac{1}{2} [\sin \varepsilon \cos^2 \varepsilon/2 \cos(\Delta f_3 t) \\
& + \sin \varepsilon \cos \varepsilon \cos(\Delta f_3 (t - \tau)) \\
& - \sin \varepsilon \sin^2 \varepsilon/2 \cos(\Delta f_3 (t - 2\tau))] \\
& \dots (II.93)
\end{aligned}$$

where $\tau \gg t_w$

$$t > (\tau + 2t_w) \text{ and } \varepsilon = 2\omega_1 t_w$$

II.D.1(ii) Irradiation near f_2 frequency:

If we wish to observe the signal corresponds to frequency f_2 we need to apply the r.f. pulse with this frequency about the Y-axis of the crystal. The r.f. Hamiltonian for this case is given by

$$\begin{aligned}
\tilde{\mathcal{H}}_1 &= -i 2\omega_1 \cos(f_2 t) \tilde{T}_1^1(s) \\
&\approx -i\omega_1 \tilde{T}_1^1(s) \dots (II.94)
\end{aligned}$$

The evolution of tensor operators under the influence of the Hamiltonian $\tilde{\mathcal{H}}_1 = -i\omega_1 \tilde{T}_1^1(s)$ can be obtained from Table 4 of ref. [8]. Making use of the Table II.8 of this thesis and Table 4 of ref. [8] the expectation values of the magnetization operators in the case of single and two pulses can be written as,

II.D.1(ii)a Single-pulse response:

$$\langle \tilde{M}_y \rangle = \frac{2}{3} \frac{\omega_Q}{kT} \frac{(1 - \eta/3)}{2} \sin \varepsilon \cos(\Delta f_2 t') \dots (II.95)$$

where $t' = t - t_w$; and $\langle \tilde{M}_x \rangle = \langle \tilde{M}_z \rangle = 0$.

II.D.1(ii)b Two-pulse response:

$$\begin{aligned}
\langle \tilde{M}_Y \rangle &= \frac{2}{3} \frac{\omega_Q}{kT} \frac{(1-\eta/3)}{2} \left[\sin \xi \cos^2 \xi/2 \cos(\Delta f_2 t) \right. \\
&\quad \left. + \sin \xi \cos \xi \cos(\Delta f_2 (t-\tau)) \right. \\
&\quad \left. - \sin \xi \sin^2 \xi/2 \cos(\Delta f_2 (t-2\tau)) \right] \\
&\quad \dots \text{(II.96)}
\end{aligned}$$

$$\langle \tilde{M}_X \rangle = \langle \tilde{M}_Z \rangle = 0$$

where $\tau \gg t_w$

$$t > (\tau + 2t_w)$$

II.D.1(iii) Irradiation near f_1 frequency:

In order to detect the signal corresponding to frequency f_1 we need to apply the r.f. pulse with this frequency about the Z-axis of the crystal.

The r.f. Hamiltonian corresponding to this situation is

$$\mathcal{H}_1 = -2\omega_1 \cos(f_1 t) \tilde{T}_O^1 \quad \dots \text{(II.97)}$$

In the interaction representation it is given by

$$\tilde{\mathcal{H}}_1 = -2\omega_1 \cos(f_1 t) \tilde{T}_O^1 \approx -\omega_1 \tilde{T}_O^1 \quad \dots \text{(II.98)}$$

The evolution of tensor operators under the influence of $\tilde{\mathcal{H}}_1$ can be written as (see ref. [8]),

$$\exp(-i \tilde{\mathcal{H}}_1 t_w) T_Q^n(s) \exp(i \tilde{\mathcal{H}}_1 t_w)$$

$$= T_Q^n(s) \cos(q \cdot \omega_1 t_w) + i T_Q^n(a) \sin(q \cdot \omega_1 t_w) \quad \dots (II.99)$$

$T_Q^n(s)$'s will also have a similar form. Using these relationships and Table II.9 the expectation value of the magnetization operator after single and two-pulses (see Fig. II.1) can be obtained.

II.D.1(iii)a Single-pulse response:

$$\langle \tilde{M}_z \rangle = \frac{2}{3} \frac{\omega_Q}{kT} \left(\frac{2}{3} \eta \right) \frac{1}{2} \sin \xi \cos(\Delta f_1 t') \quad \dots (II.100)$$

$$\text{Also } \langle \tilde{M}_x \rangle = \langle \tilde{M}_y \rangle = 0 ; t' = t - t_w.$$

II.D.1(iii)b Two-pulse response:

$$\begin{aligned} \langle \tilde{M}_z \rangle = \frac{2}{3} \frac{\omega_Q}{kT} \left(\frac{2}{3} \eta \right) \frac{1}{2} [& \sin \xi \cos^2 \xi / 2 \cos(\Delta f_1 t) \\ & + \sin \xi \cos \xi \cos(\Delta f_1 (t - \tau)) \\ & - \sin \xi \sin^2 \xi / 2 \cos(\Delta f_1 (t - 2\tau))] \quad \dots (II.101) \end{aligned}$$

$$\langle \tilde{M}_x \rangle = \langle \tilde{M}_y \rangle = 0$$

where $\tau \gg t_w ; t > (\tau + 2t_w) .$

II.D.2 Spin I = 3/2

In spin $I = 3/2$ case the asymmetry of the efg, does not remove the degeneracies of the energy levels. The basis $|m_I\rangle$ functions are no longer eigen functions. The asymmetric component of the efg mixes the $|-3/2\rangle$ with the $|+1/2\rangle$ function and the $|-1/2\rangle$ with the $|+3/2\rangle$ function [15]. Due to the Kramer's

degeneracy even with the asymmetric efg's only one transition is possible. The transition frequency between the two degenerate levels, is now given by [15]:

$$\omega_Q = \omega_Q (1 + \eta^2/3)^{1/2} \quad \dots (II.102)$$

$$\text{where } \omega_Q = \frac{e^2 q Q}{2}$$

The evolution of tensor operators under the Hamiltonian

$\mathcal{H}_Q = \frac{\omega_Q}{\sqrt{6}} (\mathcal{T}_0^2 + \eta/\sqrt{3} \mathcal{T}_2^2(s))$ is given in Table II.10. The r.f. Hamiltonian in this case is

$$\mathcal{H}_1 = 2\omega_1 \cos(\omega'_Q t) \mathcal{T}_1^1(a) \quad \dots (II.103)$$

$$\text{where } \omega'_Q = \omega (1 + \eta^2/3)^{1/2}$$

In the quadrupolar interaction representation, the total Hamiltonian for this case is given by

$$\tilde{\mathcal{H}} = \frac{\Delta\omega}{\sqrt{6}} [\mathcal{T}_0^2 + \eta/\sqrt{3} \mathcal{T}_2^2(s)] + \tilde{\mathcal{H}}_1 \quad \dots (II.104)$$

where

$$\begin{aligned} \tilde{\mathcal{H}}_1 &= 2\omega_1 \cos(\omega'_Q t) U \mathcal{T}_1^1(a) U^{-1} \\ &\approx \omega_1 \left[\frac{1}{3\rho^2} \left\{ \frac{(3+\eta)^2}{5} \mathcal{T}_1^1(a) + \frac{(2-\eta)(3+\eta)}{\sqrt{15}} \mathcal{T}_1^3(a) \right. \right. \\ &\quad \left. \left. - \frac{\eta(3+\eta)}{3} \mathcal{T}_3^3(a) \right\} \right] \quad \dots (II.105) \end{aligned}$$

Table II.10. The Evolution of Tensor Operators T^n Under a Quadrupole Interaction $\mathcal{H}_Q = \frac{\omega_Q}{\sqrt{6}} [\tilde{T}_0^2 + \eta/\sqrt{3} \tilde{T}_2^2(s)]$ for spin $I = 3/2$

$$U \tilde{T}_0^1 U^{-1} = \frac{1}{\rho^2} [\tilde{T}_0^1 \{ \frac{15\rho^2 + 4\eta^2 (\cos(\omega t) - 1)}{15} \} - \tilde{T}_2^3(s) \frac{2\sqrt{2}}{3\sqrt{3}} \eta (\cos(\omega t) - 1) \\ - \tilde{T}_0^3 \frac{2\sqrt{2}}{9\sqrt{5}} \eta^2 (\cos(\omega t) - 1) + i \tilde{T}_2^2(a) \frac{\sqrt{2}}{3} \rho \eta \sin(\omega t)]$$

$$U \tilde{T}_1^1(s) U^{-1} = \frac{1}{\rho^2} [\tilde{T}_1^1(s) \frac{1}{15} \{ (3-\eta)^2 \cos(\omega t) + 2(3+2\eta^2) \} \\ + \tilde{T}_1^3(s) \frac{1}{3\sqrt{15}} \{ (2+\eta)(3-\eta)(\cos(\omega t) - 1) \} \\ - \tilde{T}_3^3(s) \frac{1}{9} \eta(3-\eta)(\cos(\omega t) - 1) \\ - i \tilde{T}_1^2(a) \frac{1}{3\sqrt{2}} (3-\eta) \rho \sin(\omega t)]$$

$$U \tilde{T}_1^1(a) U^{-1} = \frac{1}{\rho^2} [\tilde{T}_1^1(a) \frac{1}{15} \{ 3\rho^2 \cos(\omega t) + 2(3+2\eta^2-3\eta) \} \\ + \tilde{T}_1^3(a) \frac{(2-\eta)(3+\eta)}{3\sqrt{15}} (\cos(\omega t) - 1) \\ - \tilde{T}_3^3(a) \frac{\eta}{9} (3+\eta)(\cos(\omega t) - 1) \\ - i \tilde{T}_1^2(s) \frac{(3+\eta)}{3\sqrt{2}} \rho \sin(\omega t)]$$

$$U \tilde{T}_0^2 U^{-1} = \frac{1}{\rho^2} [\tilde{T}_0^2 \frac{1}{3} \{ 3\rho^2 + \eta^2 (\cos(\omega t) - 1) \} \\ - \tilde{T}_2^2(s) \frac{\eta}{\sqrt{3}} (\cos(\omega t) - 1) + i \tilde{T}_2^3(a) \frac{2\eta\rho}{3} \sin(\omega t)]$$

able II.10 (contd.)

$$\begin{aligned} \tilde{T}_1^2(s)U^{-1} &= \frac{1}{\rho} \left[\tilde{T}_1^2(s) \rho \cos(\omega t) - i \tilde{T}_1^1(a) \frac{\sqrt{2}}{5} (3+\eta) \sin(\omega t) \right. \\ &\quad \left. - i \tilde{T}_1^3(a) \frac{\sqrt{2}}{\sqrt{15}} (2-\eta) \sin(\omega t) + i \tilde{T}_3^3(a) \frac{\sqrt{2}}{3} \eta \sin(\omega t) \right] \end{aligned}$$

$$\begin{aligned} \tilde{T}_1^2(a)U^{-1} &= \frac{1}{\rho} \left[\tilde{T}_1^2(a) \cos(\omega t) \rho - i \tilde{T}_1^1(s) \frac{\sqrt{2}}{5} (3-\eta) \sin(\omega t) \right. \\ &\quad \left. - i \tilde{T}_1^3(s) \frac{\sqrt{2}}{\sqrt{15}} (2+\eta) \sin(\omega t) + i \tilde{T}_3^3(s) \frac{\sqrt{2}}{3} \eta \sin(\omega t) \right] \end{aligned}$$

$$\begin{aligned} \tilde{T}_2^2(s)U^{-1} &= \frac{1}{\rho^2} \left[\tilde{T}_2^2(s) \{ \rho^2 + (\cos(\omega t) - 1) \} - \tilde{T}_0^2 \frac{\eta}{\sqrt{3}} (\cos(\omega t) - 1) \right. \\ &\quad \left. - i \tilde{T}_2^3(a) \frac{2\rho}{\sqrt{3}} \sin(\omega t) \right] \end{aligned}$$

$$\begin{aligned} \tilde{T}_2^2(a)U^{-1} &= \frac{1}{\rho} \left[\tilde{T}_2^2(a) \rho \cos(\omega t) - i \tilde{T}_2^3(s) \frac{2}{\sqrt{3}} \sin(\omega t) \right. \\ &\quad \left. + i \tilde{T}_0^1 \frac{4}{5} \frac{\eta}{\sqrt{2}} \sin(\omega t) - i \tilde{T}_0^3 \frac{2\eta}{3\sqrt{5}} \sin(\omega t) \right] \end{aligned}$$

$$\begin{aligned} \tilde{T}_1^3(s)U^{-1} &= \frac{1}{\rho^2} \left[\tilde{T}_1^3(s) \frac{1}{30} \{ 3(4+4\eta + \eta^2) \cos(\omega t) + (18+7\eta^2-12\eta) \} \right. \\ &\quad \left. + \tilde{T}_1^1(s) \frac{3}{10\sqrt{15}} \{ (2+\eta)(3-\eta)(\cos(\omega t)-1) \} \right. \\ &\quad \left. - \tilde{T}_3^3(s) \frac{\eta(2+\eta)}{2\sqrt{15}} (\cos(\omega t)-1) \right. \\ &\quad \left. - i \tilde{T}_1^2(a) \frac{\sqrt{3}}{2\sqrt{10}} \{ (2+\eta)\rho \sin(\omega t) \} \right] \end{aligned}$$

$$\begin{aligned} \tilde{T}_1^3(a)U^{-1} &= \frac{1}{\rho^2} \left[\tilde{T}_1^3(a) \frac{1}{30} \{ 3(4-4\eta+\eta^2) \cos(\omega t) + (24+7\eta^2-12\eta) \} \right. \\ &\quad \left. + \tilde{T}_1^1(a) \frac{3}{10\sqrt{15}} (2-\eta)(3+\eta)(\cos(\omega t)-1) \right. \\ &\quad \left. - \tilde{T}_3^3(a) \frac{\eta(2-\eta)}{2\sqrt{15}} (\cos(\omega t)-1) - i \tilde{T}_1^2(s) \frac{\sqrt{3}}{2\sqrt{10}} (2-\eta)\rho \sin(\omega t) \right] \end{aligned}$$

Table II.10 (contd.)

$$U \tilde{T}_0^3 U^{-1} = \frac{1}{\rho^2} \left[\tilde{T}_0^3 \frac{1}{15} \{ 15 \rho^2 + \eta^2 (\cos(\omega t) - 1) \} + \tilde{T}_2^3(s) \frac{\eta}{\sqrt{15}} (\cos(\omega t) - 1) \right. \\ \left. - \tilde{T}_0^1 \frac{2}{5\sqrt{10}} \eta^2 (\cos(\omega t) - 1) - i \tilde{T}_2^2(a) \frac{\eta \rho}{2\sqrt{5}} \sin(\omega t) \right]$$

$$U \tilde{T}_2^3(s) U^{-1} = \frac{1}{\rho^2} \left[\tilde{T}_2^3(s) \{ \rho^2 + (\cos(\omega t) - 1) \} - \tilde{T}_0^1 \frac{\sqrt{6}}{5} \eta (\cos(\omega t) - 1) \right. \\ \left. + \tilde{T}_0^3 \frac{\eta}{\sqrt{15}} (\cos(\omega t) - 1) - i \tilde{T}_2^2(a) \frac{\sqrt{3} \rho}{2} \sin(\omega t) \right]$$

$$U \tilde{T}_2^3(a) U^{-1} = \frac{1}{\rho} \left[\tilde{T}_2^3(a) \cos(\omega t) \rho - i \tilde{T}_2^2(s) \frac{\sqrt{3}}{2} \sin(\omega t) + i \tilde{T}_0^2 \frac{\eta}{2} \sin(\omega t) \right]$$

$$U \tilde{T}_3^3(s) U^{-1} = \frac{1}{\rho^2} \left[\tilde{T}_3^3(s) \frac{1}{6} \{ 6 \rho^2 + \eta^2 (\cos(\omega t) - 1) \} - \tilde{T}_1^3(s) \frac{\eta(2+\eta)}{2\sqrt{15}} (\cos(\omega t) - 1) \right. \\ \left. - \tilde{T}_1^1(s) \frac{\eta}{10} (3-\eta) (\cos(\omega t) - 1) + i \tilde{T}_1^2(a) \frac{\eta \rho}{2\sqrt{2}} \sin(\omega t) \right]$$

$$U \tilde{T}_3^3(a) U^{-1} = \frac{1}{\rho^2} \left[\tilde{T}_3^3(a) \frac{1}{6} \{ 6 \rho^2 + \eta^2 (\cos(\omega t) - 1) \} \right. \\ \left. - \tilde{T}_1^1(a) \frac{\eta}{10} (3+\eta) (\cos(\omega t) - 1) \right. \\ \left. + \tilde{T}_1^3(a) \frac{\eta(2-\eta)}{2\sqrt{15}} (\cos(\omega t) - 1) + i \tilde{T}_1^2(s) \frac{\eta \rho}{2\sqrt{2}} \sin(\omega t) \right]$$

where $U = \exp(-i \mathcal{H}_Q t)$

$$\omega = \omega_Q \rho \quad ; \quad \omega_Q = \frac{e^2 q Q}{2}$$

$$\rho = (1 + \eta^2/3)^{1/2}$$

In arriving at this equation we have made use of the Table II.10, and, as usual, dropped the high frequency terms. The evolution of the tensor operators under the influence of $\tilde{\mathcal{H}}_1$ are set out in Table II.11. Having obtained the time evolution of the tensor operators under the influence of $\frac{\Delta\omega}{\sqrt{6}} \mathcal{H}'_Q$ and $\tilde{\mathcal{H}}_1$ it is a straightforward matter to obtain the expression for the pulse responses. The single- and two-pulse responses obtained in this case are:

II.D.2(i) Single-pulse response:

$$\langle \tilde{M}_x \rangle = \frac{\omega_Q}{4 kT} \frac{(1+\eta^2/3)^{1/2}}{2} \frac{(3+\eta)}{(3+\eta^2)^{1/2}} \sin\beta \cos(\Delta\omega_Q t') \quad \dots (II.106)$$

$$\text{where } \beta = \frac{(3+\eta)}{(3+\eta^2)^{1/2}} \omega_1 t_w \quad \dots (II.107)$$

$$\Delta\omega_Q = (\omega_Q - \omega)(1+\eta^2/3)^{1/2}$$

$$t' = t - t_w$$

$$\text{Also } \langle \tilde{M}_y \rangle = \langle \tilde{M}_z \rangle = 0.$$

II.D.2(ii) Two-pulse response:

$$\begin{aligned} \langle \tilde{M}_x \rangle = \frac{\omega_Q}{4 kT} \frac{(1+\eta^2/3)^{1/2}}{2} \frac{(3+\eta)}{(3+\eta^2)^{1/2}} \{ & \sin\beta \cos^2 \beta/2 \cos(\Delta\omega_Q t) \\ & + \sin\beta \cos\beta \cos(\Delta\omega_Q (t-\tau)) \\ & - \sin\beta \sin^2 \beta/2 \cos(\Delta\omega_Q (t-2\tau)) \} \end{aligned}$$

.. (II.108)

Table II.11. The Evolution of the Tensor Operators \tilde{T}_q^n Under the Influence of the Hamiltonian $\tilde{\mathcal{H}}_1$ for $I = 3/2$

$$\begin{aligned} U \tilde{T}_0^1 U^{-1} &= \frac{1}{\rho^2} [\tilde{T}_0^1 \frac{1}{15} \{15 \rho^2 + (3+5 \eta^2)(\cos\beta-1)\} \\ &\quad - \tilde{T}_2^3(s) \frac{4}{3\sqrt{6}} \eta(\cos\beta-1) + \tilde{T}_0^3 \frac{4}{3\sqrt{10}}(\cos\beta-1) \\ &\quad + i \tilde{T}_1^1(s) \frac{1}{5\sqrt{3}} (3+\eta) \rho \sin\beta + i \tilde{T}_1^3(s) \frac{(2-\eta)}{3\sqrt{5}} \sin\beta \\ &\quad - i \tilde{T}_3^3(s) \frac{\eta}{\sqrt{3}} \rho \sin\beta] \end{aligned}$$

$$\begin{aligned} U \tilde{T}_1^1(s) U^{-1} &= \frac{1}{\rho^2} [\tilde{T}_1^1(s) \frac{1}{15} \{15 \rho^2 + 2(6+\eta^2-3\eta)(\cos\beta-1)\} \\ &\quad + \tilde{T}_1^3(s) \frac{1}{3\sqrt{15}} (3+\eta-2\eta^2)(\cos\beta-1) \\ &\quad - \tilde{T}_3^3(s) \frac{(1+\eta)}{3} (\cos\beta-1) + i \tilde{T}_0^1 \frac{1}{5\sqrt{3}} (3+\eta) \rho \sin\beta \\ &\quad - i \tilde{T}_2^3(s) \frac{\sqrt{2}}{3} \rho \sin\beta + i \tilde{T}_0^3 \frac{\sqrt{2}}{\sqrt{15}} (2-\eta) \rho \sin\beta] \end{aligned}$$

$$\begin{aligned} U \tilde{T}_1^1(a) U^{-1} &= \frac{1}{\rho^2} [\tilde{T}_1^1(a) \frac{1}{15} \{15 \rho^2 + 3(1-\eta^2)(\cos\beta-1)\} \\ &\quad - \tilde{T}_3^3(a) \frac{(1-\eta)}{3} (\cos\beta-1) - \tilde{T}_1^3(a) \frac{1}{3\sqrt{15}} (3+2\eta)(1-\eta)(\cos\beta-1) \\ &\quad - i \tilde{T}_2^3(a) \frac{\sqrt{2}}{3} \rho (1-\eta) \sin\beta] \end{aligned}$$

$$U \tilde{T}_0^2 U^{-1} = \frac{1}{\rho^2} [\tilde{T}_0^2 \{ \rho^2 + (\cos\beta-1) \} + \tilde{T}_2^2(s) \frac{\eta}{\sqrt{3}} (\cos\beta-1) + i \tilde{T}_1^2(s) \rho \sin\beta]$$

$$U \tilde{T}_1^2(s) U^{-1} = \frac{1}{\rho} [\tilde{T}_1^2(s) \rho \cos\beta + i \tilde{T}_2^2(s) \frac{\eta}{\sqrt{3}} \sin\beta + i \tilde{T}_0^2 \sin\beta]$$

$$\begin{aligned} U \tilde{T}_2^2(s) U^{-1} &= \frac{1}{\rho^2} [\tilde{T}_2^2(s) \frac{1}{3} \{3 \rho^2 + \eta^2(\cos\beta-1)\} + \tilde{T}_0^2 \frac{1}{\sqrt{3}} (\cos\beta-1) \\ &\quad + i \tilde{T}_1^2(s) \frac{\eta}{\sqrt{3}} \rho \sin\beta] \end{aligned}$$

.. contd.

Table II.11 (contd.)

$$\begin{aligned}
 U \tilde{T}_0^3 U^{-1} &= \frac{1}{\rho^2} \left[\tilde{T}_0^3 \frac{1}{15} \{ 15 \rho^2 + (5\eta^2 + 12)(\cos\beta - 1) \} + \tilde{T}_2^3(s) \frac{\eta}{\sqrt{15}} (\cos\beta - 1) \right. \\
 &\quad + \tilde{T}_0^1 \frac{6}{5\sqrt{10}} (\cos\beta - 1) + i \tilde{T}_1^3(s) \frac{\sqrt{2}}{10} (4 + 3\eta) \rho \sin\beta \\
 &\quad \left. + i \tilde{T}_1^1(s) \frac{3}{5\sqrt{30}} (2 - \eta) \rho \sin\beta - i \tilde{T}_3^3(s) \frac{\eta}{\sqrt{30}} \rho \sin\beta \right]
 \end{aligned}$$

$$\begin{aligned}
 U \tilde{T}_1^3(s) U^{-1} &= \frac{1}{\rho^2} \left[\tilde{T}_1^3(s) \frac{1}{10} \{ 10 \rho^2 + (7 + 2\eta^2 + 4\eta)(\cos\beta - 1) \} \right. \\
 &\quad + \tilde{T}_3^3(s) \frac{1}{2\sqrt{15}} (3 - 2\eta)(\cos\beta - 1) \\
 &\quad + \tilde{T}_1^1(s) \left[\frac{3}{10\sqrt{15}} (3 + \eta - 2\eta^2)(\cos\beta - 1) \right] + i \tilde{T}_2^3(s) \frac{\sqrt{3}}{\sqrt{10}} \rho \sin\beta \\
 &\quad \left. + i \tilde{T}_0^3 \frac{\sqrt{2}}{10} (4 + 3\eta) \rho \sin\beta + i \tilde{T}_0^1 \frac{3}{10\sqrt{5}} (2 - \eta) \rho \sin\beta \right]
 \end{aligned}$$

$$\begin{aligned}
 U \tilde{T}_1^3(a) U^{-1} &= \frac{1}{\rho^2} \left[\tilde{T}_1^3(a) \frac{1}{30} \{ 30 \rho^2 + (3 + 2\eta)^2 (\cos\beta - 1) \} \right. \\
 &\quad + \tilde{T}_3^3(a) \frac{1}{2\sqrt{15}} (3 + 2\eta)(\cos\beta - 1) \\
 &\quad - \tilde{T}_1^1(a) \frac{3}{10\sqrt{15}} (3 + 2\eta)(1 - \eta)(\cos\beta - 1) \\
 &\quad \left. + i \tilde{T}_2^3(a) \frac{1}{\sqrt{30}} (3 + 2\eta) \sin\beta \right]
 \end{aligned}$$

$$\begin{aligned}
 U \tilde{T}_2^3(a) U^{-1} &= \frac{1}{\rho} \left[\tilde{T}_2^3(a) \rho \cos\beta + i \tilde{T}_3^3(a) \frac{1}{\sqrt{2}} \sin\beta + i \tilde{T}_1^3(a) \frac{1}{\sqrt{30}} (3 + 2\eta) \sin\beta \right. \\
 &\quad \left. - i \tilde{T}_1^1(a) \frac{3}{5\sqrt{2}} (1 - \eta) \sin\beta \right]
 \end{aligned}$$

$$\begin{aligned}
 U \tilde{T}_2^3(s) U^{-1} &= \frac{1}{\rho^2} \left[\tilde{T}_2^3(s) \{ \rho^2 + (\cos\beta - 1) \} - \tilde{T}_0^1 \frac{\sqrt{6}}{5} \eta (\cos\beta - 1) \right. \\
 &\quad + \tilde{T}_0^3 \frac{\eta}{\sqrt{15}} (\cos\beta - 1) + i \tilde{T}_2^3(s) \frac{\rho}{\sqrt{2}} \sin\beta \\
 &\quad \left. + i \tilde{T}_1^3(s) \frac{\sqrt{3}}{\sqrt{10}} \rho \sin\beta - i \tilde{T}_1^1(s) \frac{3\rho}{5\sqrt{2}} \sin\beta \right]
 \end{aligned}$$

...contd.

Table II.11 (contd.)

$$\begin{aligned}
 U \tilde{T}_3^3(s) U^{-1} = & \frac{1}{\rho^2} [\tilde{T}_3^3(s) \frac{1}{6} [6\rho^2 + (3+2\eta^2)(\cos\beta-1) \\
 & + \tilde{T}_1^3(s) \frac{1}{2\sqrt{15}} (3-2\eta)(\cos\beta-1) - \tilde{T}_1^1(s) \frac{3(1+\eta)}{10} (\cos\beta-1) \\
 & + i \tilde{T}_2^3(s) \frac{\rho}{\sqrt{2}} \sin\beta - i \tilde{T}_0^1 \frac{2}{10\sqrt{3}} \eta \rho \sin\beta - i \tilde{T}_0^3 \frac{\eta \rho}{10\sqrt{3}} \sin\beta]
 \end{aligned}$$

$$\begin{aligned}
 U \tilde{T}_3^3(a) U^{-1} = & \frac{1}{\rho^2} [\tilde{T}_3^3(a) \frac{1}{2} \{2\rho^2 + (\cos\beta - 1)\} \\
 & + \tilde{T}_1^3(a) \frac{1}{2\sqrt{15}} (3+2\eta)(\cos\beta - 1) \\
 & - \tilde{T}_1^1(a) \frac{3}{10} (1-\eta)(\cos\beta-1) + i \tilde{T}_2^3(a) \frac{\rho}{\sqrt{2}} \sin\beta]
 \end{aligned}$$

where $U = \exp(-i \tilde{\mathcal{H}}_1 t_w)$

$$\tilde{\mathcal{H}}_1 = \omega_1 \left[\frac{1}{3\rho^2} [\tilde{T}_1^1(a) \frac{(3+\eta)^2}{5} + \frac{(2-\eta)(3+\eta)}{\sqrt{15}} \tilde{T}_1^3(a) - \frac{\eta(3+\eta)}{3} \tilde{T}_3^3(a)] \right]$$

$$\beta = \omega_1 \frac{(3+\eta)}{\sqrt{3}\rho} t_w$$

$$\rho = (1 + \eta^2/3)^{1/2}$$

where $\tau \gg t$

$$t > (\tau + 2t_w)$$

II.D.3 Calculation in the 'Diagonal Frame'

Pulse response calculations can be considerably simplified if we work in a representation in which the quadrupolar Hamiltonian is in diagonal form. It can be easily shown that (for $I = 3/2$) that quadrupolar Hamiltonian can be brought into the diagonal form by the transformation operator

$$U_d = \exp \left(\frac{2}{\sqrt{3}} x T_2^3(a) \right) \quad \dots (II.109)$$

$$\text{where } x = \tan^{-1} \eta / \sqrt{3} \quad \dots (II.110)$$

The transformation of a few selected tensor operators under U_d are set out in Table II.12. The total Hamiltonian in the diagonal frame can be written as

$$\mathcal{H}^d(t) = \mathcal{H}_Q^d + \mathcal{H}_1^d \quad \dots (II.111)$$

$$\text{where } \mathcal{H}_Q^d = U_d \mathcal{H}_Q U_d^{-1} = \frac{\omega_Q}{\sqrt{6}} (1 + \eta^2/3)^{1/2} T_0^2 = \frac{\omega_Q}{\sqrt{6}} T_0^2 \quad \dots (II.112)$$

$$\begin{aligned} \text{and } \mathcal{H}_1^d = 2 \cos(\omega_Q' t) & \left[T_1^1(a) \{1 + 4/5(\cos x - 1)\} \right. \\ & + T_1^3(a) \left\{ \frac{1}{\sqrt{15}}(\cos x - 1) + \frac{\sqrt{5}}{3} \sin x \right\} \\ & \left. + T_3^3(a) \left\{ \frac{1}{\sqrt{3}} \sin x - \frac{1}{3}(\cos x - 1) \right\} \right] \quad \dots (II.113) \end{aligned}$$

'd' refers to the diagonal frame.

Table II.12. Transformation of a few Selected Irreducible Tensor Operators in the Frame Defined by the Transformation Operator $U_d = \exp (2/\sqrt{3} \times T_2^3(a))$, for $I = 3/2$

$$U_d T_{\sim 0}^2 U_d^{-1} = T_{\sim 0}^2 \cos X - \sin X T_{\sim 2}^2(s)$$

$$U_d T_{\sim 2}^2(s) U_d^{-1} = T_{\sim 2}^2(s) \cos X + T_{\sim 0}^2 \sin X$$

$$U_d T_{\sim 1}^1(a) U_d^{-1} = T_{\sim 1}^1(a) [1 + 4/5 (\cos X - 1)] + T_{\sim 1}^3(a) \left[\frac{1}{\sqrt{15}} (\cos X - 1) + \frac{\sqrt{5}}{3} \sin X \right] + T_{\sim 3}^3(a) \left[\frac{1}{\sqrt{3}} \sin X - 1/3 (\cos X - 1) \right]$$

$$U_d T_{\sim 1}^1(s) U_d^{-1} = T_{\sim 1}^1(s) [1 + \frac{4}{5} (\cos X - 1)] + T_{\sim 1}^3(s) \left[\frac{1}{\sqrt{15}} (\cos X - 1) - \frac{\sqrt{5}}{3} \sin X \right] + T_{\sim 3}^3(s) \left[\frac{1}{3} (\cos X - 1) + \frac{1}{\sqrt{3}} \sin X \right]$$

$$U_d T_{\sim 0}^1 U_d^{-1} = T_{\sim 0}^1 [1 + \frac{4}{5} (\cos X - 1)] - T_{\sim 0}^3 \left[\frac{4}{3\sqrt{10}} (\cos X - 1) \right] - T_{\sim 2}^3(s) \left[\frac{2\sqrt{2}}{3} \sin X \right]$$

where $\cos X = (1 + \eta^2/3)^{-1/2}$;

$$\sin X = \frac{\eta}{(3 + \eta^2)^{1/2}}$$

Now the evolution of tensor operators under the influence of \mathcal{H}_Q^d can be obtained from Table II.2 by substituting ω_Q by ω_q . In the interaction representation defined by the transformation operator

$$U_q = \exp \left(i \frac{\omega'_q}{\sqrt{6}} T_0^2 \right), \quad \dots (II.114)$$

the total Hamiltonian given in Eqn. II.111 can be written as

$$\tilde{\mathcal{H}}^d = \frac{\Delta\omega_q}{\sqrt{6}} T_0^2 + \tilde{\mathcal{H}}_1^d \quad \dots (II.115)$$

where $\Delta\omega_q = (\omega_q - \omega'_q)$

and $\tilde{\mathcal{H}}_1^d = U_q \mathcal{H}_1^d U_q^{-1}$

$$\simeq \omega_1 \left\{ \frac{(3+\eta)}{3\rho} \right\} \left[\frac{3}{5} T_1^1(a) + \frac{2}{\sqrt{15}} T_1^3(a) \right] \quad \dots (II.116)$$

In arriving at this equation the high frequency terms have been omitted as usual. The evolution of tensor operators under $\tilde{\mathcal{H}}_1^d$ can be obtained from Table II.3 by substituting ξ by β

$$\text{where } \beta = \frac{\omega_1 (3+\eta) t_w}{(3+\eta^2)^{1/2}} \quad \dots (II.117)$$

Using the evolution of tensor operators under \mathcal{H}_Q^d and $\tilde{\mathcal{H}}_1^d$ and proceeding as earlier, the single- and two-pulse responses obtained are exactly same as those given by Eqns. II.106 and

II.108, respectively. From here onwards we present all the calculations in the 'diagonal frame' only.

II.E PULSE RESPONSES IN THE PRESENCE OF A WEAK ZEEMAN FIELD FOR NUCLEAR SPIN $I = 3/2$ IN NON-AXIALLY SYMMETRIC FIELD GRADIENTS

In this section we present the calculation of pulse responses in the presence of a weak Zeeman field applied along X-, Y-, and Z- principal axes of the efg tensor. In this analysis we assume that $\omega_0 \ll \omega_q$ and also neglect the effect of Zeeman field during the r.f. pulse assuming that the spins scarcely precess during the period when r.f. is on.

II.E.1 Zeeman Field Applied Along X-Axis of the efg

The Hamiltonian corresponding to the Zeeman interaction for this case is given by

$$\mathcal{H}_{ZX} = \omega_0 T_1^1(a) \quad \dots (II.118)$$

Using Tables II.2 and II.12

$$\begin{aligned} \tilde{\mathcal{H}}_Z^d &= U_q U_d \mathcal{H}_Z U_d^{-1} U_q^{-1} \\ &\approx \omega_0 \left[\frac{1}{5} \left\{ 1 + \frac{1}{\rho} (1-\eta) \right\} T_1^1(a) - \frac{1}{\sqrt{15}} \left\{ 1 + \frac{1}{\rho} (1-\eta) \right\} T_1^3(a) \right. \\ &\quad \left. + \frac{1}{3} \left\{ 1 - \frac{1}{\rho} (1-\eta) \right\} T_3^3(a) \right] \quad \dots (II.119) \end{aligned}$$

$$\text{where } \rho = (1 + \eta^2/3)^{1/2} \quad \dots (II.120)$$

The evolution of a few selected tensor operators under this Hamiltonian are tabulated in Table II.13. The single- and two-pulse responses obtained for this case (for $\Delta\omega_q = 0$) are:

II.E.1(i) Single-pulse response:

$$\langle \tilde{M}_x \rangle = \frac{\omega_Q}{4 kT} (1 + \eta^2/3)^{1/2} \frac{(3+\eta)}{(3+\eta^2)^{1/2}} \sin\beta \cos\left(\frac{\omega_o(1-\eta)}{\rho} t'\right) \quad \dots (II.121)$$

where $\beta = \omega_1 \frac{(3+\eta)}{(3+\eta^2)^{1/2}} t_w$; $t' = t - t_w$

II.E.1(ii) Two-pulse response:

$$\begin{aligned} \langle \tilde{M}_x \rangle = & \frac{\omega_Q}{4 kT} (1 + \eta^2/3)^{1/2} \frac{(3+\eta)}{(3+\eta^2)^{1/2}} \\ & \left[\sin\beta \cos^2\beta / 2 \cos\left(\omega_o \frac{(1-\eta)}{\rho} t\right) \right. \\ & + \sin\beta \cos\beta \cos\left(\omega_o \frac{(1-\eta)}{\rho} (t-\tau)\right) \\ & \left. - \sin\beta \sin^2\beta / 2 \cos\left(\omega_o \frac{(1-\eta)}{\rho} (t-2\tau)\right) \right] \quad \dots (II.122) \end{aligned}$$

where $\tau \gg t_w$,

$$t \gg (\tau + 2t_w)$$

II.E.2 Zeeman Field Applied Along Y-Axis of efg

The Zeeman Hamiltonian corresponding to this situation is

$$\mathcal{H}_Z = -i\omega_o T_1^1(s) \quad \dots (II.123)$$

Table II.13. The Evolution of a few Selected Irreducible Tensor Operators Under the Action of the Hamiltonian $\tilde{\mathcal{H}}_{ZX}^d$

$$\begin{aligned}
 U \tilde{T}_1^2(s) U^{-1} &= \tilde{T}_1^2(s) \cos(\omega_0 \frac{(1-\eta)}{\rho} t) + i \tilde{T}_2^2(s) \sin(\omega_0 \frac{(1-\eta)}{\rho} t) \\
 U \tilde{T}_1^2(a) U^{-1} &= \tilde{T}_1^2(a) \cos(\omega_0 t) + i \tilde{T}_2^2(a) \sin(\omega_0 t) \\
 U \tilde{T}_2^2(s) U^{-1} &= \tilde{T}_2^2(s) \cos(\omega_0 \frac{(1-\eta)}{\rho} t) + i \tilde{T}_1^2(s) \sin(\omega_0 \frac{(1-\eta)}{\rho} t) \\
 U \tilde{T}_2^2(a) U^{-1} &= \tilde{T}_2^2(a) \cos(\omega_0 t) + i \tilde{T}_1^2(a) \sin(\omega_0 t) \\
 U \tilde{T}_0^2 U^{-1} &= \tilde{T}_0^2
 \end{aligned}$$

where $U = \exp(-i \tilde{\mathcal{H}}_{ZX}^d t)$

$$\begin{aligned}
 \tilde{\mathcal{H}}_{ZX}^d &= \omega_0 \left[\tilde{T}_1^1(a) \frac{1}{5} \left\{ 1 + \frac{1}{\rho} (1-\eta) \right\} - \tilde{T}_1^3(a) \frac{1}{\sqrt{15}} \left\{ 1 + \frac{1}{\rho} (1-\eta) \right\} \right. \\
 &\quad \left. + \tilde{T}_3^3(a) \frac{1}{3} \left\{ 1 - \frac{1}{\rho} (1-\eta) \right\} \right]
 \end{aligned}$$

$$\rho = (1 + \eta^2/3)^{1/2}$$

$$\omega_0 = \gamma H_0$$

Now, $\tilde{\mathcal{H}}_z^d = U_q U_d \mathcal{H}_z U_d^{-1} U_q^{-1}$.. (II.124)

Using Tables II.2 and II.12 and dropping the high frequency terms, we get

$$\begin{aligned} \tilde{\mathcal{H}}_z^d \approx & -i\omega_0 \left[\frac{1}{5} \left(1 + \frac{1}{\rho} (1-\eta) \right) T_1^1(s) - \frac{1}{\sqrt{15}} \left(1 + \frac{1}{\rho} (1+\eta) \right) T_1^3(s) \right. \\ & \left. + \frac{1}{3} \left(-1 + \frac{1}{\rho} (1+\eta) \right) T_3^3(s) \right] \end{aligned}$$

.. (II.125)

The evolution of a few selected tensor operators under this Hamiltonian are given in Table II.14. Pulse responses obtained in this case are as under.

II.E.2(i) Single-pulse response:

$$\langle \tilde{M}_x \rangle = \frac{\omega_Q}{4 kT} (1 + \eta^2/3)^{1/2} \frac{(3+\eta)}{(3+\eta^2)^{1/2}} \sin\beta \cos\left(\omega_0 \frac{(1+\eta)}{\rho} t'\right]$$

.. (II.126)

where $t' = t - t_w$

II.E.2(ii) Two-pulse response:

$$\begin{aligned} \langle \tilde{M}_x \rangle = & \frac{\omega_Q}{4 kT} (1 + \eta^2/3)^{1/2} \frac{(3+\eta)}{(3+\eta^2)^{1/2}} \left[\sin\beta \cos^2\beta/2 \cos\left(\omega_0 \frac{(1+\eta)}{\rho} t\right) \right. \\ & + \sin\beta \cos\beta \cos\left(\omega_0 \frac{(1+\eta)}{\rho} (t-\tau)\right) \\ & \left. - \sin\beta \sin^2\beta/2 \cos\left(\omega_0 \frac{(1+\eta)}{\rho} (t-2\tau)\right) \right] \end{aligned}$$

.. (II.127)

where $\tau \gg t_w$

$t \geq (\tau + 2t_w)$

Table II.14. The Evolution of a few Selected Irreducible Tensor Operators Under the Action of the Hamiltonian $\tilde{\mathcal{H}}_{ZY}^d$

$$UT_1^2(s)U^{-1} = T_1^2(s) \cos(\omega_0 t) - T_2^2(a) \sin(\omega_0 t)$$

$$UT_1^2(a)U^{-1} = T_1^2(a) \cos\left(\omega_0 \frac{(1+\eta)}{\rho} t\right) - T_2^2(s) \sin\left(\omega_0 \frac{(1+\eta)}{\rho} t\right)$$

$$UT_2^2(s)U^{-1} = T_2^2(s) \cos\left(\omega_0 \frac{(1+\eta)}{\rho} t\right) + T_1^2(a) \sin\left(\omega_0 \frac{(1+\eta)}{\rho} t\right)$$

$$UT_2^2(a)U^{-1} = T_2^2(a) \cos(\omega_0 t) + T_1^2(s) \sin(\omega_0 t)$$

$$UT_0^2U^{-1} = T_0^2$$

where $U = \exp(-i \tilde{\mathcal{H}}_{ZY}^d t)$

$$\begin{aligned} \tilde{\mathcal{H}}_{ZY}^d = & -i\omega_0 \left[T_1^1(s) \frac{1}{5} \left\{ 1 + \frac{1}{\rho} (1+\eta) \right\} - T_1^3(s) \frac{1}{\sqrt{15}} \left\{ 1 + \frac{1}{\rho} (1+\eta) \right\} \right. \\ & \left. + T_3^3(s) \frac{1}{3} \left\{ -1 + \frac{1}{\rho} (1+\eta) \right\} \right] \end{aligned}$$

$$\omega_0 = \gamma H_0,$$

$$\rho = (1 + \eta^2/3)^{1/2}$$

II.E.3 Zeeman Field Applied Along Z-Axis of efg

The Zeeman Hamiltonian for this case is given by

$$\mathcal{H}_Z = -\omega_o T_o^1 \quad \dots (II.128)$$

and

$$\begin{aligned} \tilde{\mathcal{H}}_Z^d &= U_q U_d \mathcal{H}_Z U_d^{-1} U_q^{-1} \\ &\approx -\omega_o \left[\frac{1}{5}(1+4/\rho) T_o^1 - \frac{4}{3\sqrt{10}} \left(\frac{1}{\rho} - 1 \right) T_o^3 \right] \quad \dots (II.129) \end{aligned}$$

The evolution of a few selected tensor operators under the influence of this Hamiltonian are set out in Table II.15. Pulse responses obtained in this case are as follows.

II.E.3(i) Single-pulse response:

$$\langle \tilde{M}_x \rangle = \frac{\omega_Q}{4 kT} (1 + \eta^2/3)^{1/2} \frac{(3+\eta)}{(3+\eta^2)^{1/2}} \sin\beta \cos(\omega_o t') \quad \dots (II.130)$$

where $t' = t - t_w$

II.E.3(ii) Two-pulse response:

$$\begin{aligned} \langle \tilde{M}_x \rangle &= \frac{\omega_Q}{4 kT} (1 + \eta^2/3)^{1/2} \frac{(3+\eta)}{(3+\eta^2)^{1/2}} [\sin\beta \cos^2\beta/2 \cos(\omega_o t) \\ &\quad + \sin\beta \cos\beta \cos(\omega_o(t-\tau)) \\ &\quad - \sin\beta \sin^2\beta/2 \cos(\omega_o(t-2\tau))] \quad \dots (II.131) \end{aligned}$$

where $\tau \gg t_w$

$t \gg (\tau + 2t_w)$

Table II.15. The Evolution of a few Selected Irreducible
Tensor Operators Under the Action of the
Hamiltonian $\tilde{\mathcal{H}}_{zz}^d$

$$U \tilde{T}_1^2(s) U^{-1} = \tilde{T}_1^2(s) \cos(\omega_0 t) - i \tilde{T}_1^2(a) \sin(\omega_0 t)$$

$$U \tilde{T}_1^2(a) U^{-1} = \tilde{T}_1^2(a) \cos(\omega_0 t) - i \tilde{T}_1^2(s) \sin(\omega_0 t)$$

$$U \tilde{T}_2^2(s) U^{-1} = \tilde{T}_2^2(s) \cos(\omega_0 \frac{2}{\rho} t) - i \tilde{T}_2^2(a) \sin(\omega_0 \frac{2}{\rho} t)$$

$$U \tilde{T}_2^2(a) U^{-1} = \tilde{T}_2^2(a) \cos(\omega_0 \frac{2}{\rho} t) - i \tilde{T}_2^2(s) \sin(\omega_0 \frac{2}{\rho} t)$$

where $U = \exp(-i \tilde{\mathcal{H}}_{zz}^d t)$

$$\tilde{\mathcal{H}}_{zz}^d = -\omega_0 \left[T_0^1 \frac{1}{5} \left(1 + \frac{4}{\rho} \right) - T_0^3 \frac{4}{3\sqrt{10}} \left(\frac{1}{\rho} - 1 \right) \right]$$

$$\rho = (1 + \eta^2/3)^{1/2}, \quad \omega_0 = \gamma H_0$$

Before concluding this section, it is worth mentioning here that since the calculation of the evolution of complete set of tensor operators (for spin $I = 3/2$) under the action of Zeeman Hamiltonian in different situations, becomes cumbersome we have presented here the results of the evolution of only a selected set of operators.

II.F THE EVOLUTION OF TENSOR OPERATORS UNDER THE ACTION OF r.f. HAMILTONIAN: ROLE OF PHASE OF r.f.

So far we have considered the r.f. pulses, in a two-pulse sequence with the same phase. However, if we wish to study the response of a nuclear spin system to an r.f. pulse as a function of phase then the r.f. Hamiltonian should be modified as follows:

$$(\mathcal{H}_1)_\emptyset = 2\omega_1 \cos(\omega t + \emptyset) \tilde{T}_1^1(a) \quad \dots (II.132)$$

where \emptyset is the phase of the r.f.

We consider the case of spin $I = 3/2$. In the interaction representation it is given by

$$(\tilde{\mathcal{H}}_1^d)_\emptyset = U_q U_d (\mathcal{H}_1)_\emptyset U_d^{-1} U_q^{-1} \quad \dots (II.133)$$

$$\begin{aligned} \approx \frac{(3+\eta)}{\sqrt{3}(3+\eta^2)^{1/2}} \omega_1 \left[\left(\frac{3}{5} \tilde{T}_1^1(a) + \frac{2}{\sqrt{15}} \tilde{T}_1^3(a) \right) \cos \emptyset \right. \\ \left. - i \sin \emptyset \frac{1}{\sqrt{2}} \tilde{T}_1^2(s) \right] \end{aligned} \quad \dots (II.134)$$

For $\phi = 0$ this reduces to Eqn. II.116.

$$\text{For } \phi = 90^\circ, \tilde{\mathcal{H}}_1^d = - \frac{(3+\eta) \omega_1}{\sqrt{3}(3+\eta)^{1/2}} i \frac{1}{\sqrt{2}} T_1^2(s) \quad \dots \text{ (II.135)}$$

In arriving at the Eqn. II.134 we have made use of the Tables II.2 and II.12 and dropped the high frequency terms. The evolution of tensor operators under the influence of $(\tilde{\mathcal{H}}_1^d)_\phi$ is set out in Table II.16. Tables II.16 and II.2 can be used to calculate the responses of spin 3/2 nuclei to sequence of pulses involving different relative phases.

It should be quite evident now from the above presentation that the tensor operator formalism can be used with relative ease to describe the pulse responses in pure NQR.

SUMMARY

Tensor operator formalism has been applied to pulsed NQR spectroscopy for the first time. The versatility of the formalism has been illustrated by calculating the single- and two-pulse responses in various situations in the case of spin $I = 1, 3/2$ and $5/2$ nuclei in single crystals. The results obtained here are in full agreement with those of others, wherever available in the literature. The evolution of tensor operators under the action of the r.f. Hamiltonian including arbitrary phase is presented for the spin 3/2 case. For the sake of illustration typical recordings of pulse responses are also included.

Table II.16. The Evolution of the Tensor Operators $T_q^n(a,s)$ Under the Influence of the Hamiltonian $(\tilde{\mathcal{H}}_1^d)_0$ for $I = 3/2$

$$\begin{aligned}
 U T_0^1 U^{-1} &= T_0^1 [1 + \frac{3}{5} (\cos\beta - 1)] + \frac{2\sqrt{2}}{3\sqrt{5}} T_0^3 (\cos\beta - 1) \\
 &\quad + \sin\beta [i\{\frac{\sqrt{3}}{5} T_1^1(s) + \frac{2}{3\sqrt{5}} T_1^3(s)\} \cos\varnothing + \frac{1}{\sqrt{6}} T_1^2(a) \sin\varnothing] \\
 U T_1^1(a) U^{-1} &= T_1^1(a) [1 + \frac{1}{5} (1 + 3 \sin^2\varnothing)(\cos\beta - 1)] - \frac{1}{\sqrt{15}} T_1^3(a) \cos 2\varnothing (\cos\beta - 1) \\
 &\quad + i \frac{1}{2\sqrt{2}} T_1^2(s) \sin 2\varnothing (\cos\beta - 1) - \frac{1}{3} T_3^3(a) (\cos\beta - 1) \\
 &\quad - i \sin\beta [-i\{\frac{1}{\sqrt{6}} T_2^2(s) + \frac{1}{\sqrt{2}} T_0^2\} \sin\varnothing + \frac{\sqrt{2}}{3} T_2^3(a) \cos\varnothing] \\
 U T_1^1(s) U^{-1} &= T_1^1(s) [1 + \frac{1}{5} (3 \cos^2\varnothing + 1)(\cos\beta - 1)] + \frac{1}{\sqrt{15}} T_1^3(s) \cos 2\varnothing (\cos\beta - 1) \\
 &\quad - i \frac{1}{2\sqrt{2}} T_1^2(a) \sin 2\varnothing (\cos\beta - 1) - \frac{1}{3} T_3^3(s) (\cos\beta - 1) \\
 &\quad + \sin\beta [i\{\frac{\sqrt{3}}{5} T_0^1 - \frac{\sqrt{2}}{3} T_2^3(s) + \frac{2\sqrt{2}}{\sqrt{15}} T_0^3\} \cos\varnothing - \frac{1}{\sqrt{6}} T_2^2(a) \sin\varnothing] \\
 U T_0^2 U^{-1} &= T_0^2 \cos\beta + \sin\beta [i T_1^2(s) \cos\varnothing + \frac{1}{\sqrt{2}} \{\frac{6\sqrt{3}}{5} T_1^1(a) + \frac{4}{\sqrt{15}} T_1^3(a)\} \sin\varnothing] \\
 U T_1^2(a) U^{-1} &= T_1^2(a) [1 + \sin^2\varnothing (\cos\beta - 1)] + i [\frac{3}{5\sqrt{2}} T_1^1(s) + \frac{2}{\sqrt{30}} T_1^3(s)] \sin 2\varnothing (\cos\beta - 1) \\
 &\quad - [\frac{\sqrt{6}}{5} T_0^1 + \frac{4}{\sqrt{15}} T_0^3] \sin\varnothing \sin\beta \\
 U T_1^2(s) U^{-1} &= T_1^2(s) [1 + \cos^2\varnothing (\cos\beta - 1)] - \frac{i}{2\sqrt{6}} [\frac{6\sqrt{3}}{5} T_1^1(a) + \frac{4}{\sqrt{5}} T_1^3(a)] \sin 2\varnothing (\cos\beta - 1) \\
 &\quad + i T_0^2 \cos\varnothing \sin\beta \\
 U T_2^2(a) U^{-1} &= T_2^2(a) [1 + \sin^2\varnothing (\cos\beta - 1)] + i \frac{1}{\sqrt{3}} T_2^3(s) \sin 2\varnothing (\cos\beta - 1) \\
 &\quad + \sin\beta [+ \frac{\sqrt{6}}{5} T_1^1(s) - \frac{\sqrt{2}}{\sqrt{5}} T_1^3(s) - \frac{\sqrt{2}}{\sqrt{3}} T_3^3(s)] \sin\varnothing \\
 U T_2^2(s) U^{-1} &= T_2^2(s) [1 + \sin^2\varnothing (\cos\beta - 1)] + i \frac{1}{\sqrt{3}} T_2^3(a) \sin 2\varnothing (\cos\beta - 1) \\
 &\quad + \sin\beta [\frac{\sqrt{6}}{5} T_1^1(a) - \frac{\sqrt{2}}{\sqrt{5}} T_1^3(a) - \frac{\sqrt{2}}{\sqrt{3}} T_3^3(a)] \sin\varnothing \\
 U T_0^3 U^{-1} &= T_0^3 [1 + \frac{4}{5} (\cos\beta - 1)] + \frac{3\sqrt{2}}{5\sqrt{5}} T_0^1 (\cos\beta - 1) \\
 &\quad + \sin\beta [i\{\frac{9\sqrt{2}}{5\sqrt{15}} T_1^1(s) + \frac{2\sqrt{2}}{5} T_1^3(s)\} \cos\varnothing + \frac{\sqrt{3}}{\sqrt{5}} \sin\varnothing T_1^2(a)]
 \end{aligned}$$

...contd.

Table II.16 (contd.)

$$\begin{aligned}
 U \tilde{T}_1^3(a) U^{-1} &= \tilde{T}_1^3(a) \left[1 + \frac{1}{10} (3 + 4 \sin^2 \varnothing) (\cos \beta - 1) \right] + (\cos \beta - 1) \left[\frac{\sqrt{3}}{2\sqrt{5}} \tilde{T}_3^3(a) \right. \\
 &\quad \left. - \frac{9}{10\sqrt{15}} \tilde{T}_1^1(a) \cos 2\varnothing + i \frac{1}{2\sqrt{10}} \sin 2\varnothing \tilde{T}_1^2(s) \right] + i \sin \beta \\
 &\quad \left[i \left\{ \frac{\sqrt{3}}{\sqrt{10}} \tilde{T}_0^2 - \frac{3}{2\sqrt{10}} \tilde{T}_2^2(s) \right\} \sin \varnothing + \frac{\sqrt{3}}{\sqrt{10}} \tilde{T}_2^3(a) \cos \varnothing \right]
 \end{aligned}$$

$$\begin{aligned}
 U \tilde{T}_1^3(s) U^{-1} &= \tilde{T}_1^1(s) \frac{9}{10\sqrt{15}} \cos 2\varnothing (\cos \beta - 1) + \tilde{T}_1^3(s) \left[1 + \frac{1}{10} (3 + 4 \cos^2 \varnothing) (\cos \beta - 1) \right] \\
 &\quad + \frac{\sqrt{3}}{2\sqrt{5}} \tilde{T}_3^3(s) (\cos \beta - 1) - i \frac{3}{2\sqrt{30}} \tilde{T}_1^2(a) \sin 2\varnothing (\cos \beta - 1) \\
 &\quad + \sin \beta \left[i \left\{ \frac{3}{5\sqrt{5}} \tilde{T}_0^1 + \frac{2\sqrt{2}}{5} \tilde{T}_0^3 + \frac{\sqrt{3}}{\sqrt{10}} \tilde{T}_2^3(s) \right\} \cos \varnothing - \frac{3}{2\sqrt{10}} \tilde{T}_2^2(s) \sin \varnothing \right]
 \end{aligned}$$

$$\begin{aligned}
 U \tilde{T}_2^3(a) U^{-1} &= \tilde{T}_2^3(a) \left[1 + \cos^2 \varnothing (\cos \beta - 1) \right] - i \frac{\sqrt{3}}{4} \tilde{T}_2^2(s) \sin 2\varnothing (\cos \beta - 1) \\
 &\quad + i \sin \beta \left[\left\{ -\frac{3}{5\sqrt{2}} \tilde{T}_1^1(a) + \frac{\sqrt{3}}{\sqrt{10}} \tilde{T}_1^3(a) + \frac{1}{\sqrt{2}} \tilde{T}_3^3(a) \right\} \cos \varnothing \right]
 \end{aligned}$$

$$\begin{aligned}
 U \tilde{T}_2^3(s) U^{-1} &= \tilde{T}_2^3(s) \left[1 + \cos^2 \varnothing (\cos \beta - 1) \right] - i \frac{\sqrt{3}}{4} \tilde{T}_2^2(a) \sin 2\varnothing (\cos \beta - 1) \\
 &\quad + i \sin \beta \left[\left\{ -\frac{3}{5\sqrt{2}} \tilde{T}_1^1(s) + \frac{\sqrt{3}}{\sqrt{10}} \tilde{T}_1^3(s) + \frac{1}{\sqrt{2}} \tilde{T}_3^3(s) \right\} \cos \varnothing \right]
 \end{aligned}$$

$$\begin{aligned}
 U \tilde{T}_3^3(a) U^{-1} &= \tilde{T}_3^3(a) \left[1 + \frac{1}{2} (\cos \beta - 1) \right] + \left[\frac{\sqrt{3}}{2\sqrt{5}} \tilde{T}_1^3(a) - \frac{3}{10} \tilde{T}_1^1(a) \right] (\cos \beta - 1) \\
 &\quad + \sin \beta \left[\frac{\sqrt{3}}{2\sqrt{2}} \sin \varnothing \tilde{T}_2^2(s) + \frac{1}{\sqrt{2}} \tilde{T}_2^3(a) \cos \varnothing \right]
 \end{aligned}$$

$$\begin{aligned}
 U \tilde{T}_3^3(s) U^{-1} &= \tilde{T}_3^3(s) \left[1 + \frac{1}{2} (\cos \beta - 1) \right] + \left[\frac{\sqrt{3}}{2\sqrt{15}} \tilde{T}_1^3(s) - \frac{3}{10} \tilde{T}_1^1(s) \right] (\cos \beta - 1) \\
 &\quad + \sin \beta \left[\frac{\sqrt{3}}{2\sqrt{2}} \tilde{T}_2^2(a) \sin \varnothing + \frac{1}{\sqrt{2}} \tilde{T}_2^3(s) \cos \varnothing \right]
 \end{aligned}$$

$$\text{where } (\tilde{\mathcal{H}}_1^d)_\varnothing = \omega_1 \frac{(3+\eta)}{\sqrt{3}(3+\eta^2)^{1/2}} \left[\left(\frac{3}{5} \tilde{T}_1^1(a) + \frac{2}{\sqrt{15}} \tilde{T}_1^3(a) \right) \cos \varnothing - i \frac{1}{\sqrt{2}} \tilde{T}_1^2(s) \sin \varnothing \right]$$

$$U = \exp (-i (\tilde{\mathcal{H}}_1^d)_\varnothing t)$$

$$\beta = \frac{(3+\eta)}{(3+\eta^2)^{1/2}} \omega_1 t$$

REFERENCES

- [1] R.R. Ernst, G. Bodenhausen and A. Wokaun, "Principles of Nuclear Magnetic Resonance in one and two Dimensions", Clarendon Press, Oxford (1987).
- [2] a) S. Vega and A. Pines, J. Chem. Phys., 66, 5624 (1977).
b) S. Vega, J. Chem. Phys., 63, 3769 (1975).
- [3] R.S. Cantor and J.S. Waugh, J. Chem. Phys., 73, 1054 (1980).
- [4] a) D. Ya. Osokin, Phys. Status Solidi(b), 102, 681 (1980).
b) D. Ya. Osokin, J. Molec. Struct., 83, 243 (1982).
c) D. Ya. Osokin, Phys. Status Solidi(b), 109, K7 (1982).
- [5] M. Matti Maricq, Phys. Rev., E33, 4501 (1986).
- [6] S. Vega, J. Chem. Phys., 68, 5518 (1978).
- [7] A. Wokaun and R.R. Ernst, J. Chem. Phys., 67, 1752 (1977).
- [8] G.J. Bowden and W.D. Hutchison, J. Magn. Reson., 67, 403 (1986).
- [9] G.J. Bowden, W.D. Hutchison and J. Khachan, J. Magn. Reson., 67, 415 (1986).
- [10] G.J. Bowden and W.D. Hutchison, J. Magn. Reson., 70, 361 (1986).
- [11] G.J. Bowden and W.D. Hutchison, J. Magn. Reson., 71, 61 (1987).
- [12] a) A.R. Edmonds, "Angular Momentum in Quantum Mechanics", Princeton Univ. Press, Princeton, N.J. (1957).
b) M.E. Rose, "Elementary Theory of Angular Momentum", John Wiley, New York (1967).
c) H.A. Buckmaster, R. Chatterjee and Y.H. Shing, Phys. Status Solidi, 13, 9 (1972).

- [13] W.D. Hutchison, Ph.D. Thesis, University of New South Wales, New South Wales, Australia (1987).
- [14] A.K. Saha and T.P. Das, "Theory and Applications of Nuclear Induction", Saha Institute of Nuclear Physics, Calcutta (1957).
- [15] T.P. Das and E.L. Hahn, "Solid State Physics", Suppl. I, Academic Press (1958).
- [16] M. Bloom, E.L. Hahn and B. Herzog, Phys. Rev., 97, 1699 (1955).

CHAPTER III

APPLICATION OF TENSOR OPERATOR
FORMALISM FOR THE STUDY OF ZEEMAN
PERTURBED SPIN ECHO ENVELOPE MODULA
TIONS IN SPIN $I = 3/2$ NUCLEI

This chapter deals with the theoretical investigation of Zeeman-perturbed spin echo envelope modulations (ZSEEM) in spin $I = 3/2$ nuclei in polycrystalline specimens. It consists of two sections. Section III.A presents a brief discussion on spin echo envelope modulations while section III.B outlines the details of the calculation of ZSEEM function for the case of spin $I = 3/2$ using tensor operator formalism.

III.A ZEEMAN-PERTURBED SPIN ECHO ENVELOPE MODULATIONS

The parameters that characterize the NQR spectrum are the quadrupole coupling constant (e^2qQ) and the asymmetry parameter η of the efg. As has been pointed out in Chapter I, in the case of the nuclei with spin $I = 3/2$ in the absence of a Zeeman field there is only one transition with a frequency

$$\omega_q = \frac{e^2qQ}{2} (1 + \eta^2/3)^{1/2} \quad \dots \text{(III.1)}$$

Between the pairs of doubly degenerate energy levels. Hence, it is not possible to obtain both the quadrupole interaction parameters e^2qQ and η by measuring ω_q alone. It is necessary to apply a weak Zeeman field to lift the degeneracies of the energy levels and then the resulting four transition frequencies (see Fig. III.1) can be used for the determination of both these parameters [1,2].

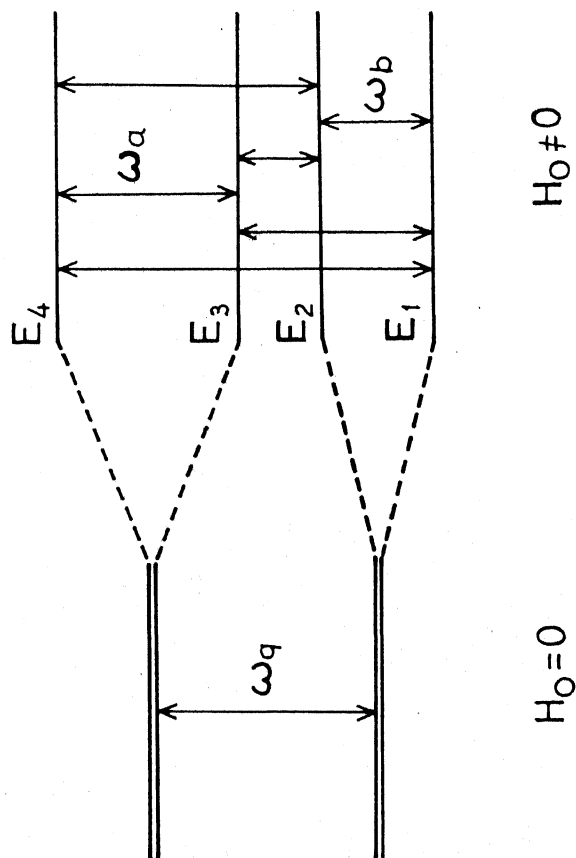


Fig.III.1 The energy level diagram of spin $I = 3/2$ nucleus in the presence of a weak Zeeman Field.

Zeeman NQR spectroscopy has been used to obtain these interaction parameters in single crystals [3] as well as in powder samples [4-6].

The ZSEEM method is ideally suited for obtaining η using pulsed NQR spectroscopy. One can employ both two-pulse and stimulated echo sequences for this study. However, we confine ourselves, in this chapter, to two-pulse SEEM. Spin echo envelope modulation techniques are well known in the area of ESR spectroscopy [7]. The energy level diagram of a Zeeman-perturbed quadrupolar nucleus with spin $I = 3/2$ is given in Fig. III.1. A coherent pulse excitation of all branching transitions would lead to modulations of spin echo signals and the echo amplitude $\mathcal{E}(2\tau)$ plotted as a function of τ , the interval between the two pulses will exhibit modulations (see Fig. III.2). The frequencies of these modulations correspond to the Zeeman splittings in steady-state experiments. The echo envelope modulations can be seen even when the modulations on the FID and spin echo signals are damped down due to static inhomogeneities. Since the energy levels of a Zeeman-perturbed quadrupolar nucleus are η -dependent the Zeeman perturbed spin echo envelope modulations (ZSEEM) function $\mathcal{E}(2\tau)$ is expected to contain information on η . $\mathcal{E}(2\tau)$ also depends on θ and ϕ which define the mutual orientation of the external fields and the principal axes of the efg tensor, owing to the dependence of the various energy levels and the transition probabilities on these angles.

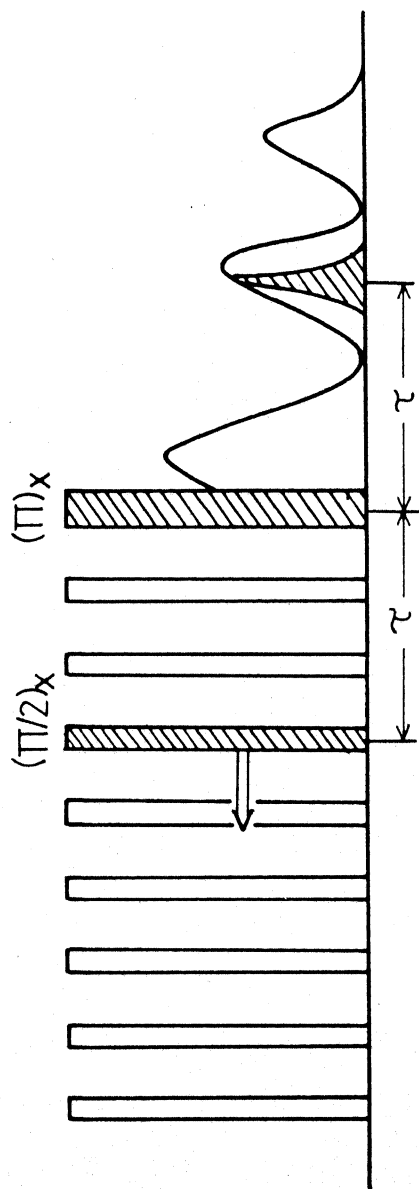


Fig. III.2 Two-pulse spin-echo envelope modulation experiment. The echo amplitude is monitored pointwise by incrementing τ from experiment to experiment.

In order to observe the Zeeman-perturbed spin echo envelope modulations the following conditions are to be satisfied. i) The Zeeman splittings, ω_a and ω_b (see Fig. III.1) are larger than the frequency width of the spin packets that make up the inhomogeneously broadened NQR line. ii) The r.f. field should satisfy the condition $\gamma H_1 \gg \omega_a$ and ω_b . The first condition ensures the occurrence of several modulation periods within the echo decay time while the latter ensures the excitation of all the branching transitions.

There have been several reports in the literature regarding the ZSEEM patterns for spin $I = 3/2$ nuclei in polycrystalline samples [8-12]. Ramachandran and Narasimhan [11] have given a more general analysis of ZSEEM patterns. In their approach, they have followed the evolution of the density matrix of the spin system by matrix transformation of the density matrix following r.f. pulses and during evolution periods and obtained an expression for ZSEEM function, $\varepsilon(2\tau)$. They have computer simulated the average value of this function, $\overline{\varepsilon(2\tau)}$, over complete (θ, ϕ) space, for various values of H_0 and η and compared the simulated ZSEEM patterns with those obtained experimentally for polycrystalline samples. Their study shows that $\varepsilon(2\tau)$ contains the frequency components ω_a , ω_b , $(\omega_a + \omega_b)$ and $(\omega_a - \omega_b)$ (see Fig. III.1) contrary to the earlier reports in the literature. The sensitivity of $\varepsilon(2\tau)$ to η is clearly reflected in the ZSEEM patterns obtained by them.

Recently, Narsimha Reddy and Narasimhan [13] have implemented the extended time excitation technique due to Schweiger et al. [14] in pure NQR to obtain ZSEEM pattern in a single short experiment.

Before presenting the theoretical analysis, we illustrate here, with some experimental recordings, the nature of ZSEEM patterns. In a two-pulse ZSEEM experiment, the echo amplitude is sampled as a function of τ , the pulse separation, to obtain the echo envelope. Since in the presence of a weak Zeeman field the echo amplitude gets modulated the echo envelope also shows modulations (see Fig. II.2). Figures III.3(a) and III.3(b) show the experimental ZSEEM patterns obtained from ^{35}Cl in polycrystalline sample of AgClO_3 . From these recordings it can be seen that the modulation period decreases as the strength of the magnetic field increases. The overall decay of echo envelope modulation is due to the spin-spin relaxation processes. If this experiment has to be done by manually varying τ and sampling the echo amplitude, mostly by a boxcar, it would take more than an hour. The ZSEEM patterns shown in Figs. III.3(a) & III.3(b) were obtained using a microprocessor-controlled pulsed NQR spectrometer described earlier (see Sec. I.C.3). In the ZSEEM experiment, with this spectrometer, the generation of two pulse sequence and incrementation of τ was done by microprocessor under software control. For each τ value the complete echo has been acquired into the signal analyzer. The echo maximum points have been chosen, off-line, with the help of a BASIC program to obtain ZSEEM pattern. Thus, with

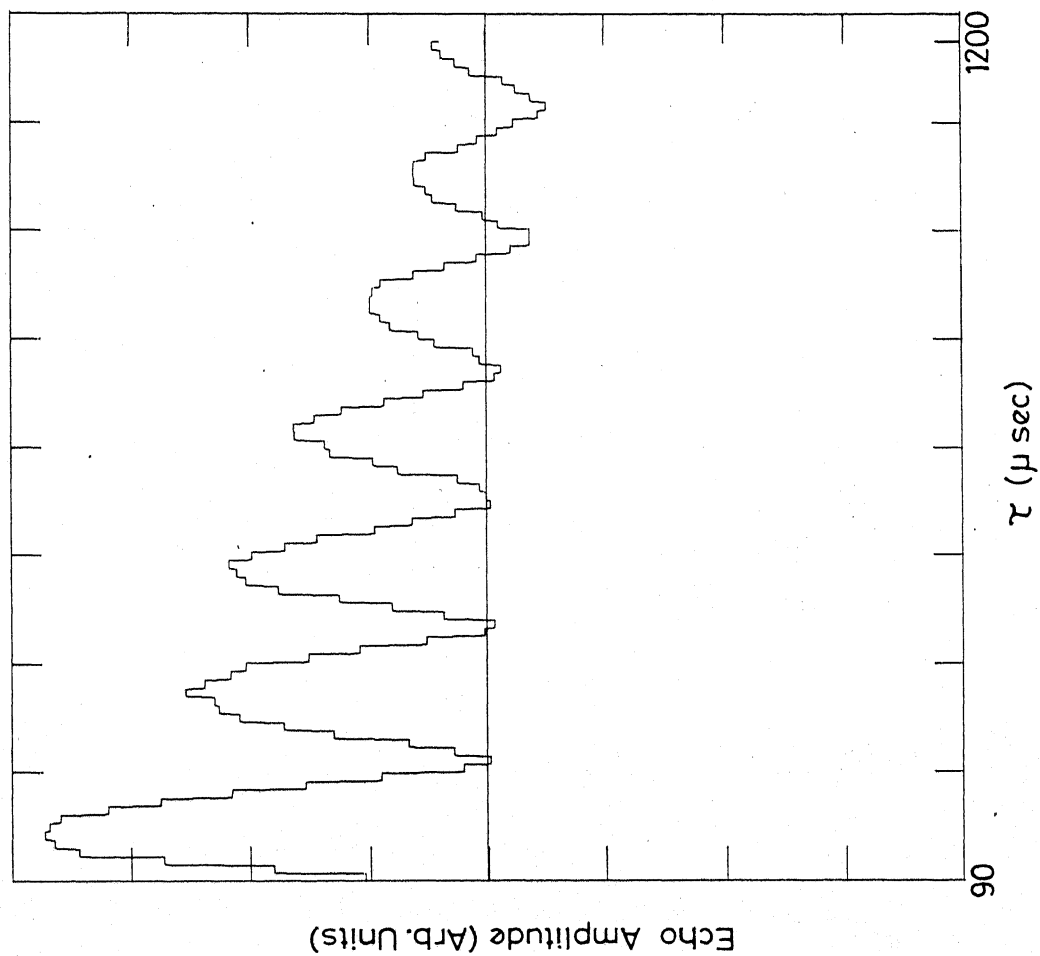


Fig.III-3(a) Experimental ZSEEM Pattern from ^{35}Cl in poly-crystalline sample of AgClO_3 ($\nu=28.851$ MHz) with a magnetic field of ≈ 9.75 Gauss.

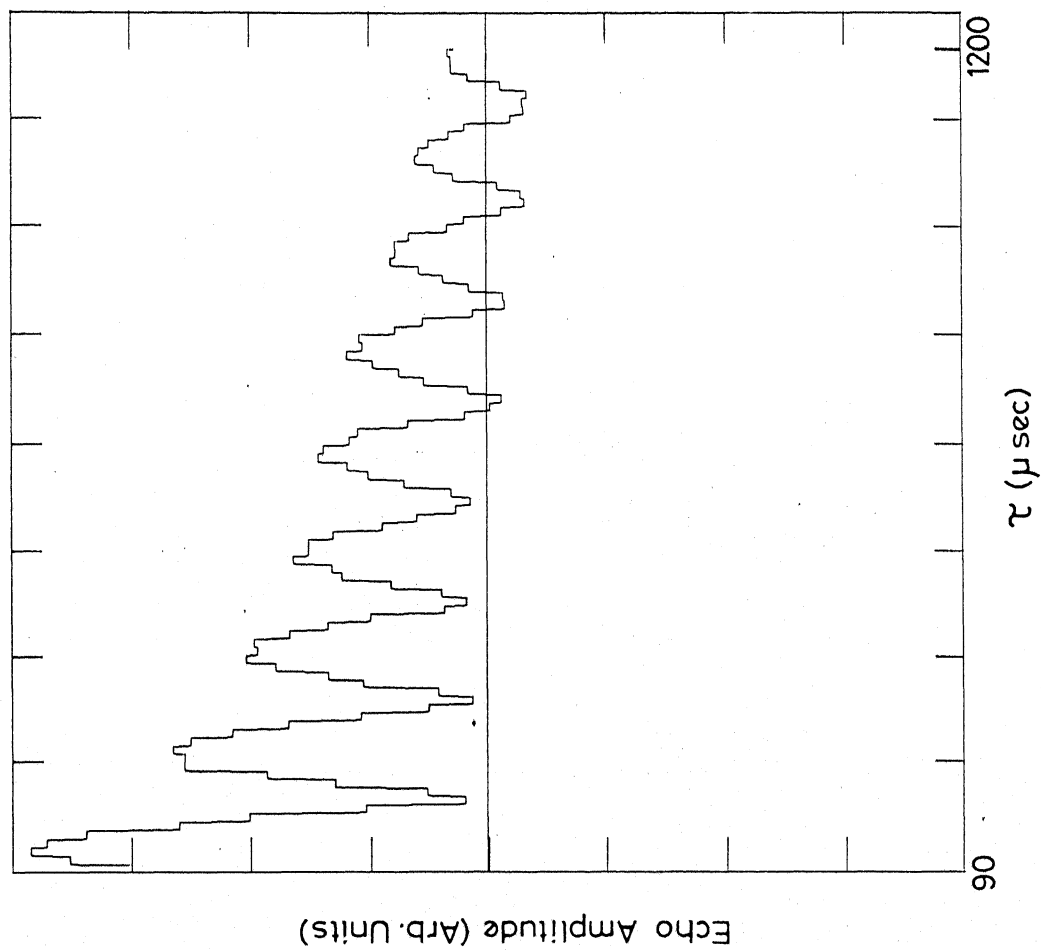


Fig.III-3(b) Experimental ZSEEM Pattern from ^{35}Cl in poly-crystalline sample of AgClO_3 ($\nu = 28.851$ MHz) with a magnetic field of ≈ 13 Gauss.

this spectrometer a complete ZSEEM pattern can be obtained in about 10 minutes.

The application of tensor operator formalism [15-20] for obtaining the two-pulse ZSEEM pattern for spin $I = 3/2$ nuclei in polycrystalline samples will be discussed in the next section.

III.B THEORETICAL INVESTIGATION OF ZSEEM USING TENSOR OPERATOR FORMALISM

III.B.1 Eigen Values of Spin $I = 3/2$ Nuclei with Non-axial Field Gradients, in the Presence of a Weak Zeeman Field

The net Hamiltonian in the laboratory frame for a spin $I = 3/2$ nucleus in a non-axially symmetric electric field gradient and in the presence of a Zeeman field can be written as

$$\mathcal{H} = \mathcal{H}_Q + \mathcal{H}_Z \quad \dots (III.2)$$

$$\text{where } \mathcal{H}_Q = \frac{e^2 q Q}{4I(2I-1)} [3 \tilde{I}_Z^2 - \tilde{I}^2 + \eta(\tilde{I}_X^2 - \tilde{I}_Y^2)] \quad \dots (III.3)$$

is the quadrupolar Hamiltonian and

$$\begin{aligned} \mathcal{H}_Z &= -\gamma H_0 \hbar \cdot \tilde{I} \\ &= -\gamma H_0 \cdot [\tilde{I}_X \sin\theta \cos\phi + \tilde{I}_Y \sin\theta \sin\phi + \tilde{I}_Z \cos\theta] \end{aligned} \quad \dots (III.4)$$

is the Hamiltonian corresponding to the interaction of the nucleus with the Zeeman field which is applied in a direction with polar coordinates (θ, ϕ) in the principal axes system of efg. I is the nuclear spin, γ is the gyromagnetic ratio of the nucleus and H_0 is the applied magnetic field strength. If H_0 is zero, there are two pairs of doubly generate energy levels for $I = 3/2$, which are given by

$$E_{1,2} = -\left(\frac{e^2 q Q}{4}\right) \wp \quad \dots (III.5)$$

$$E_{3,4} = \left(\frac{e^2 q Q}{4}\right) \wp \quad \dots (III.6)$$

$$\text{where } \wp = (1 + \eta^2/3)^{1/2} \quad \dots (III.7)$$

The transition frequency between these energy levels is

$$\nu_Q = \nu'_Q \wp = \frac{e^2 q Q}{2h} \wp \quad \dots (III.8)$$

In the presence of the magnetic field the energy levels are split depending upon the strength and the direction of H_0 relative to the principal axes of the crystalline efg. For arbitrary η values, assuming the magnetic field to be weak, i.e., $\hbar\omega_0 \ll e^2 q Q$, the energy levels can be obtained by treating the Zeeman term as a perturbation on the quadrupole levels. For arbitrary values of η the energy levels are given by [1,3]

$$E_{1,2} = -E_Q \pm \left[\frac{\hbar\omega_Q}{2\beta} \right] \left[(2-\beta)^2 \cos^2\theta + \sin^2\theta \{ (\beta+1)^2 + \eta^2 - 2(\beta+1) \cdot \right. \\ \left. \eta \cos(2\theta) \} \right]^{1/2} \quad \dots \text{(III.9)}$$

$$E_{3,4} = E_Q \pm \left[\frac{\hbar\omega_Q}{2\beta} \right] \left[(2+\beta)^2 \cos^2\theta + \sin^2\theta \{ (\beta-1)^2 + \eta^2 + 2(\beta-1) \cdot \right. \\ \left. \eta \cos(2\theta) \} \right]^{1/2} \quad \dots \text{(III.10)}$$

$$\text{where } E_Q = \frac{\hbar\omega_Q}{2} = \frac{e^2 g_Q}{2} \beta \quad \dots \text{(III.11)}$$

The energy levels diagram of a spin $I = 3/2$ nucleus, in the presence of a weak Zeeman field is shown in Fig. III.1.

In the following sub-section we present the explicit expressions for the interaction Hamiltonians, required for the discussion of ZSEEM.

III.B.2 Relevant Hamiltonians

III.B.2(i) r.f. Hamiltonian:

We are interested in the calculation of the pulse responses of spin $I = 3/2$ nuclear spin system for the case $H_0 \parallel H_1$ and for an arbitrary orientation of these fields relative to the efg principal axes system. The r.f. Hamiltonian for this case is

$$\mathcal{H}_1(t) = -2\omega_1 \hbar \cos(\omega_Q t) [I_x \sin\theta \cos\phi + I_y \sin\theta \sin\phi \\ + I_z \cos\theta] \quad \dots \text{(III.12)}$$

The frequency of the r.f. field is chosen to be equal to ω_Q ,

the resonance frequency in the absence of the Zeeman field. In the above eqn. θ and ϕ are the polar and azimuthal angles of the r.f. field vector in the principal axes system and $\omega_1 = \gamma H_1$,

$$\omega_q = \omega_Q \rho.$$

where γ is the gyromagnetic ratio of the nucleus

H_1 is the amplitude of the r.f. field

$$\text{and } \omega_Q = e^2 q Q / 2.$$

IIIB.2(ii) Total Hamiltonian in terms of tensor operators:

The total Hamiltonian in the presence of an r.f. field is given by

$$\mathcal{H}(t) = \mathcal{H}_Q + \mathcal{H}_Z + \mathcal{H}_1(t) \quad \dots \text{(III.13)}$$

where \mathcal{H}_Q , \mathcal{H}_Z & $\mathcal{H}_1(t)$ are given respectively by Eqns. III.3, III.4 and III.12. In terms of tensor operators (see Table II.1) these operators can be written as

$$\mathcal{H}_Q = \frac{\omega_Q}{\sqrt{6}} [\mathcal{T}_0^2 + \eta/\sqrt{3} \mathcal{T}_2^2(s)] \quad \dots \text{(III.14)}$$

$$\mathcal{H}_Z = -\omega_Q \hbar [-\mathcal{T}_1^1(a) P_1 + \mathcal{T}_1^1(s) P_2 + \mathcal{T}_0^1 P_3] \quad \dots \text{(III.15)}$$

$$\text{and } \mathcal{H}_1(t) = -2\omega_1 \hbar [\cos(\omega_q t)] [-\mathcal{T}_1^1(a) P_1 + \mathcal{T}_1^1(s) P_2 + \mathcal{T}_0^1 P_3] \quad \dots \text{(III.16)}$$

where $\omega_Q = \gamma H_Q$

$$P_1 = \sin\theta \cos\phi, P_2 = i \sin\theta \sin\phi, P_3 = \cos\theta \quad \dots \text{(III.17)}$$

III.B.2(iii) Total Hamiltonian in the 'Diagonal frame':

As pointed out in Chapter II, the pulse response calculations can be considerably simplified by working in a representation in which the quadrupolar Hamiltonian is diagonal. In all the subsequent calculations in this chapter we set $\hbar = 1$, and express energies in units of radians per sec. The transformation into the 'diagonal frame' can be effected by the operator defined by

$$U_d = \exp \left(\frac{2}{\sqrt{3}} \times T_2^3(a) \right) \quad \dots (III.18)$$

Making use of Table II.12 (see Chapter II) the total Hamiltonian in the 'diagonal frame' can be written as

$$\mathcal{H}^d(t) = U_d \mathcal{H}(t) U_d^{-1} = \mathcal{H}_Q^d + \mathcal{H}_Z^d + \mathcal{H}_1^d(t) \quad \dots (III.19)$$

$$\text{where } \mathcal{H}_Q^d = \frac{\omega_Q}{\sqrt{6}} T_0^2 \quad \dots (III.20)$$

$$\mathcal{H}_Z^d = -\omega_0 [J] \quad \dots (III.21)$$

$$\text{and } \mathcal{H}_1^d(t) = -2\omega_1 \cos(\omega_Q t) [J] \quad \dots (III.22)$$

$$\begin{aligned} \text{with } [J] = & -P_1 \{ a_1 T_1^1(a) + a_2 T_1^3(a) + a_3 T_3^3(a) \} \\ & + P_2 \{ a_4 T_1^1(s) + a_5 T_1^3(s) + a_6 T_3^3(s) \} \\ & + P_3 \{ a_7 T_0^1 + a_8 T_0^3 + a_9 T_2^3(s) \} \quad \dots (III.23) \end{aligned}$$

and $a_1 = a_4 = a_7 = \left(\frac{\rho+4}{5\rho}\right)$

$$a_2 = \frac{1}{3\sqrt{15}\rho} [3(1-\rho) + 5\eta]$$

$$a_3 = \frac{1}{3\rho} (\rho + \eta - 1)$$

$$a_5 = \frac{1}{3\sqrt{15}} [3(1-\rho) - 5\eta]$$

$$a_6 = \frac{1}{3\rho} [1 - \rho + \eta]$$

$$a_8 = -\frac{4}{3\sqrt{10}\rho} [1-\rho]$$

$$a_9 = -\frac{2\sqrt{2}}{3\sqrt{3}} \frac{\eta}{\rho} \quad \dots \text{(III.24)}$$

Since we will be doing all the spin dynamics calculations by following the density matrix of the spin system in the quadrupolar interaction representation (QIR) we now transform the total Hamiltonian in the 'diagonal frame', \mathcal{H}^d , into the QIR.

III.B.2(iv) Total Hamiltonian, $\mathcal{H}_1^d(t)$ in the quadrupolar interaction representation:

The total Hamiltonian in the 'diagonal frame', \mathcal{H}^d , can be transformed into the quadrupolar interaction representation by the transformation operator

$$U_Q = \exp(i\mathcal{H}_Q^d t) \quad \dots \text{(III.25)}$$

and is given by

$$\tilde{\mathcal{H}}^d(t) = U_Q \mathcal{H}^d(t) U_Q^{-1} = \tilde{\mathcal{H}}_Z^d + \tilde{\mathcal{H}}_1^d(t) \quad \dots \text{(III.26)}$$

where

$$\begin{aligned}
 \tilde{\mathcal{H}}_1^d(t) &= -2\omega_1 \cos(\omega_q t) U_q[J]U_q^{-1} \\
 \tilde{\mathcal{H}}_1^d &\approx \omega_1 \frac{1}{3\beta} [P_1\{(3+\eta)[\frac{3}{5} \tilde{T}_1^1(a) + \frac{2}{\sqrt{15}} \tilde{T}_1^3(a)]\} \\
 &\quad - P_2\{(3-\eta)[\frac{3}{5} \tilde{T}_1^1(s) + \frac{2}{\sqrt{15}} \tilde{T}_1^3(s)]\} \\
 &\quad + P_3\{+\frac{2\sqrt{2}}{\sqrt{3}}\eta [\tilde{T}_2^3(s)]\}] \quad \dots \text{(III.27)}
 \end{aligned}$$

$$\begin{aligned}
 \text{and } \tilde{\mathcal{H}}_2^d &= -\omega_o U_q[J]U_q^{-1} \\
 &\approx \omega_o \frac{1}{\beta} [P_1\{\frac{1}{5} [\beta + (1-\eta)] \tilde{T}_1^1(a) - \frac{1}{\sqrt{15}} [\beta + (1-\eta)] \tilde{T}_1^3(a) \\
 &\quad + \frac{1}{3} [\beta - (1-\eta)] \tilde{T}_3^3(a)\} \\
 &\quad - P_2\{\frac{1}{5} [\beta + (1+\eta)] \tilde{T}_1^1(s) - \frac{1}{\sqrt{15}} [\beta + (1+\eta)] \tilde{T}_1^3(s) \\
 &\quad + \frac{1}{3} [-\beta + (1+\eta)] \tilde{T}_3^3(s)\} \\
 &\quad - P_3\{\frac{1}{5} (\beta + 4) \tilde{T}_0^1 - \frac{4}{3\sqrt{10}} (-1 + \beta) \tilde{T}_0^3\}] \quad \dots \text{(III.28)}
 \end{aligned}$$

In arriving at Eqns. III.27 and III.28 we have made use of Table III.1 which gives the evolution of tensor operators under the influence of the quadrupolar interaction \mathcal{H}_Q^d . As usual, high frequency terms have been dropped since they are non-secular terms.

In order to calculate the pulse responses by studying the time evolution of the density matrix in QIR following the r.f. pulses and during the evolution under the Zeeman interaction we

Table III.1. The Evolution of the Tensor Operators $T_q^n(s, a)$
 Under a Quadrupolar Interaction $\tilde{\mathcal{H}}_Q^d = \frac{\omega_Q}{\sqrt{6}} T_0^2$
 for $I = 3/2$

$$U_q T_1^1(s) U_q^{-1} = T_1^1(s) \left[\frac{3}{5} \cos(\omega_q t) + \frac{2}{5} \right] \\
- i T_1^2(a) \frac{1}{\sqrt{2}} \sin(\omega_q t) + T_1^3(s) \frac{2}{\sqrt{15}} [\cos(\omega_q t) - 1]$$

$$U_q T_1^2(s) U_q^{-1} = -i T_1^1(a) \left[\frac{3\sqrt{2}}{5} \sin(\omega_q t) \right] + T_1^2(s) \cos(\omega_q t) \\
- i T_1^3(a) \frac{2\sqrt{2}}{\sqrt{15}} \sin(\omega_q t)$$

$$U_q T_2^2(s) U_q^{-1} = T_2^2(s) \cos(\omega_q t) - i T_2^3(a) \frac{2}{\sqrt{3}} \sin(\omega_q t)$$

$$U_q T_1^3(s) U_q^{-1} = T_1^1(s) \frac{3}{5} \sqrt{\frac{3}{5}} [\cos(\omega_q t) - 1] \\
- i T_1^2(a) \frac{\sqrt{3}}{\sqrt{10}} \sin(\omega_q t) + T_1^3(s) \left[\frac{2}{5} \cos(\omega_q t) + \frac{3}{5} \right]$$

$$U_q T_2^3(s) U_q^{-1} = -i T_2^2(a) \frac{\sqrt{3}}{2} \sin(\omega_q t) + T_2^3(s) \cos(\omega_q t)$$

where $U_q = \exp(-i \tilde{\mathcal{H}}_Q^d t)$

For the antisymmetric combinations $T_q^n(a, s)$ replace s
 by a and a by s in the above equations. $\omega_q = \frac{e^2 q Q}{2} (1 + \frac{\eta^2}{3})^{1/2}$;
 T_0^1 , T_0^2 , $T_3^3(s)$ and $T_3^3(a)$ all commute with the Hamiltonian.

need to know the time evolution of the tensor operators under the r.f. Hamiltonian $\tilde{\mathcal{H}}_1^d$ and $\tilde{\mathcal{H}}_z^d$ respectively. In what follows we present the calculation of the time evolution of tensor operators under these interactions.

III.B.3 The Evolution of Tensor Operators Under the Influence of the Hamiltonian $\tilde{\mathcal{H}}_1^d$

In order to evaluate the time evolution of tensor operators under the influence of any interaction characterized by an Hamiltonian, first of all one has to establish the commutation relationships of the tensor operators with that Hamiltonian. One may use either the technique of "nested commutation relationships" [19] or the "harmonics of the motion method" to arrive at the evolution of tensor operators under that Hamiltonian. The commutation relationships between the Hamiltonian $\tilde{\mathcal{H}}_1^d$ and the tensor operators can be grouped into two distinct sets. It is noted that these two sets do not mix, in the sense that commutation of any member of a given set with the Hamiltonian $\tilde{\mathcal{H}}_1^d$ produces only members of that set. The set which is relevant for the present calculations is given in Table III.2. The time evolution of a few related tensor operators under the action of $\tilde{\mathcal{H}}_1^d$ calculated using the 'nested commutation relationships' is given in Table III.3.

Table III.2. The Commutation Relationships of a few Selected
Tensor Operators with the Hamiltonian $\tilde{\mathcal{H}}_1^d$ for
 $I = 3/2$

$$[\tilde{\mathcal{H}}_1^d, \tilde{T}_0^2] = \omega_1 \frac{1}{\sqrt{3}\rho} [-P_1 \tilde{T}_1^2(s)(3+\eta) + P_2 \tilde{T}_1^2(a)(3-\eta) - P_3 \tilde{T}_2^2(a) 2\eta]$$

$$[\tilde{\mathcal{H}}_1^d, \tilde{T}_1^2(s)] = \omega_1 \frac{1}{\sqrt{3}\rho} [-P_1 \tilde{T}_0^2(3+\eta)]$$

$$[\tilde{\mathcal{H}}_1^d, \tilde{T}_1^2(a)] = \omega_1 \frac{1}{\sqrt{3}\rho} [-P_2 \tilde{T}_0^2(3-\eta)]$$

$$[\tilde{\mathcal{H}}_1^d, \tilde{T}_2^2(a)] = \omega_1 \frac{1}{\sqrt{3}\rho} [-P_3 2\eta \tilde{T}_0^2]$$

$$[\tilde{\mathcal{H}}_1^d, \tilde{T}_2^2(s)] = 0$$

$$\begin{aligned} \text{where } \tilde{\mathcal{H}}_1^d = \omega_1 \frac{1}{3\rho} \{ & P_1(3+\eta) \left[\frac{3}{5} \tilde{T}_1^1(a) + \frac{2}{\sqrt{15}} \tilde{T}_1^3(a) \right] \\ & - P_2(3-\eta) \left[\frac{3}{5} \tilde{T}_1^1(s) + \frac{2}{\sqrt{15}} \tilde{T}_1^3(s) \right] \\ & + P_3 \frac{2\sqrt{2}}{\sqrt{3}} \eta [\tilde{T}_2^3(s)] \} \end{aligned}$$

$$P_1 = \cos\theta \sin\phi$$

$$P_2 = i \sin\theta \sin\phi$$

$$P_3 = \cos\theta$$

$$\rho = (1 + \eta^2/3)^{1/2}$$

Table III.3. The Evolution of a few Selected Tensor Operators
Under the Influence of the Hamiltonian $\tilde{\mathcal{H}}_1^d$ *

$$U \tilde{T}_0^2 U^{-1} = \tilde{T}_0^2 \cos \xi + i \sin \xi [C_1 \tilde{T}_1^2(s) + C_2 \tilde{T}_1^2(a) + C_3 \tilde{T}_2^2(a)]$$

$$U \tilde{T}_1^2(s) U^{-1} = \tilde{T}_1^2(s) + (\cos \xi - 1) [C_1^2 \tilde{T}_1^2(s) + C_1 C_2 \tilde{T}_1^2(a) + C_1 C_3 \tilde{T}_2^2(a)] + i C_1 \tilde{T}_0^2 \sin \xi$$

$$U \tilde{T}_1^2(a) U^{-1} = \tilde{T}_1^2(a) + (\cos \xi - 1) [-C_1 C_2 \tilde{T}_1^2(s) - C_2^2 \tilde{T}_1^2(a) - C_2 C_3 \tilde{T}_2^2(a)] - i C_2 \tilde{T}_0^2 \sin \xi$$

$$U \tilde{T}_2^2(a) U^{-1} = \tilde{T}_2^2(a) + (\cos \xi - 1) [C_1 C_3 \tilde{T}_1^2(s) + C_2 C_3 \tilde{T}_1^2(a) + C_3^2 \tilde{T}_2^2(a)] + i C_3 \tilde{T}_0^2 \sin \xi$$

$$U \tilde{T}_2^2(s) U^{-1} = \tilde{T}_2^2(s)$$

where $U = \exp(-i \tilde{\mathcal{H}}_1^d t_w)$

$$C_1 = \frac{P_1(3+\eta)}{\sqrt{3} \rho x}, \quad C_2 = \frac{-P_2(3-\eta)}{\sqrt{3} \rho x}, \quad C_3 = \frac{2\eta P_3}{\sqrt{3} \rho x}$$

$$x = \left[\frac{1}{(3+\eta^2)} [\sin^2 \theta \{ (9+\eta^2) - 6\eta \cos 2\theta \} + 4\eta^2 \cos^2 \theta] \right]^{1/2}$$

$$\xi = x \omega_1 t_w$$

* $\tilde{\mathcal{H}}_1^d$ is defined in Table III.2.

III.B.4 The Evolution of Tensor Operators Under the Influence of the Hamiltonian $\tilde{\mathcal{H}}_z^d$

In this case also the commutation relationships between tensor operators and $\tilde{\mathcal{H}}_z^d$ can be grouped into two distinct sets. The commutation relationships of the tensor operators in one of the two sets with $\tilde{\mathcal{H}}_z^d$ are presented in Table III.4. From this table it is clear that the operators in this set cannot be divided, any further into sub-groups such that commutation of $\tilde{\mathcal{H}}_z^d$ with any linear combination of the first sub-group produces a linear combination of the second sub-group and vice-versa. Hence, it is not possible to evaluate the time evolution of these operators under the action of $\tilde{\mathcal{H}}_z^d$ using the 'harmonics of the motion method'. Also, it is rather difficult to get closed-form expressions for the time evolution of these operators using the technique of 'nested commutation relationships'. However, if we set $\theta = 0$, then from Table III.4 it is evident that the commutation relationships can be divided into two sub-groups which enable one to use the 'harmonics of the motion method' to evaluate the time evolution of the tensor operators in this particular case. The time evolution of this set of tensor operators in this particular case are given in Table III.5.

Since neither of the two methods discussed above could be used for the calculation of time evolution of the tensor operators under the action of $\tilde{\mathcal{H}}_z^d$ (see Eqn. III.28) we have resorted to the matrix multiplication approach for this purpose. First

Table III.4. The Commutation Relationships of a few Selected Tensor Operators with the Hamiltonian $\tilde{\mathcal{H}}_z^d$

$$[\tilde{\mathcal{H}}_z^d, \tilde{T}_1^2(s)] = \omega_0 [-P_1 \tilde{T}_2^2(s) \frac{(1-\eta)}{\rho} - P_2 \tilde{T}_2^2(a) - P_3 \tilde{T}_1^2(a)]$$

$$[\tilde{\mathcal{H}}_z^d, \tilde{T}_1^2(a)] = \omega_0 [-P_1 \tilde{T}_2^2(a) + P_2 \tilde{T}_2^2(s) \frac{(1+\eta)}{\rho} - P_3 \tilde{T}_1^2(s)]$$

$$[\tilde{\mathcal{H}}_z^d, \tilde{T}_2^2(s)] = \omega_0 [-P_1 \tilde{T}_1^2(s) \frac{(1-\eta)}{\rho} - P_2 \tilde{T}_1^2(a) \frac{(1+\eta)}{\rho} - P_3 \tilde{T}_2^2(a) \frac{2}{\rho}]$$

$$[\tilde{\mathcal{H}}_z^d, \tilde{T}_2^2(a)] = \omega_0 [-P_1 \tilde{T}_1^2(a) - P_2 \tilde{T}_1^2(s) - P_3 \tilde{T}_2^2(s) \frac{2}{\rho}]$$

where $\omega_0 = \gamma H_0$

$$\begin{aligned} \tilde{\mathcal{H}}_z^d = \omega_0 \frac{1}{\rho} [& P_1 \{ \frac{1}{5} [\rho + (1-\eta)] \tilde{T}_1^1(a) - \frac{1}{\sqrt{15}} [\rho + (1-\eta)] \tilde{T}_1^3(a) \\ & + \frac{1}{3} [\rho - (1-\eta)] \tilde{T}_3^3(a) \} \\ & - P_2 \{ \frac{1}{5} [\rho + (1-\eta)] \tilde{T}_1^1(s) - \frac{1}{\sqrt{15}} [\rho + (1-\eta)] \tilde{T}_1^3(s) \\ & + \frac{1}{3} [-\rho + (1+\eta)] \tilde{T}_3^3(s) \} \\ & - P_3 \{ \frac{1}{5} (\rho + 4) \tilde{T}_0^1 - \frac{4}{3\sqrt{10}} (-1 + \rho) \tilde{T}_0^3 \}] \end{aligned}$$

P_1, P_2, P_3 and ρ are defined in Table III.2

Table III.5. The Evolution of a few Selected Tensor Operators
Under the Influence of $\tilde{\mathcal{H}}_Z^d$ for $I = 3/2$

$$\begin{aligned} U_Z T_{\sim 1}^2(s) U_Z^{-1} = & T_{\sim 1}^2(s) \left[-\frac{h_2}{h_3} \cos(Rt) + \frac{h_1}{h_3} \cos(St) \right] \\ & - T_{\sim 2}^2(a) \left[\frac{h_1 h_2}{gh_3} (\cos(Rt) - \cos(St)) \right] \\ & + i \{ T_{\sim 1}^2(a) \left[\frac{e_1 h_2}{gh_3} \sin(Rt) - \frac{e_2 h_1}{gh_3} \sin(St) \right] \} \\ & + T_{\sim 2}^2(s) \left[\frac{f_1 h_2}{gh_3} \sin(Rt) - \frac{f_2 h_1}{gh_3} \sin(St) \right] \}; \end{aligned}$$

$$\begin{aligned} U_Z T_{\sim 1}^2(a) U_Z^{-1} = & T_{\sim 1}^2(a) \left[\frac{e_1 f_2}{f_3} \cos(Rt) - \frac{e_2 f_1}{f_3} \cos(St) \right] \\ & + T_{\sim 2}^2(s) \left[\frac{f_1 f_2}{f_3} (\cos(Rt) - \cos(St)) \right] \\ & - i \{ T_{\sim 1}^2(s) \left[\frac{gf_2}{f_3} \sin(Rt) - \frac{gf_1}{f_3} \sin(St) \right] \} \\ & + T_{\sim 2}^2(a) \left[\frac{f_2 h_1}{f_3} \sin(Rt) - \frac{f_1 h_2}{f_3} \sin(St) \right] \}; \end{aligned}$$

$$\begin{aligned} U_Z T_{\sim 2}^2(a) U_Z^{-1} = & T_{\sim 1}^2(s) \frac{g}{h_3} [\cos(Rt) - \cos(St)] \\ & + T_{\sim 2}^2(a) \left[\frac{h_1}{h_3} \cos(Rt) - \frac{h_2}{h_3} \cos(St) \right] \\ & - i \{ T_{\sim 1}^2(a) \left[\frac{e_1}{h_3} \sin(Rt) - \frac{e_2}{h_3} \sin(St) \right] \} \\ & + T_{\sim 2}^2(s) \left[\frac{f_1}{h_3} \sin(Rt) - \frac{f_2}{h_3} \sin(St) \right] \}; \end{aligned}$$

...contd.

Table III.5 (contd.)

$$\begin{aligned}
 U_Z T_2^2(s) U_Z^{-1} = & - T_1^2(a) \frac{e_1 e_2}{f_3} [\cos(Rt) - \cos(St)] - T_2^2(s) \left[\frac{f_1 e_2}{f_3} \cos(Rt) \right. \\
 & \left. - \frac{f_2 e_1}{f_3} \cos(St) \right] - i \{ T_1^2(s) \left[\frac{g e_2}{f_3} \sin(Rt) - \frac{e_1 g}{f_3} \sin(St) \right] \\
 & + T_2^2(a) \left[\frac{h_1 e_2}{f_3} \sin(Rt) - \frac{h_2 e_1}{f_3} \sin(St) \right] \}
 \end{aligned}$$

$$U_Z T_0^2 U_Z^{-1} = T_0^2$$

In this table the following definitions hold:

$$U_Z = \exp(-i \tilde{\mathcal{H}}_Z^d t)$$

$$\begin{aligned}
 \tilde{\mathcal{H}}_Z^d = \omega_0 \frac{1}{f} [& P_1 \{ \frac{1}{5} [\rho + (1-\eta)] T_1^1(a) - \frac{1}{\sqrt{15}} [\rho + (1-\eta)] T_1^3(a) \\
 & + \frac{1}{3} [\rho - (1-\eta)] T_3^3(a) \}
 \end{aligned}$$

$$- P_3 \{ \frac{1}{5} [\rho + 4] T_0^1 - \frac{4}{3\sqrt{10}} [1-\rho] T_0^3 \}]$$

$$P_1 = \sin\theta, P_3 = \cos\theta, a_1 = \frac{1}{f} (1-\eta), c_1 = \frac{2}{f}$$

$$K_{1,2} = \frac{1}{2} [\{ P_1^2 (1+a_1^2) + P_3^2 (1+c_1^2) \} \pm \sqrt{\{ [P_1^2 (1+a_1^2) + P_3^2 (1+c_1^2)]^2 - 4(P_1^2 a_1^2 - P_3^2 c_1^2) \}}]$$

$$r_1 = \sqrt{K_1}, r_2 = \sqrt{K_2}, R = r_1 \omega_0, S = r_2 \omega_0, \omega_0 = \gamma H_0$$

$$g = P_1 P_3 (1+a_1 c_1), h_{1,2} = [(P_3^2 + a_1^2 P_1^2) - K_{1,2}]$$

$$e_{1,2} = -[P_3 g + P_1 h_{1,2}] / \sqrt{K_{1,2}}$$

$$f_{1,2} = -[P_1 a_1 g + P_3 c_1 h_{1,2}] / \sqrt{K_{1,2}}, h_3 = (h_1 - h_2)$$

$$f_3 = e_1 f_2 - e_2 f_1$$

we have converted the $\tilde{\mathcal{H}}_z^d$ into its equivalent matrix form (see Table III.6 for the matrix representation of tensor operators), which is given by

$$\tilde{\mathcal{H}}_z^d = \omega_o \begin{bmatrix} a & 0 & 0 & b \\ 0 & c & d & 0 \\ 0 & d^* & -c & 0 \\ b^* & 0 & 0 & -a \end{bmatrix} = \omega_o [B] \quad \dots (III.29)$$

where

$$\begin{aligned} a &= -1/2 P_3 \frac{(\rho+2)}{\rho} \\ b &= \frac{1}{2\rho} [-P_1\{\rho-(1-\eta)\} + P_2\{(1+\eta)-\rho\}] \\ b^* &= \frac{1}{2\rho} [-P_1\{\rho-(1-\eta)\} - P_2\{(1+\eta)-\rho\}] \\ c &= \frac{1}{2\rho} [P_3(\rho-2)] \\ d &= \frac{1}{2\rho} [-P_1\{\rho+(1-\eta)\} + P_2\{\rho+(1+\eta)\}] \\ d^* &= \frac{1}{2\rho} [-P_1\{\rho+(1-\eta)\} - P_2\{\rho+(1+\eta)\}] \end{aligned} \quad \dots (III.30)$$

Now, $U_z = \exp(-i \tilde{\mathcal{H}}_z^d t)$.. (III.31)

$$\begin{aligned} &= \exp(-i[B]\omega_o t) \\ &= \cos([B]\omega_o t) - i \sin([B]\omega_o t) \end{aligned}$$

Since we find

$$[B]^2 = \begin{bmatrix} k_1^2 & 0 & 0 & 0 \\ 0 & k_2^2 & 0 & 0 \\ 0 & 0 & k_2^2 & 0 \\ 0 & 0 & 0 & k_1^2 \end{bmatrix}$$

...contd.

Table III.6. Matrix Representation of Tensor Operators for Spin $I = 3/2$

$ \frac{3}{2}\rangle$	$ \frac{1}{2}\rangle$	$ \frac{1}{2}\rangle$	$ \frac{3}{2}\rangle$
$T_1^1(a) = -\frac{\sqrt{3}}{2} \begin{bmatrix} 0 & 1 & 0 & 0 \\ 1 & 0 & 2/\sqrt{3} & 0 \\ 0 & 2/\sqrt{3} & 0 & 1 \\ 0 & 0 & 1 & 0 \end{bmatrix}$	$T_1^1(s) = -\frac{\sqrt{3}}{2} \begin{bmatrix} 0 & -1 & 0 & 0 \\ 0 & 0 & -2/\sqrt{3} & 0 \\ 0 & 2/\sqrt{3} & 0 & 1 \\ 0 & 0 & 1 & 0 \end{bmatrix}$	$T_1^1 = \frac{3}{2} \begin{bmatrix} 1 & 0 & 0 & 0 \\ 0 & 1/3 & 0 & 0 \\ 0 & 0 & -1/3 & 0 \\ 0 & 0 & 0 & -1 \end{bmatrix}$	
$T_0^2 = \frac{\sqrt{6}}{2} \begin{bmatrix} 1 & 0 & 0 & 0 \\ 0 & -1 & 0 & 0 \\ 0 & 0 & -1 & 0 \\ 0 & 0 & 0 & 1 \end{bmatrix}$	$T_1^2(a) = \frac{\sqrt{6}}{2} \begin{bmatrix} 0 & -1 & 0 & 0 \\ -1 & 0 & 0 & 0 \\ 0 & 0 & 0 & 1 \\ 0 & 0 & 1 & 0 \end{bmatrix}$	$T_1^2(s) = \frac{\sqrt{6}}{2} \begin{bmatrix} 0 & -1 & 0 & 0 \\ 1 & 0 & 0 & 0 \\ 0 & 0 & 0 & 1 \\ 0 & 0 & -1 & 0 \end{bmatrix}$	
$T_2^2(a) = \frac{\sqrt{6}}{2} \begin{bmatrix} 0 & 0 & 1 & 0 \\ 0 & 0 & 0 & 1 \\ -1 & 0 & 0 & 0 \\ 0 & -1 & 0 & 0 \end{bmatrix}$	$T_2^2(s) = \frac{\sqrt{6}}{2} \begin{bmatrix} 0 & 0 & 1 & 0 \\ 0 & 0 & 0 & 1 \\ 1 & 0 & 0 & 0 \\ 0 & 1 & 0 & 0 \end{bmatrix}$	$T_0^3 = \frac{3}{2\sqrt{10}} \begin{bmatrix} 1 & 0 & 0 & 0 \\ 0 & -3 & 0 & 0 \\ 0 & 0 & 3 & 0 \\ 0 & 0 & 0 & -1 \end{bmatrix}$	
$T_1^3(a) = \frac{-3}{2\sqrt{5}} \begin{bmatrix} 0 & 1 & 0 & 0 \\ 1 & 0 & -\sqrt{3} & 0 \\ 0 & -\sqrt{3} & 0 & 1 \\ 0 & 0 & 1 & 0 \end{bmatrix}$	$T_1^3(s) = \frac{3}{2\sqrt{5}} \begin{bmatrix} 0 & -1 & 0 & 0 \\ 1 & 0 & \sqrt{3} & 0 \\ 0 & -\sqrt{3} & 0 & 1 \\ 0 & 0 & 1 & 0 \end{bmatrix}$	$T_2^3(a) = \frac{-3}{2\sqrt{2}} \begin{bmatrix} 0 & 0 & -1 & 0 \\ 0 & 0 & 0 & 1 \\ 1 & 0 & 0 & 0 \\ 0 & -1 & 0 & 0 \end{bmatrix}$	
$T_2^3(s) = \frac{3}{2\sqrt{2}} \begin{bmatrix} 0 & 0 & 1 & 0 \\ 0 & 0 & 0 & -1 \\ 1 & 0 & 0 & 0 \\ 0 & -1 & 0 & 0 \end{bmatrix}$	$T_3^3(a) = \frac{-3}{2} \begin{bmatrix} 0 & 0 & 0 & 1 \\ 0 & 0 & 0 & 0 \\ 0 & 0 & 0 & 0 \\ 1 & 0 & 0 & 0 \end{bmatrix}$	$T_3^3(s) = \frac{3}{2} \begin{bmatrix} 0 & 0 & 0 & -1 \\ 0 & 0 & 0 & 0 \\ 0 & 0 & 0 & 0 \\ 1 & 0 & 0 & 0 \end{bmatrix}$	

$$[B]^3 = B[B]^2, [B]^4 = [[B]^2]^2$$

$$[B]^5 = B[B]^4, \dots$$

where $k_1^2 = a^2 + bb^*$

$$k_2^2 = c^2 + dd^*$$

$$k_1 = \frac{1}{2\varphi} [\cos^2\theta (2+\varphi)^2 + \{(\varphi-1)^2 + \eta^2 + 2(\varphi-1)\eta \cos 2\varnothing\} \sin^2\theta]^{1/2}$$

.. (III.32)

and

$$k_2 = \frac{1}{2\varphi} [\cos^2\theta (\varphi-2)^2 + \{(\varphi+1)^2 + \eta^2 - 2(\varphi+1)\eta \cos 2\varnothing\} \sin^2\theta]^{1/2}$$

.. (III.33)

U_z can be written in the matrix form, with the matrix elements given as follows:

$$[U_z(t)]_{11} = \cos(\omega_A t) - i \frac{a}{k_1} \sin(\omega_A t)$$

$$[U_z(t)]_{12} = [U_z(t)]_{13} = 0$$

$$[U_z(t)]_{14} = -i \frac{b}{k_1} \sin(\omega_A t)$$

$$[U_z(t)]_{21} = 0$$

$$[U_z(t)]_{22} = \cos(\omega_B t) - i \frac{c}{k_2} \sin(\omega_B t)$$

$$[U_z(t)]_{23} = -i \frac{d}{k_2} \sin(\omega_B t)$$

$$[U_z(t)]_{24} = 0$$

$$[U_z(t)]_{31} = 0$$

$$[U_z(t)]_{32} = -i \frac{d^*}{k_2} \sin(\omega_B t)$$

...contd.

$$[U_Z(t)]_{33} = \cos(\omega_B t) + i \frac{c}{k_2} \sin(\omega_B t)$$

$$[U_Z(t)]_{34} = 0$$

$$[U_Z(t)]_{41} = -i \frac{b^*}{k_1} \sin(\omega_A t)$$

$$[U_Z(t)]_{42} = [U_Z(t)]_{43} = 0$$

$$[U_Z(t)]_{44} = \cos(\omega_A t) + i \frac{a}{k_1} \sin(\omega_A t) \quad \dots (III.34)$$

$$\text{where } \omega_A = k_1 \omega_0 = \frac{\omega_a}{2}$$

$$\omega_B = k_2 \omega_0 = \frac{\omega_b}{2} \quad \dots (III.35)$$

Also, it can be seen that $U_Z U_Z^{-1} = \mathbb{1}$. Having obtained U_Z in the form of matrix, it is now straightforward to arrive at the time evolution of tensor operators. In calculating the evolution of tensor operators the expressions of the form

$$U_Z T_1^2(s) U_Z^{-1}$$

have been evaluated by multiplying the corresponding matrices. The resulting matrix has been converted back into equivalent tensor operators. The evolution of a few selected tensor operators obtained in this manner are tabulated in Table III.7. Having obtained the evolution of tensor operators under the action of $\tilde{\mathcal{H}}_1^d$ and $\tilde{\mathcal{H}}_Z^d$ the calculation of pulse responses is now straightforward.

Table III.7. The Evolution of a few Selected Tensor Operators
Under the Influence of the Hamiltonian $\tilde{\mathcal{H}}_z^d$

$$\begin{aligned}
 U_z T_{\sim 1}^2(s) U_z^{-1} = & T_{\sim 1}^2(s) [A_{11} \cos \frac{1}{2}(\omega_a - \omega_b)t] + A_{12} \cos[\frac{1}{2}(\omega_a + \omega_b)t] \\
 & + T_{\sim 1}^2(a) [A_{21} \{ \cos[\frac{1}{2}(\omega_a - \omega_b)t] - \cos[\frac{1}{2}(\omega_a + \omega_b)t] \} \\
 & \quad A_{22} \sin[\frac{1}{2}(\omega_a + \omega_b)t] + A_{23} \sin[\frac{1}{2}(\omega_a - \omega_b)t]] \\
 & + T_{\sim 2}^2(a) [A_{31} \{ \cos[\frac{1}{2}(\omega_a - \omega_b)t] - \cos[\frac{1}{2}(\omega_a + \omega_b)t] \} \\
 & \quad + A_{32} \{ \sin[\frac{1}{2}(\omega_a + \omega_b)t] \} + A_{33} \{ \sin[\frac{1}{2}(\omega_a - \omega_b)t] \}] \\
 & + T_{\sim 2}^2(s) [A_{41} \{ \cos[\frac{1}{2}(\omega_a - \omega_b)t] - \cos[\frac{1}{2}(\omega_a + \omega_b)t] \} \\
 & \quad + A_{42} \sin[\frac{1}{2}(\omega_a + \omega_b)t] + A_{43} \sin[\frac{1}{2}(\omega_a - \omega_b)t]] \\
 \\
 U_z T_{\sim 1}^2(a) U_z^{-1} = & T_{\sim 1}^2(s) [B_{11} \{ \cos[\frac{1}{2}(\omega_a - \omega_b)t] - \cos[\frac{1}{2}(\omega_a + \omega_b)t] \} \\
 & + B_{12} \{ \sin[\frac{1}{2}(\omega_a + \omega_b)t] \} + B_{13} \{ \sin[\frac{1}{2}(\omega_a - \omega_b)t] \}] \\
 & + T_{\sim 1}^2(a) [B_{21} \cos[\frac{1}{2}(\omega_a - \omega_b)t] + B_{22} \cos[\frac{1}{2}(\omega_a + \omega_b)t]] \\
 & + T_{\sim 2}^2(a) [B_{31} \{ \cos[\frac{1}{2}(\omega_a - \omega_b)t] - \cos[\frac{1}{2}(\omega_a + \omega_b)t] \} \\
 & \quad + B_{32} \sin[\frac{1}{2}(\omega_a + \omega_b)t] + B_{33} \sin[\frac{1}{2}(\omega_a - \omega_b)t]] \\
 & + T_{\sim 2}^2(s) [B_{41} \{ \cos[\frac{1}{2}(\omega_a - \omega_b)t] - \cos[\frac{1}{2}(\omega_a + \omega_b)t] \} \\
 & \quad + B_{42} \sin[\frac{1}{2}(\omega_a + \omega_b)t] + B_{43} \sin[\frac{1}{2}(\omega_a - \omega_b)t]]
 \end{aligned}$$

Table III.7 (contd.)

$$\begin{aligned}
U_z T_2^2(a) U_z^{-1} = & T_1^2(s) [D_{11} \{ \cos[\frac{1}{2} (\omega_a - \omega_b) t] - \cos[\frac{1}{2} (\omega_a + \omega_b) t] \} \\
& + D_{12} \sin[\frac{1}{2} (\omega_a + \omega_b) t] + D_{13} \sin[\frac{1}{2} (\omega_a - \omega_b) t]] \\
& + T_1^2(a) [D_{21} \{ \cos[\frac{1}{2} (\omega_a - \omega_b) t] - \cos[\frac{1}{2} (\omega_a + \omega_b) t] \} \\
& + D_{22} \sin[\frac{1}{2} (\omega_a + \omega_b) t] + D_{23} \sin[\frac{1}{2} (\omega_a - \omega_b) t]] \\
& + T_2^2(a) [D_{31} \cos[\frac{1}{2} (\omega_a + \omega_b) t] + D_{32} \cos[\frac{1}{2} (\omega_a - \omega_b) t]] \\
& + T_2^2(s) [D_{41} \{ \cos[\frac{1}{2} (\omega_a + \omega_b) t] - \cos[\frac{1}{2} (\omega_a - \omega_b) t] \} \\
& + D_{42} \sin[\frac{1}{2} (\omega_a + \omega_b) t] + D_{43} \sin[\frac{1}{2} (\omega_a - \omega_b) t]]
\end{aligned}$$

$$\begin{aligned}
U_z T_2^2(s) U_z^{-1} = & T_1^2(s) [G_{11} \{ \cos[\frac{1}{2} (\omega_a - \omega_b) t] - \cos[\frac{1}{2} (\omega_a + \omega_b) t] \} \\
& + G_{12} \sin[\frac{1}{2} (\omega_a + \omega_b) t] + G_{13} \sin[\frac{1}{2} (\omega_a - \omega_b) t]] \\
& + T_1^2(a) [G_{21} \{ \cos[\frac{1}{2} (\omega_a + \omega_b) t] - \cos[\frac{1}{2} (\omega_a - \omega_b) t] \} \\
& + G_{22} \sin[\frac{1}{2} (\omega_a + \omega_b) t] + G_{23} \sin[\frac{1}{2} (\omega_a - \omega_b) t]] \\
& + T_2^2(a) [G_{31} \{ \cos[\frac{1}{2} (\omega_a - \omega_b) t] - \cos[\frac{1}{2} (\omega_a + \omega_b) t] \} \\
& + G_{32} \{ \sin[\frac{1}{2} (\omega_a + \omega_b) t] \} + G_{33} \sin[\frac{1}{2} (\omega_a - \omega_b) t]] \\
& + T_2^2(s) [G_{41} \{ \cos[\frac{1}{2} (\omega_a + \omega_b) t] \} + G_{42} \cos[\frac{1}{2} (\omega_a - \omega_b) t]]
\end{aligned}$$

Table III.7 (contd.)

where $U_z = \exp(-i \tilde{\mathcal{H}}_z^d t)$

The Hamiltonian $\tilde{\mathcal{H}}_z^d$ is defined in Table III.4.

$$\begin{aligned}
 A_{11} &= (k_1 k_2 + 1 + ac)/2 \, k_1 k_2 \\
 A_{12} &= [k_1 k_2 - (1 + ac)]/2 \, k_1 k_2 \\
 A_{21} &= -B_{11} = m/2 \, k_1 k_2 \\
 A_{22} &= B_{12} = D_{43} = G_{33} = i(ck_1 - ak_2)/2 \, k_1 k_2 \\
 A_{23} &= B_{13} = D_{42} = G_{32} = -i(ck_1 + ak_2)/2 \, k_1 k_2 \\
 A_{31} &= D_{11} = (cs_1 - aq_1)/2 \, k_1 k_2 \\
 A_{32} &= -D_{12} = i(s_2 k_2 - q_2 k_1)/2 \, k_1 k_2 \\
 A_{33} &= -D_{13} = i(s_2 k_2 + q_2 k_1)/2 \, k_1 k_2 \\
 A_{41} &= -G_{11} = (cs_2 - aq_2)/2 \, k_1 k_2 \\
 A_{42} &= B_{33} = G_{12} = -D_{23} = i(s_1 k_2 - q_1 k_1)/2 \, k_1 k_2 \\
 A_{43} &= -B_{32} = G_{13} = -D_{22} = i(q_1 k_1 + s_1 k_2)/2 \, k_1 k_2 \\
 B_{21} &= (k_1 k_2 + ac - 1)/2 \, k_1 k_2 \\
 B_{22} &= (k_1 k_2 - (ac - 1))/2 \, k_1 k_2 \\
 B_{31} &= -D_{21} = [-(aq_2 + cs_2)]/2 \, k_1 k_2 \\
 B_{41} &= G_{21} = -(q_1 a + s_1 c)/2 \, k_1 k_2 \\
 B_{42} &= -G_{22} = -i(q_2 k_1 + s_2 k_2)/2 \, k_1 k_2 \\
 B_{43} &= G_{23} = -i(q_2 k_1 - s_2 k_2)/2 \, k_1 k_2 \\
 D_{31} &= (k_1 k_2 + ca + s_1 q_1 + s_2 q_2)/2 \, k_1 k_2 \\
 D_{32} &= [k_1 k_2 - (-ca + s_1 q_1 + s_2 q_2)]/2 \, k_1 k_2 \\
 D_{41} &= (s_1 q_1 + s_2 q_1)/2 \, k_1 k_2 \\
 G_{31} &= (s_1 q_2 + s_2 q_1)/2 \, k_1 k_2 \\
 G_{41} &= [k_1 k_2 - (-cs + s_1 q_1 + s_2 q_2)]/2 \, k_1 k_2 \\
 G_{42} &= [k_2 k_2 - ca + s_1 q_1 + s_2 q_2]/2 \, k_1 k_2
 \end{aligned}$$

...contd.

Table III.7 (contd.)

with

$$k_1 = \frac{1}{2\rho} [\cos^2 \theta (2+\rho)^2 + \{(\rho-1)^2 + \eta^2 + 2(\rho-1)\eta \cos 2\theta\} \sin^2 \theta]^{1/2}$$

$$k_2 = \frac{1}{2\rho} [\cos^2 \theta (\rho-2)^2 + \{(\rho+1)^2 + \eta^2 - 2(1+\rho)\eta \cos 2\theta\} \sin^2 \theta]^{1/2}$$

$$l = \frac{1}{4\rho^2} [P_1^2 \{\rho^2 - (1-\eta)^2\} + P_2^2 \{(1+\eta)^2 - \rho^2\}]$$

$$m = P_1 P_2 \frac{\eta}{2\rho}$$

$$q_1 = -\frac{1}{2\rho} P_1 [\rho + (1-\eta)]$$

$$q_2 = -\frac{1}{2\rho} P_2 [\rho + (1+\eta)]$$

$$s_1 = -\frac{1}{2\rho} P_1 [\rho - (1-\eta)]$$

$$s_2 = -\frac{1}{2\rho} P_2 [\rho - (1+\eta)]$$

P_1 , P_2 , P_3 and ρ are defined in Table III.2.

III.B.5 Evaluation of Two-Pulse Response: ZSEEM Pattern

We are interested in calculating the two-pulse response of non-interacting nuclei with spin $I = 3/2$ in polycrystalline samples in the presence of a weak Zeeman field. In all the calculations the relaxation effects and efg inhomogeneities are not considered.

We assume a configuration in which the Zeeman and r.f. fields are oriented parallel to each other and their axis is oriented randomly with respect to the principal axes of efg tensor. The total Hamiltonian for this situation is given in Eqn. III.13. In the quadrupolar interaction representation (see Eqn. III.25) the total Hamiltonian is given by Eqn. III.26.

As mentioned in the previous chapters of this thesis the two-pulse response in this case also can be obtained by following the time evolution of the density matrix under r.f. and Zeeman interactions in QIR. As the magnetic field is assumed to be weak, i.e., $\omega_0 \ll \omega_Q$, the thermal equilibrium reduced density matrix (see Chapter I, Section I.D.1) for this case also is given by

$$\rho(0) = T_0^2 \quad \dots \text{ (III.36)}$$

In QIR then

$$\tilde{\rho}(0) = \tilde{T}_0^2 \quad \dots \text{ (III.37)}$$

In the following calculations we neglect the effect of the Zeeman field during the time when pulse is 'on', assuming that

\mathcal{H}_z causes negligible precession of the spins during application of the pulse.

Now, consider the response of nuclear spin $I = 3/2$ system, in the presence of a weak Zeeman field, to the two-pulse sequence shown in Fig. III.4.

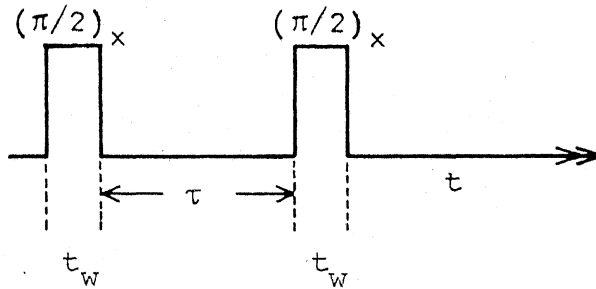


Fig. III.4. Two Pulse Spin-Echo Sequence

Immediately following the application of r.f. pulse the density matrix is given by (see Table III.3)

$$\tilde{\rho}(t_w) = T_0^2 \cos \xi + i \sin \xi [C_1 T_1^2(s) + C_2 T_1^2(a) + C_3 T_2^2(a)] \quad \dots (III.38)$$

where ξ , C_1 , C_2 and C_3 are defined in Table III.3.

Following the removal of the pulse the spin system evolves under the influence of Zeeman interaction and the density matrix is given by

$$\tilde{\rho}(\tau) = U_z \tilde{\rho}(t_w) U_z^{-1} \quad \dots (III.39)$$

$$\text{where } U_z = \exp(-i \mathcal{H}_z^d \tau) \quad \dots (III.40)$$

Similarly, the density matrix after the second pulse can be written as

$$\tilde{\rho}(t-\tau) = U_Z(t-\tau) U_R(t_w) \tilde{\rho}(\tau) U_R^{-1}(t_w) U_Z^{-1}(t-\tau) \dots \text{ (III.41)}$$

$$\text{where } U_R(t_w) = \exp(-i \tilde{\mathcal{H}}_1^d t_w) \dots \text{ (III.42)}$$

$$U_Z(t-\tau) = \exp[-i \tilde{\mathcal{H}}_Z^d (t-\tau)] \dots \text{ (III.43)}$$

Now, in any experiment, we can only measure the magnetization and it can be obtained by considering the expectation value of the magnetization operator [21]. The signal is proportional to the expectation value of the magnetization operator. The magnetization operators (at the resonance frequency) in phase and 90° out of phase w.r.t. the applied r.f. pulses, in the laboratory frame can be written, respectively as

$$M_x' = 2 \cos(\omega_q t) \{-T_1^1(a) P_1 + P_2 T_1^1(s) + P_3 T_{\infty}^1\} \\ \text{(in units of } \gamma \hbar) \dots \text{ (III.44)}$$

and

$$M_x = -2 \sin(\omega_q t) \{-T_1^1(a) P_1 + P_2 T_1^1(s) + P_3 T_0^1\} \\ \text{(in units of } \gamma \hbar) \dots \text{ (III.45)}$$

In QIR these are given by

$$\tilde{M}_x' = 2 \cos(\omega_q t) \{U_q U_d [-T_1^1(a) P_1 + T_1^1(s) P_2 + T_{\infty}^1 P_3] \\ U_d^{-1} U_q^{-1}\}$$

...contd.

$$\begin{aligned}
&\approx [-P_1 \frac{3(3+\eta)}{\rho} \{ \frac{3}{5} T_1^1(a) + \frac{2}{\sqrt{15}} T_1^3(a) \} \\
&\quad + P_2 \frac{3(3-\eta)}{\rho} \{ \frac{3}{5} T_1^1(s) + \frac{2}{\sqrt{15}} T_1^3(s) \} \\
&\quad + P_3 \{ -\frac{2}{3} \frac{\sqrt{2}\eta}{\sqrt{3}\rho} \} T_2^3(s)] \quad \dots \text{(III.46)}
\end{aligned}$$

and

$$\begin{aligned}
\tilde{M}_x &= -2 \sin(\omega_q t) \{ U_q U_d [-T_1^1(a) P_1 + T_1^1(s) P_2 + T_0^1 P_3] \\
&\quad U_d^{-1} U_q^{-1} \} \\
&\approx -\frac{i}{\sqrt{2}} [-P_1 \frac{(3+\eta)}{3\rho} T_1^2(s) + P_2 \frac{(3-\eta)}{3\rho} T_1^2(a) - P_3 \frac{2\eta}{3\rho} T_2^2(a)] \\
&\approx -\frac{i}{\sqrt{2}} [C_4 T_1^2(s) + C_5 T_1^2(a) + C_6 T_2^2(a)] \quad \dots \text{(III.47)}
\end{aligned}$$

where $C_4 = -P_1 \frac{(3+\eta)}{3\rho}$

$$C_5 = P_2 \frac{(3-\eta)}{3\rho}$$

$$C_6 = -P_3 \frac{2\eta}{3\rho} \quad \dots \text{(III.48)}$$

In arriving at Eqns. III.46 and III.47 we have made use of Tables III.1 and II.12 and dropped the high frequency terms. Now, making use of Tables III.3 and III.7 and Eqns. III.41 and III.47 and considering only the terms that contribute to echo, the expectation value of the magnetization operator \tilde{M}_x can be written as

$$\begin{aligned}
\langle \tilde{M}_x \rangle &= \frac{\sqrt{3}\omega}{4 kT} g \sin \epsilon \{ F_1 \cos[\frac{1}{2} (\omega_a + \omega_b) t] + F_2 \cos[\frac{1}{2} (\omega_a - \omega_b) t] \\
&\quad + F_3 \sin[\frac{1}{2} (\omega_a + \omega_b) t] + F_4 \sin[\frac{1}{2} (\omega_a - \omega_b) t]
\end{aligned}$$

...contd.

$$\begin{aligned}
& + F_5 \cos\left[\frac{1}{2} (\omega_a + \omega_b)(t - 2\tau)\right] + F_6 \cos\left[\frac{1}{2} (\omega_a - \omega_b)(t - 2\tau)\right] \\
& + F_7 \sin\left[\frac{1}{2} (\omega_a + \omega_b)(t - 2\tau)\right] + F_8 \sin\left[\frac{1}{2} (\omega_a - \omega_b)(t - 2\tau)\right] \\
& + F_9 \cos\left[\frac{1}{2} (\omega_a + \omega_b)\tau + \frac{1}{2}(\omega_a - \omega_b)(t - \tau)\right] \\
& + F_{10} \cos\left[\frac{1}{2} (\omega_a + \omega_b)\tau - \frac{1}{2} (\omega_a - \omega_b)(t - \tau)\right] \\
& + F_{11} \cos\left[\frac{1}{2} (\omega_a - \omega_b)\tau + \frac{1}{2} (\omega_a + \omega_b)(t - \tau)\right] \\
& + F_{12} \cos\left[\frac{1}{2} (\omega_a + \omega_b)(t - \tau) - \frac{1}{2} (\omega_a - \omega_b)\tau\right] \\
& + F_{13} \sin\left[\frac{1}{2} (\omega_a - \omega_b)(t - \tau) + \frac{1}{2} (\omega_a + \omega_b)\tau\right] \\
& + F_{14} \sin\left[\frac{1}{2} (\omega_a - \omega_b)(t - \tau) - \frac{1}{2} (\omega_a + \omega_b)\tau\right] \\
& + F_{15} \sin\left[\frac{1}{2} (\omega_a + \omega_b)(t - \tau) + \frac{1}{2} (\omega_a - \omega_b)\tau\right] \\
& + F_{16} \sin\left[\frac{1}{2} (\omega_a + \omega_b)(t - \tau) - \frac{1}{2} (\omega_a - \omega_b)\tau\right] \} \quad \dots \text{(III.49)}
\end{aligned}$$

where F's are as given in Table III.8. Similarly, it can be easily shown that the expectation value of the in-phase component of the magnetization, i.e., $\langle \tilde{M}'_x \rangle$ is zero.

The magnetization corresponding to the echo at $t = 2\tau$ is obtained by setting $t = 2\tau$ in Eqn. III.49. Thus,

$$\begin{aligned}
\varepsilon(2\tau) & \propto \frac{\sqrt{3}\omega_g}{4kT} \sin\varepsilon \{ F_1 \cos[(\omega_a + \omega_b)\tau] + F_2 \cos[(\omega_a - \omega_b)\tau] \\
& + F_3 \sin[(\omega_a + \omega_b)\tau] + F_4 \sin[(\omega_a - \omega_b)\tau] \\
& + (F_9 + F_{11}) \cos(\omega_a \tau) + (F_{10} + F_{12}) \cos(\omega_b \tau) \\
& + (F_{13} + F_{15}) \sin(\omega_a \tau) + (F_{14} + F_{16}) \sin(\omega_b \tau) + (F_5 + F_6) \} \\
& \dots \text{(III.50)}
\end{aligned}$$

Table III.8. Expressions for F's

$$F_1 = C_4 (X_1 - \cos^2 \epsilon / 2 E_{11}) + C_5 (Y_1 - \cos^2 \epsilon / 2 E_{21}) \\ + C_6 (Z_1 - \cos^2 \epsilon / 2 E_{31})$$

$$F_2 = C_4 (X_2 - \cos^2 \epsilon / 2 E_{12}) + C_5 (Y_2 - \cos^2 \epsilon / 2 E_{22}) \\ + C_6 (Z_2 - \cos^2 \epsilon / 2 E_{32})$$

$$F_3 = C_4 (X_3 - \cos^2 \epsilon / 2 E_{13}) + C_5 (Y_3 - \cos^2 \epsilon / 2 E_{23}) \\ + C_6 (Z_3 - \cos^2 \epsilon / 2 E_{33})$$

$$F_4 = C_4 (X_4 - \cos^2 \epsilon / 2 E_{14}) + C_5 (Y_4 - \cos^2 \epsilon / 2 E_{24}) \\ + C_6 (Z_4 - \cos^2 \epsilon / 2 E_{34})$$

$$F_5 = C_4 X_5 + C_5 Y_5 + C_6 Z_5$$

$$F_6 = C_4 X_6 + C_5 Y_6 + C_6 Z_6$$

$$F_7 = C_4 X_7 + C_5 Y_7 + C_6 Z_7$$

$$F_8 = C_4 X_8 + C_5 Y_8 + C_6 Z_8$$

$$F_9 = C_4 X_9 + C_5 Y_9 + C_6 Z_9$$

$$F_{10} = C_4 X_{10} + C_5 Y_{10} + C_6 Z_{10}$$

$$F_{11} = C_4 X_{11} + C_5 Y_{11} + C_6 Z_{11}$$

$$F_{12} = C_4 X_{12} + C_5 Y_{12} + C_6 Z_{12}$$

$$F_{13} = C_4 X_{13} + C_5 Y_{13} + C_6 Z_{13}$$

....contd.

Table III.8. (contd.)

$$F_{14} = C_4 X_{14} + C_5 Y_{14} + C_6 Z_{14}$$

$$F_{15} = C_4 X_{15} + C_5 Y_{15} + C_6 Z_{15}$$

$$F_{16} = C_4 X_{16} + C_5 Y_{16} + C_6 Z_{16}$$

$$\text{where } C_4 = -\frac{P_1(3+\eta)}{3\rho}, C_5 = \frac{P_2(3-\eta)}{3\rho}, C_6 = \frac{-2\eta}{3\rho}$$

ξ is defined in Table III.3.

P_1, P_2, P_3 and ρ are defined in Table III.2.

E's, X's, Y's and Z's are defined, respectively,
in Tables III.9, III.10, III.11 and III.12.

Table III.9. Expressions for E's and H's

$$E_{11} = C_1 A_{12} - C_2 B_{11} - C_3 D_{11}$$

$$E_{12} = C_1 A_{11} + C_2 B_{11} + C_3 D_{11}$$

$$E_{13} = C_2 B_{12} + C_3 D_{12}$$

$$E_{14} = C_2 B_{13} + C_3 D_{13}$$

$$E_{21} = -C_1 A_{21} + C_2 B_{22} - C_3 D_{21}$$

$$E_{22} = C_1 A_{21} + C_3 D_{21} + C_2 B_{21}$$

$$E_{23} = C_1 A_{22} + C_3 D_{22}$$

$$E_{24} = C_1 A_{23} + C_3 D_{23}$$

$$E_{31} = -C_1 A_{31} - C_2 B_{31} + C_3 D_{31}$$

$$E_{32} = C_1 A_{31} + C_2 B_{31} + C_3 D_{32}$$

$$E_{33} = C_1 A_{32} + C_2 B_{32}$$

$$E_{34} = C_1 A_{33} + C_2 B_{33}$$

$$E_{41} = -C_1 A_{41} - C_2 B_{41} + C_3 D_{41}$$

$$E_{42} = C_1 A_{41} + C_2 B_{41} - C_3 D_{41}$$

$$E_{43} = C_1 A_{42} + C_2 B_{42} + C_3 D_{42}$$

$$E_{44} = C_1 A_{43} + C_2 B_{43} + C_3 D_{43}$$

$$H_{11} = C_1^2 A_{12} - C_2^2 B_{22} + C_3^2 D_{31}$$

$$H_{12} = C_1 C_2 (-B_{11} + A_{21}) + C_1 C_3 (-D_{11} - A_{31}) + C_2 C_3 (D_{21} - B_{31})$$

$$= -H_{22}$$

...contd.

Table III.9 (contd.)

$$H_{21} = C_1^2 A_{11} = C_2^2 B_{21} + C_3^2 D_{32}$$

$$C_1 = \frac{P_1(3+\eta)}{\sqrt{3} \rho_x}, \quad C_2 = -\frac{P_2(3-\eta)}{\sqrt{3} \rho_x}, \quad C_3 = \frac{2\eta P_3}{\sqrt{3} \rho_x}$$

$$x = \left[\frac{1}{(3+\eta^2)} \{ \sin^2 \theta [(9+\eta^2) - 6\eta \cos 2\theta] + 4\eta^2 \cos^2 \theta \} \right]^{1/2}$$

where A's, B's, D's are defined in Table III.7,

while P_1 , P_2 , P_3 and ρ are defined in Table III.2.

Table III.10. Expressions for Q's and X's

$$Q_1 = (\cos\xi - 1) [E_{11}(H_{11} + H_{12})] + I_{11}$$

$$Q_2 = (\cos\xi - 1) [E_{12}(H_{11} + H_{12})] + I_{12}$$

$$Q_3 = (\cos\xi - 1) [E_{13}(H_{11} + H_{12})] + I_{13}$$

$$Q_4 = (\cos\xi - 1) [E_{14}(H_{12} + H_{11})] + I_{14}$$

$$Q_5 = (\cos\xi - 1) [E_{11}(H_{21} - H_{12})] + I_{21}$$

$$Q_6 = (\cos\xi - 1) [E_{12}(H_{21} - H_{12})] + I_{22}$$

$$Q_7 = (\cos\xi - 1) [E_{13}(H_{21} - H_{12})] + I_{23}$$

$$Q_8 = (\cos\xi - 1) [E_{14}(H_{21} - H_{12})] + I_{24}$$

$$X_1 = Q_1 - I_{33}$$

$$X_9 = Q_2 - I_{34}$$

$$X_2 = Q_6 - I_{44}$$

$$X_{10} = Q_2 + I_{34}$$

$$X_3 = Q_3 + I_{31}$$

$$X_{11} = Q_5 - I_{43}$$

$$X_4 = Q_8 + I_{42}$$

$$X_{12} = Q_5 + I_{43}$$

$$X_5 = Q_1 + I_{33}$$

$$X_{13} = Q_4 + I_{32}$$

$$X_6 = Q_6 + I_{44}$$

$$X_{14} = Q_4 - I_{32}$$

$$X_7 = Q_3 - I_{31}$$

$$X_{15} = Q_7 + I_{41}$$

$$X_8 = Q_8 - I_{42}$$

$$X_{16} = Q_7 - I_{41}$$

...contd.

Table III.10(contd.)

$$\text{where } I_{11} = E_{11}A_{12} - E_{21}B_{11} - E_{31}D_{11} - E_{41}G_{11}$$

$$I_{12} = E_{11}A_{11} + E_{21}B_{11} + E_{31}D_{11} + E_{41}G_{11}$$

$$I_{13} = E_{21}B_{12} + E_{31}D_{12} + E_{41}G_{12}$$

$$I_{14} = E_{21}B_{13} + E_{31}D_{13} + E_{41}G_{13}$$

$$I_{21} = A_{12}E_{12} - E_{22}B_{11} - E_{32}D_{11} - E_{42}G_{11}$$

$$I_{22} = E_{12}A_{11} + E_{22}B_{11} + E_{32}D_{11} + E_{42}G_{11}$$

$$I_{23} = E_{22}B_{12} + E_{32}D_{12} + E_{42}G_{12}$$

$$I_{24} = E_{22}B_{13} + E_{32}D_{13} + E_{42}G_{13}$$

$$I_{31} = E_{13}A_{12} - E_{23}B_{11} - E_{33}D_{11} - E_{43}G_{11}$$

$$I_{32} = E_{13}A_{11} + E_{23}B_{11} + E_{33}D_{11} + E_{43}G_{11}$$

$$I_{33} = E_{23}B_{12} + E_{33}D_{12} + E_{43}G_{12}$$

$$I_{34} = E_{23}B_{13} + E_{33}D_{13} + E_{43}G_{13}$$

$$I_{41} = E_{14}A_{12} - E_{24}B_{11} - E_{34}D_{11} - E_{44}G_{11}$$

$$I_{42} = E_{14}A_{11} + E_{24}B_{11} + E_{34}D_{11} + E_{44}G_{11}$$

$$I_{43} = E_{24}B_{12} + E_{34}D_{12} + E_{44}G_{12}$$

$$I_{44} = E_{24}B_{13} + E_{34}D_{13} + E_{44}G_{13}$$

ε is defined in Table III.3.

A's, B's, D's and G's are defined in Table III.7.

C's, E's and H's are defined in Table III.9.

Table III.11. Expressions for R's and V's

$$R_1 = (\cos\xi - 1) [E_{21}(H_{11} + H_{12})] + J_{11}$$

$$R_2 = (\cos\xi - 1) [E_{22}(H_{11} + H_{12})] + J_{12}$$

$$R_3 = (\cos\xi - 1) [E_{23}(H_{11} + H_{12})] + J_{13}$$

$$R_4 = (\cos\xi - 1) [E_{24}(H_{11} + H_{12})] + J_{14}$$

$$R_5 = (\cos\xi - 1) [E_{21}(H_{21} - H_{12})] + J_{21}$$

$$R_6 = (\cos\xi - 1) [E_{22}(H_{21} - H_{12})] + J_{22}$$

$$R_7 = (\cos\xi - 1) [E_{23}(H_{21} - H_{12})] + J_{23}$$

$$R_8 = (\cos\xi - 1) [E_{24}(H_{21} - H_{12})] + J_{24}$$

$$Y_1 = R_1 - J_{33}$$

$$Y_2 = R_6 - J_{44}$$

$$Y_3 = R_3 + J_{31}$$

$$Y_4 = R_8 + J_{42}$$

$$Y_5 = R_1 + J_{33}$$

$$Y_6 = R_6 + J_{44}$$

$$Y_7 = R_3 - J_{31}$$

$$Y_8 = R_8 - J_{42}$$

$$Y_9 = R_2 - J_{34}$$

$$Y_{10} = R_2 + J_{34}$$

$$Y_{11} = R_5 - J_{43}$$

$$Y_{12} = R_5 + J_{43}$$

$$Y_{13} = R_4 + J_{32}$$

$$Y_{14} = R_4 - J_{32}$$

$$Y_{15} = R_7 + J_{41}$$

$$Y_{16} = R_7 - J_{41}$$

...contd.

Table III.11 (contd.)

where

$$\begin{aligned}
 J_{11} &= -E_{11}A_{21} + E_{21}B_{22} - E_{31}D_{21} - E_{41}G_{21} \\
 J_{12} &= E_{11}A_{21} + E_{21}B_{21} + E_{31}D_{21} + E_{41}G_{21} \\
 J_{13} &= E_{11}A_{22} + E_{31}D_{22} + E_{41}G_{22} \\
 J_{14} &= E_{11}A_{23} + E_{31}D_{23} + E_{41}G_{23} \\
 J_{21} &= -E_{12}A_{21} + E_{22}B_{22} - E_{32}D_{21} - E_{42}G_{21} \\
 J_{22} &= E_{12}A_{21} + E_{22}B_{21} + E_{32}D_{21} + E_{42}G_{21} \\
 J_{23} &= E_{12}A_{22} + E_{22}D_{22} + E_{42}G_{22} \\
 J_{24} &= E_{12}A_{23} + E_{32}D_{23} + E_{42}G_{23} \\
 J_{31} &= E_{13}A_{21} + E_{23}B_{22} - E_{33}D_{21} - E_{43}G_{21} \\
 J_{32} &= E_{13}A_{21} + E_{23}B_{21} + E_{33}D_{21} + E_{43}G_{21} \\
 J_{33} &= E_{13}A_{22} + E_{33}D_{22} + E_{43}G_{22} \\
 J_{34} &= E_{13}A_{23} + E_{33}D_{23} + E_{43}G_{23} \\
 J_{41} &= E_{14}A_{21} + E_{24}B_{22} - E_{34}G_{21} \\
 J_{42} &= E_{14}A_{21} + E_{24}B_{21} + E_{34}D_{21} + E_{44}G_{21} \\
 J_{43} &= E_{14}A_{22} + E_{34}D_{22} + E_{44}G_{22} \\
 J_{44} &= E_{14}A_{23} + E_{34}D_{23} + E_{44}G_{23}
 \end{aligned}$$

ξ is defined in Table III.3.

A's, B's, D's and G's are defined in Table III.7.

C's, E's and H's are defined in Table III.9.

Table III.12. Expressions for S's and Z's

$$S_1 = (\cos\xi - 1) [E_{31}(H_{11} + H_{12})] + K_{11}$$

$$S_2 = (\cos\xi - 1) [E_{32}(H_{11} + H_{12})] + K_{12}$$

$$S_3 = (\cos\xi - 1) [E_{33}(H_{11} + H_{12})] + K_{13}$$

$$S_4 = (\cos\xi - 1) [E_{34}(H_{11} + H_{12})] + K_{14}$$

$$S_5 = (\cos\xi - 1) [E_{31}(H_{21} - H_{12})] + K_{21}$$

$$S_6 = (\cos\xi - 1) [E_{32}(H_{21} - H_{12})] + K_{22}$$

$$S_7 = (\cos\xi - 1) [E_{33}(H_{21} - H_{12})] + K_{23}$$

$$S_8 = (\cos\xi - 1) [E_{34}(H_{21} - H_{12})] + K_{24}$$

$$Z_1 = S_1 - K_{33}$$

$$Z_2 = S_2 - K_{44}$$

$$Z_3 = S_3 + K_{31}$$

$$Z_4 = S_8 + K_{42}$$

$$Z_5 = S_1 + K_{33}$$

$$Z_6 = S_6 + K_{44}$$

$$Z_7 = S_3 - K_{31}$$

$$Z_8 = S_8 - K_{42}$$

$$Z_9 = S_2 - K_{34}$$

$$Z_{10} = S_2 + K_{34}$$

$$Z_{11} = S_5 - K_{43}$$

$$Z_{12} = S_5 + K_{43}$$

$$Z_{13} = S_4 + K_{32}$$

$$Z_{14} = S_4 - K_{32}$$

$$Z_{15} = S_7 + K_{41}$$

$$Z_{16} = S_7 - K_{41}$$

...contd.

Table III.12 (contd.)

$$\begin{aligned}
\text{where } K_{11} &= -E_{11}A_{31} - E_{21}B_{31} + E_{31}D_{31} - E_{41}G_{31} \\
K_{12} &= E_{11}A_{31} + E_{21}B_{31} + E_{31}D_{31} + E_{41}G_{31} \\
K_{13} &= E_{11}A_{32} + E_{21}B_{32} + E_{41}G_{32} \\
K_{14} &= E_{11}A_{33} + E_{21}B_{33} + E_{41}G_{33} \\
K_{21} &= E_{12}A_{31} - E_{22}B_{31} + E_{32}D_{31} - E_{42}G_{31} \\
K_{22} &= E_{12}A_{31} + E_{22}B_{31} + E_{32}D_{32} + E_{42}G_{31} \\
K_{23} &= E_{12}A_{32} + E_{22}B_{32} + E_{42}G_{32} \\
K_{24} &= E_{12}A_{33} + E_{22}B_{33} + E_{42}G_{33} \\
K_{31} &= -E_{13}A_{31} - E_{23}B_{31} + E_{33}D_{31} - E_{43}G_{31} \\
K_{32} &= E_{13}A_{31} + E_{23}B_{31} + E_{33}D_{32} + E_{43}G_{31} \\
K_{33} &= E_{13}A_{32} + E_{23}B_{32} + E_{43}G_{32} \\
K_{34} &= E_{13}A_{33} + E_{23}B_{33} + E_{43}G_{33} \\
K_{41} &= -E_{14}A_{31} - E_{24}B_{31} + E_{34}D_{31} - E_{43}G_{31} \\
K_{42} &= E_{14}A_{31} + E_{24}B_{31} + E_{34}D_{32} + E_{43}G_{31} \\
K_{43} &= E_{14}A_{32} + E_{24}B_{32} + E_{43}G_{32} \\
K_{44} &= E_{14}A_{33} + E_{24}B_{33} + E_{43}G_{33}
\end{aligned}$$

E is defined in Table III.3.

A's, B's, D's and G's are defined in Table III.7.

C's, E's and H's are defined in Table III.9.

From Eqn. III.50 it is evident that the expression for the Zeeman-perturbed spin echo envelope modulations contains all the frequency components ω_a, ω_b ($\omega_a + \omega_b$) and ($\omega_a - \omega_b$) as reported earlier by Ramachandran and Narasimhan.

In the following special cases the expression for $\mathcal{E}(2\tau)$ reduces to those given in [1] (also see Chapter II).

Case 1: For $\eta = 0$, $H_0 = 0$, and $\mathcal{H}_1 = +2\omega_1 \cos(\omega_q t) T_1^1(a)$

$$\omega_a = \omega_b = 0,$$

$$\mathcal{E} = \sqrt{3}\omega_1 t_w$$

$$\mathcal{E}(2\tau) \propto \sin \mathcal{E} \sin^2 \mathcal{E}/2 \quad \dots \text{(III.51)}$$

Case 2: For $\eta = 0$, $H_0 = f n(\theta)$ and $\mathcal{H}_1 = 2\omega_1 \cos(\omega_q t) T_1^1(a)$

$$\mathcal{E} = 3\omega_1 t_w$$

$$f = (1 + 4 \tan^2 \theta)^{1/2}$$

$$\begin{aligned} \mathcal{E}(2\tau) \propto \sin \mathcal{E} \sin^2(\mathcal{E}/2) & \left[\left(\frac{f^2 - 1}{2f^2} \right) \{ \cos(\omega_a \tau) + \cos(\omega_b \tau) \right. \\ & \left. - \cos(\omega_a \tau) \cos(\omega_b \tau) \} \right. \\ & \left. + \left(\frac{f+1}{2f} \right)^2 + \left(\frac{f-1}{2f} \right)^2 \right] \end{aligned}$$

$$\dots \text{(III.52)}$$

III.B.5(i) Powder averaging:

Since in the above calculations we have assumed that the r.f. and Zeeman fields are randomly oriented with respect to the efg principal axes system, the expression for $\mathcal{E}(2\tau)$ is also

applicable for this situation. The response of a quadrupolar spin ensemble in a polycrystalline specimen, where all values of θ and ϕ occur with equal probability is obtained by considering a weighted average overall orientations,

$$\langle \overline{\epsilon(2\tau)} \rangle \propto \frac{1}{4\pi} \int_0^{2\pi} \int_0^\pi \epsilon(2\tau) \sin\theta \, d\theta \, d\phi \quad \dots \text{(III.53)}$$

$\epsilon(2\tau)$ obtained using the tensor operator formalism (Eqn. III.50) is inserted in Eqn. III.53 which has to be then evaluated to obtain Zeeman-perturbed spin echo envelope modulation pattern from polycrystalline samples.

From the above presentation it is clear that the tensor operator formalism can be used for the theoretical analysis of ZSEEM in spin $I = 3/2$ nuclei in polycrystalline specimens. However, before concluding this section, the following points may be mentioned. As pointed out earlier in this section in the calculation of the expression which gives the ZSEEM pattern from polycrystalline specimens one needs to evaluate the time evolution of tensor operators under r.f. and Zeeman interaction Hamiltonians corresponding to general (θ, ϕ) orientation. The calculation of the time evolution of tensor operators under the action of the r.f. Hamiltonian is straightforward. However, it is rather difficult to obtain closed-form expressions for the time evolution of tensor operators under the Zeeman Hamiltonian by any of the two methods, viz., the method of 'nested commutation

relationships' or the 'harmonics of the motion method'. Hence, we had to resort to the matrix representation method for evaluating the time evolution of the operators and reconvert the resulting matrix into the tensor operators. On this account, the calculation became rather cumbersome. The tensor operator formalism per se does not seem to offer any additional advantage over the other approaches for the analysis of ZSEEM.

SUMMARY

Tensor operator formalism has been applied for the theoretical analysis of Zeeman-perturbed spin echo envelope modulations in spin $I = 3/2$ nuclei in polycrystalline specimens. The present results are in agreement with those obtained earlier by Ramachandran and Narasimhan. The tensor operator formalism, however, does not offer any special advantage over the other approaches on account of the complexity in the calculation of the evolution of tensor operators under the action of Zeeman Hamiltonian.

REFERENCES

- [1] T.P. Das and E.L. Hahn, "Nuclear Quadrupole Resonance," Solid State Physics, Supplement 1, Academic Press, New York (1958).
- [2] E.A.C. Lucken, "Nuclear Quadrupole Coupling Constants," Academic Press, New York (1969).
- [3] C. Dean, Phys. Rev., 96, 1053 (1954).
- [4] Y. Morino and M. Toyama, J. Chem. Phys., 35, 1289 (1961).
- [5] K.V. Raman and P.T. Narasimhan, Pure Appl. Chem., 32, 271 (1972).
- [6] V. Harihara Subramanian and P.T. Narasimhan, J. Molec. Struct., 58, 193 (1980) and references therein.
- [7] W.B. Mims, Phys. Rev., B5, 2409 (1972).
- [8] N.E. Ainbinder, V.S. Grechishkin, A.D. Gordeev, A.S. Osipenko, Soviet Phys. Solid St., 10, 1592 (1969).
- [9] Yu. E. Sapozhnikov and Ya. B. Yasman, Bull. Acad. Sci. USSR, Phys. Ser., 42, 210 (1978).
- [10] D.U. Zakirov and I.A. Safin, J. Molec. Struct., 83, 253 (1982).
- [11] (a) R. Ramachandran and P.T. Narasimhan, Molec. Phys., 48, 267 (1983).
(b) R. Ramachandran, Ph.D. Thesis, Indian Institute of Technology, Kanpur, India (1982).
- [12] (a) Narsimha Reddy, Arun L. Bhavsar and P.T. Narasimhan, Z. Naturforsch., 41a, 449 (1987).

(b) Narsimha Reddy, Ph.D. Thesis, Indian Institute of Technology, Kanpur, India (1987).

- [13] Narsimha Reddy and P.T. Narasimhan, Proceedings of the IX International Symposium on Magnetic Resonance, Rio de Janeiro, Brazil (1986), Abstract A54.
- [14] A. Schweiger, L. Braunschweiler, J.M. Fauth and R.R. Earnst, Phys. Rev. Lett., 54, 1241 (1985).
- [15] H.A. Buckmaster, R. Chatterjee and Y.H. Shing, Phys. Status Solidi, 13, 9 (1972).
- [16] G.J. Bowden and W.D. Hutchison, J. Magn. Reson., 67, 403 (1986).
- [17] G.J. Bowden, W.D. Hutchison and J. Khachan, J. Magn. Reson., 67, 415 (1986).
- [18] G.J. Bowden and W.D. Hutchison, J. Magn. Reson., 70, 361 (1986).
- [19] G.J. Bowden and W.D. Hutchison, J. Magn. Reson., 72, 61 (1987).
- [20] W.D. Hutchison, Ph.D. Thesis, University of New South Wales, NSW, Australia (1987).
- [21] R.S. Cantor and J.S. Waugh, J. Chem. Phys., 73, 1054 (1980).

CHAPTER IV

EXPERIMENTAL AND THEORETICAL INVESTIGATIONS OF RESPONSES OF QUADRUPOLEAR NUCLEI TO SOME MULTIPLE-PULSE SEQUENCES

The NMR spectrum of a solid sample is usually broad, mostly due to dipole-dipole interactions in solid-state masking information about chemical shifts and spin couplings. To achieve high resolution NMR spectra from solid samples, various experimental techniques have been developed, many of which are based on multiple r.f. pulses. [1,2]. The first multiple-pulse experiment in NMR of solids was due to Ostroff and Waugh [3] and Mansfield and Ware [4]. These workers observed that the application of modified Carr-Purcell (CP) sequence leads to a lengthening of the decay of transverse magnetization. Since then a variety of multiple pulse sequences have been designed to achieve prolonged transverse magnetization. These sequences not only achieve long transverse magnetization but also give rise to selective averaging thereby leaving chemical shift interactions active and leading to the high resolution NMR spectrum from solids. Multiple-pulse experimental techniques in NMR of solids are now well established [1,2].

The interest in the study of multiple-pulse experiments in NQR stems from the following considerations. Multiple-pulse sequences in NQR could also lead to prolonged transverse magnetization and thus to a narrowed line. Information on various internal interactions which broaden or split the line can be then obtained. This may help in a better understanding of the chemical environment of the quadrupolar nucleus in the solid state. Relaxation times in rotating reference frame may also be obtained from a study of NQR multiple pulse experiments.

Multiple pulse experiments can be effectively used in achieving enhanced S/N. Under the multiple r.f. pulse irradiation a sensitive double resonance experiment can be performed to detect rare quadrupolar nuclei. Thus, the multiple pulse investigations in NQR could yield valuable structural and dynamical information in the solid state.

This chapter consists of four sections. The first section gives a brief review of the multiple pulse investigations in NQR. Section IV.B deals with the experimental investigations of a variety of multiple pulse sequence on spin $3/2$ and $5/2$ nuclei. Section IV.C gives the results of a double resonance experiment under multiple pulse spin locking condition. The last section outlines theoretical analysis of a few multiple pulse experiments in NQR of spin $3/2$ nuclei using tensor operator formalism.

IV.A MULTIPLE PULSE INVESTIGATIONS IN PURE NQR - A REVIEW

The first experimental investigations of multiple pulse sequences in NQR were due to Marino and Klainer (MK) [5]. They employed the Ostroff-Waugh (OW) sequence to study ^{14}N ($I = 1$) in a polycrystalline sample of NaNO_2 and found effects very similar to those observed in NMR experiments, namely, a persistence of the transverse magnetization for times long compared to, T_2 , spin-spin relaxation time. Following this, Osokin [6-9] investigated the effect of phase alternated multiple pulse sequence (PAPS), Carr-Purcell-Meiboom-Gill (CPMG) and OW sequence on NQR of spin $I = 1$ nuclei. Ainbinder et al. [10] have studied the

influence of CPMG sequence on ^{35}Cl ($I = 3/2$) and ^{123}Sb ($I = 7/2$) in polycrystalline samples. Recently, Narsimha Reddy and Narasimhan [11] have carried out experimental investigations of the influence of CP, CPMG, OW and PAPS sequences in the case of spin $I = 3/2$ nuclei in polycrystalline samples. In all the above mentioned investigations, the persistence of the transverse magnetization for times much longer than T_2 was observed. Recently, Ermakov and Osokin [12] studied the influence of the well-known pulse sequence, WAHUHA [13], which is known to suppress the dipole-dipole interactions in NMR of solids, on ^{14}N ($I = 1$) NQR in a single crystal of NaNO_2 .

Apart from the above experimental investigations there are some theoretical studies in the area of multiple pulse NQR. Using different approaches attempts have been made to give a theoretical explanation for the long time and short time behaviour of the magnetization in the MK experiment [14-16].

Cantor and Waugh [14] employed an approximation method to theoretically investigate the short time behaviour and to some extent long time behaviour of the magnetization in MK's experiment. Hitrin et al. [15] employed a canonical transformation technique to obtain solution for the density matrix, and obtained theoretical agreement with the experimentally observed short and long time behaviour of the magnetization. Matti Marick [16] used a generalized version of the Average Hamiltonian Theory (AHT) based on Floquet solution of the periodic, time-dependent, Schrödinger equation to analyze the MK experiment and compared

the results with those obtained in the case of NMR.

In all the aforesaid cases the theoretical investigations were carried out on spin-1 nuclei only. Recently, Ainbinder et al. [17,18] have developed a theory which is applicable for general spin I . They employed the method of canonical transformations and Krylov-Bogolyubov-Mitropolski averaging method [19]. They have shown that in the multiple pulse sequence, $(\pi/2)_x - [\tau - (\theta)_{x+\phi} - \tau]_n$, referred hereafter as spin-locking sequence (SLS), spin locking occurs for arbitrary θ values when $\phi = (2K+1)\pi/2$ where K is an integer. Ainbinder and Furman [17] proposed that like in NMR, multiple-pulse experiments in NQR spectroscopy lead to two types of averaging of internal interactions which broaden the NQR line. These are termed as: (i) general averaging, and (ii) selective averaging. A pulse sequence that influences the broadening interactions as a whole, regardless of their nature, is said to cause general averaging.

The influence of relaxation processes on the quasi-equilibrium state of the magnetization in the spin-locking experiments has also been investigated in the literature [10].

The theoretical investigations of PAPS on spin $I = 1$ nuclei have also been carried out in the literature [6-8]. In these investigations AHT has been employed. Ermakov and Osokin [12] have investigated the influence of PAPS on a system of two dipolar coupled equivalent spin $I = 1$ nuclei and predicted the quasi-equilibrium state of the magnetization. Osokin [9]

studied the influence of spin-lattice relaxation process on the the quasi-equilibrium state of the magnetization in PAPS experiment.

It may be mentioned that in a multiple-pulse experiment an internal interaction is said to be averaged out if the average Hamiltonian $\overline{\mathcal{H}}_{\text{int}}^{(i)}$ of that interaction over the cycle of the pulse sequence satisfies the condition [20]

$$\overline{\mathcal{H}}_{\text{int}}^{(i)} = 0 \text{ or } [\rho_i, \overline{\mathcal{H}}_{\text{int}}^{(i)}] = 0$$

where ρ_i is the initial density operator prepared by the preparatory pulse. Employing the "fictitious spin-1/2 operator formalism" [21] Osokin [6-8] has shown that under the influence of PAPS, the average Hamiltonian $\overline{\mathcal{H}}_{\text{int}}^{(0)}$ corresponding to the internal interactions due to (i) inhomogeneities in efg's, (ii) torsional oscillations of molecules, (iii) heteronuclear dipole-dipole interactions commutes with the initial density operator, ρ_i . Thus, he concluded that under the action of PAPS the above mentioned internal interactions are averaged out. Osokin [7,8] has also shown that the homonuclear dipole-dipole interaction is not averaged out under the action of PAPS. Theoretical analysis of some of the multiple pulse sequences in NQR have been considered earlier by Zueva et al. [22]. Using the fictitious spin-1/2 operator formalism Ermakov and Osokin [12] have analyzed the influence of WAHUHA sequence on a model system of two dipolar-coupled spin-1 nuclei.

In the next section we present our experimental results of some multiple pulse sequences in NQR of spin $I = 3/2$ and $5/2$ nuclei.

IV.B EXPERIMENTAL INVESTIGATIONS OF RESPONSES OF QUADRUPOLEAR NUCLEI TO MULTIPLE PULSE SEQUENCES

As has been discussed earlier, under the action of multiple pulse sequences some or all contributions of the interactions which lead to line broadening can be removed and thus one can achieve a narrowed line. This kind of resolution enhancement, in principle, enables one to study the weaker interactions in solid state.

In this section we present our experimental investigations of the influence of a few multiple pulse sequences on quadrupolar nuclei. The nuclei investigated are: (a) ^{35}Cl ($I = 3/2$) in a single crystal of NaClO_3 , and in polycrystalline samples of NaClO_3 , KClO_3 and SbCl_3 . (b) ^{187}Re & ^{185}Re (both $I = 5/2$) in polycrystalline specimen of KReO_4 .

The multiple pulse sequences investigated are:

- i) Spin locking sequence (SLS): $(\pi/2)_x - (\tau - \theta_{(x+\phi)} - \tau)_n$
- ii) PAPS : $(\pi/2)_x - (\tau - \theta_{-x} - 2\tau - \theta_x - \tau)_n$
- iii) WAHUA sequence : $(\pi/2)_x - \tau - (\pi/2)_{-x} - \tau - (\pi/2)_y - 2\tau - (\pi/2)_{-y} - \tau - (\pi/2)_x - \tau -)_n$

From the spin locking sequence one can derive well known sequences

like CP ($\theta = \pi$, $\phi = 0$), OW ($\theta = \pi/2$, $\phi = 90^\circ$), CPMG ($\theta = \pi$, $\phi = 90^\circ$) by choosing appropriate θ and ϕ values.

II.B.1 Experimental

All the experiments discussed in this chapter have been carried out using the pulsed NQR spectrometer described earlier (see Section I.C.3). The DC pulse sequences generated by the micro-processor system under the software control have been used to gate the r.f. The gating scheme for generating various phases in WAHUHA sequence is shown in Fig. IV.1. Same gating scheme can be used, with slight modification for generating PAPS sequence also. Delay line is employed to get arbitrary values of phase shifts. In this spectrometer despite the receiver gating the transmitter pulse feed-through could not be avoided. In all the experiments the responses of multiple pulse sequences have been acquired into the signal analyzer. These signals are processed, off-line, in the signal analyzer to remove the transmitter pulse feed-through. The processed signals can be either stored in a minifloppy disk or can be recorded on a plotter interfaced to the signal analyzer.

Since in some of the experiments the multiple pulse responses are studied as a function of the flip angle of the sequence pulses it is worth mentioning here the definition of the pulse flip angles in the case of the polycrystalline samples. We discuss only the case of axially symmetric field gradients ($\eta = 0$). In polycrystalline samples a pulse which gives rise to

- (1) μp : Microprocessor
- (2) PSCQ, PSCT are broad band hybrid junctions from Mini-circuits, USA
- (3) Double balanced mixers (DBM) are from Hewlett-Packard USA (model 10514A)
- (4) Power combiners are from Engelmann Micro wave, USA (model PSK-210).

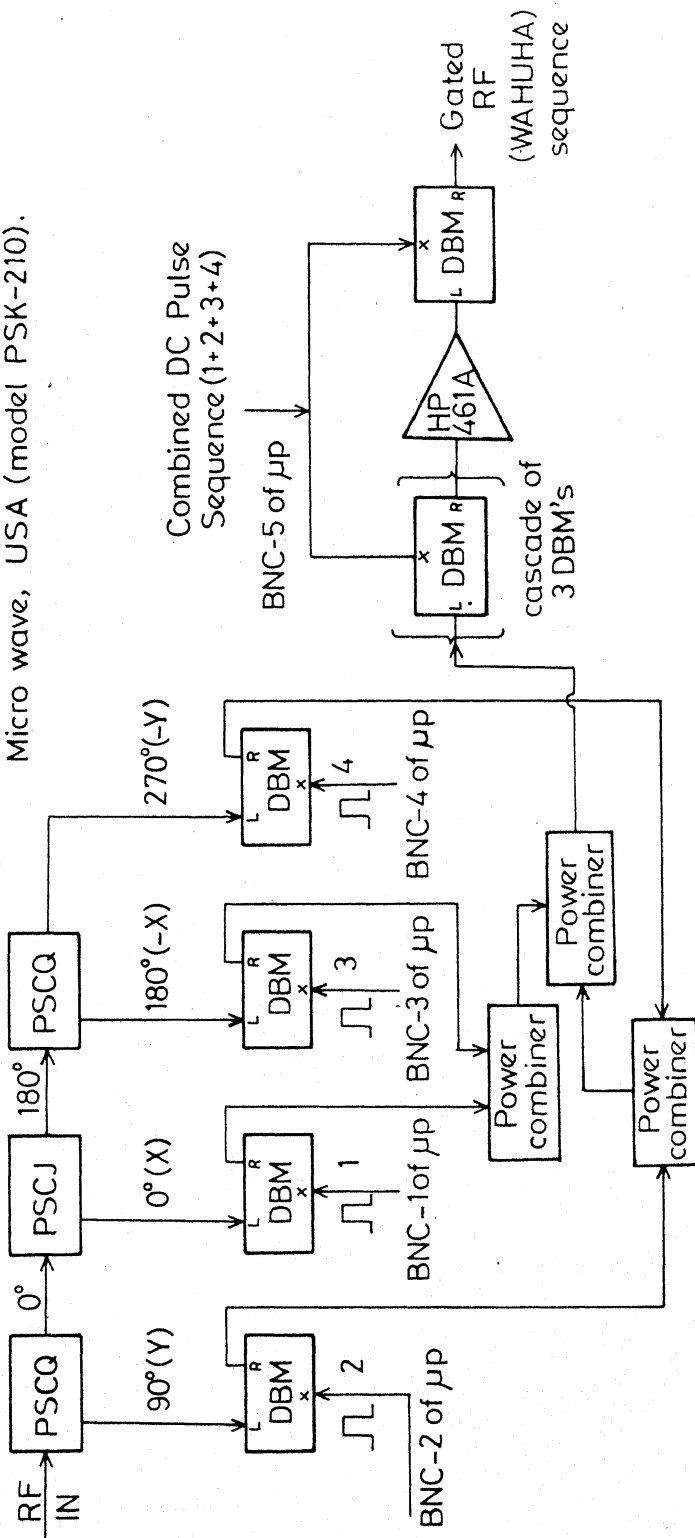


Fig. IV.1 RF Gating scheme for the generation of WAHUHA sequence.

a maximum FID is referred to as a 90° pulse. This 90° pulse flip angle is not equal to $\pi/2$ but it is 0.66π (for arbitrary spin I). Similarly the flip angle of a 180° refocussing pulse is equal to 1.22π [23]. In all our experiments we have followed the above-mentioned definitions in adjusting the pulse widths.

IV.B.2 Results

In what follows we present the results of experimental investigations of spin-locking, PAPS and WAHUA sequences.

IV.B.2(i) Spin-locking sequence (SLS):

We first studied the influence of spin-locking sequence on ^{35}Cl in a single crystal of NaClO_3 . The crystal was oriented such that the r.f. field is perpendicular to the (1,0,0) plane. Under the influence of the spin-locking sequence the establishment of a quasi-equilibrium state of the magnetization could be observed. The magnetization has been observed to last for times much longer than the spin-spin relaxation time T_2 . In the case of ^{35}Cl in a single crystal of NaClO_3 , $T_2^* \approx 300 \mu\text{sec}$ and T_1 , the spin-lattice relaxation time, is $\approx 23 \text{ msec}$ [24]. Results obtained with OW, CP, CPMG sequences are shown respectively in Fig. IV.2(a), IV.2(b) and IV.2(c), while Fig. IV.2(d) to IV.2(f) show the results obtained with arbitrary combinations of θ and ϕ values in SLS sequence. From these figures it is evident that even in a single crystal the quasi-equilibrium state of the magnetization can be achieved with arbitrary θ , ϕ values for the

Fig. IV.2(a) . Response of ^{35}Cl in a single crystal of NaClO_3
to
Fig. IV.2(f) to spin-locking sequence, $(\pi/2)_x - (\tau - \theta_{(x+\phi)} - \tau)_n$.
The plots are given for various combination of
 θ, ϕ in SLS. In all the cases $\nu = 29.9232 \text{ MHz}$,
the resonance off-set, $\Delta\omega \approx -4 \text{ KHz}$ and $\tau = 180$
 μsec . The relative signal amplitudes in all
the figures are in the same scale.

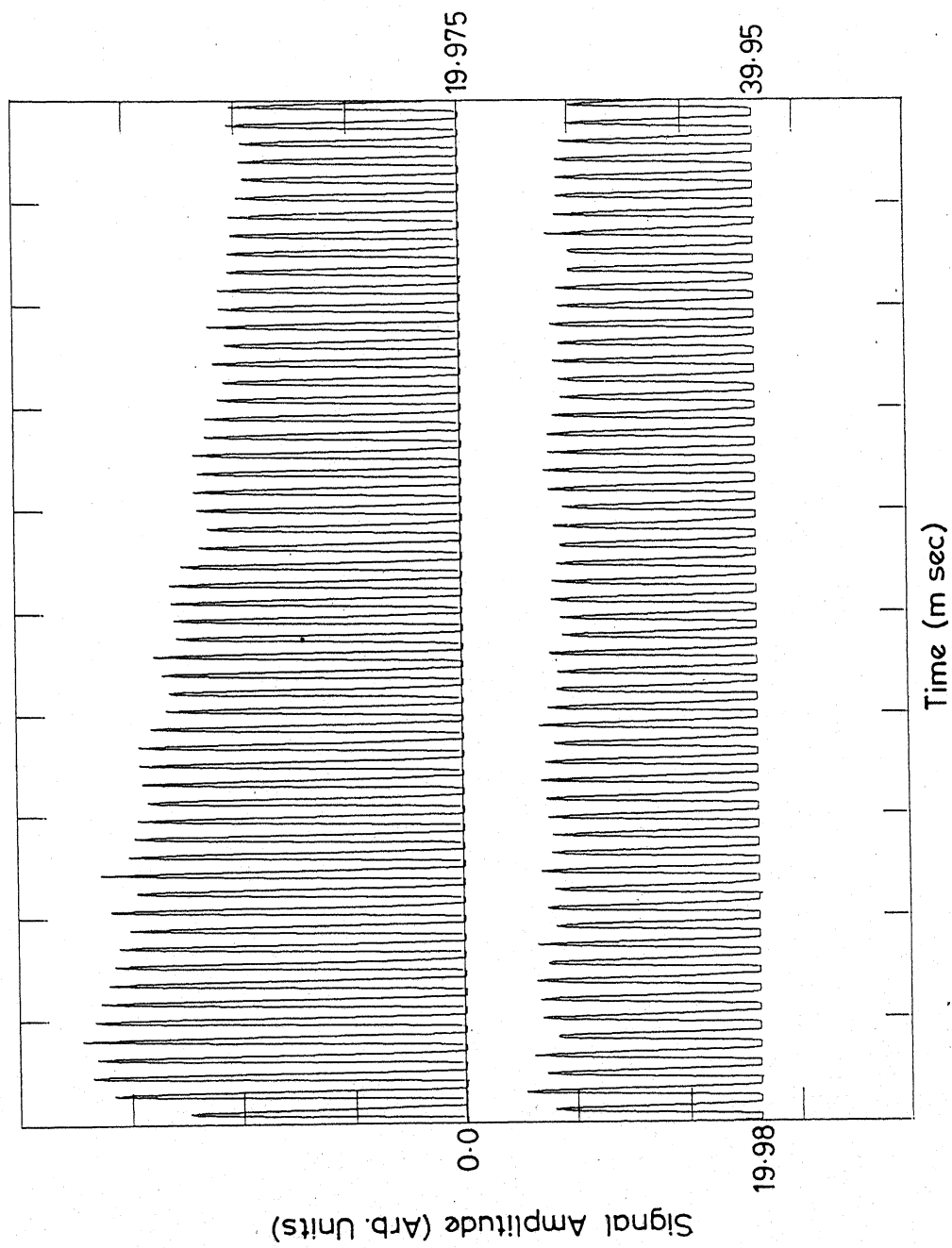


Fig. IV-2(a) OW-Sequence, $\theta = \pi/2$, $\phi = 90^\circ$

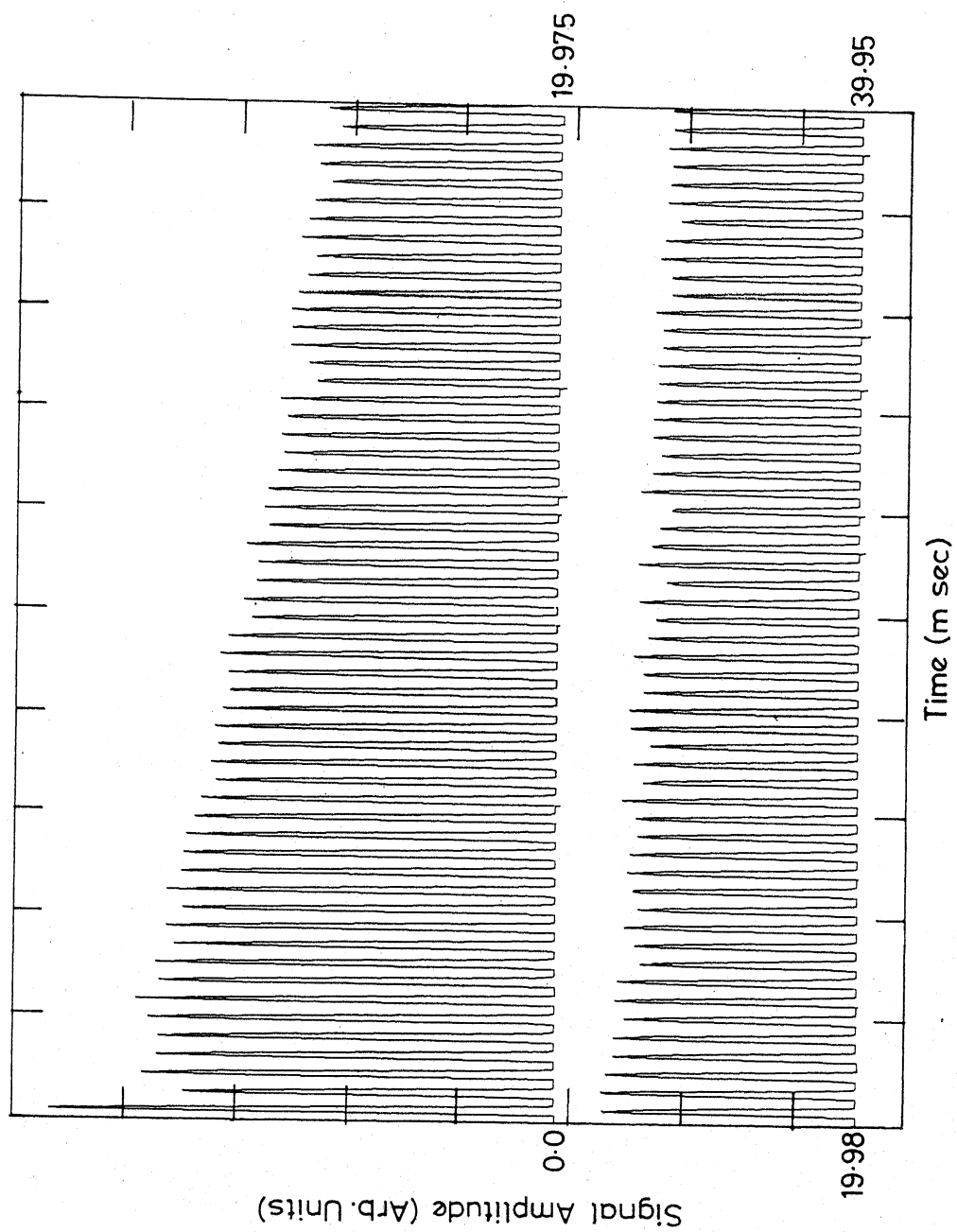


Fig. IV-2(b) CP Sequence: $\theta = \pi$, $\phi = 0$

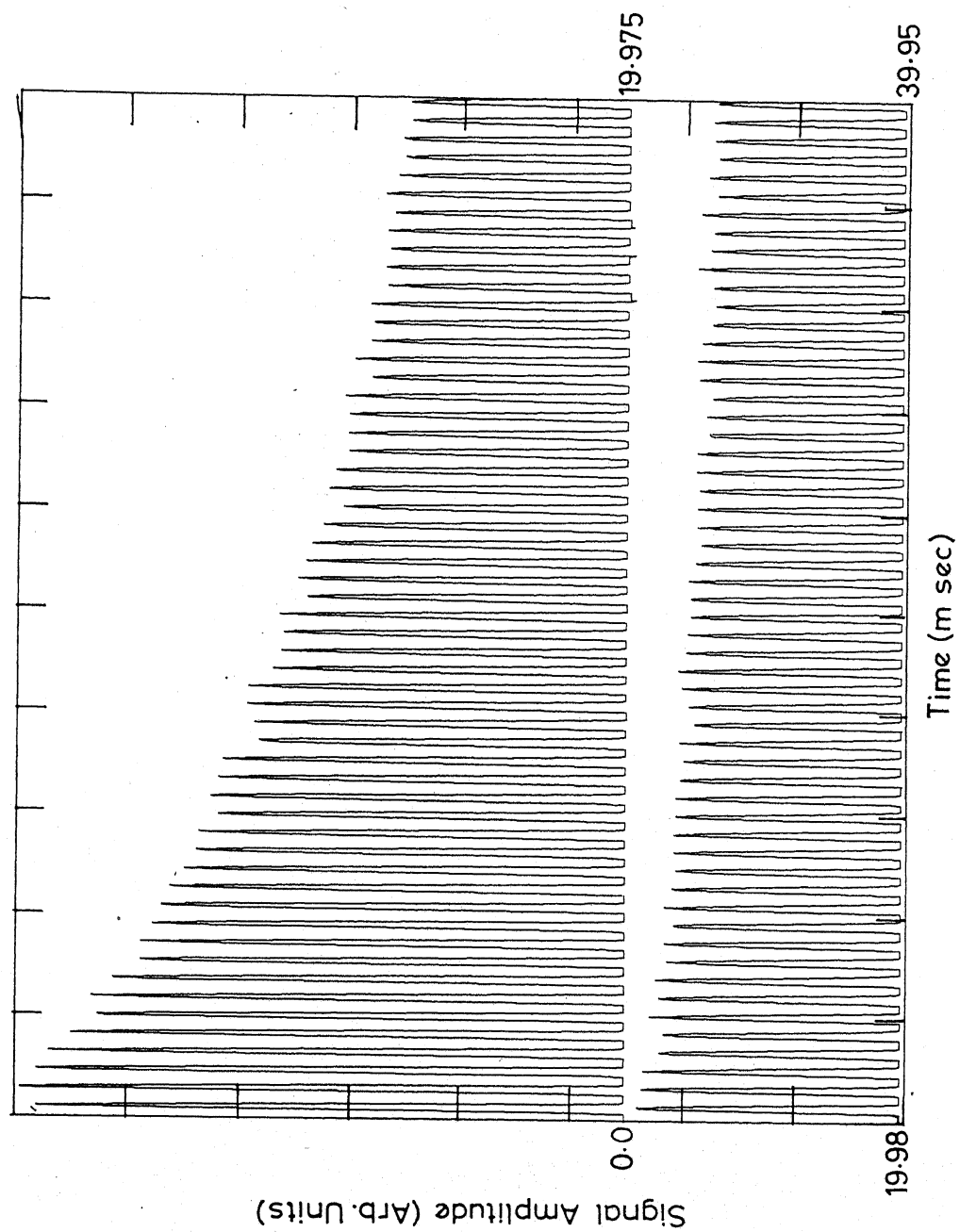


Fig. IV-2(c) CPMG Sequence: $\theta = \pi$, $\phi = 90^\circ$

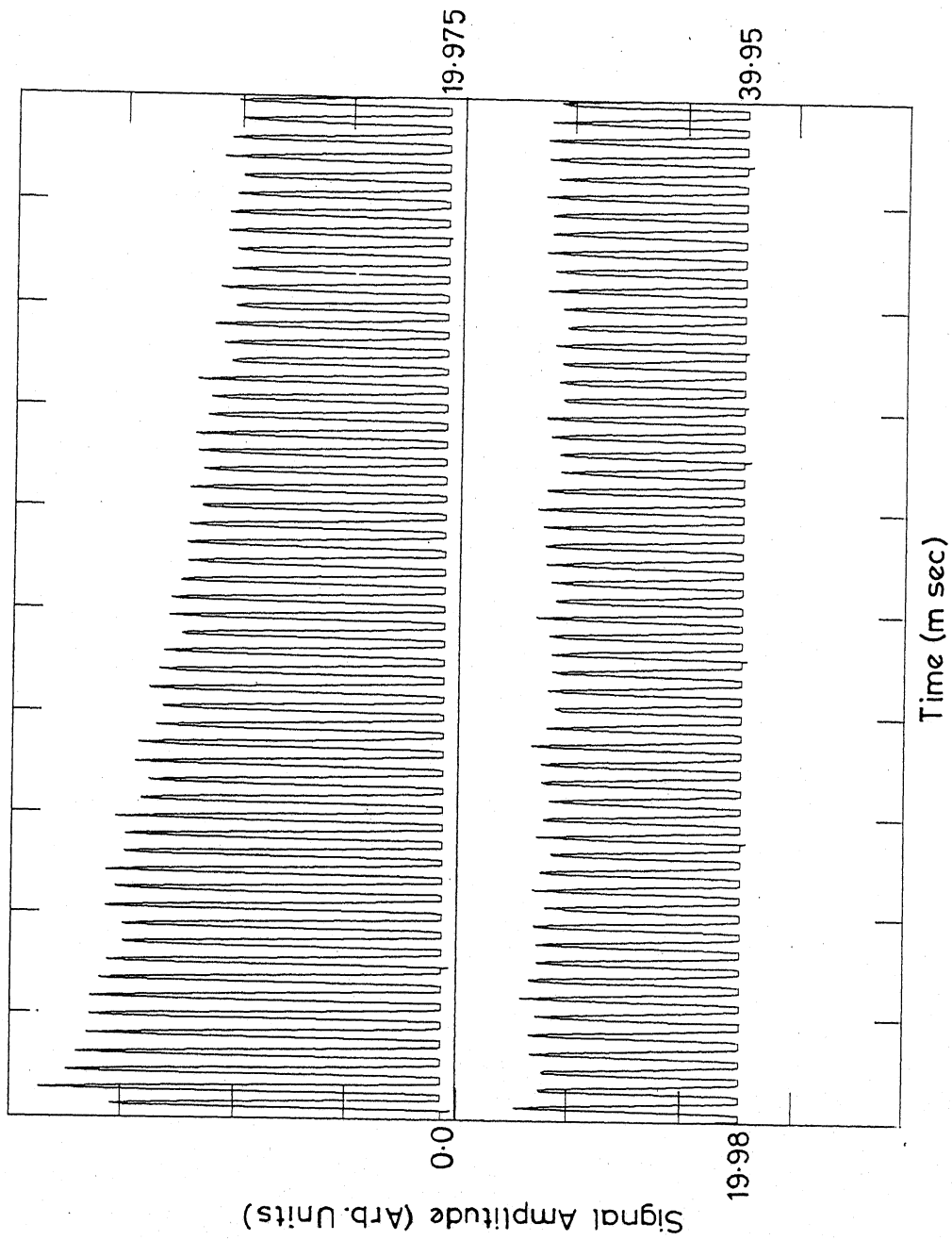


Fig. IV-2(d) $\theta = \pi/2, \phi = 0$

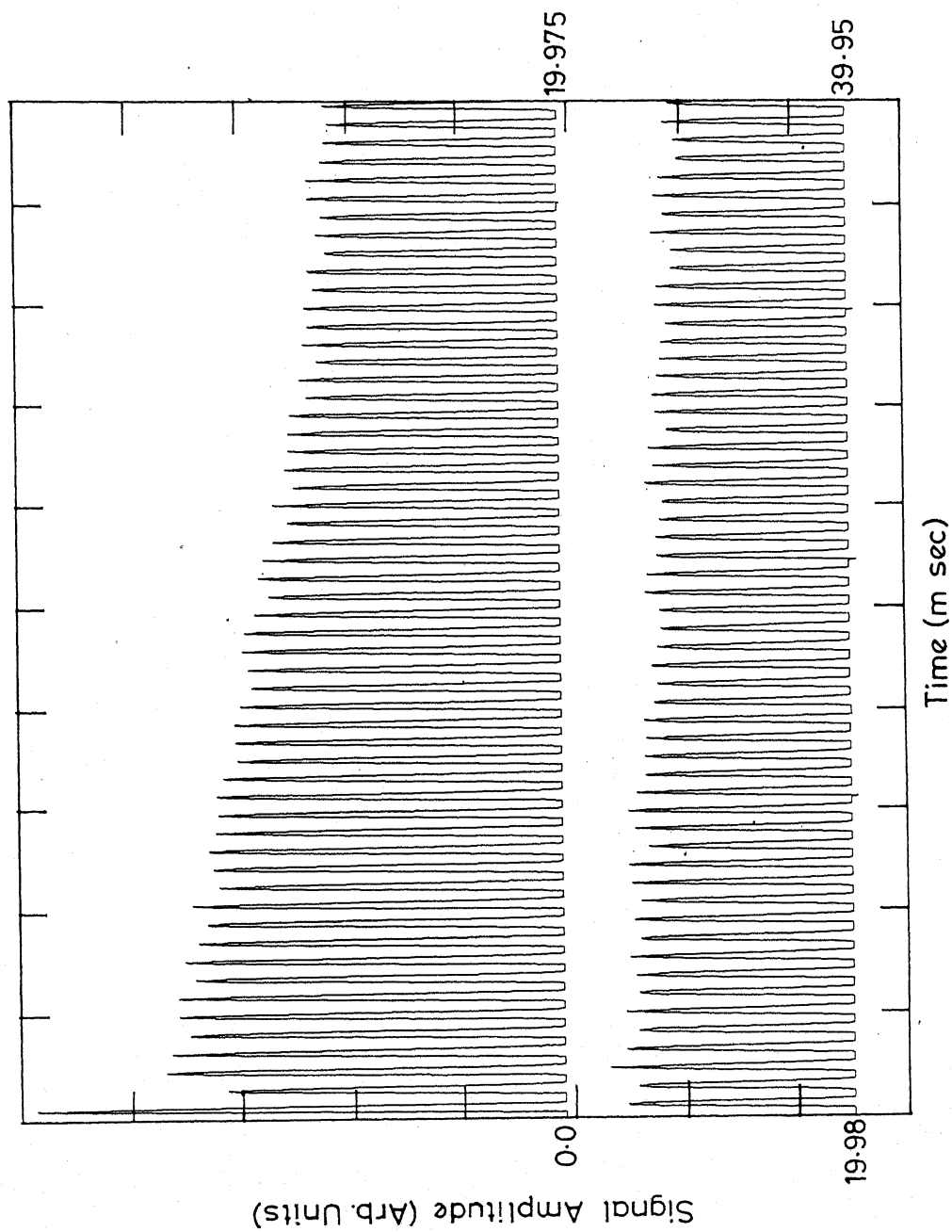


Fig. IV.2(e) $\theta = \pi/2$, $\phi = 180^\circ$

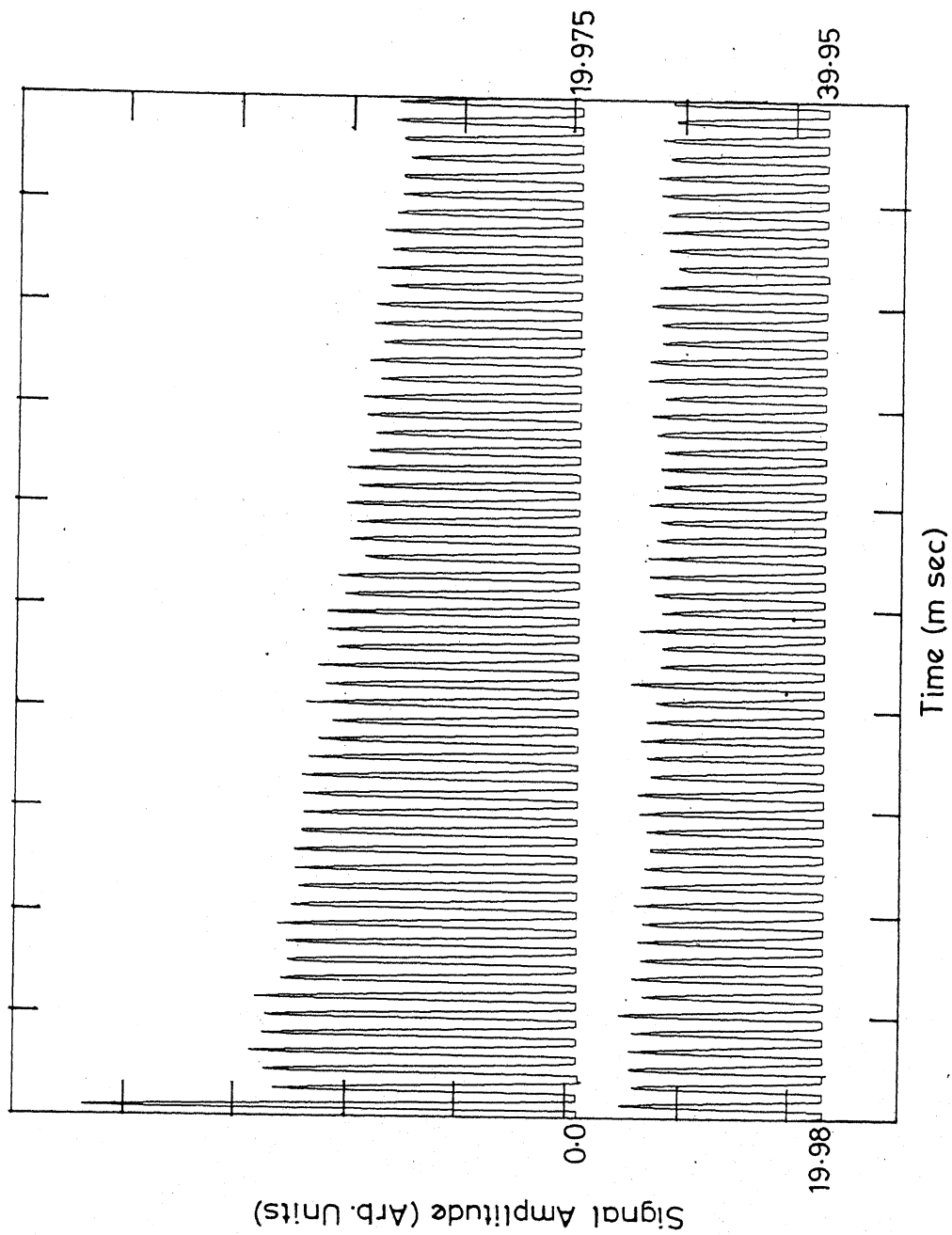


Fig. IV-2(f) $\theta = \pi$, $\phi = 180^\circ$

sequence pulses. The results of dependence of the decay of the quasi-equilibrium magnetization (QEM) on θ , ϕ , τ and resonance off-set, $\Delta\omega$, parameters will be presented in subsequent sections.

In order to ascertain whether the spin-locking phenomenon is confined to only specific spin I values or it is general for any spin, we have studied the influence of SLS on ^{187}Re , ^{185}Re (both with $I = 5/2$) in the polycrystalline sample of KReO_4 . To our surprise we observed the spin-locking effect in these cases also. In the case of ^{187}Re the results obtained with OW, CP and CPMG sequences are shown respectively in Fig. IV.3(a), IV.3(b) and IV.3(c), while Fig. IV.3(d) to IV.3(f) show the results with arbitrary combinations of θ , ϕ in the SLS. In the case of ^{185}Re , the responses of OW, CP, and CPMG are shown in Fig. IV.4(a), IV.4(b) and IV.4(c). The results obtained with arbitrary θ , ϕ combinations in SLS are shown in Fig. IV.4(d) - IV.4(f). The spin-spin relaxation time of ^{187}Re in polycrystalline sample of KReO_4 is $\approx 90 \mu\text{sec}$. Now, from Fig. IV.3 it can be easily seen that the decay of QEM lasts for times much longer than T_2 . These results and the results reported earlier in the literature [5,10,11,23] indicate that the spin-locking phenomenon is a general one and can be observed for any arbitrary spin I .

IV.B.2(i)a Study of flip-angle ' θ ' dependence:

We have employed OW sequence for investigating the dependence of the decay of QEM, on the flip-angle, ' θ ', of the sequence pulses. The resonance off-set is fixed at -4 KHz and τ is chosen

Fig. IV.3(a) Response of ^{187}Re in polycrystalline specimen of KReO_4 , to spin-locking sequence,

Fig. IV.3(f) $(\pi/2)_x - (\tau - \theta_{(x+\phi)} - \tau)_n$. The plots are given for various combinations of θ , ϕ in the SLS. In all the cases $\nu = 26.7817$ MHz, the resonance off-set, $\Delta\omega$, is about -8 KHz. The relative signal amplitudes in all the figures are in the same scale.

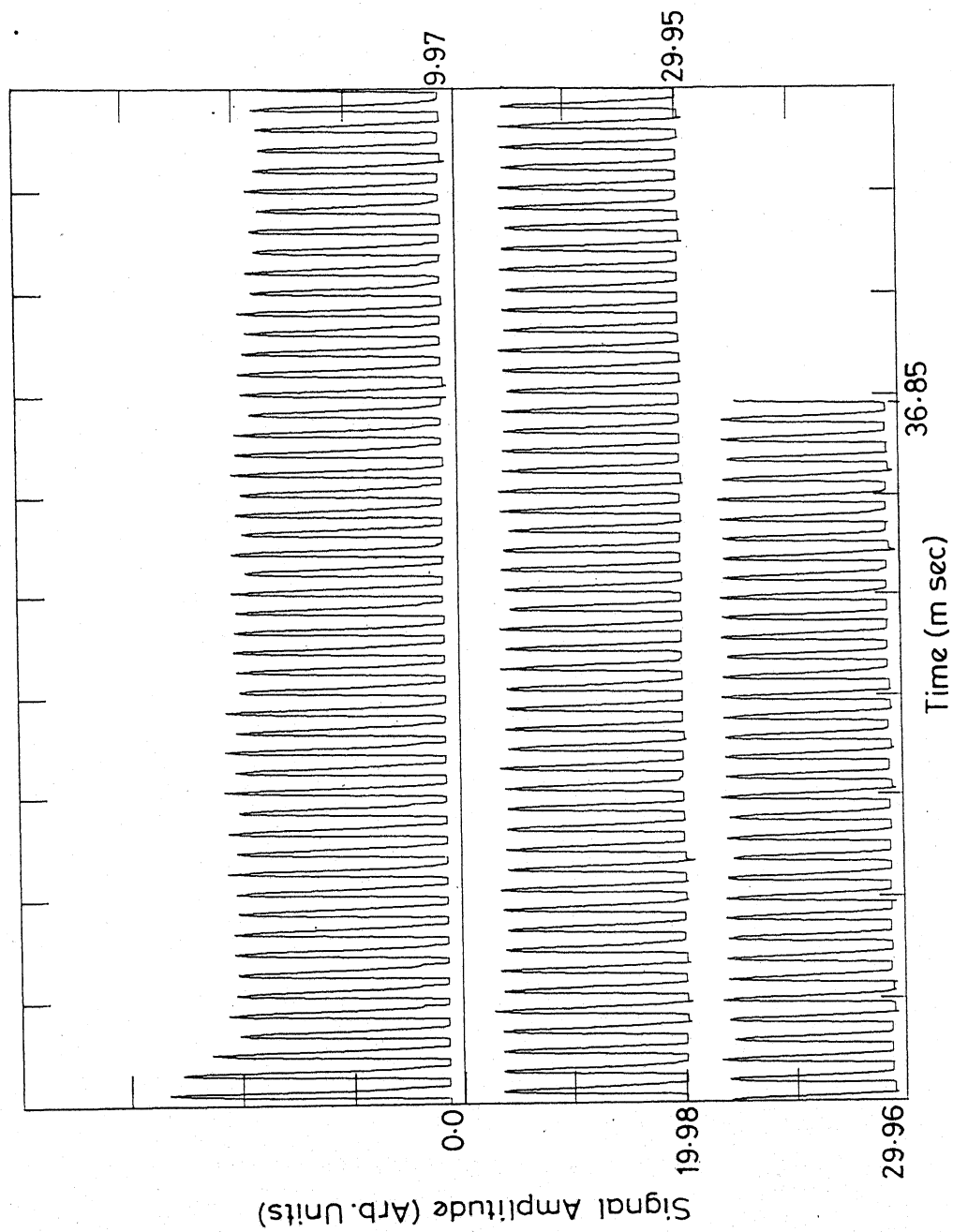


Fig. IV.3(a) O-W Sequence: $\theta = \pi/2$, $\phi = 90^\circ$, $\tau = 100 \mu\text{sec}$

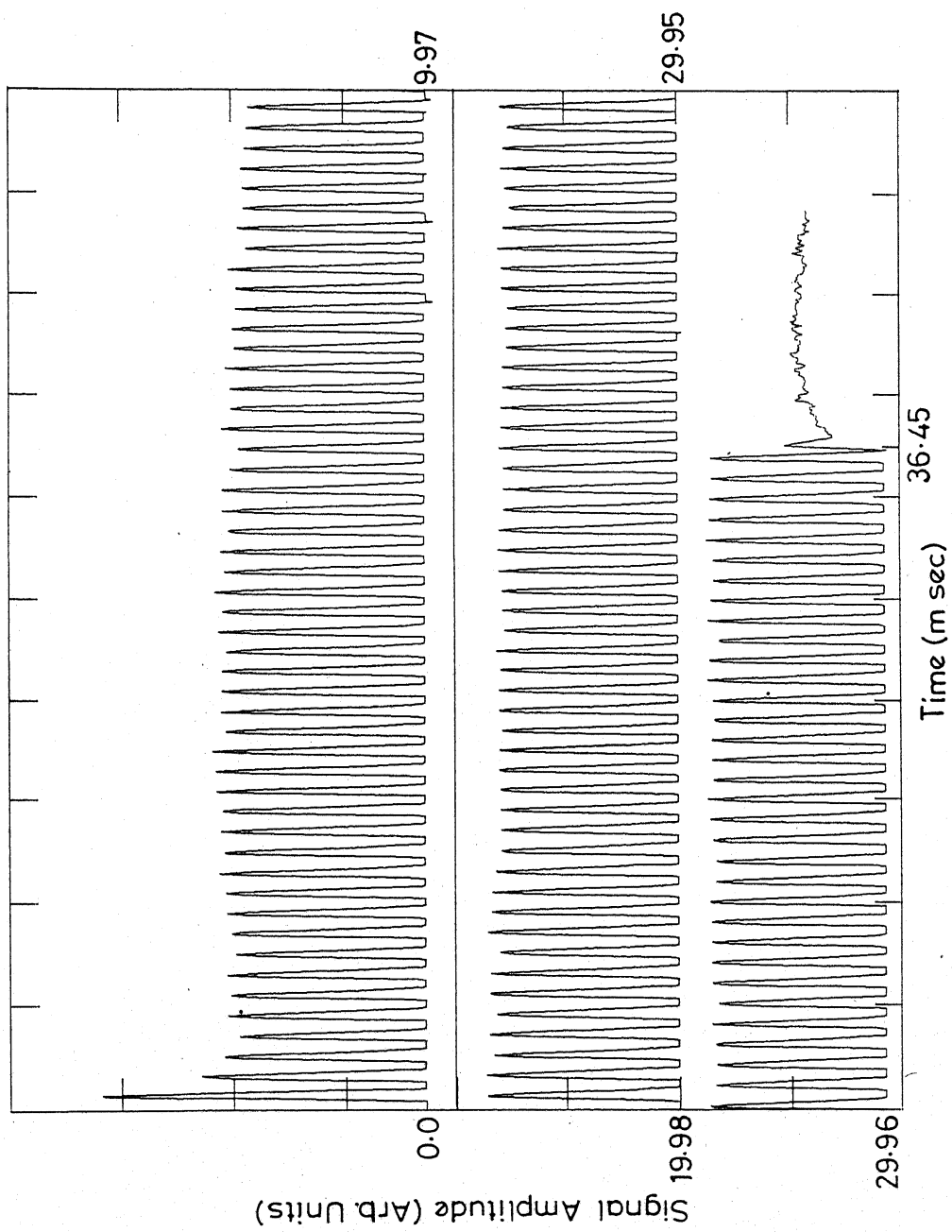


Fig. IV.3(b) CP Sequence: $\theta = \pi$, $\phi = 0$, $\tau = 100 \mu \text{sec}$

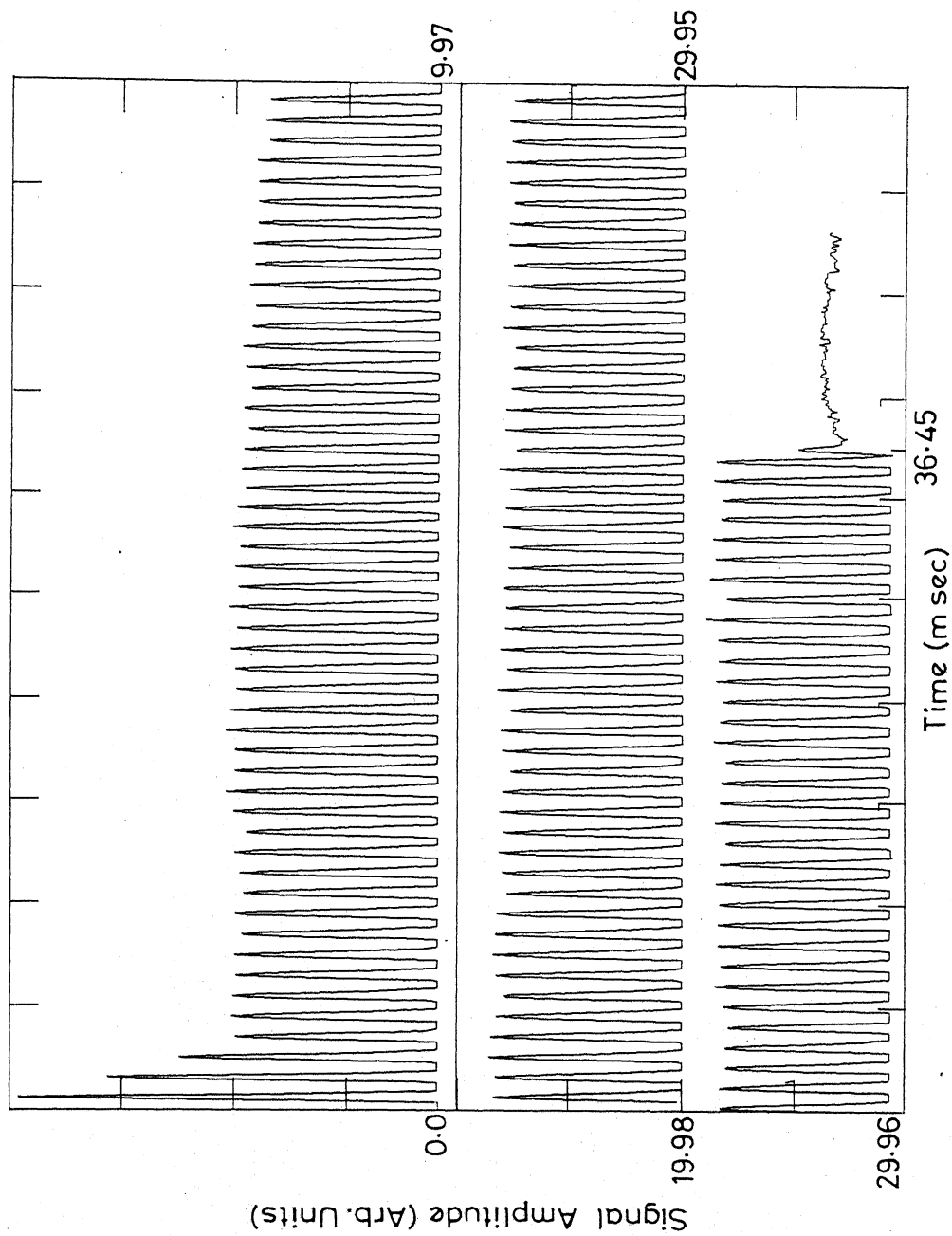


Fig. IV-3(c) CPMG Sequence : $\theta = \pi$, $\phi = 90^\circ$, $\tau = 100 \mu \text{sec}$

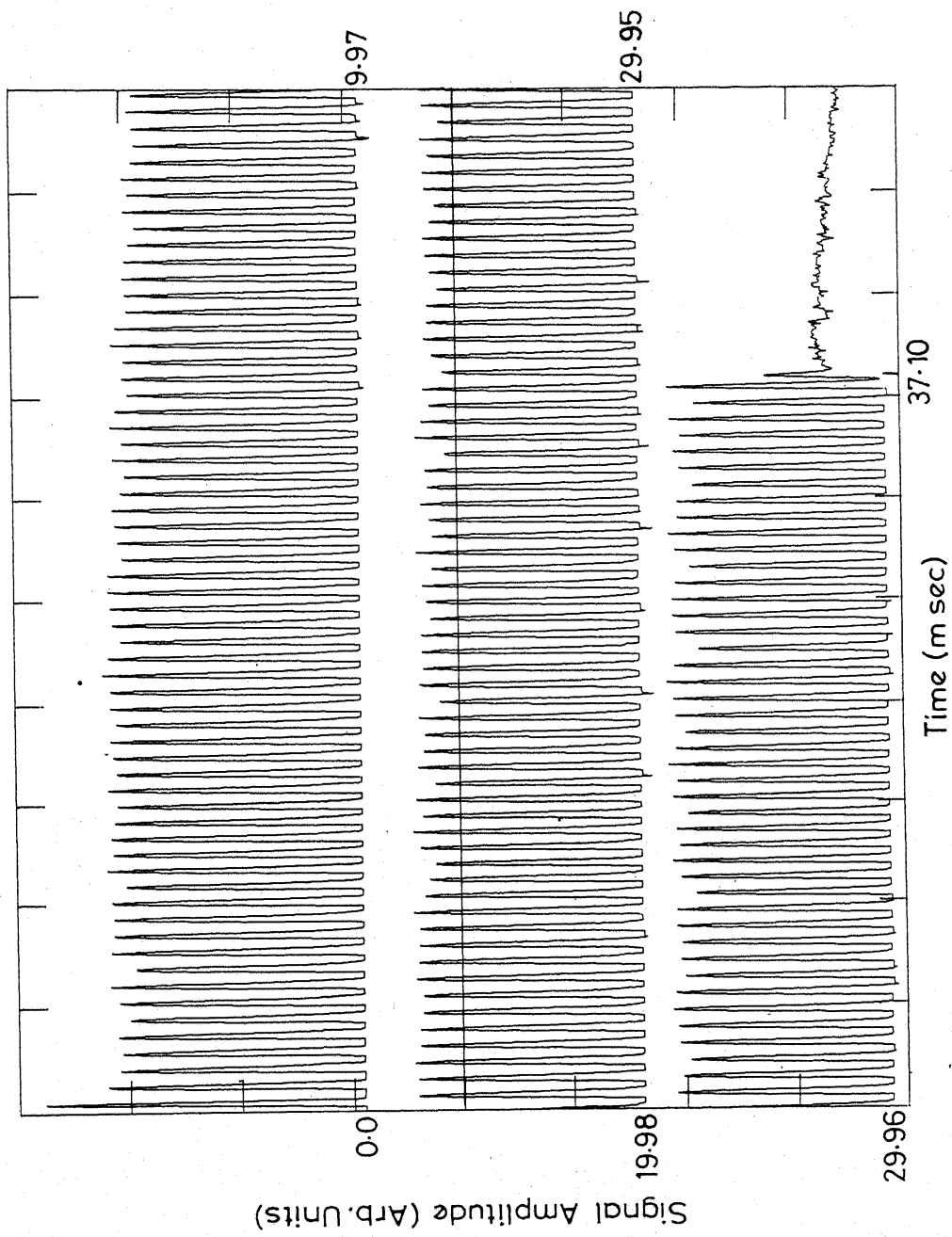


Fig. IV.3(d) $\theta = \pi/2$, $\phi = 180^\circ$, $\tau = 80 \mu \text{ sec}$

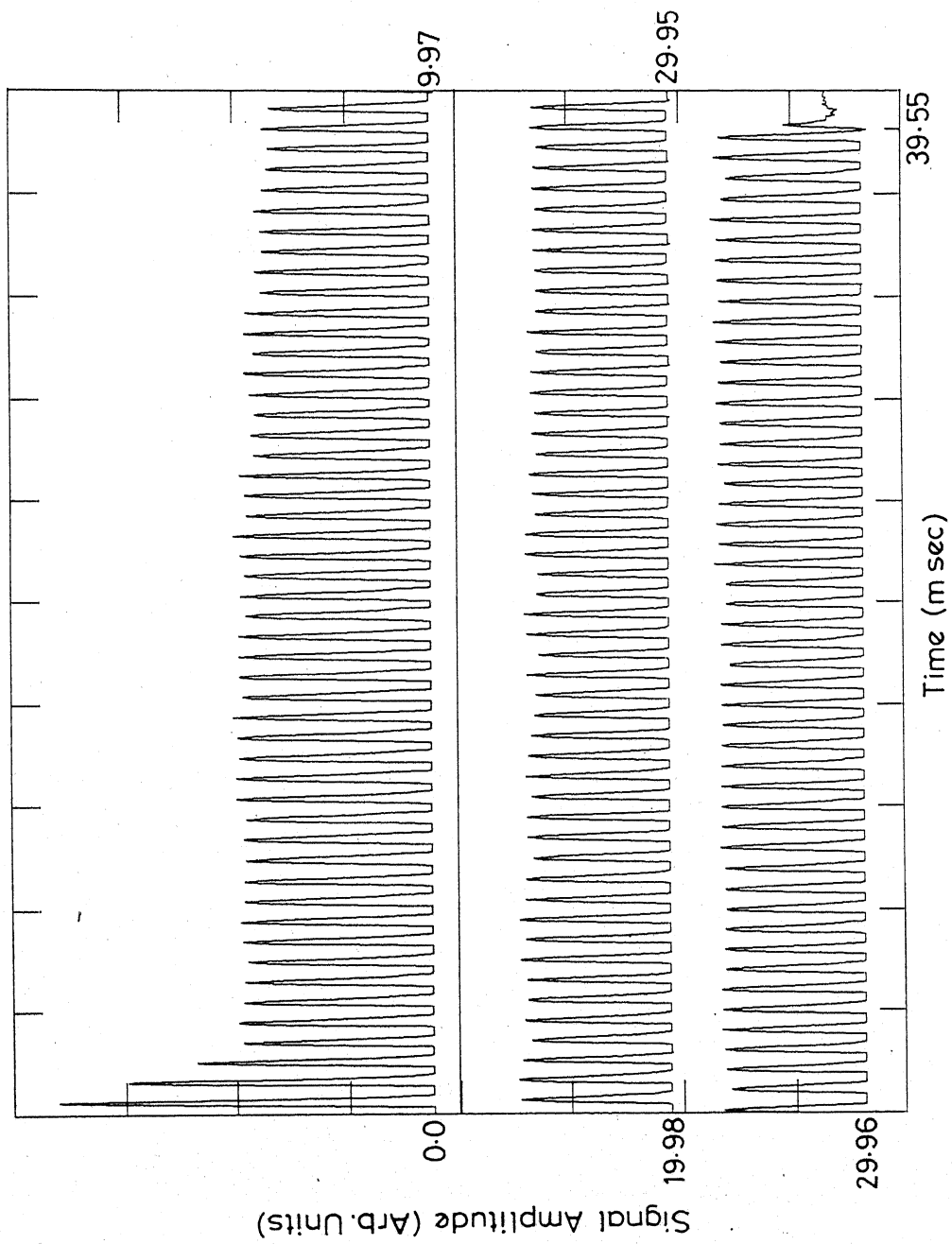


Fig. IV-3(e) $\theta \approx 145^\circ$, $\Phi = 90^\circ$, $\tau = 100 \mu \text{ sec}$

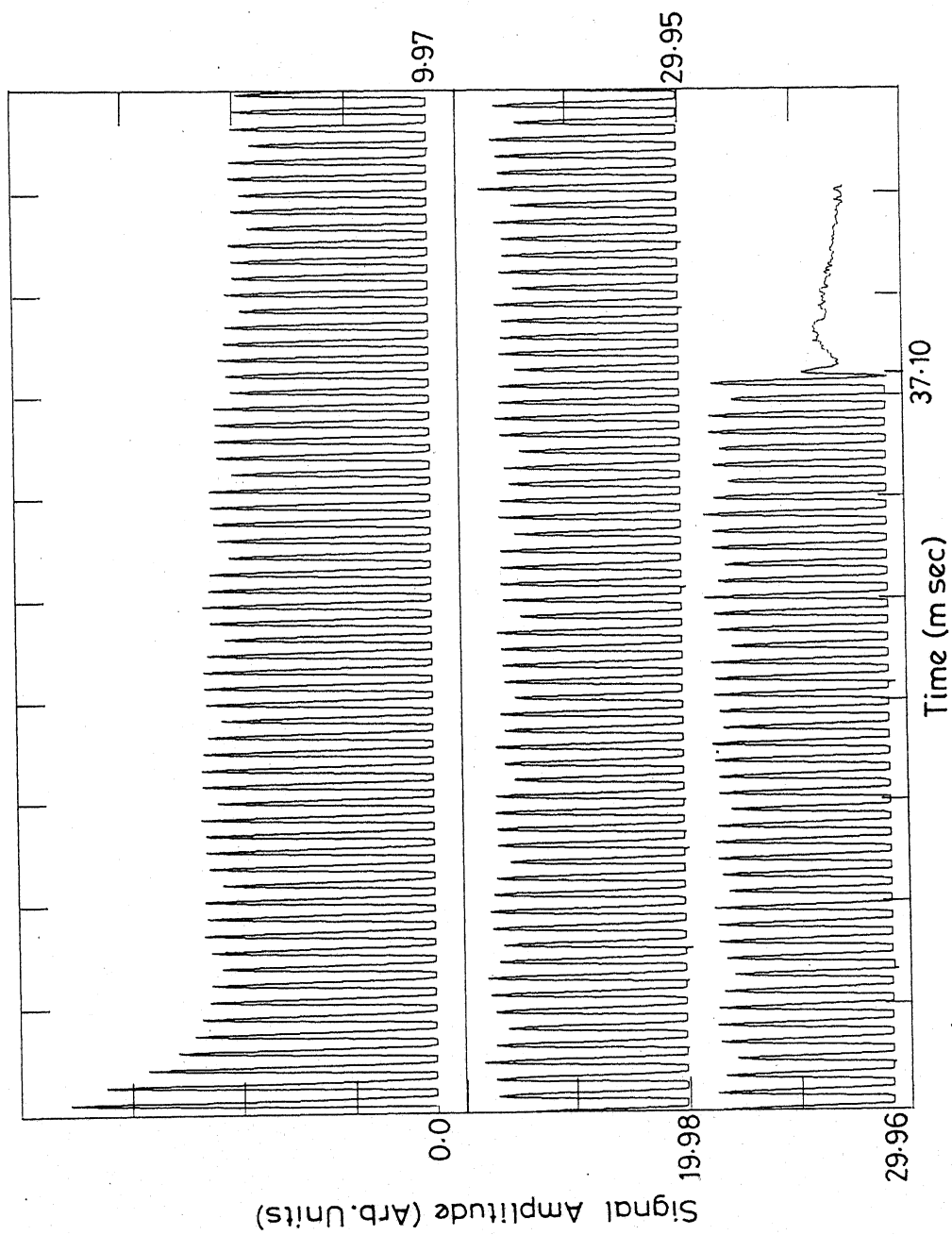


Fig.IV.3(f) O-W Sequence: $\theta = \pi/2$, $\Phi = 90^\circ$, $\tau = 80 \mu \text{sec}$

Fig. IV.4(a) Response of ^{185}Re in polycrystalline sample
to of KReO_4 to spin-locking sequence, $(\pi/2)_x -$
Fig. IV.4(f) $(\tau - \theta_{(x+\phi)} - \tau)_n$. Fig. 4(a) to 4(f) give the
results for various combinations of θ , ϕ in
the SLS. In all the cases $\nu = 28.3043 \text{ MHz}$,
Resonance off-set, $\Delta\omega$, $\approx -8 \text{ KHz}$ and $\tau = 80$
 μsec . The relative signal amplitudes in
all the figures are in the same scale.

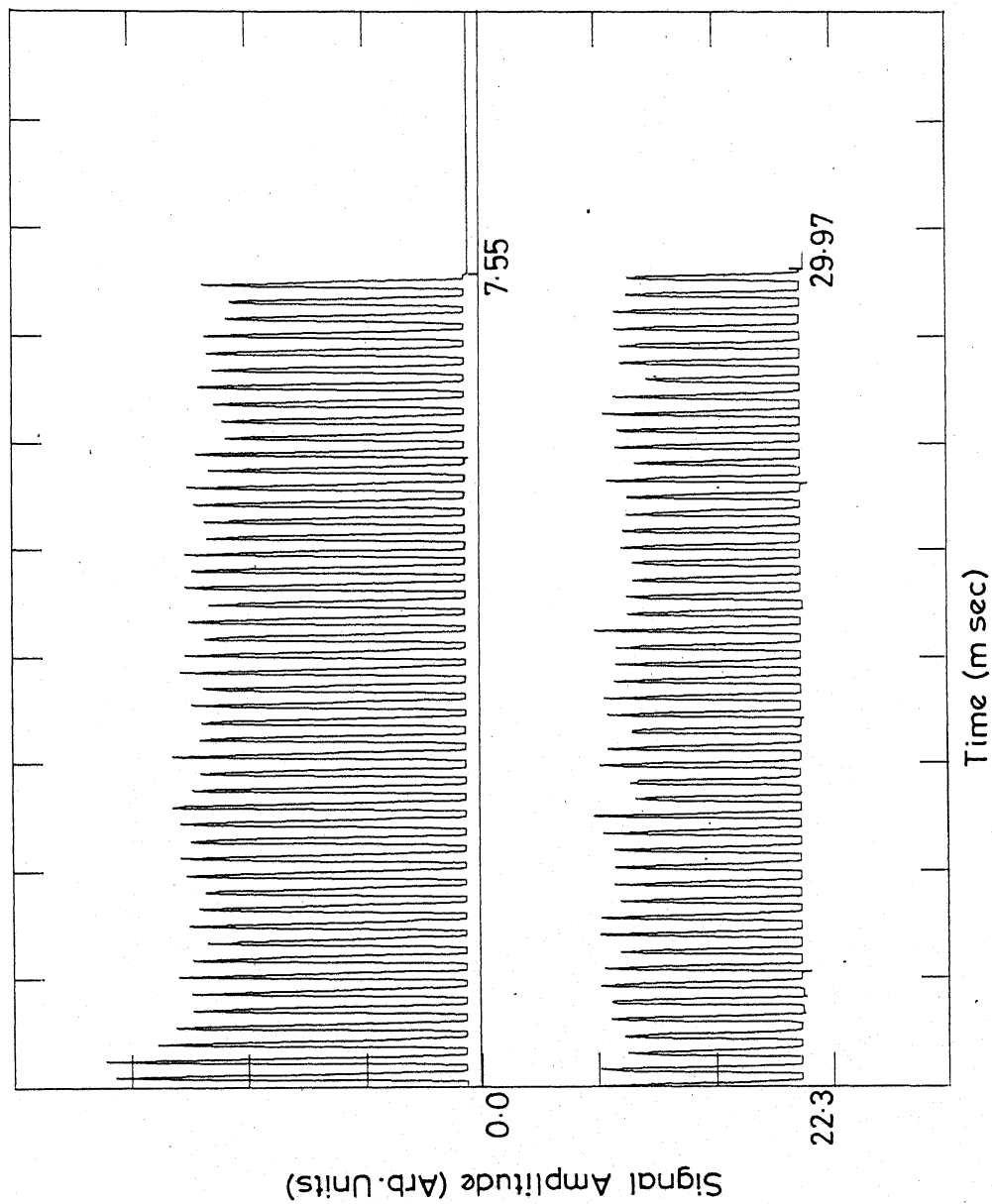


Fig. IV.4(a) OW Sequence: $\theta = \pi/2$, $\phi = 90^\circ$

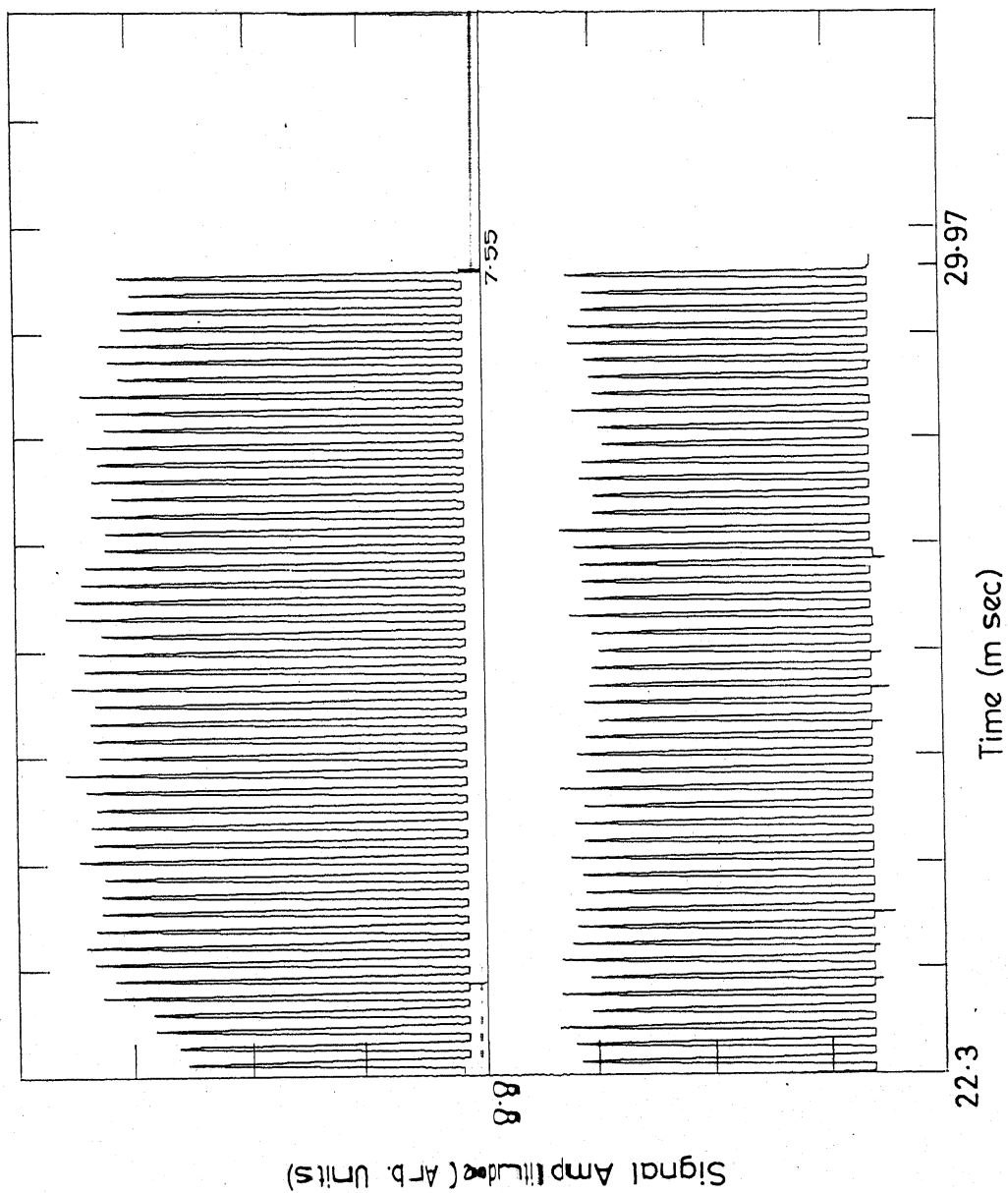


Fig. IV-4(b) CP Sequence : $\theta = \pi$, $\phi = 0$

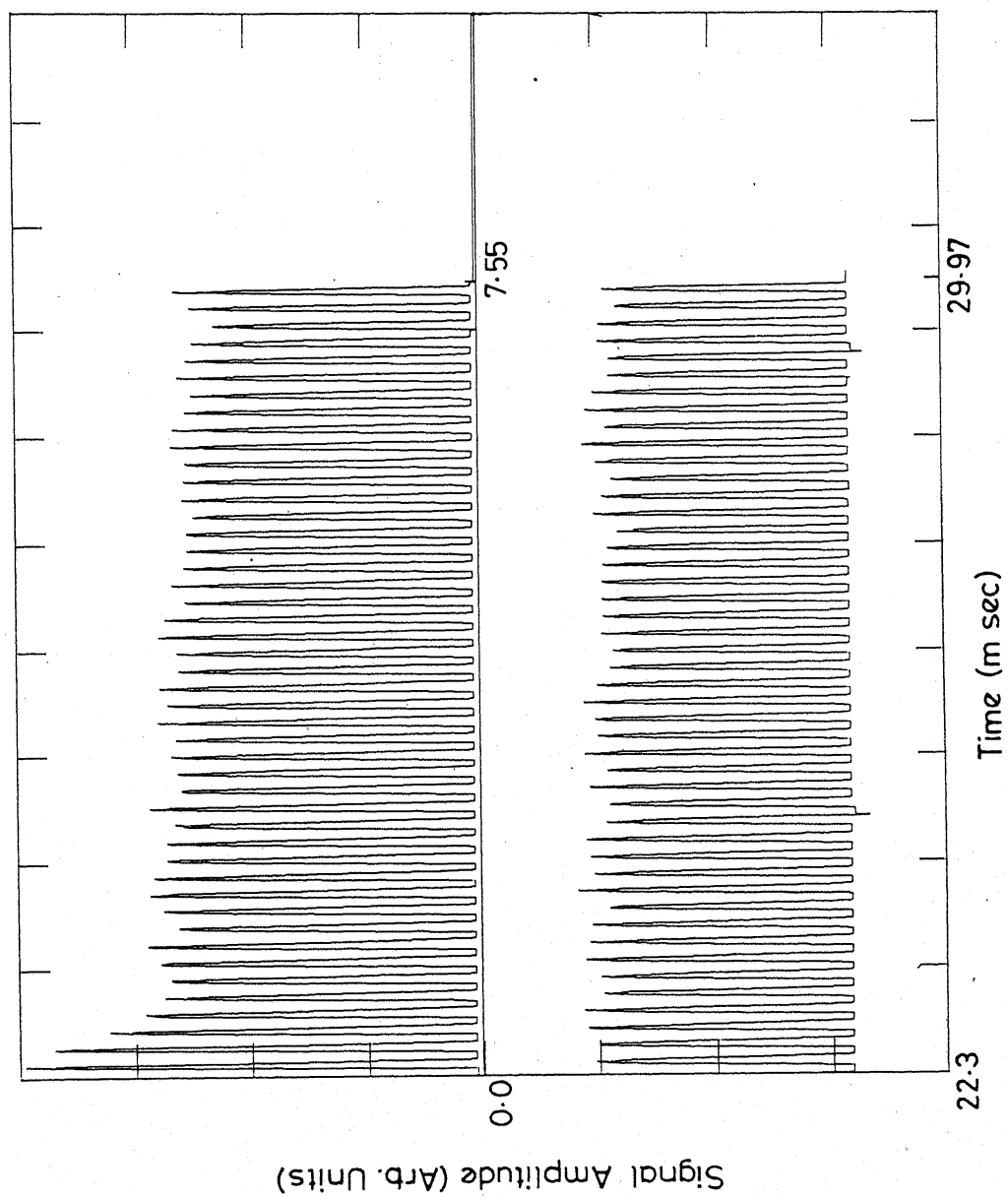


Fig. IV.4(c) CPMG Sequence: $\theta = \pi$, $\phi = 90^\circ$

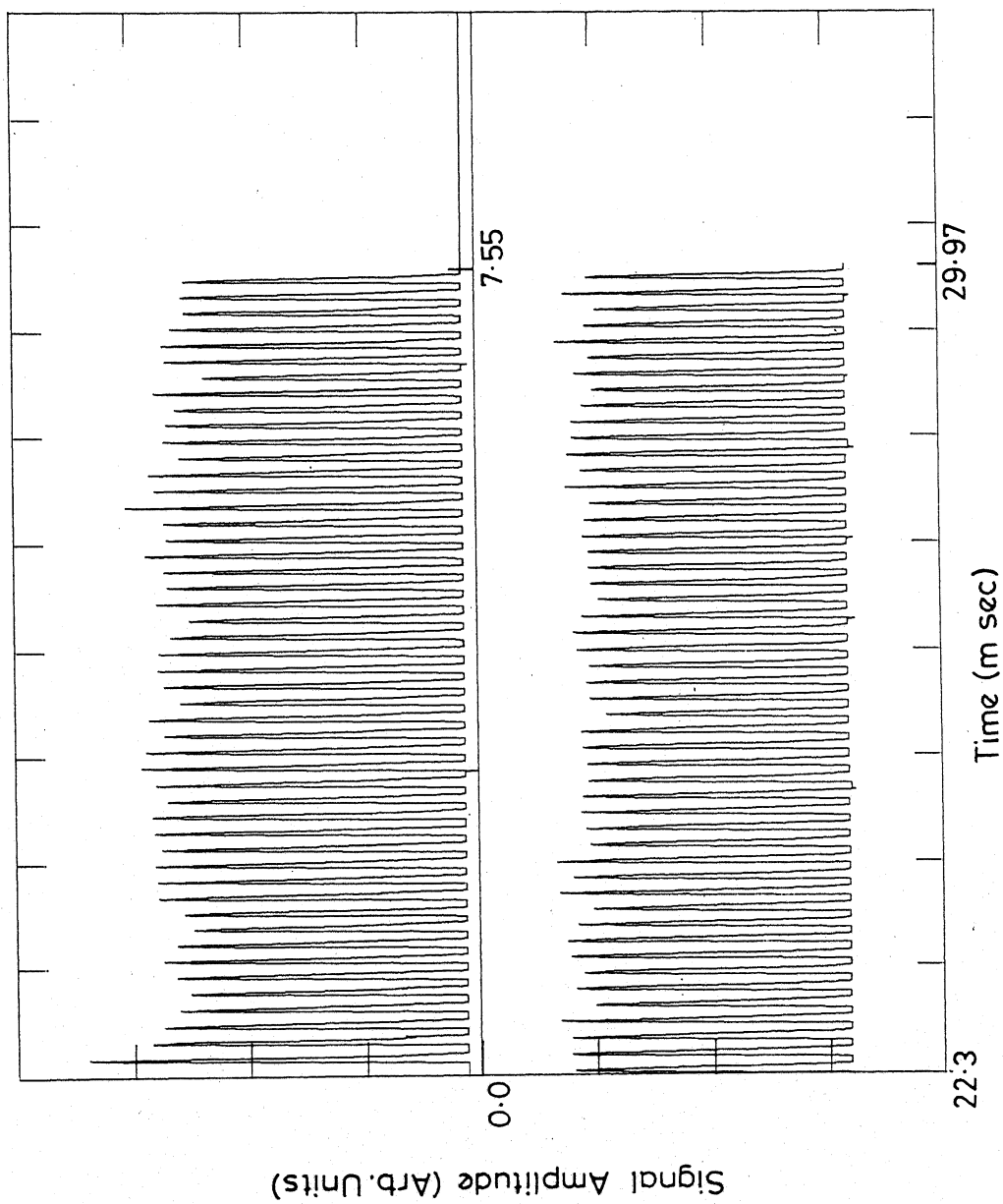


Fig. IV-4(d) $\theta = \pi/2$, $\phi = 180^\circ$

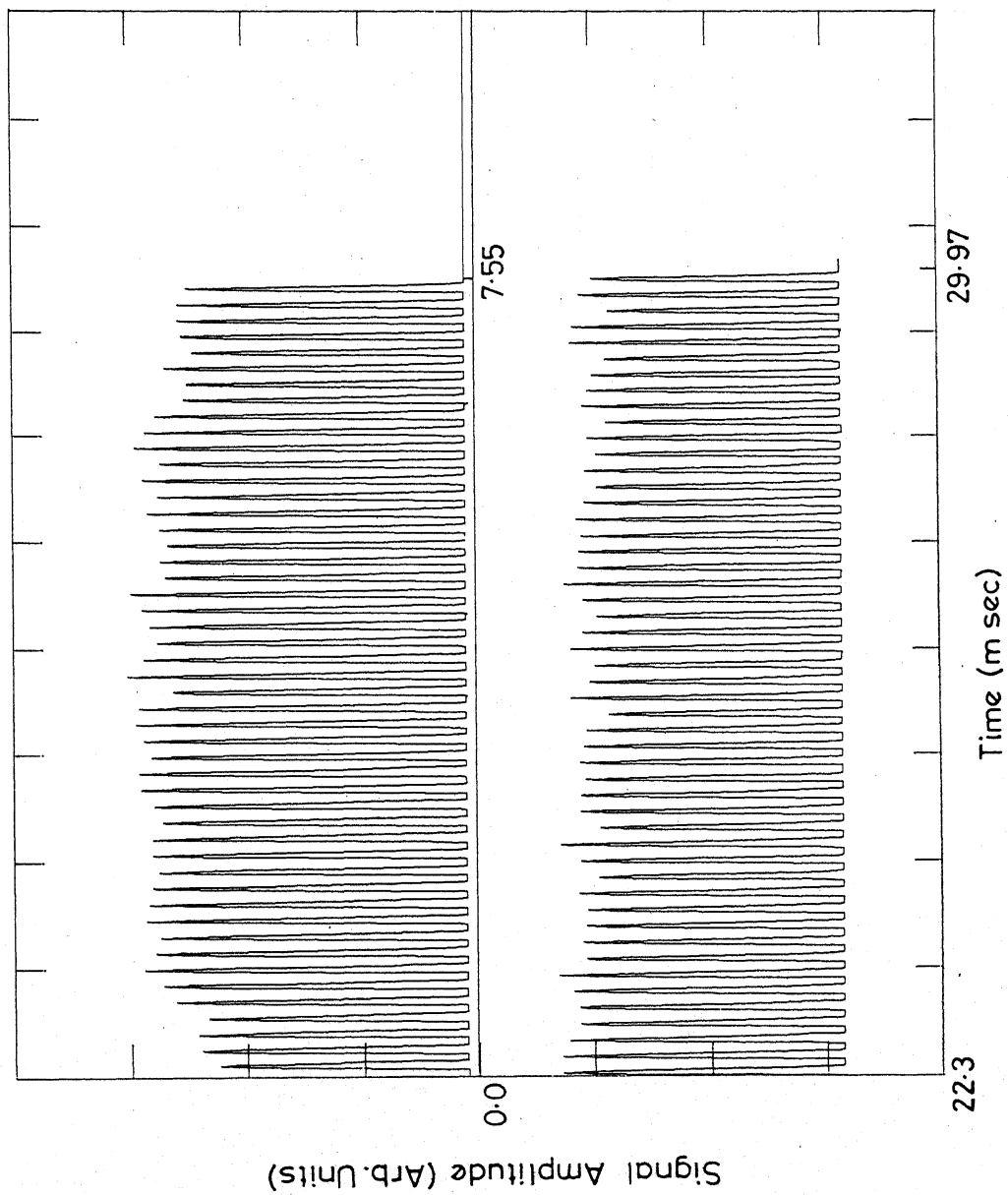


Fig. IV.4(e) $\theta = \pi/2$, $\phi = 0$

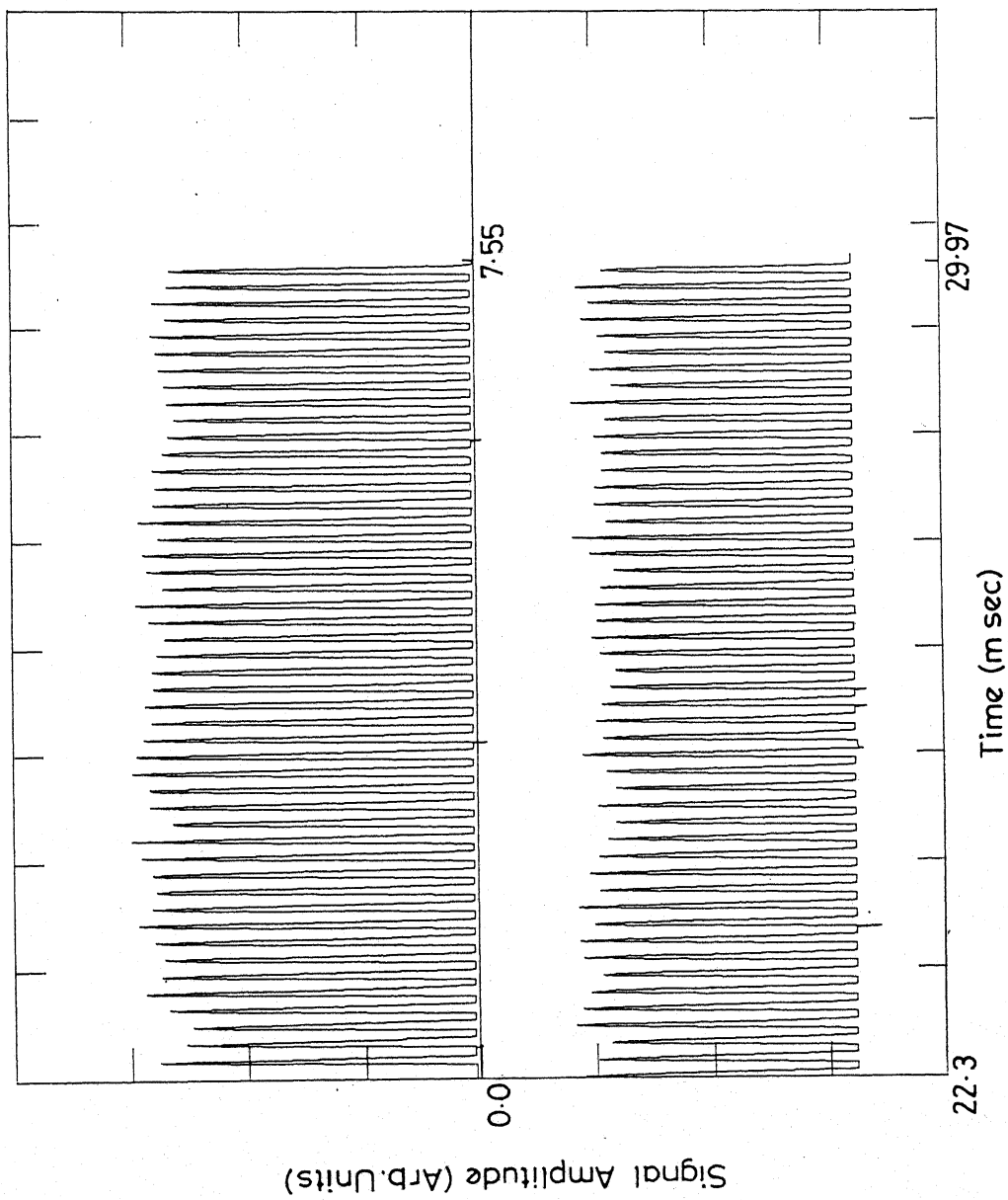


Fig. IV-4(f) $\theta = \pi$, $\phi = 180^\circ$

to be 180 μ sec. For each ' θ ' value we have computed the time constant for the decay of the QEM, T_{2e} , by fitting the experimental data to an exponential function. The T_{2e} values obtained for various values of θ both in the case of ^{35}Cl in single crystal as well as in polycrystalline sample of NaClO_3 are given in Table IV.1.

Table IV.1. Dependence of the Quasi-Equilibrium Magnetization Decay Time Constant, T_{2e} , on the Flip-Angle of the Sequence Pulses in the SLS

$$\Delta\omega = -4 \text{ KHz}; \tau = 180 \mu\text{sec}$$

θ_y	T_{2e} (in msec)	
	For ^{35}Cl in single crystal of NaClO_3	For ^{35}Cl in Powder sample of NaClO_3
45°	11.7	17.6
90°	10.5	16.8
180°	9.2	14.0

From the above table it is clear that as ' θ ' is decreased T_{2e} increases indicating that the spin-locking effect is more effective with smaller flip-angles of the sequence pulses. It is also evident from this table that T_{2e} for a given ' θ ' in the case of polycrystalline sample is higher than that in for the single crystal. Similar kind of behaviour has been observed by Osokin, in the case of ^{14}N in NaNO_2 [6].

IV.B.2(i)b Study of \varnothing and τ dependence:

Until recently, there has been no rigorous experimental investigations of the dependence of the spin-locking phenomenon on \varnothing in SLS. Only recently Narsimha Reddy and Narasimhan [11,21] have studied in detail the dependence of spin-locking effect on \varnothing and found that in the case of nuclei with $I = 3/2$ in polycrystalline specimens spin-locking effect could be observed with arbitrary \varnothing values in SLS. Their results contradict the theoretical predictions due to Ainbinder and Furman [17].

We have carried out the spin-locking experiments on ^{187}Re and ^{185}Re in polycrystalline specimens of KReO_4 and observed the establishment of QEM for different \varnothing values. From Figs. IV.3(a)-IV.3(f) and Figs. IV.4(a)-IV.4(f) it can be seen that (for $\Theta = \pi/2, \pi$) with $\varnothing = 0, \pi/2, \pi$ spin-locking can be achieved in the case of ^{187}Re and ^{185}Re also. These results indicate that the observation of QEM with arbitrary \varnothing values in SLS, in the case of polycrystalline samples is not restricted to spin $I = 3/2$ only but it is valid even for higher spins.

One of the reasons for this observation of the spin-locking phenomenon with arbitrary \varnothing values could be the polycrystalline nature of the sample where the crystallites are randomly oriented with respect to each other and have their own efg principal axes systems which make a distribution of angles with respect to the applied r.f. field.

In order to verify the above reasoning we carried out spin-locking experiments on ^{35}Cl in a single crystal of NaClO_3 , with different \emptyset values. In all these experiments we set $\Delta\omega = -4$ KHz, $\tau = 180 \mu\text{sec}$, $\theta = \pi/2$ or π . The results obtained with $\theta = 45, 135, 225$ are shown respectively in Figs. IV.5(a), IV.5(b) and IV.5(c). The T_{2e} values obtained for $\emptyset = 45, 135$ and 225 are set out in Table IV.2. Now, from Fig. IV.2(a) - IV.2(f) and Fig. IV.5(a) - IV.5(c) it is evident that even in the case of single crystal QEM has been established for arbitrary values of \emptyset .

Table IV.2. T_{2e} Values Obtained from the Study of SLS in the case of ^{35}Cl in Single Crystal of NaClO_3

$\Delta\omega = -4$ KHz ; $\theta = \pi/2$; $\tau = 180 \mu\text{sec}$

\emptyset (in deg)	T_{2e} (msec)
45	10.6
135	11.9
225	13.2

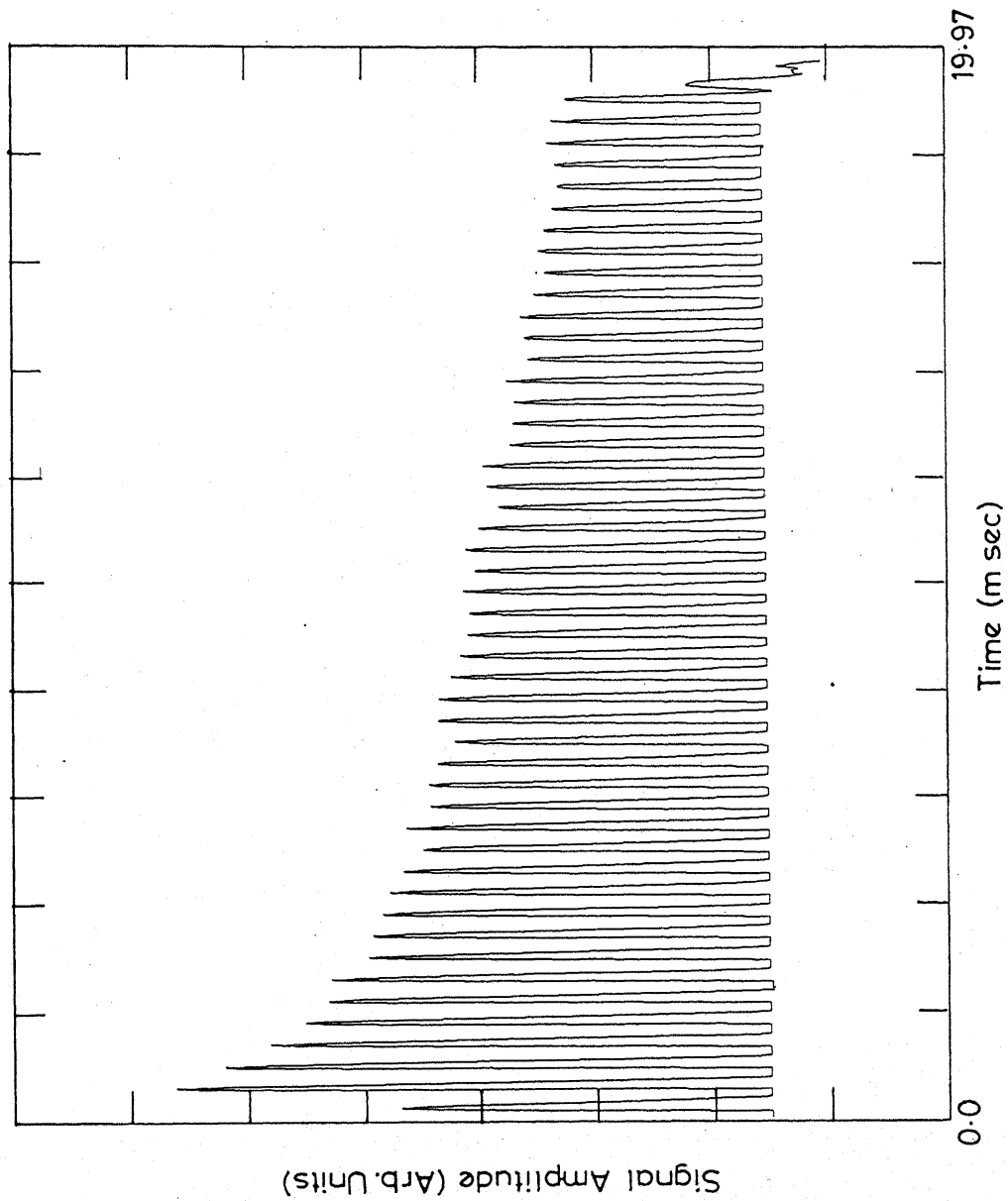


Fig. IV.5(a) Response of ^{35}Cl in a single crystal of NaClO_3 to SLS.
 $\Delta\omega = -4\text{ KHz}$, $\tau = 180\text{ }\mu\text{sec}$, $\theta = \pi/2$, $\phi = 45$, $\nu = 29.9232\text{ MHz}$

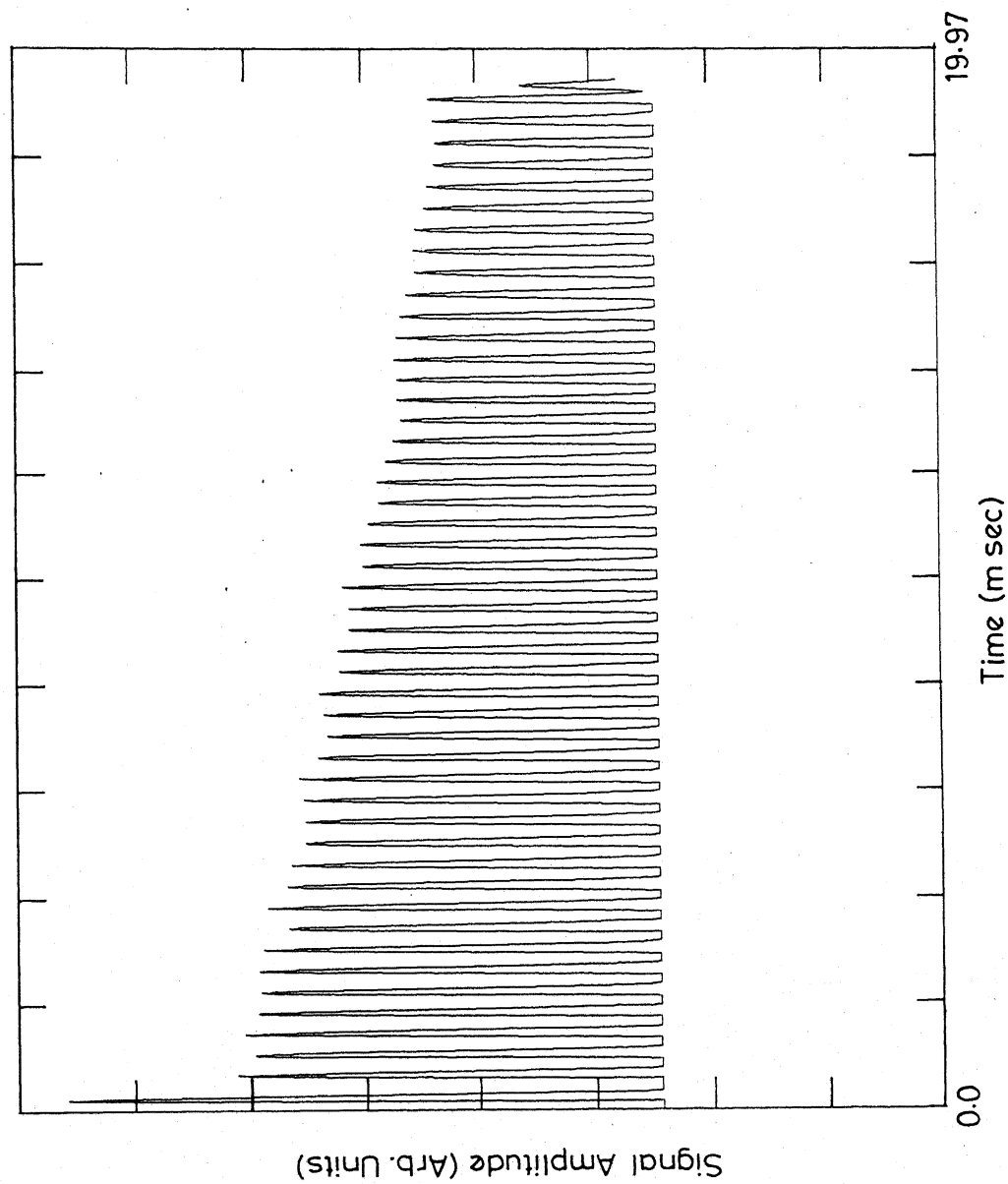


Fig. IV.5(b) Response of ^{35}Cl in single crystal of NaClO_3 to SLS. $\Delta\omega = -4\text{ KHz}$, $\tau = 180\text{ }\mu\text{sec}$, $\theta = \pi/2$, $\phi = 135^\circ$, $\nu = 29\text{ }9232\text{ MHz}$.

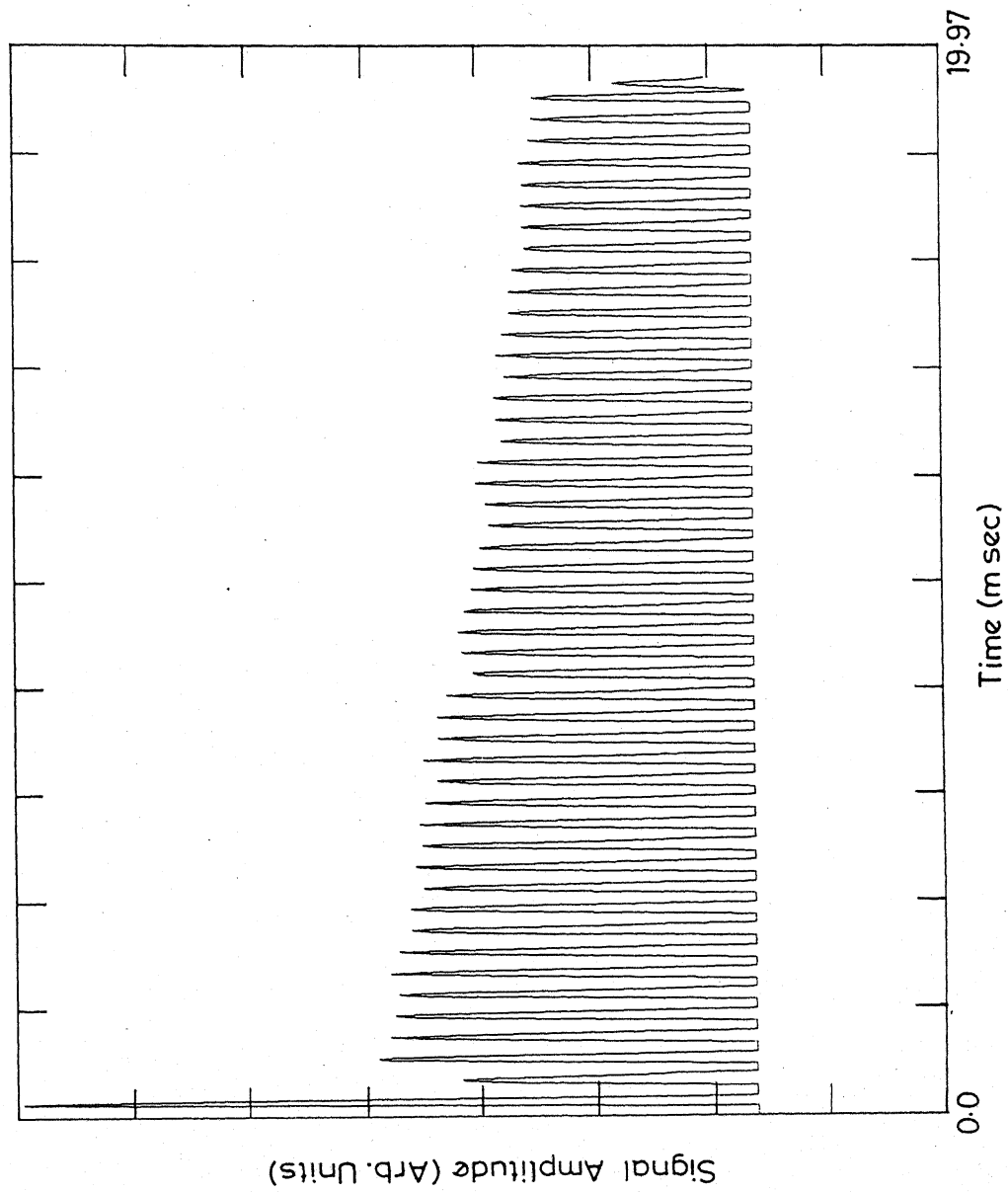


Fig. IV-5(c) Response of ^{35}Cl in a single crystal of NaClO_3 to SLS $\Delta\omega = -4\text{ KHz}$,
 $\tau = 180\text{ }\mu\text{sec}$ $\theta = \pi/2$, $\phi = 225$, $\nu = 29.9232\text{ MHz}$.

Thus from this study it may be inferred that the spin-locking phenomenon can be observed both in polycrystalline samples as well as in single crystal with arbitrary ϕ values.

Marino and Klainer [5] who carried out the first spin-locking experiment in NQR of ^{14}N [$I = 1$] have investigated the dependence of the T_{2e} on τ , and found that $T_{2e} \propto \tau^{-5}$. However, Osokin [8] who also studied the spin-locking experiments on ^{14}N in NaNO_2 has shown that the dependence of T_{2e} on τ is a complex one and that there is no simple relation which exists between them. Similar results have been obtained by Ainbinder et al. [10] in the case of spin $I = 3/2$ nuclei in polycrystalline sample.

In all our experiments we have observed spin-locking effect for all values of $\tau \leq T_2$. However, as the T_{2e} values obtained by us are not very accurate owing to the transmitter pulse feed-through problem, we could not fit our experimental data to any simple relation between T_{2e} and τ .

IV.B.2(i)c Study of resonance off-set, $\Delta\omega$, dependence:

Although the spin-locking effect has been observed on resonance as well as off-resonance we have presented all the results so far with finite resonance off-set. This is on account of the fact that the spin-locked signal amplitude is much smaller at resonance than that in the case with finite resonance off-set.

Table IV.3. Dependence of the Quasi-Equilibrium Magnetization Decay Time Constant T_{2e} on the Flip-Angle of the Sequence Pulses in the PAPS, $\Delta\omega = 0$; $\tau = 180 \mu\text{sec}$

θ_{-x}	T_{2e} (msec)	
	For ^{35}Cl in single crystal of NaClO_3	For ^{35}Cl in powder sample of NaClO_3
45°	15.2	28.4
90°	13.5	27.0
180°	11.6	24.4

Table IV.4. Dependence of the Quasi-Equilibrium Magnetization Decay Time Constant T_{2e} (obtained from ^{35}Cl in Powder Sample of SbCl_3) on the Flip-Angle of the Sequence Pulses in the PAPS

$\Delta\omega = 0$; $\tau = 150 \mu\text{sec}$

θ_{-x}	T_{2e} (msec)
45°	11.2
90°	10.0
180°	8.4

In the case of ^{35}Cl in NaClO_3 single crystal, CPMG sequence (with $\tau = 200 \mu\text{sec}$) while in the case of ^{187}Re in polycrystalline sample of KReO_4 OW sequence (with $\tau = 80 \mu\text{sec}$) are employed to study the dependence of QEM on resonance off-set. A plot of $\Delta\omega$ versus the amplitude of QEM obtained in these cases are given in Fig. IV.6 and Fig. IV.7, respectively. Similar kind of behaviour of QEM has been theoretically predicted for the case of spin $I = 1$ [16].

IV.B.2(ii) Phase alternated pulse sequence (PAPS):

We have investigated influence of PAPS on ^{35}Cl in both single crystal and powder sample of NaClO_3 , and in polycrystalline sample of SbCl_3 . In this case all the experiments have been carried out on resonance. The decay constant of QEM as a function of ' θ ' of the sequence pulses has been calculated and the results obtained in the case of NaClO_3 are given in Table IV.3 and those obtained in the case of SbCl_3 are given in Table IV.4.

Typical recordings of responses of PAPS (with $\tau = 160 \mu\text{sec}$, $\Delta\omega = 0$) obtained from ^{35}Cl in a single crystal and in polycrystalline sample of NaClO_3 are shown respectively in Figs. IV.8(a) and IV.8(b). In Figs. IV.9(a) and IV.9(b) we have compared the results of PAPS (with same τ value and $\Delta\omega = 0$) obtained from ^{35}Cl in single crystal and powder sample of NaClO_3 .

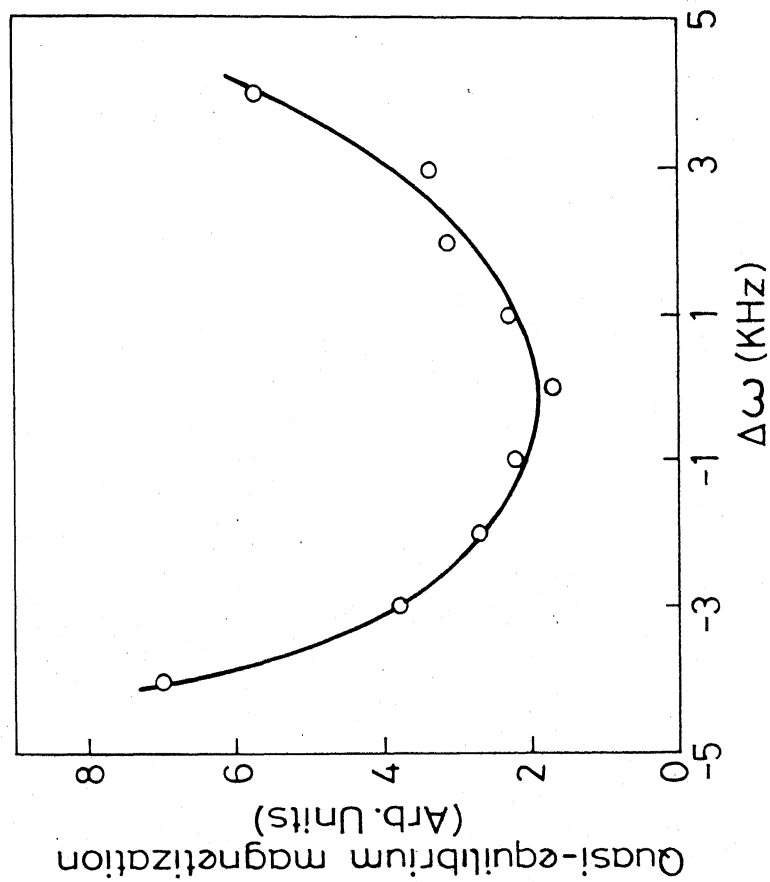


Fig.IV.6 A plot of quasi-equilibrium magnetization, obtained as a response to CPMG sequence from ^{35}Cl in a single crystal of NaClO_3 , vs $\Delta\omega$, the resonance off-set.

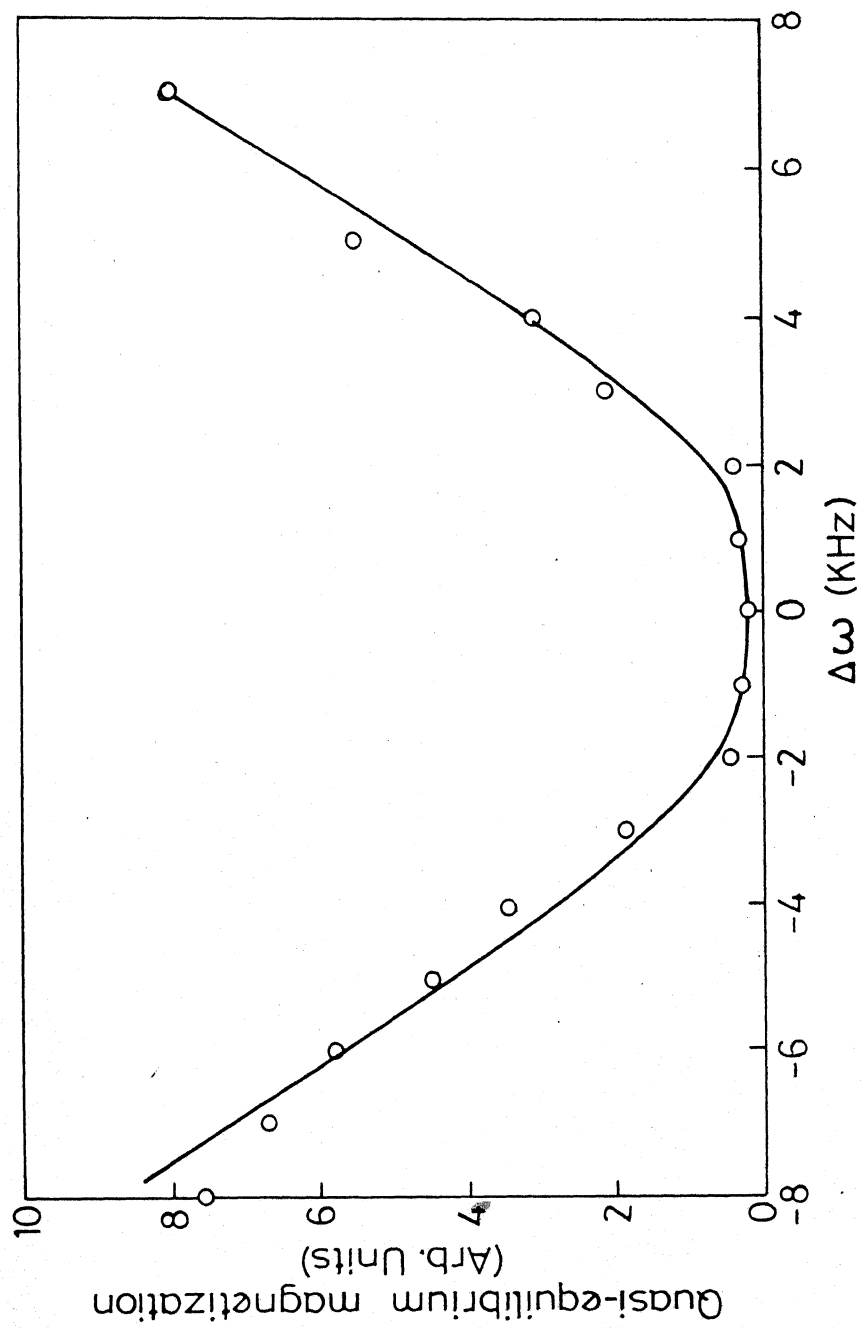


Fig. IV.7 A plot of quasi-equilibrium magnetization, obtained as a response to OW sequence from ^{187}Re in polycrystalline sample of KReO_4 , vs $\Delta\omega$, the resonance off-set.

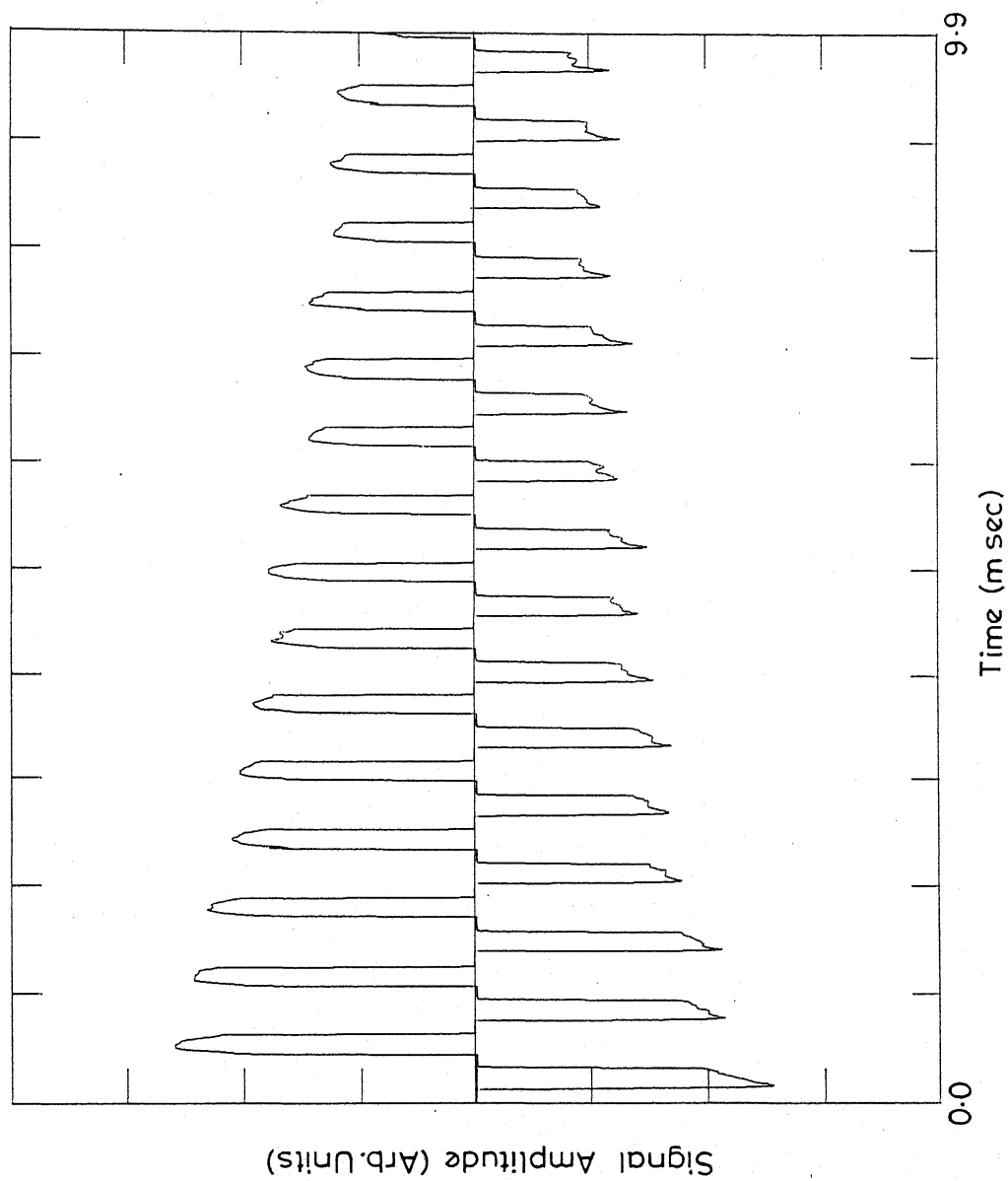


Fig.IV.8(a) Response of ^{35}Cl in a single crystal of NaClO_3 to PAPS.
 $\Theta_x = (\pi)_{-x}$, $\Delta\omega=0$, $\tau=160\mu\text{sec}$ and $\nu=29.9232\text{MHz}$.

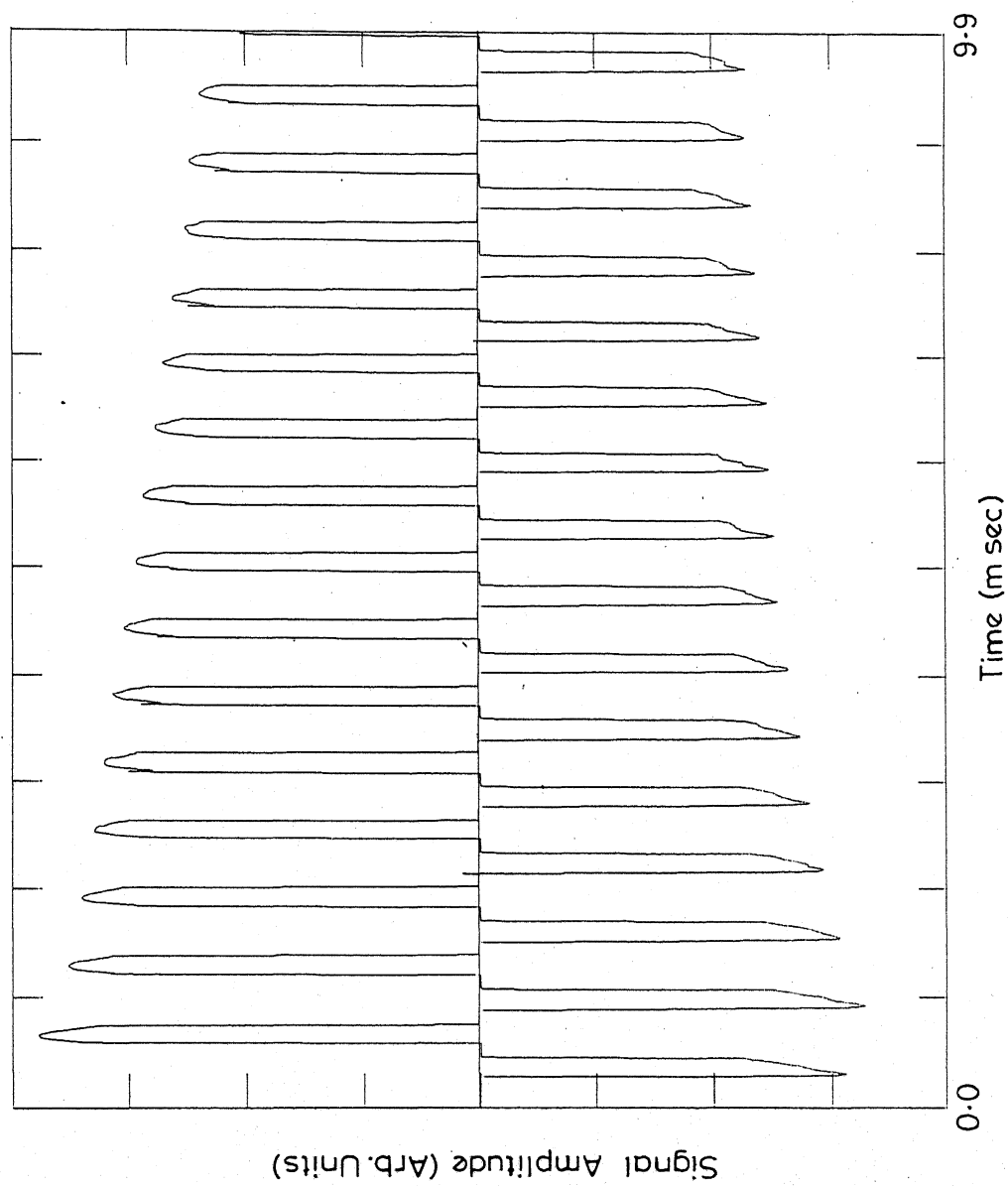


Fig IV 8(b) Response of ^{35}Cl in polycrystalline specimen of NaClO_3 to PAPS.
 $\Theta_{-x} = (\pi)_{-x}$, $\Delta\omega = 0$, $\tau = 160 \mu\text{sec}$ and $\nu = 29.9232 \text{ MHz}$.

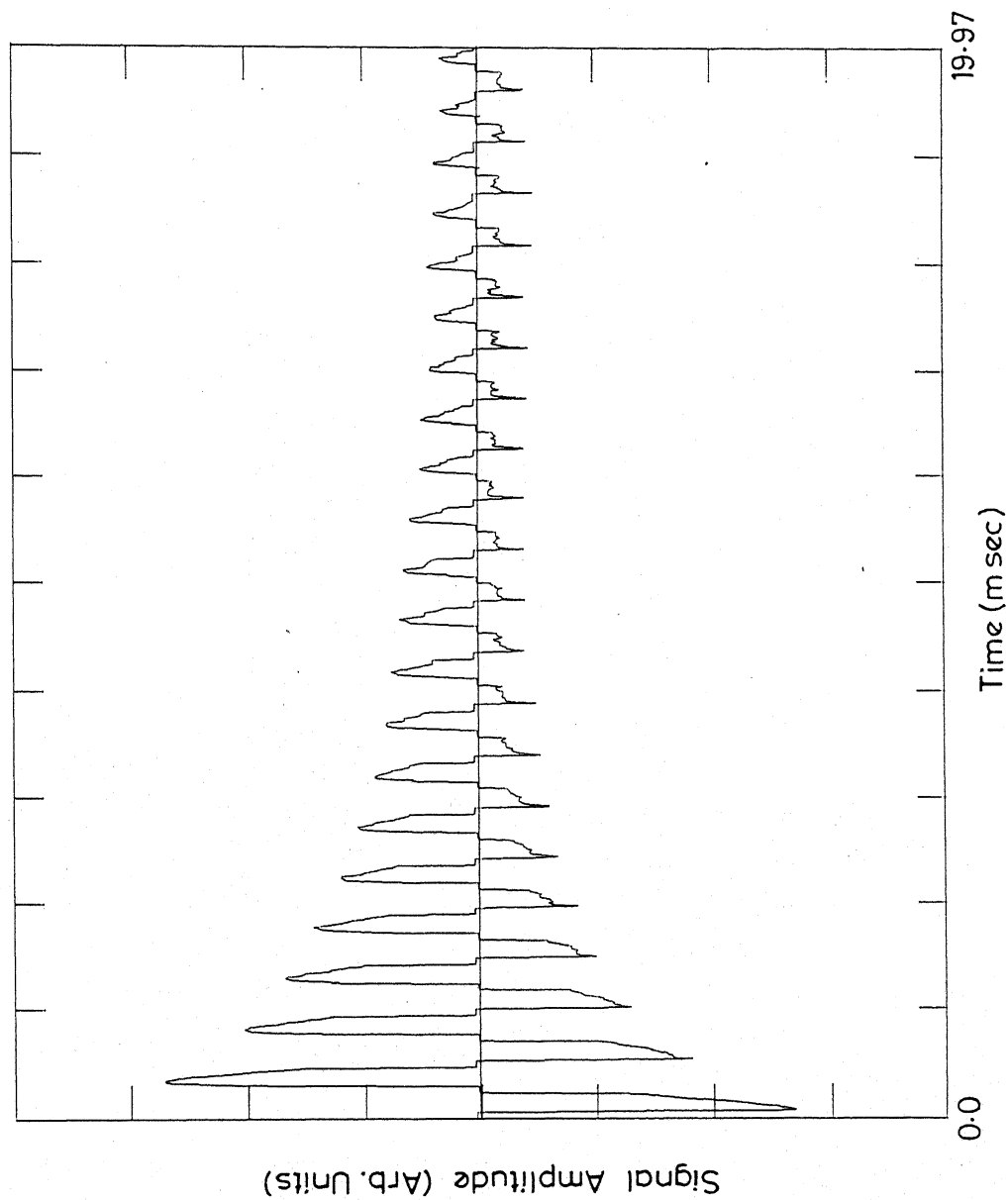


Fig. IV.9(a) Response of ^{35}Cl in a single crystal of NaClO_3 to PAPS.
 $\Theta_{-X} = (\pi)_{-X}$, $\Delta\omega = 0$, $\tau = 240 \mu\text{sec}$ and $\nu = 29.9232 \text{ MHz}$.

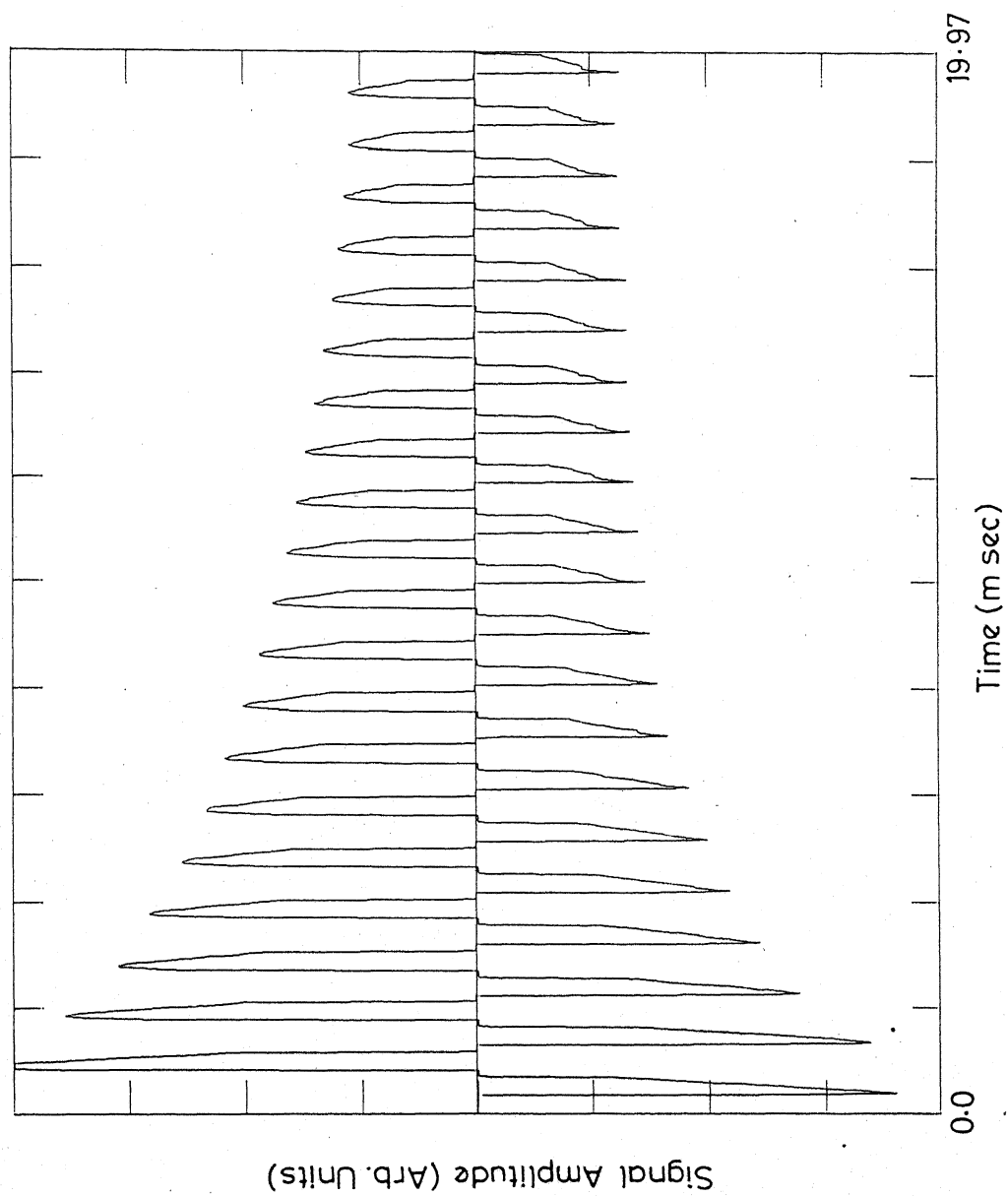


Fig.IV.9(b) Response of ^{35}Cl in polycrystalline sample of NaClO_3 to PAPS.
 $\theta_{-x} = (\pi)_{-x}$, $\Delta\omega = 0$, $\tau = 240 \mu\text{sec}$ and $\nu = 29.9232 \text{ MHz}$.

A typical recording of response of ^{35}Cl in SbCl_3 to PAPS (with $\tau = 120 \mu\text{sec}$, $\Delta\omega = 0$) is given in Fig. IV.10. The spin-spin relaxation time, T_2 , of ^{35}Cl in polycrystalline sample of SbCl_3 is about 0.5 msec. In the case of ^{35}Cl in polycrystalline sample of NaClO_3 T_2 is of the order of a msec and $T_1 \approx 45 \text{ msec}$ [25].

From the above results again one can infer that under the action of PAPS the decay constant of QEM is much larger than the spin-spin relaxation time. From Table IV.2 it may be noted that the smaller ' θ ' values lead to longer T_{2e} values, also T_{2e} for a given θ, τ values, in the case of single crystal is less than that in the case of polycrystalline sample of NaClO_3 . Response of ^{187}Re in KReO_4 to PAPS (with $\tau = 80 \mu\text{sec}$, $\Delta\omega = 0$) is shown in Fig. IV.11.

IV.B.2(iii) WAHUA sequence:

WAHUHA sequence is well known in high resolution NMR of solids. It suppresses the dipole-dipole interactions and leaves the chemical shift interaction active by selective averaging and lead to high resolution NMR spectrum.

In the case of pure NQR, the only report on the study of WAHUHA sequence is that of Ermakov et al. [12] who investigated the influence of this sequence on ^{14}N ($I = 1$) in a single crystal of NaNO_2 . To the best of our knowledge there has been no literature report on the study of WAHUHA sequence in the case of spin $I > 1$.

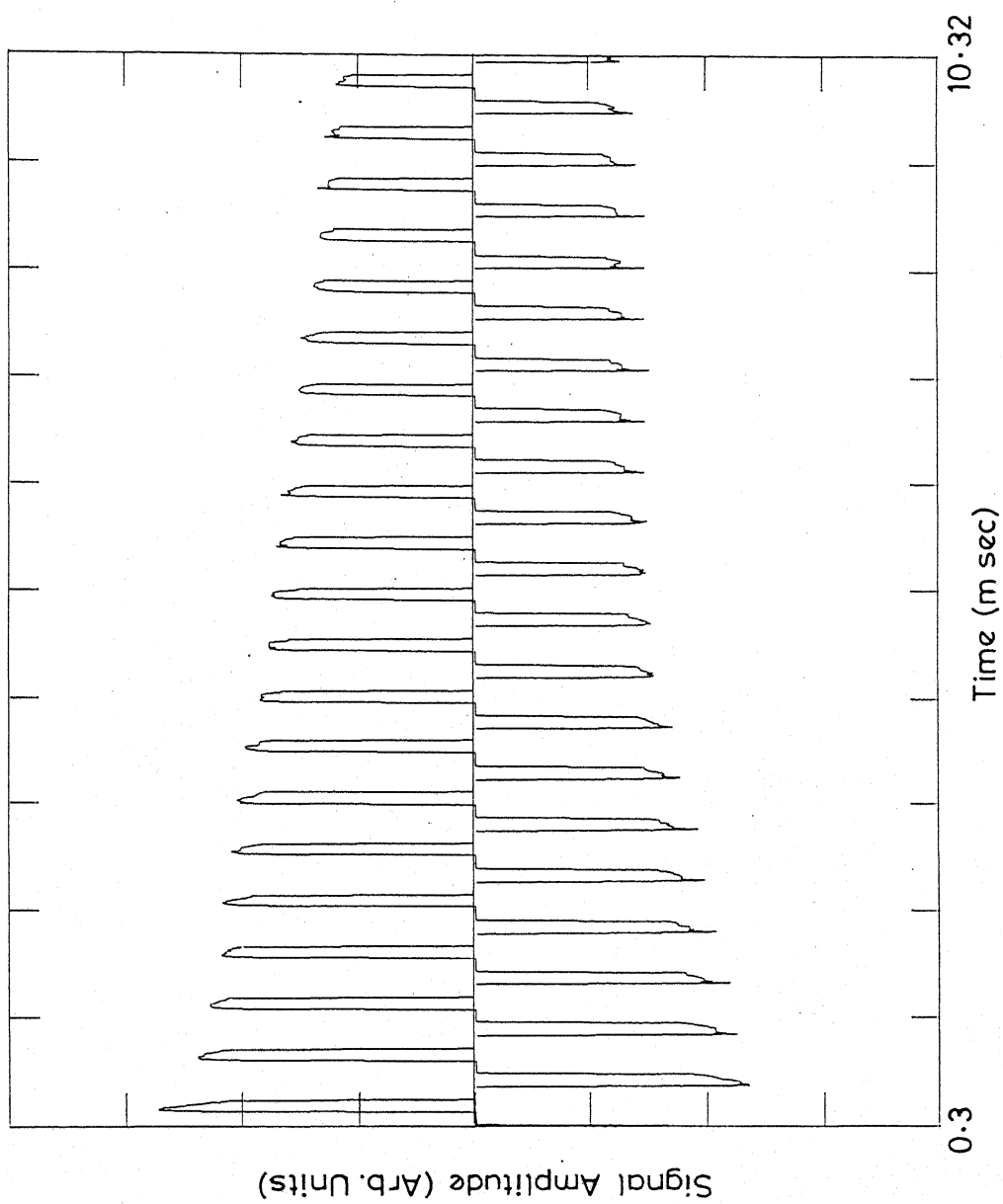


Fig.IV.10 Response of ^{35}Cl in polycrystalline specimen of SbCl_3 to PAPS.
 $\Theta_{-x} = (\pi)_{-x}$, $\Delta\omega = 0$, $\tau = 120 \mu\text{sec}$ and $\nu = 19.175 \text{ MHz}$.

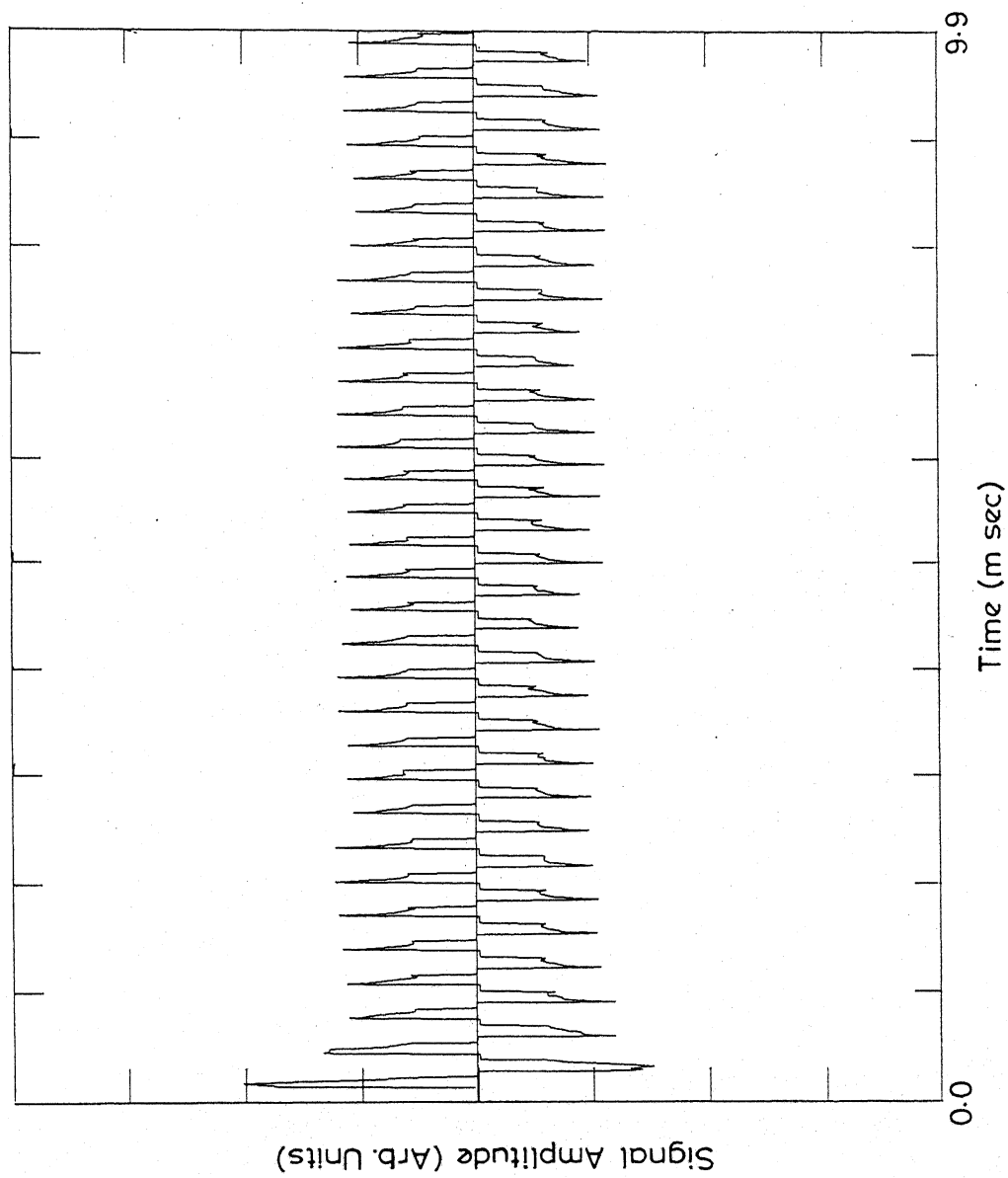


Fig. IV.11 Response of ^{187}Re in polycrystalline sample of KReO_4 to PAPS.
 $\Theta_{-x} = (\pi)_{-x}$, $\Delta\omega = 0$, $\tau = 80 \mu\text{sec}$ and $\nu = 26.7817 \text{ MHz}$.

We have experimentally investigated the action of WAHUHA sequence on ^{35}Cl in the polycrystalline samples of NaClO_3 and KClO_3 and on ^{187}Re in KReO_4 . The results obtained in the case of NaClO_3 and KClO_3 are shown respectively in Fig. IV.12 and Fig. IV.13 while Fig. IV.14 gives the results of ^{187}Re . From these figures the lengthening of the decay of the magnetization is quite evident. This suggests that under the action of WAHUHA sequence some of the internal interactions which contribute to the line width are getting averaged out. It should be mentioned here that one of the important criterion for any multiple pulse sequence to be effective in averaging out the internal interactions is that the cycle time τ_c , should be much less than T_2^* , i.e., $\tau_c \ll T_2^*$ [1]. However, because of the pulsewidth requirements the cycle times employed in all the cases studied were more than or equal to T_2^* . Despite the large cycle times the lengthening of the decay of the magnetization could be observed. The decay constants of the magnetization as a function of τ obtained in the case of ^{35}Cl in polycrystalline sample are set out in Table IV.5.

Table IV.5. T_{2e} Values Obtained from a Study of WAHUHA Sequence in the Case of ^{35}Cl in Polycrystalline Sample of NaClO_3

$\tau (\mu\text{sec})$	$T_{2e} (\text{msec})$
100	20.5
120	18.0
150	17.2

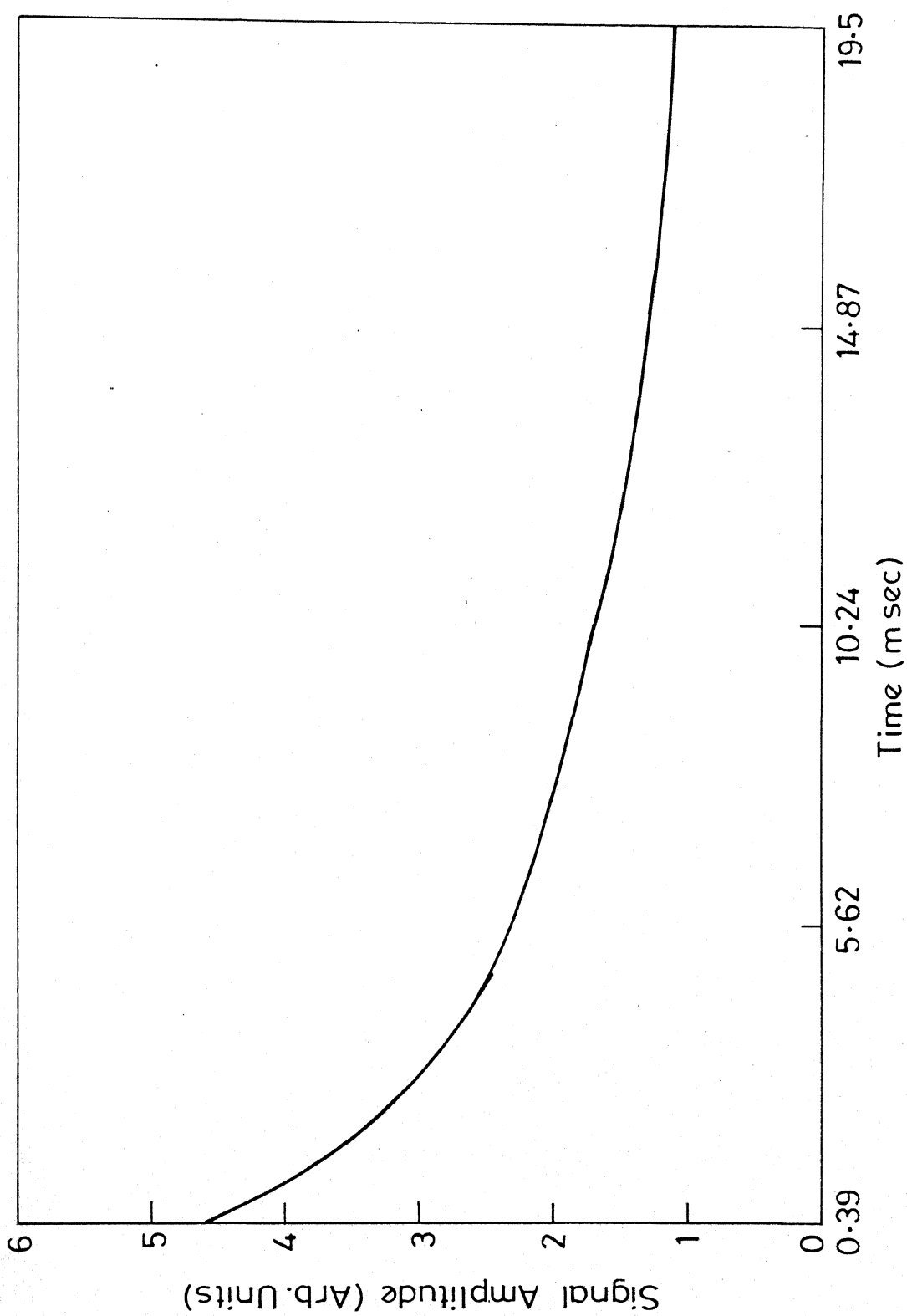


Fig.IV.12 Response of ^{35}Cl in polycrystalline sample of NaClO_3 to WAHUA sequence: $\Delta\omega=0$, $\tau=150\text{ }\mu\text{sec}$, $\nu=29.9232\text{ MHz}$.

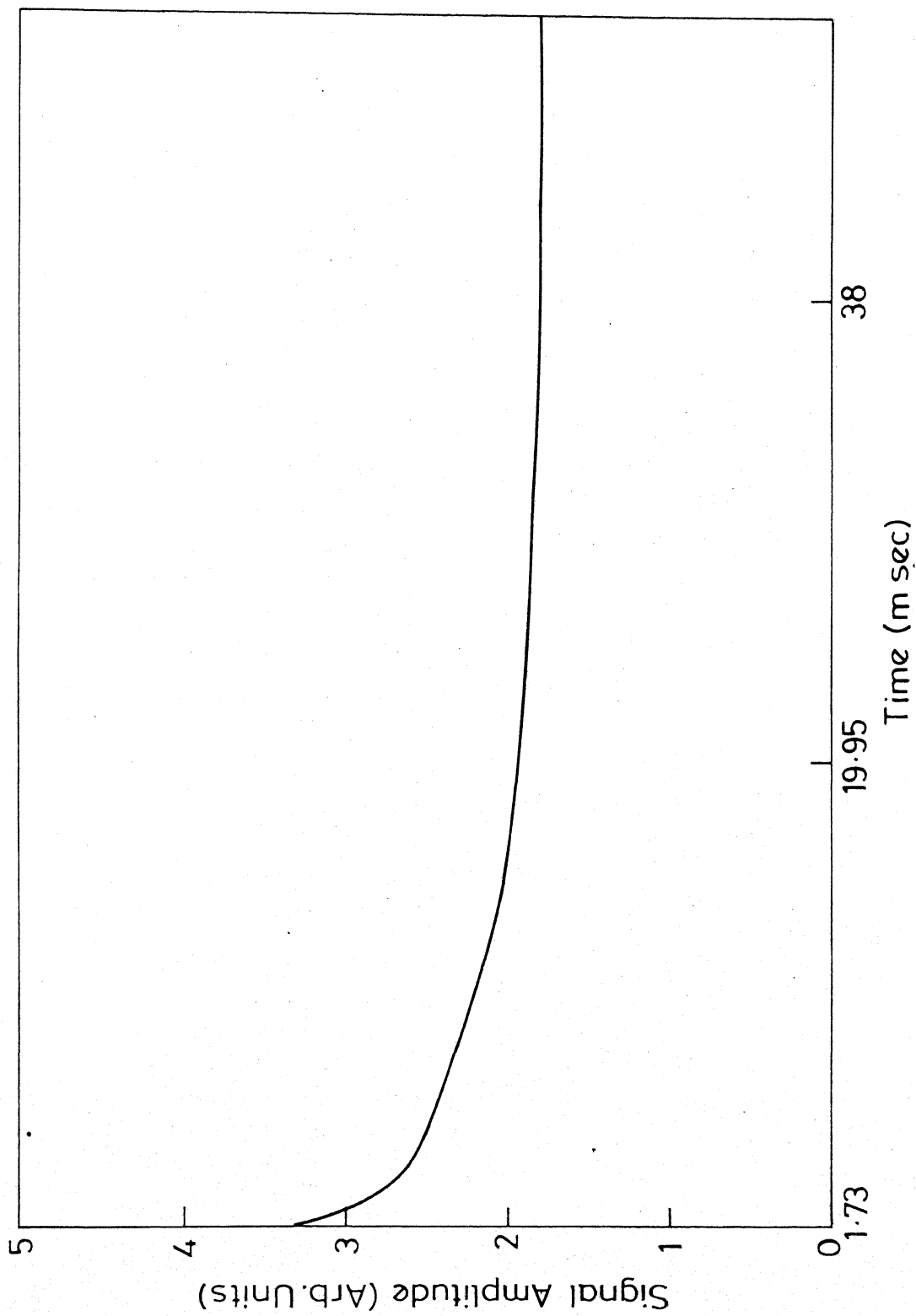


Fig. IV.13 Response of ^{35}Cl in polycrystalline sample of KClO_3 to WAHUHA sequence: $\Delta\omega = 0$, $\tau = 300 \mu\text{sec}$, $\nu = 28.0623 \text{ MHz}$.

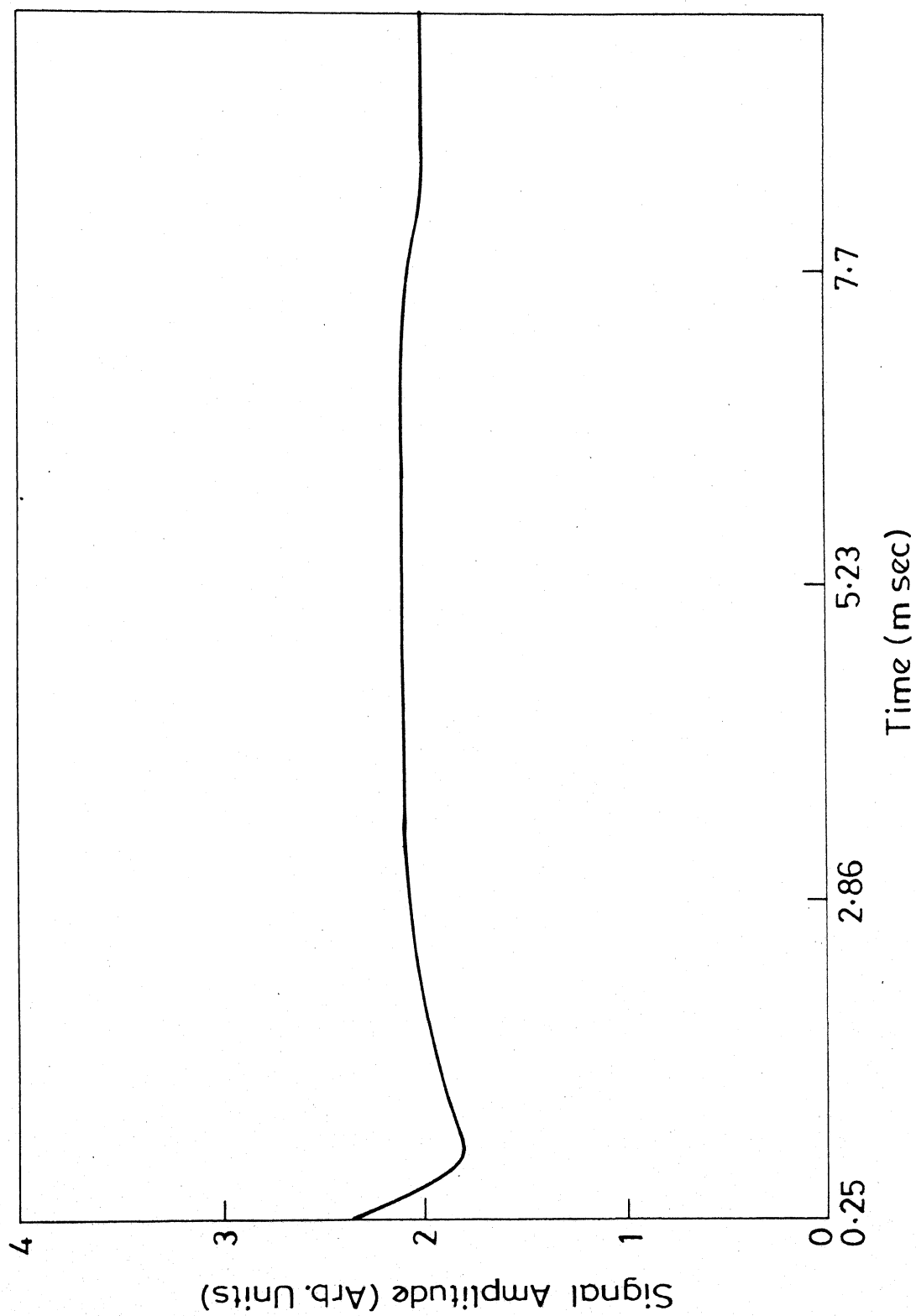


Fig.IV.14 Response of ^{187}Re in polycrystalline sample of KReO_4 to WAHUHA sequence: $\Delta\omega=0$, $\tau=80\ \mu\text{sec}$, $\nu=26.7817\ \text{MHz}$.

From the above table it is clear that the smaller τ values yield larger decay time constants. Similar trend has been observed in the case of ^{35}Cl in KClO_3 and ^{187}Re in KReO_4 .

IV.C DOUBLE RESONANCE UNDER MULTIPLE-PULSE SPIN-LOCKING

As discussed in Chapter I, in NQR the direct detection of quadrupolar nuclei having low-natural abundance and/or low quadrupole coupling constant (such nuclei termed as rare nuclei) is rather difficult. Double resonance methods offer better sensitivity in detecting such rare nuclei. There have been several double resonance techniques available in the literature (see Chapter I, Section I.C.2).

Marino and Klainer [5] who carried out the first spin-locking experiment in NQR have proposed that, in principle, the sensitivity of double resonance scheme of Emswiller, Hahn and Kaplan [26] could be enhanced under the spin-locking condition. Encouraged by this proposition, we have carried out ^{23}Na - ^{35}Cl (in polycrystalline sample of NaClO_3) double resonance experiment under the spin-locked condition. In what follows we present the experimental details and the results of the double resonance experiment.

IV.C.1 Experimental

For this double resonance experiment we have chosen CPMG sequence. The DC pulse sequence in this case has also been

generated by the microprocessor. First the preparatory ($\pi/2$) pulse and the sequence of π pulses were generated respectively at BNC-1 and BNC-2 of the microprocessor system. The π pulse sequence was passed through a current driver. One of the two outputs available at the current driver was used to gate the r.f. in ^{23}Na channel while the other output was used to gate the 90° phase shifted r.f. in ^{35}Cl channel and which is subsequently used to generate the CPMG sequence in ^{35}Cl channel. The experimental set-up in ^{35}Cl channel is same as described earlier in Chapter I. The gated r.f. pulse sequence in the ^{23}Na channel has been amplified by an r.f. amplifier (Model GR 1233-A, 20 Hz to 3 MHz from General Radio, USA) which gives a maximum power of 15 watts, and coupled to the double resonance probe. Thus, basically this experiment is an extension of the Spin Echo Double Resonance (SEDOR) experiment [26].

IV.C.2 Results

Although we have tried various combinations of θ , ϕ in the spin-locking sequence, CPMG sequence was found to be more sensitive in this experiment. Since, on resonance, the spin-locked signal intensity is rather small we have set an off-set of -3.5 KHz in ^{35}Cl channel. Upon irradiation in ^{23}Na channel at the resonance frequency of ^{23}Na , the amplitude of the spin-echo train in ^{35}Cl channel has been found to be reduced considerably. The superimposition of the two echo trains obtained in the presence and absence of the double resonance irradiation is shown in Fig. IV.15.

A plot of the ^{35}Cl spin-echo amplitude, monitored after $\approx 5 T_2$ time, versus the frequency of ^{23}Na channel is given in Fig. IV.16. From this figure it is evident that the resonance frequency of ^{23}Na is ≈ 397.5 KHz at 295 K which is in good agreement with that obtained earlier by other double resonance methods in the literature.

From the experimental results of multiple-pulse sequences presented in Sections IV.B and IV.C the following conclusions can be drawn.

- i) Spin-locking phenomenon can be observed with arbitrary values of ϕ in SLS, in polycrystalline samples as well as in single crystals. These results cannot be explained by any of the theories currently available in the literature on the spin-locking phenomenon in NQR. A more detailed theoretical analysis of spin-locking phenomenon in NQR of polycrystalline samples as well as in single crystals is therefore warranted.
- ii) It appears that spin-locking effect is not restricted to spin $I = 1$ or $3/2$ nuclei only but it can be observed in the case of nuclei with any arbitrary spin I .
- iii) Spin-locked signals have higher intensity in the presence of a finite resonance off-set.
- iv) Enormous improvement in the S/N can be achieved by co-adding all the echoes in the spin locked spin echo train.

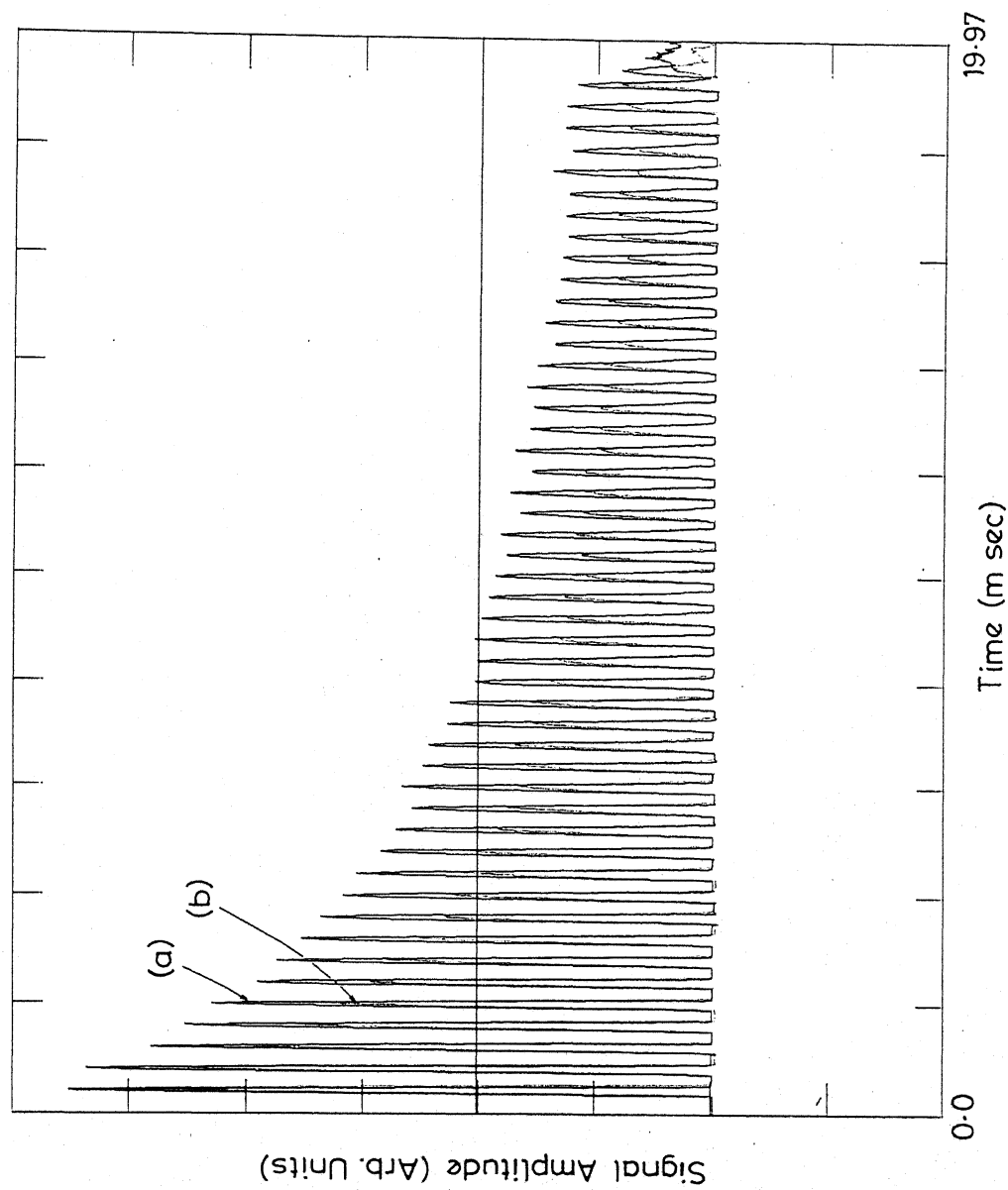


Fig. IV.15 Response of ^{35}Cl in polycrystalline sample of NaClO_3 ($\omega = 29.9232\text{ MHz}$) to CPMG sequence under ($^{23}\text{Na} - ^{35}\text{Cl}$) double resonance condition. ^{35}Cl resonance off set, $\Delta\omega$, is $\approx -3.5\text{ KHz}$.

(a) In the absence of double resonance irradiation.

(b) In the presence of double resonance irradiation. Double resonance channel frequency (^{23}Na resonance frequency) $= 397.5\text{ KHz}$.

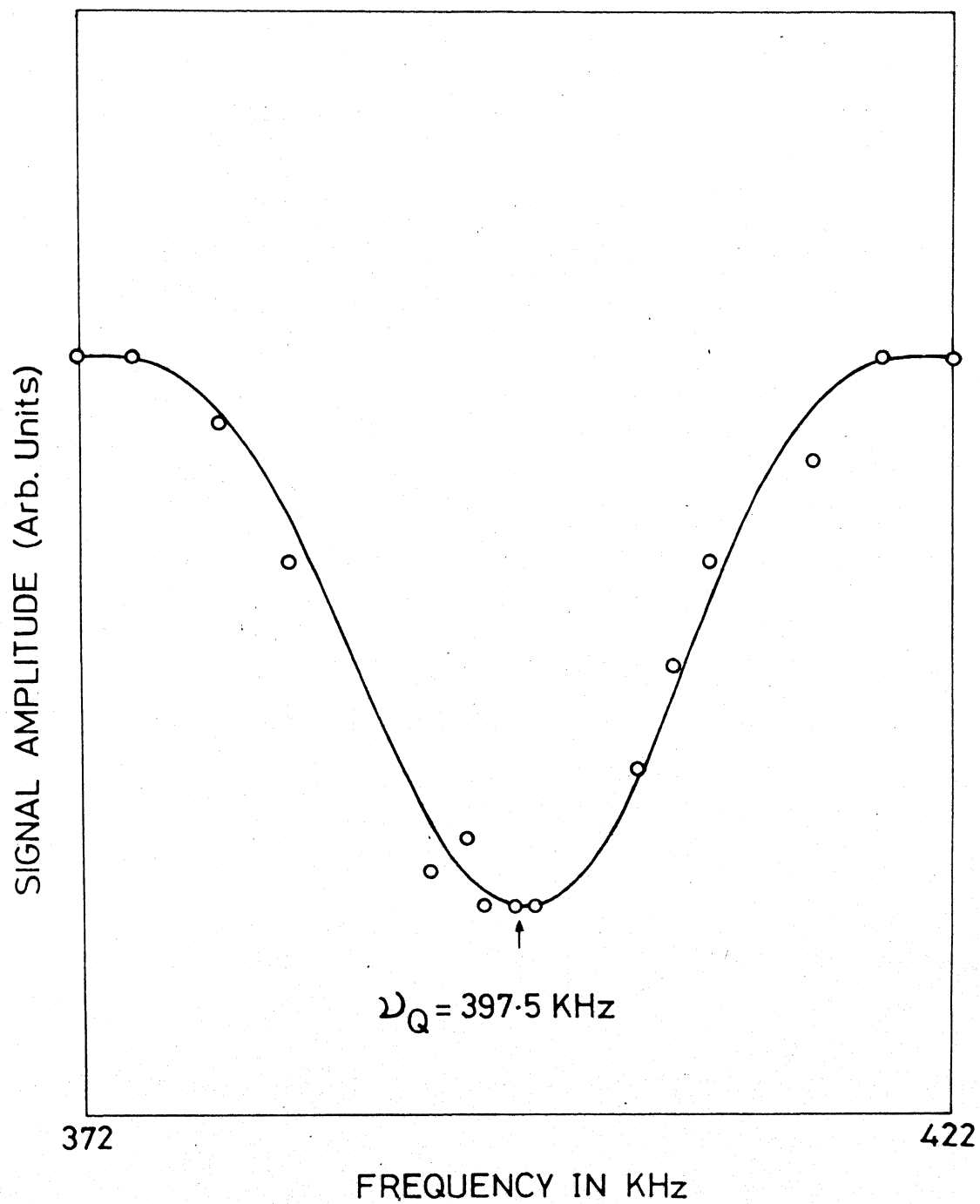


Fig. IV.16 ^{23}Na double resonance spectrum of NaClO_3 .

- v) Under the influence of SLS and PAPS the decay time constant of QEM increases as the flip-angle of the sequence pulses is decreased indicating that spin-locking is more effective with short flip angle pulses.
- vi) Under the action of PAPS the lengthening of the transverse magnetization could be observed for arbitrary θ values of the sequence pulses for nuclear spins with general spin I .
- vii) WAHUHA sequence leads to the lengthening of the transverse magnetization in the case of NQR of spin $I = 3/2$ and $5/2$ also
- viii) As pointed out in the beginning of this chapter a sensitive double resonance experiment under spin-locking condition can be carried out to detect rare quadrupolar nuclei.

To summarize all the aforesaid multiple-pulse sequences lead to the lengthening of the decay of the transverse magnetization implying a narrowed NQR line in the frequency domain.

In order to understand the kind of internal interactions that are averaged out under a particular sequence one needs a theoretical analysis of the influence these sequences.

We have carried out theoretical analysis of some of the multiple pulse sequences, using the tensor operator formalism, the details of which will be presented in the next section.

IV.D THEORETICAL ANALYSIS OF A FEW MULTIPLE PULSE EXPERIMENTS IN NQR OF SPIN $I = 3/2$ NUCLEI

In this section we present our theoretical analysis of the influence of multiple-pulse sequences such as PAPS, WAHUHA [13] and Mansfield-Rhim-Elleman-Vaughan (MREV-8) [27] on spin $3/2$ nuclei. We have employed the Average Hamiltonian Theory [1] and tensor operator formalism [28-32] in this investigation.

In NQR spectroscopy the main internal interactions which lead to line broadening are [6,33],

- i) inhomogeneities in the efg's
- ii) torsional oscillations of molecules
- iii) heteronuclear dipole-dipole interactions
- and iv) homo-nuclear dipole-dipole interactions.

In the present analysis we consider only the first three of the above four interactions. The Hamiltonians corresponding to these three internal interactions are listed below.

IV.D.1 Hamiltonians of Internal Interactions

We consider a nuclear spin system with $I = 3/2$ in a non-axial efg.

IV.D.1(i) Hamiltonian of inhomogeneous efg:

The Hamiltonian which defines the internal interaction due to inhomogeneous efg can be written as

$$\mathcal{H}_{\text{inhom}} = \frac{\Delta\omega_q}{\sqrt{6}} [3\tilde{I}_z^2 - \tilde{I}^2 + \eta(\tilde{I}_x^2 - \tilde{I}_y^2)] \quad \dots \text{(IV.1)}$$

where $\Delta\omega_q$ is the frequency deviation from an average value $\omega_q = e^2 q Q / 2$. In terms of tensor operators this Hamiltonian can be written as

$$\mathcal{H}_{\text{inhom}} = \frac{\Delta\omega_q}{\sqrt{6}} \left[T_0^2 + \eta/\sqrt{3} T_2^2(s) \right] \quad \dots (IV.2)$$

IV.D.1(ii) Hamiltonian corresponding to torsional oscillations:

Let us assume that the molecule containing the quadrupolar nucleus undergoes torsional motions about the three principal axes of the field gradient. The axes fixed in space are denoted by primes and the axes fixed in the molecule without primes. Then for small rotations θ_X , θ_Y and θ_Z about the three axes X, Y, Z it may be shown [33] that the primed and unprimed components of the field gradient tensor are related by the following equations:

$$\begin{aligned} V_{X'X'} &= (1 - \theta_Y^2 - \theta_Z^2) V_{XX} + \theta_Z^2 V_{YY} + \theta_Y^2 V_{ZZ} \\ V_{Y'Y'} &= \theta_Z^2 V_{XX} + (1 - \theta_X^2 - \theta_Z^2) V_{YY} + \theta_X^2 V_{ZZ} \\ V_{Z'Z'} &= \theta_Y^2 V_{XX} + \theta_X^2 V_{YY} + (1 - \theta_X^2 - \theta_Y^2) V_{ZZ} \\ V_{X'Y'} &= -\theta_Z V_{XX} + (\theta_X \theta_Y + \theta_Z) V_{YY} - \theta_X \theta_Y V_{ZZ} \\ V_{Y'Z'} &= \theta_Y \theta_Z V_{XX} - \theta_X V_{YY} - (\theta_Y \theta_Z - \theta_X) V_{ZZ} \\ V_{Z'X'} &= -\theta_Y V_{XX} - \theta_X \theta_Z V_{YY} + (\theta_X \theta_Z + \theta_Y) V_{ZZ} \end{aligned} \quad \dots (IV.3)$$

where $V_{XX} = eq/2 (\eta - 1)$; $V_{YY} = -eq/2 (1 + \eta)$

and $V_{ZZ} = eq$.

The quadrupolar Hamiltonian of a nucleus in a molecule which is undergoing torsional oscillations can be written as

$$\mathcal{H} = \frac{eQ}{6I(2I-1)} [\mathbf{I} \cdot \mathbf{V}' \cdot \mathbf{I}] \quad \dots (\text{IV.4})$$

where \mathbf{V}' is the efg tensor.

The above Eqn. can be rewritten as

$$\mathcal{H} = \mathcal{H}_Q + \mathcal{H}'_{\text{tors}} \quad \dots (\text{IV.5})$$

$$\text{where } \mathcal{H}_Q = \frac{\omega_Q}{\sqrt{6}} [\mathcal{T}_0^2 + \eta/\sqrt{3} \mathcal{T}_2^2(s)] \quad \dots (\text{IV.6})$$

is the pure quadrupolar Hamiltonian and $\mathcal{H}'_{\text{tors}}$ is the Hamiltonian which defines the interaction between the spin system and torsional oscillations. We are mainly interested in $\mathcal{H}'_{\text{tors}}$. Considering only the secular part of $\mathcal{H}'_{\text{tors}}$ i.e., $\mathcal{H}_{\text{tors}}$ it can be shown that

$$\mathcal{H}_{\text{tors}} = \omega_x \epsilon_x (\mathcal{I}_Y^2 - \mathcal{I}_Z^2) + \omega_Y \epsilon_Y (\mathcal{I}_Z^2 - \mathcal{I}_X^2) + \omega_Z \epsilon_Z (\mathcal{I}_X^2 - \mathcal{I}_Y^2) \quad \dots (\text{IV.6})$$

$$\text{where } \omega_x = \frac{1}{9} \omega_Q \frac{(3+\eta)}{2}, \omega_Y = \frac{1}{9} \omega_Q \frac{(\eta-3)}{2}, \omega_Z = \frac{-\omega_Q}{9} 2\eta$$

$$\epsilon_x = e_x^2, \epsilon_Y = e_Y^2 \text{ and } \epsilon_Z = e_Z^2$$

$$\text{with } \omega_Q = e^2 q Q / 2$$

In terms of tensor operators $\mathcal{H}_{\text{tors}}$ can be written as

$$\mathcal{H}_{\text{tors}} = T_0^2 b_1 + T_2^2(s) b_2 \quad \dots \text{(IV.6a)}$$

$$\text{where } b_1 = \frac{\sqrt{6}}{2} (-\omega_x \varepsilon_x + \omega_y \varepsilon_y) \quad \dots \text{(IV.6b)}$$

$$b_2 = \frac{1}{\sqrt{2}} (-\omega_x \varepsilon_x - \omega_y \varepsilon_y + \omega_z \varepsilon_z) \quad \dots \text{(IV.6c)}$$

IV.D.1(iii) Hamiltonian of heteronuclear dipole-dipole interactions:

The dipolar interaction between the two magnetic moments

$\vec{\mu}_1 = \gamma_1 \hbar \vec{I}_1$, $\vec{\mu}_2 = \gamma_2 \hbar \vec{I}_2$ is given by the Hamiltonian [34]

$$\mathcal{H}_{\text{dip}} = \gamma_1 \gamma_2 \hbar^2 \left[\frac{(\vec{I}_1 \cdot \vec{I}_2)}{r^3} - \frac{3(\vec{I}_1 \cdot \vec{r})(\vec{I}_2 \cdot \vec{r})}{r^5} \right] \quad \dots \text{(IV.7)}$$

where γ_1, γ_2 are gyromagnetic ratios of the nuclear spins.

The above equation can also be written as [34]:

$$\mathcal{H}_{\text{dip}} = -\gamma_2 \hbar \vec{I}_2 \cdot H_{12}$$

where H_{12} is called the local field produced by spin 1 at the site of spin 2.

Thus, the heteronuclear dipole-dipole interaction can be treated as the interaction of the resonant nuclear spin with a local magnetic field produced by the non-resonant nuclear spin at the site of the resonant spin. Thus,

$$\mathcal{H}_{\text{het}} = -\gamma \sum_{m=x}^z I_m H_m \quad \dots \text{(IV.8)}$$

where we have set $\hbar = 1$, and H_m is the component of the local field in 'm' direction.

In terms of tensor operators \mathcal{H}_{het} can be written as

$$\mathcal{H}_{het} = -\gamma [-T_1^1(a) H_x + T_1^1(s) H_y + T_0^1 H_z] \quad \dots (IV.9)$$

As mentioned in Section IV.A, under the action of a multiple-pulse sequence an internal interaction is said to be averaged out if the following conditions are satisfied [20]:

$$\overline{\mathcal{H}}_{int}^{(i)} = 0 \text{ or } [\rho_i, \overline{\mathcal{H}}_{int}^{(i)}] = 0 \quad \dots (IV.10)$$

where $\overline{\mathcal{H}}_{int}^{(i)}$ is the average Hamiltonian, of i^{th} order, of an internal interaction, and ρ_i is the density matrix prepared by the preparatory pulse of the sequence.

Since in this section we are mainly interested in the status of the various internal interactions under the action of the multiple-pulse sequences we first calculate the average Hamiltonians (we restrict ourselves only to the zeroth order average Hamiltonian) of the internal interactions and then evaluate the density matrix following the preparatory pulse and subsequently look for the commutation relationship of the form given in Eqn. IV.10. Depending upon the result of the commutator between ρ_i and $\overline{\mathcal{H}}_{int}^{(0)}$ we infer whether a particular internal interaction under a given sequence averaged out or not.

In order to present a coherent discussion on the above mentioned aspects in the next sub-section we give a brief outline of average Hamiltonian theory and in the subsequent sections we discuss the evaluation of zeroth order average Hamiltonians of the internal interactions, under some of the multiple-pulse sequences, and their commutation with the ρ_i .

IV.D.2 Multiple-Pulse NQR and the Average Hamiltonian

Average Hamiltonian theory is well documented [1]. In this sub-section we closely follow the treatment outlined by Haeberlen [1]. From here onwards in all the calculations in this chapter we set $\hbar = 1$.

Let us consider a nuclear spin system governed by a total Hamiltonian $\mathcal{H}(t)$, given by

$$\mathcal{H}(t) = \mathcal{H}_Q + \mathcal{H}_1(t) + \mathcal{H}_{int} \quad \dots (IV.11)$$

where \mathcal{H}_Q is the quadrupolar Hamiltonian, $\mathcal{H}_1(t)$ is the Hamiltonian for the interaction between the r.f. field and the nuclear spins, and \mathcal{H}_{int} represents the Hamiltonian corresponding to the internal interactions.

In the quadrupolar interaction representation (QIR) defined by

$$U_Q = \exp(i \mathcal{H}_Q t) \quad \dots (IV.12)$$

The total Hamiltonian is given by

$$\tilde{\mathcal{H}} = \tilde{\mathcal{H}}_1(t) + \tilde{\mathcal{H}}_{\text{int}} \quad \dots (\text{IV.13})$$

In QIR, the equation of motion of the density matrix ρ is given by

$$\frac{d\tilde{\rho}}{dt} = -i [(\tilde{\mathcal{H}}_1(t) + \tilde{\mathcal{H}}_{\text{int}}), \tilde{\rho}] \quad \dots (\text{IV.14})$$

Now let us make a transformation

$$\tilde{\rho}(t) = U_1(t) \tilde{\tilde{\rho}}(t) U_1(t)^{-1} \quad \dots (\text{IV.15})$$

$$\text{where } U_1(t) = T \exp \left(-i \int_0^t \tilde{\mathcal{H}}_1(t') dt' \right) \quad \dots (\text{IV.16})$$

T is the Dyson time-ordering operator

In this new frame the motion of $\tilde{\tilde{\rho}}$ is governed by

$$\frac{d\tilde{\tilde{\rho}}}{dt} = -i [\tilde{\mathcal{H}}_{\text{int}}, \tilde{\tilde{\rho}}] \quad \dots (\text{IV.17})$$

$$\text{with } \tilde{\mathcal{H}}_{\text{int}}(t) = U_1^{-1}(t) \tilde{\mathcal{H}}_{\text{int}} U_1(t) \quad \dots (\text{IV.18})$$

The formal solution of Eqn. (IV.17) is given by

$$\tilde{\tilde{\rho}}(t) = U_{\text{int}}(t) \tilde{\tilde{\rho}}(0) U_{\text{int}}^{-1}(t) \quad \dots (\text{IV.19})$$

$$\text{where } U_{\text{int}}(t) = T \exp \left(-i \int_0^t \tilde{\mathcal{H}}_{\text{int}}(t') dt' \right) \quad \dots (\text{IV.20})$$

Then from Eqns. IV.15 and IV.19, we have

$$\tilde{\rho}(t) = U_1(t) U_{\text{int}}(t) \tilde{\rho}(0) U_{\text{int}}^{-1}(t) U_1^{-1}(t) \quad \dots (\text{IV.21})$$

Since the average Hamiltonian theory is based on the cyclicity of the r.f. pulse interactions, $\mathcal{H}_1(t)$, we now briefly discuss the cyclicity and periodicity of the multiple pulse sequences.

A pulse sequence is said to be cyclic if the propagator operator $U_1(t_c)$ defined by the sequence at a cycle time t_c is unity [35], i.e.,

$$U_1(t_c) = T \exp \left(-i \int_0^{t_c} \tilde{\mathcal{H}}_1(t) dt \right) = 1 \quad \dots (\text{IV.22})$$

Using Magnus expansion [36] the above equation can be rewritten as

$$U_1(t_c) = \exp \{ -it_c [\bar{\mathcal{H}}_1^{(0)} + \bar{\mathcal{H}}_1^{(1)} + \dots] \} \quad \dots (\text{IV.23})$$

$$\text{where } \bar{\mathcal{H}}_1^{(0)} = \frac{1}{t_c} \int_0^{t_c} \tilde{\mathcal{H}}_1(t) dt \quad \dots (\text{IV.24})$$

$$\bar{\mathcal{H}}_1^{(1)} = - \frac{i}{2t_c} \int_0^{t_c} dt \int_0^t dt' [\tilde{\mathcal{H}}_1(t), \tilde{\mathcal{H}}_1(t')] \quad \dots (\text{IV.25})$$

From Eqn. IV.23 it is evident that a sufficient condition for designing a cyclic sequence is by the requirement that

$$\bar{\mathcal{H}}_1^{(i)} = 0 \text{ for all } i \quad \dots (\text{IV.26})$$

A sequence is said to be periodic, i.e., the sequence is repeated periodically with a cycle time t_c

$$\text{if } \tilde{\mathcal{H}}_1(t) = \tilde{\mathcal{H}}_1(t + Nt_c) \quad \dots \text{ (IV.27)}$$

For a sequence both cyclic and periodic

$$U_1(Nt_c) = 1 \quad (N = 0, 1, 2, \dots) \quad \dots \text{ (IV.28)}$$

Now let us assume that our observation Windows in the experiment are set at the integral multiples of the cycle time i.e., $t = Nt_c$. Then from Eqn. IV.21

$$\begin{aligned} \tilde{\rho}(t) &= \tilde{\rho}(Nt_c) = U_1(Nt_c) U_{\text{int}}(Nt_c) \tilde{\rho}(0) U_{\text{int}}^{-1}(Nt_c) U_1^{-1}(Nt_c) \\ &= U_{\text{int}}(Nt_c) \tilde{\rho}(0) U_{\text{int}}^{-1}(Nt_c) \quad \dots \text{ (IV.29)} \end{aligned}$$

Since $U_1(t) = U_1(Nt_c) = 1$ for a cyclic sequence

Since $U_1(t)$ is periodic i.e., $U_1(t) = U_1(t + t_c)$ and $\tilde{\mathcal{H}}_{\text{int}}$ is determined through Eqn. IV.18

$$\tilde{\mathcal{H}}_{\text{int}}(t + Nt_c) = \tilde{\mathcal{H}}_{\text{int}}(t) \quad \dots \text{ (IV.30)}$$

$$\text{hence } U_{\text{int}}(Nt_c) = [U_{\text{int}}(t_c)]^N \quad \dots \text{ (IV.31)}$$

Consequently,

$$\tilde{\rho}(Nt_c) = [U_{\text{int}}(t_c)]^N \tilde{\rho}(0) [U_{\text{int}}^{-1}(t_c)]^N \quad \dots \text{ (IV.32)}$$

Thus, this equation implies that, in order to describe the state of the system, under the action of a cyclic multiple-pulse

sequence, at any integer multiple of the cycle time t_c it is sufficient to know its short-time evolution over one cycle.

We can now make use of Magnus expansion [36] to evaluate $U_{\text{int}}(t_c)$,

$$U_{\text{int}}(t_c) = \exp \{-it_c [\overline{\mathcal{H}}_{\text{int}}^{(0)} + \overline{\mathcal{H}}_{\text{int}}^{(1)} + \dots]\} \quad \dots \text{ (IV.33)}$$

with

$$\overline{\mathcal{H}}_{\text{int}}^{(0)} = \frac{1}{t_c} \int_0^{t_c} \tilde{\mathcal{H}}_{\text{int}}(\tau) d\tau \quad \dots \text{ (IV.34)}$$

$$\overline{\mathcal{H}}_{\text{int}}^{(1)} = -\frac{i}{2t_c} \int_0^{t_c} d\tau [\tilde{\mathcal{H}}_{\text{int}}(\tau), \int_0^{\tau} d\vartheta \tilde{\mathcal{H}}_{\text{int}}(\vartheta)] \quad \dots \text{ (IV.35)}$$

and higher order terms.

$\overline{\mathcal{H}}_{\text{int}}^{(0)}$ is referred to as the zeroth-order average Hamiltonian while $\overline{\mathcal{H}}_{\text{int}}^{(1)}$ is the first-order average Hamiltonian.

In order that this series is strongly convergent

$$t_c |\tilde{\mathcal{H}}_{\text{int}}(\tau)| \simeq t_c \omega_{\text{int}} \ll 1 \quad \dots \text{ (IV.36)}$$

In our theoretical analysis we are mainly concerned with $\overline{\mathcal{H}}_{\text{int}}^{(0)}$.

IV.D.3 Theoretical Analysis

In this section we first present the explicit expressions for relevant Hamiltonians in QIR and then proceed on to evaluate zeroth order average Hamiltonians of the internal interactions.

Consider a non-interacting nuclear spin system which is characterized by a total Hamiltonian, $\mathcal{H}(t)$ (see Eqn. IV.11) given by:

$$\mathcal{H}(t) = \mathcal{H}_Q + \mathcal{H}_1(t) + \mathcal{H}_{\text{int}}$$

where \mathcal{H}_Q is the pure quadrupolar Hamiltonian defined in Eqn. IV.5.

If we assume that the r.f. pulses are applied along x-axis of the crystal with a frequency ω_Q and amplitude H_1 then we have for the r.f. Hamiltonian,

$$\mathcal{H}_1(t) = + 2\omega_1 \cos(\omega_Q t + \varphi) T_1^1(a) \quad \dots (\text{IV.37})$$

with $\omega_1 = \gamma H_1$; γ is the gyromagnetic ratio of the nucleus and φ is the phase of the r.f. Considering specific cases of φ values we have

$$\text{for } \varphi = 0 \quad \mathcal{H}_1(t) = 2\omega_1 \cos(\omega_Q t) T_1^1(a)$$

$$\text{for } \varphi = 90^\circ \quad \mathcal{H}_1(t) = -2\omega_1 \sin(\omega_Q t) T_1^1(a)$$

$$\text{for } \varphi = 180^\circ \quad \mathcal{H}_1(t) = -2\omega_1 \cos(\omega_Q t) T_1^1(a)$$

$$\text{and for } \varphi = 270^\circ \quad \mathcal{H}_1(t) = 2\omega_1 \sin(\omega_Q t) T_1^1(a) \quad \dots (\text{IV.38})$$

$$\mathcal{H}_{\text{int}} = \mathcal{H}_{\text{inhom}} + \mathcal{H}_{\text{tors}} + \mathcal{H}_{\text{het}} \quad \dots (\text{IV.39})$$

where $\mathcal{H}_{\text{inhom}}$, $\mathcal{H}_{\text{tors}}$ and \mathcal{H}_{het} are given respectively by Eqns. IV.2, IV.6(a) and IV.9.

As has been mentioned in previous chapters calculations will be simplified if we work in a representation in which the quadrupolar Hamiltonian is diagonal. In the 'diagonal representation' defined by the transformation operator,

$$U_d = \exp (2/\sqrt{3} \times T_2^3(a)) \quad \dots (\text{IV.40})$$

the total Hamiltonian is given by (see Table II.12),

$$\mathcal{H}^d(t) = \frac{\omega_q}{\sqrt{6}} T_0^2 + \mathcal{H}_1^d(t) + \mathcal{H}_{int}^d \quad \dots (IV.41)$$

$$\text{where } \omega_q = \frac{\omega_Q}{\sqrt{6}} \wp \quad \dots (IV.41a)$$

$$\text{with } \wp = (1 + \eta^2/3)^{1/2} \quad \dots (IV.41b)$$

$$\text{For } \varphi = 0 \quad \mathcal{H}_1^d(t) = 2\omega_1 \cos(\omega_q t) [a_1 \tilde{T}_1^1(a) + a_2 \tilde{T}_1^3(a) + a_3 \tilde{T}_3^3(a)] \quad \dots (IV.42)$$

$$\text{For } \varphi = 90^\circ \quad \mathcal{H}_1^d(t) = -2\omega_1 \sin(\omega_q t) [a_1 \tilde{T}_1^1(a) + a_2 \tilde{T}_1^3(a) + a_3 \tilde{T}_3^3(a)] \quad \dots (IV.43)$$

$\mathcal{H}_1^d(t)$ for $\varphi = 180^\circ$ and $\varphi = 270^\circ$ can be obtained, respectively from Eqns. IV.42 and IV.43 by changing the sign of Hamiltonians.

$$\mathcal{H}_{int}^d = \mathcal{H}_{inhom}^d + \mathcal{H}_{tors}^d + \mathcal{H}_{het}^d \quad \dots (IV.44)$$

where

$$\mathcal{H}_{inhom}^d = \frac{\Delta\omega_q}{\sqrt{6}} T_0^2 \quad \dots (IV.44a)$$

$$\mathcal{H}_{tors}^d = A_1 T_0^2 + A_2 T_2^2(s) \quad \dots (IV.44b)$$

$$\begin{aligned} \mathcal{H}_{het}^d = & -\gamma [-H_X [a_1 \tilde{T}_1^1(a) + a_2 \tilde{T}_1^3(a) + a_3 \tilde{T}_3^3(a)] \\ & + iH_Y \{a_4 \tilde{T}_1^1(s) + a_5 \tilde{T}_1^3(s) + a_6 \tilde{T}_3^3(s)\} \\ & + H_Z [a_7 \tilde{T}_0^1 + a_8 \tilde{T}_0^3 + a_9 \tilde{T}_2^3(s)]] \quad \dots (IV.44c) \end{aligned}$$

where $A_1 = 1/\rho (b_1 + \eta/\sqrt{3} b_2)$

$$A_2 = 1/\rho (-\eta/\sqrt{3} b_1 + b_2)$$

$$a_1 = a_4 = a_7 = (\frac{\rho+4}{5\rho})$$

$$a_2 = \frac{1}{3\sqrt{15}\rho} [3(1-\rho) + 5\eta]$$

$$a_3 = \frac{1}{3\rho} (\rho + \eta - 1)$$

$$a_5 = \frac{1}{3\sqrt{15}\rho} [3(1-\rho) - 5\eta]$$

$$a_6 = \frac{1}{3\rho} [1 - \rho + \eta]$$

$$a_8 = -\frac{4}{3\sqrt{10}\rho} (1 - \rho)$$

$$a_9 = -\frac{2\sqrt{2}}{3\sqrt{3}} \eta/\rho \quad \dots \text{(IV.44d)}$$

b_1 , b_2 and ρ are given respectively by Eqns. IV.6(b), IV.6(c) and IV.41(b). Having obtained the total Hamiltonian of the system in the diagonal representation, we now transform it into the QIR defined by

$$U_q = \exp \left(i \frac{\omega_q}{\sqrt{6}} T_o^2 t \right) \quad \dots \text{(IV.45)}$$

In the QIR, the total Hamiltonian can be written as (see Table III.1):

$$U_q \mathcal{H}^d U_q^{-1} = \tilde{\mathcal{H}}^d = \tilde{\mathcal{H}}_1^d + \tilde{\mathcal{H}}_{\text{int}}^d \quad \dots \text{(IV.46)}$$

where

$$\text{for } \varphi = 0 \quad \tilde{\mathcal{H}}_1^d = \omega_1 R, \quad \varphi = 90^\circ \quad \tilde{\mathcal{H}}_1^d = \omega_1 S$$

$$\varphi = 180^\circ \quad \tilde{\mathcal{H}}_1^d = -\omega_1 R, \quad \varphi = 270^\circ \quad \tilde{\mathcal{H}}_1^d = -\omega_1 S$$

.. (IV.47)

$$\text{with } R = \frac{(3+\eta)}{3\wp} \left[\frac{3}{5} T_1^1(a) + \frac{2}{\sqrt{15}} T_1^3(a) \right] \quad \text{.. (IV.47a)}$$

$$S = \frac{-(3+\eta)}{3\wp} \left[\frac{1}{\sqrt{2}} T_1^2(s) \right] \quad \text{.. (IV.47b)}$$

$$\text{and } \tilde{\mathcal{H}}_{\text{int}}^d = \tilde{\mathcal{H}}_{\text{inhom}}^d + \tilde{\mathcal{H}}_{\text{tors}}^d + \tilde{\mathcal{H}}_{\text{het}}^d \quad \text{.. (IV.48)}$$

$$\text{with } \tilde{\mathcal{H}}_{\text{inhom}}^d = \frac{\Delta\omega_q}{\sqrt{6}} T_0^2 \quad \text{.. (IV.48a)}$$

$$\tilde{\mathcal{H}}_{\text{tors}}^d = A_1 T_0^2 \quad \text{.. (IV.48b)}$$

$$\begin{aligned} \tilde{\mathcal{H}}_{\text{het}}^d = & -\gamma \left[-H_x \left\{ \frac{1}{\wp} (\wp+1-\eta) \left[\frac{1}{5} T_1^1(a) - \frac{1}{\sqrt{15}} T_1^3(a) \right] + \frac{1}{3\wp} (\wp+\eta-1) T_3^3(a) \right\} \right. \\ & + iH_y \left\{ \frac{1}{\wp} (\wp+1+\eta) \left[\frac{1}{5} T_1^1(s) - \frac{1}{\sqrt{15}} T_1^3(s) \right] + \frac{1}{3\wp} (-\wp+1+\eta) T_3^3(s) \right\} \\ & \left. + H_z \left\{ \frac{(4+\wp)}{5\wp} T_0^1 - \frac{4(1-\wp)}{3\sqrt{10}\wp} T_0^3 \right\} \right] \quad \text{.. (IV.48c)} \end{aligned}$$

In arriving at the Eqns. IV.48(a), IV.48(b) and IV.48(c) we have made use of the evolution of tensor operators under the action of quadrupolar Hamiltonian $\frac{\omega_q}{\sqrt{6}} T_0^2$ (see Table III.1) and dropped the high frequency terms as nonsecular terms.

The evolution of tensor operators under the action of $\tilde{\mathcal{H}}_1^d$ (for $\varphi = 0$) can be obtained from Table II.3 by substituting $\tilde{\mathcal{Z}}$ by

$\beta = \frac{(3+\eta)}{\sqrt{3} \beta} \omega_1 t_w$. From the same table, the evolution of tensor operators under $\tilde{\mathcal{H}}_1^d$ (for $\varphi = 180^\circ$) can be obtained by substituting β by $-\beta$. The evolution of tensor operators under $\tilde{\mathcal{H}}_1^d$ (for $\varphi = 90^\circ$) are set out in Table IV.6. From this table the evolution of the operators under the influence of $\tilde{\mathcal{H}}_1^d$ (for $\varphi = 270^\circ$) can be obtained by replacing β by $-\beta$.

Having obtained the Hamiltonians corresponding to the internal interactions and r.f. interaction with the spins, in the QIR, we are now ready to discuss the influence of the pulse sequences on the internal interactions.

We shall now examine whether the pulse sequences under investigation are cyclic. We begin with PAPS, i.e.,

$$(\pi/2)_x - [\tau - (\pi)_x - 2\tau - (\pi)_{-x} - \tau] \quad \dots (IV.49)$$

Considering only the zeroth order term from Eqn. (IV.24) we see that

$$\overline{\mathcal{H}}_1^{(0)} = \frac{1}{t_c} \int_0^t \tilde{\mathcal{H}}_1^d(t) dt = \frac{\omega_1}{4} (R-R) = 0 \quad \dots (IV.50)$$

$$\text{where } R = \frac{(3+\eta)}{3\beta} \left[\frac{3}{5} T_1^1(a) + \frac{2}{\sqrt{15}} T_1^3(a) \right] \quad \dots (IV.51)$$

Since in PAPS only the operator R is involved in $\tilde{\mathcal{H}}_1^d$ it can be easily shown that all higher order terms in the magnus expansion i.e., $\overline{\mathcal{H}}_1^{(i)}$ vanish. Thus, we can establish that PAPS is a cyclic sequence. Proceeding in a similar manner it can be shown that

Table IV.6. Evolution of Tensor Operators $T_q^n(a,s)$ Under the Influence of $\tilde{\mathcal{H}}_1^d$ for Spin $I = 3/2$

$$U\tilde{T}_1^1(a)U^{-1} = \tilde{T}_1^1(a)[1 + \frac{4}{5}(\cos\xi - 1)] + \frac{1}{\sqrt{15}}\tilde{T}_1^3(a)(\cos\xi - 1) - \frac{1}{3}(\cos\xi - 1)\tilde{T}_3^3(a) \\ - \frac{1}{\sqrt{2}}\sin\xi\tilde{T}_0^2 - \frac{1}{\sqrt{6}}\sin\xi\tilde{T}_2^2(s)$$

$$U\tilde{T}_1^1(s)U^{-1} = \tilde{T}_1^1(s)[1 + \frac{1}{5}(\cos\xi - 1) - \frac{1}{\sqrt{15}}\tilde{T}_1^3(s)(\cos\xi - 1) - \frac{1}{3}(\cos\xi - 1)\tilde{T}_3^3(s) \\ - \frac{1}{\sqrt{6}}\sin\xi\tilde{T}_2^2(a)$$

$$U\tilde{T}_1^2(a)U^{-1} = \cos\xi\tilde{T}_1^2(a) - \sin\xi\frac{\sqrt{6}}{5}\tilde{T}_0^1 - \sin\xi\frac{4}{\sqrt{15}}\tilde{T}_0^3$$

$$U\tilde{T}_1^2(s)U^{-1} = \tilde{T}_1^2(s)$$

$$U\tilde{T}_0^1U^{-1} = \tilde{T}_0^1[1 + \frac{1}{5}(\cos\xi - 1) + \frac{2\sqrt{2}}{3\sqrt{5}}\tilde{T}_0^3(\cos\xi - 1) + \frac{1}{\sqrt{6}}\sin\xi\tilde{T}_1^2(a)$$

$$U\tilde{T}_0^3U^{-1} = \tilde{T}_0^3 + (\cos\xi - 1)[\frac{4}{5}\tilde{T}_0^3 + \frac{3\sqrt{2}}{5\sqrt{5}}\tilde{T}_0^1] + \frac{3}{\sqrt{15}}\sin\xi\tilde{T}_1^2(a)$$

$$U\tilde{T}_0^2U^{-1} = \tilde{T}_0^2\cos\xi + \sin\xi[\tilde{T}_1^1(a)\frac{3\sqrt{2}}{5} + \frac{4}{\sqrt{30}}\tilde{T}_1^3(a)]$$

$$U\tilde{T}_2^2(a)U^{-1} = \tilde{T}_2^2(a)\cos\xi + \sin\xi[\frac{\sqrt{6}}{5}\tilde{T}_1^1(s) - \frac{2}{\sqrt{10}}\tilde{T}_1^3(s) - \frac{\sqrt{2}}{\sqrt{3}}\tilde{T}_3^3(s)]$$

$$U\tilde{T}_2^2(s)U^{-1} = \tilde{T}_2^2(s)\cos\xi + \sin\xi[\frac{\sqrt{6}}{5}\tilde{T}_1^1(a) - \frac{2}{\sqrt{10}}\tilde{T}_1^3(a) - \frac{\sqrt{2}}{\sqrt{3}}\tilde{T}_3^3(a)]$$

$$U\tilde{T}_1^3(a)U^{-1} = \tilde{T}_1^3(a) + (\cos\xi - 1)[\tilde{T}_1^3(a)\frac{7}{10} + \frac{9}{10\sqrt{15}}\tilde{T}_1^1(a) + \frac{\sqrt{3}}{2\sqrt{5}}\tilde{T}_3^3(a)] \\ + \sin\xi[-\frac{3}{\sqrt{30}}\tilde{T}_0^2 + \frac{3}{2\sqrt{10}}\tilde{T}_2^2(s)]$$

...contd.

Table IV.6 (contd.)

$$U \tilde{T}_1^3(s) U^{-1} = \tilde{T}_1^3(s) + (\cos \xi - 1) \left[\frac{3}{10} \tilde{T}_1^3(s) - \frac{9}{10\sqrt{15}} \tilde{T}_1^1(s) + \frac{\sqrt{3}}{2\sqrt{5}} \tilde{T}_3^3(s) \right] \\ + \sin \xi \left[\frac{3}{2\sqrt{10}} \tilde{T}_2^2(a) \right]$$

$$U \tilde{T}_2^3(a) U^{-1} = \tilde{T}_2^3(a)$$

$$U \tilde{T}_2^3(s) U^{-1} = \tilde{T}_2^3(s)$$

$$U \tilde{T}_3^3(a) U^{-1} = \tilde{T}_3^3(a) [(\cos \xi - 1)] \left[\frac{1}{2} \tilde{T}_3^3(a) - \frac{3}{10} \tilde{T}_1^1(a) + \frac{\sqrt{3}}{2\sqrt{5}} \tilde{T}_1^3(a) \right] \\ + \frac{\sqrt{3}}{2\sqrt{2}} \sin \xi [\tilde{T}_2^2(s)]$$

$$U \tilde{T}_3^3(s) U^{-1} = \tilde{T}_3^3(s) \left[1 + \frac{1}{2} (\cos \beta - 1) \right] + \left[\frac{\sqrt{3}}{2\sqrt{15}} \tilde{T}_1^3(s) - \frac{3}{10} \tilde{T}_1^1(s) \right] (\cos \beta - 1) \\ + \frac{\sqrt{3}}{2\sqrt{2}} \tilde{T}_2^2(a) \sin \beta$$

where $\tilde{\mathcal{H}}_1^d = \frac{(3+\eta)}{3\rho} \omega_1 \left[-\frac{i}{\sqrt{2}} \tilde{T}_1^2(s) \right]$

$$U = \exp(-i \tilde{\mathcal{H}}_1^d t)$$

$$\beta = \omega_1 \frac{(3+\eta)}{\sqrt{3}\rho} t$$

WAHUHA, i.e.,

$$(\pi/2)_{\mathbf{x}}^{-\tau} (\tau - (\pi/2))_{-\mathbf{x}}^{-\tau - (\pi/2)} \mathbf{y}^{-2\tau - (\pi/2)}_{\mathbf{y}}_{-\mathbf{y}}^{-\tau - (\pi/2)} \mathbf{x}^{-\tau -} \mathbf{n} \dots \text{.. (IV.52)}$$

and MREV-8, i.e.,

$$(\pi/2)_{\mathbf{x}}^{-\tau} (\tau - (\pi/2))_{-\mathbf{x}}^{-\tau - (\pi/2)} \mathbf{y}^{-2\tau - (\pi/2)}_{\mathbf{y}}_{-\mathbf{y}}^{-\tau - (\pi/2)} \mathbf{x}^{-\tau -} \mathbf{n} \dots \text{.. (IV.53)}$$

Pulse sequences are cyclic at least to zeroth order.

IV.D.3(i) Zeroth-order average Hamiltonians of internal interactions under the influence of PAPS and their commutation with ρ_i : case of single crystals:

In this sub-section we first evaluate the zeroth-order average Hamiltonians of internal interactions and seek their commutation with ρ_i , the initial density matrix prepared by the preparatory pulse.

The Hamiltonians corresponding to the internal interactions are given by Eqns. IV.44(a) - IV.44(c). Making use of Eqn. IV.34 the zeroth-order average Hamiltonian for efg inhomogeneity can be shown to be,

$$\begin{aligned} \tilde{\mathcal{H}}_{\text{inhom}}^{(0)} &= \frac{1}{t_c} \int_0^{t_c} \tilde{\mathcal{H}}_{\text{inhom}}^d(\tau) d\tau \\ &= \frac{\Delta\omega_q}{\sqrt{6.2}} \left[T_0^2 (1 + \cos\beta_2) + i \sin\beta_2 T_1^2(s) \right] \dots \text{.. (IV.54)} \end{aligned}$$

Similarly,

$$\bar{\mathcal{H}}_{\text{tors}}^{(0)} = A_1/2 [T_0^2 (1 + \cos \beta_2) + i \sin \beta_2 T_1^2(s)] \quad \dots \text{(IV.55)}$$

and

$$\begin{aligned} \bar{\mathcal{H}}_{\text{het}}^{(0)} = & \gamma [-H_X \{ [(1-\eta) \cos \beta_2 + \rho] [\frac{1}{\rho} (\frac{1}{5} T_1^1(a) - \frac{1}{\sqrt{15}} T_1^3(a))] \\ & + \frac{1}{3\rho} [-(1-\eta) \cos \beta_2 + \rho] T_3^3(a) \\ & + i \sin \beta_2 \frac{\sqrt{2}}{3\rho} (\eta-1) T_2^3(a) \} \\ & + i H_Y \{ [(1+\eta) + \cos \beta_2 \rho] [\frac{1}{\rho} (\frac{1}{5} T_1^1(s) - \frac{1}{\sqrt{15}} T_1^3(s))] \\ & + \frac{1}{3\rho} [(1+\eta) - \cos \beta_2 \rho] T_2^3(s) \\ & - i \sin \beta_2 \frac{\sqrt{2}}{3} T_2^3(s) \} \\ & + H_Z \{ \frac{1}{5\rho} (\cos \beta_2 \rho + 4) T_0^1 \\ & + \frac{4}{3\sqrt{10}\rho} (\cos \beta_2 \rho - 1) T_0^3 \\ & + i \sin \beta_2 [\frac{\sqrt{3}}{5} T_1^1(s) + \frac{2}{3\sqrt{5}} T_1^3(s)] \} \} \\ & \dots \text{(IV.56)} \end{aligned}$$

$$\text{where } \beta_2 = 2(\omega_1 \frac{(3+\eta)}{\sqrt{3}\rho} t_w) \quad \dots \text{(IV.52)}$$

In obtaining Eqns. IV.54, IV.55, IV.56 we have made use of the Table II.3 which gives the evolution of tensor operators under the action of $\tilde{\mathcal{H}}_1^d$ (for $\varphi = 0$) when ξ is replaced by $\beta = \omega_1 \frac{(3+\eta)}{\sqrt{3}\rho} t_w$. In obtaining the evolution of the operators under $\tilde{\mathcal{H}}_1^d$ (for $\varphi = 180$) we substituted ξ by $-\beta$ in Table II.3.

The initial density matrix prepared by the preparatory pulse is given by

$$\tilde{\rho}(t_w) = T_0^2 \cos \beta_1 + i \sin \beta_1 T_1^2(s) \quad \dots (IV.58)$$

$$\text{where } \beta = \omega_1 \cdot \frac{(3+\eta)}{\sqrt{3}} t_w \quad \dots (IV.59)$$

Now, from Eqns. IV.54, IV.55, IV.56 and IV.58 and commutation relationships of tensor operators for spin $I = 3/2$ (see [29]) it can be easily shown that

$$[\tilde{\rho}, \overline{\mathcal{H}}_{\text{inhom}}^{(0)}] = 0$$

$$[\tilde{\rho}, \overline{\mathcal{H}}_{\text{tors}}^{(0)}] = 0$$

$$[\tilde{\rho}, \overline{\mathcal{H}}_{\text{het}}^{(0)}] = 0 \quad \dots (IV.60)$$

when $2\beta_1 = \beta_2$.

Thus, from the above discussion it is clear that under the influence of PAPS the internal interactions defined by $\mathcal{H}_{\text{inhom}}$, $\mathcal{H}_{\text{tors}}$, \mathcal{H}_{het} are averaged out when the pulse widths of the cycle pulses are twice to that of the preparatory pulse. This indicates that the PAPS sequence is effecting a kind of general averaging leading to the lengthening of the decay of the magnetization. This is in agreement with the experimental results of PAPS on single crystal presented in Section IV.B.

IV.D.3(ii) Influence of PAPS on spin $I = 3/2$ nuclei in polycrystalline samples:

In the preceeding sub-section we dealt with the action of PAPS on spin $I = 3/2$ nuclei in single crystals. In this section we examine the influence of PAPS on spin $I = 3/2$ nuclei in polycrystalline samples. In the case of polycrystalline samples the crystallites are oriented randomly and hence each crystallite will make a different angle with respect to the applied r.f. field. Hence, the r.f. Hamiltonian for this situation should be written as

$$\mathcal{H}_1(t) = -2\omega_1 \cos(\omega_q t + \varphi) [I_x P_1 + I_y P_2 + I_z P_3] \quad \dots (IV.61)$$

where $P_1 = \sin\theta \cos\varphi$, $P_2 = \sin\theta \sin\varphi$, $P_3 = \cos\theta$, θ and φ are the polar and azimuthal angles of the applied r.f. field vector and φ is the phase of r.f.

In terms of tensor operators the above equation can be written as

$$\mathcal{H}_1(t) = -2\omega_1 \cos(\omega_q t + \varphi) [-T_1^1(a) P_1 + T_1^1(s) P_2 + T_0^1 P_3] \quad \dots (IV.62)$$

$$\text{For } \varphi = 0 \quad \mathcal{H}_1(t) = -2\omega_1 \cos(\omega_q t) [-T_1^1(a) P_1 + T_1^1(s) P_2 + T_0^1 P_3] \quad \dots (IV.63)$$

$$\text{For } \varphi = 180^\circ \quad \mathcal{H}_1(t) = 2\omega_1 \cos(\omega_q t) [-T_1^1(a) P_1 + T_1^1(s) P_2 + T_0^1 P_3] \quad \dots (IV.64)$$

Transforming $\mathcal{H}_1(t)$ first into 'diagonal representation' and then into QIR, we have

$$\tilde{\mathcal{H}}_1^d = U_q U_d \mathcal{H}_1(t) U_d^{-1} U_q^{-1} \quad \dots (IV.65)$$

$$\begin{aligned} \text{for } \varphi = 0 \quad \tilde{\mathcal{H}}_1^d \simeq \omega_1 \frac{1}{3\varphi} & \left[P_1 (3+\eta) \left(\frac{3}{5} T_1^1(a) + \frac{2}{\sqrt{15}} T_1^3(a) \right) \right. \\ & - P_2 (3-\eta) \left(\frac{3}{5} T_1^1(s) + \frac{2}{\sqrt{15}} T_1^3(s) \right) \\ & \left. - P_3 \left(-\frac{2\sqrt{2}}{\sqrt{3}} \eta \right) T_2^3(s) \right] \quad \dots (IV.66) \end{aligned}$$

and $\tilde{\mathcal{H}}_1^d$ (for $\varphi = 180^\circ$) can be obtained from Eqn. IV.66 by just changing the sign of the Hamiltonian, i.e.,

$$(\tilde{\mathcal{H}}_1^d)_{\varphi=180^\circ} = -(\tilde{\mathcal{H}}_1^d)_{\varphi=0} \quad \dots (IV.67)$$

The evolution of tensor operators under the influence of $\tilde{\mathcal{H}}_1^d$ (for $\varphi = 0$) is set out in Table III.3. From Table III.3 the evolution of the operators under $\tilde{\mathcal{H}}_1^d$ (for $\varphi = 180^\circ$) can be obtained by replacing \mathcal{E} by $-\mathcal{E}$.

Before evaluating the zeroth order average Hamiltonian, we consider the question of cyclicity of PAPS in the case of polycrystalline samples. Again considering only the zeroth order term, from Eqn. IV.24 and using Table III.3, we see that

$$\overline{\mathcal{H}}_1^{(0)} = 1/t_c \int_0^t \tilde{\mathcal{H}}_1^d(t) dt = \omega_1/4 [T-T] = 0 \quad \dots (IV.68)$$

$$\begin{aligned} \text{where } T = \frac{1}{3\varphi} & \left[P_1 (3+\eta) \left(\frac{3}{5} T_1^1(a) + \frac{2}{\sqrt{15}} T_1^3(a) \right) \right. \\ & - P_2 (3-\eta) \left(\frac{3}{5} T_1^1(s) + \frac{2}{\sqrt{15}} T_1^3(s) \right) \\ & \left. - P_3 \left(\frac{-2\sqrt{2}}{\sqrt{3}} \eta \right) T_2^3(s) \right] \quad \dots (IV.68a) \end{aligned}$$

Thus, even in the case of polycrystalline samples PAPS is cyclic atleast to the zeroth order.

Zeroth-order average Hamiltonians of internal interactions and their commutation with ρ_1 :

In the case of polycrystalline samples we consider the internal interactions due to efg inhomogeneities and torsional oscillations only. Making use of Eqn. IV.34 and Table III.3 the zeroth order average Hamiltonian of inhomogeneous efg can be shown to be

$$\begin{aligned} \overline{\mathcal{H}}_{\text{inhom}}^{(0)} &= \frac{\Delta\omega_q}{\sqrt{6}.2} \left[\tilde{T}_O^2 (1 + \cos \xi_2) + \frac{i \sin \xi_2}{\sqrt{3} \int x} \right. \\ &\quad \left. \{ P_1(3+\eta) \tilde{T}_1^2(s) - P_2(3-\eta) \tilde{T}_1^2(a) + P_3 2\eta \tilde{T}_2^2(a) \} \right] \\ &\quad \dots \text{(IV.69)} \end{aligned}$$

Similarly,

$$\begin{aligned} \overline{\mathcal{H}}_{\text{tors}}^{(0)} &= \frac{A_1}{2} \left[\tilde{T}_O^2 (1 + \cos \xi_2) + \frac{i \sin \xi_2}{\sqrt{3} \int x} \{ P_1(3+\eta) \tilde{T}_1^2(s) \right. \\ &\quad \left. - P_2(3-\eta) \tilde{T}_1^2(a) + P_3 2\eta \tilde{T}_2^2(a) \} \right] \\ &\quad \dots \text{(IV.70)} \end{aligned}$$

The density matrix prepared by the preparatory pulse is given by

$$\begin{aligned} \rho(t_w) &= \tilde{T}_O^2 \cos \xi_1 + \frac{i \sin \xi_1}{\sqrt{3} \int x} \left[P_1(3+\eta) \tilde{T}_1^2(s) - P_2(3-\eta) \tilde{T}_1^2(a) \right. \\ &\quad \left. + 2\eta P_3 \tilde{T}_2^2(a) \right] \quad \dots \text{(IV.71)} \end{aligned}$$

$$\text{where } \varepsilon_1 = \omega_1 t_w \left[\frac{1}{(3+\eta^2)} \{ \sin^2 \theta [(9+\eta^2) - 6\eta \cos 2\theta] + 4\eta^2 \cos^2 \theta \} \right]^{1/2} \quad \dots \text{(IV.72)}$$

$$\varepsilon_2 = 2\varepsilon_1$$

From Eqns. IV.69, IV.70 and IV.71 and commutation relationships of tensor operators for spin $I = 3/2$ (see [29]) it can be easily shown that

$$[\tilde{\rho}(t_w), \overline{\mathcal{H}}_{\text{inhom}}^{(0)}] = 0 \quad \dots \text{(IV.73)}$$

$$[\tilde{\rho}(t_w), \overline{\mathcal{H}}_{\text{tors}}^{(0)}] = 0$$

Thus, even in the case of polycrystalline samples under the action of PAPS the internal interactions due to efg inhomogeneities and torsional oscillations will be averaged out, when the width of the cycle pulses is twice to that of the preparatory pulse. Similar kind of behaviour has been observed by Osokin [6] in the case of spin $I = 1$. Thus the experimentally observed, lengthening of the decay of the magnetization can be explained as, partially, due to the averaging effect of the $\mathcal{H}_{\text{inhom}}, \mathcal{H}_{\text{tors}}$. However, experimentally we have observed the lengthening of the decay of the magnetization, for arbitrary values of the width of the cycle pulses. This observation cannot be explained by the theoretical analysis presented above.

IV.D.3(III) Influence of WAHUHA and MREV-8 sequences on spin $I = 3/2$ nuclei in single crystals:

In this section we consider the influence of WAHUHA and MREV-8 sequences on internal interactions due to efg

inhomogeneities and torsional oscillations only.

(a) WAHUHA sequence:

Using Eqn. IV.34 and Tables II.3 and IV.6 the zeroth-order average Hamiltonians of $\tilde{\mathcal{H}}_{\text{inhom}}^d$, $\tilde{\mathcal{H}}_{\text{tors}}^d$ can be shown to be

$$\begin{aligned} \bar{\mathcal{H}}_{\text{inhom}}^{(0)} = \frac{\Delta\omega_q}{\sqrt{6.3}} [(1+\cos\xi + \cos^2\xi) T_0^2 - 2 \text{isin}\xi T_1^2(s) \\ - \frac{1}{\sqrt{2}} \sin 2\xi \left(\frac{3}{5} T_1^1(a) + \frac{2}{\sqrt{15}} T_1^3(a) \right)] \\ \dots \text{(IV.74)} \end{aligned}$$

$$\begin{aligned} \bar{\mathcal{H}}_{\text{tors}}^{(0)} = \frac{A_1}{3} [(1+\cos\xi + \cos^2\xi) T_0^2 - 2 \text{isin}\xi T_1^2(s) \\ - \frac{1}{\sqrt{2}} \sin 2\xi \left[\frac{3}{5} T_1^1(a) + \frac{2}{\sqrt{15}} T_1^3(a) \right]] \dots \text{(IV.75)} \end{aligned}$$

The initial density matrix prepared by the preparatory pulse is given by

$$\tilde{\rho}(t_w) = T_0^2 \cos\beta + \text{isin}\beta T_1^2(s) \dots \text{(IV.76)}$$

Now, from Eqns. IV.74, IV.75 and IV.76 and commutation relationships of tensor operators for spin $I = 3/2$ (see [29]) it can be shown that

$$\begin{aligned} [\tilde{\rho}, \bar{\mathcal{H}}_{\text{inhom}}^{(0)}] \neq 0 \\ [\rho, \bar{\mathcal{H}}_{\text{tors}}^{(0)}] \neq 0 \dots \text{(IV.77)} \end{aligned}$$

(b) MREV-8 sequence:

Proceeding as in the case of WAHUHA sequence the zeroth-order average Hamiltonians of the internal interactions corresponding to efg inhomogeneities and torsional oscillations for this case can be shown to be

$$\bar{\mathcal{H}}_{\text{inhom}}^{(0)} = \frac{\Delta\omega_q}{\sqrt{6}} \frac{1}{3} [\tilde{T}_O^2 (1 + \cos\beta + \cos^2\beta)] \quad \dots (\text{IV.78})$$

$$\text{and } \bar{\mathcal{H}}_{\text{tors}}^{(0)} = \frac{A_1}{3} [\tilde{T}_O^2 (1 + \cos\beta + \cos^2\beta)] \quad \dots (\text{IV.79})$$

the $\tilde{\rho}_i$ is given by Eqn. IV.76.

Now from Eqns. IV.76, IV.78 and IV.79 and commutation relationships of tensor operators for spin $I = 3/2$ [see 29] it can be easily seen that

$$[\tilde{\rho}, \bar{\mathcal{H}}_{\text{inhom}}^{(0)}] \neq 0$$

$$[\tilde{\rho}, \bar{\mathcal{H}}_{\text{tors}}^{(0)}] \neq 0 \quad \dots (\text{IV.80})$$

Thus, the above results indicate that under WAHUHA and MREV-8, sequences the internal interactions defined by $\mathcal{H}_{\text{inhom}}$ and $\mathcal{H}_{\text{tors}}$ do not average out. It will be interesting to study the internal interactions due to heteronuclear and homonuclear dipole-dipole interactions to verify whether there is any kind of selective averaging taking place under the influence of these sequences.

SUMMARY

Experimental results of SLS, PAPS and WAHUHA multiple pulse sequences on ^{35}Cl ($I = 3/2$) ^{187}Re and ^{185}Re (both with $I = 5/2$) nuclei are presented. In SLS, the dependence of the decay of the quasi-equilibrium magnetization on the parameters such as, θ , ϕ , τ and $\Delta\omega$ has been investigated. It is inferred that all the multiple pulse sequences investigated here lead to the lengthening of the transverse magnetization, implying a narrowed NQR line in the frequency domain. Results of ^{23}Na - ^{35}Cl double resonance experiment carried out under spin-locked condition, in a polycrystalline sample of NaClO_3 are presented.

Using average Hamiltonian theory and tensor operator formalism theoretical analysis of the influence of PAPS, WAHUHA, and MREV-8 sequences on spin $3/2$ nuclei has been carried out. In the case of spin $3/2$ nuclei in single crystals it has been shown that under the action of PAPS the zeroth order average Hamiltonians of the internal interactions ($\overline{\mathcal{H}}_{\text{int}}^{(0)}$) due to

- i) efg inhomogeneities ($\mathcal{H}_{\text{inhom}}$)
- ii) torsional oscillations ($\mathcal{H}_{\text{tors}}$)
- iii) heteronuclear dipole-dipole interaction (\mathcal{H}_{het})

commute with ρ_1 , the initial density matrix prepared by the preparatory pulse, thereby implying the averaging out of these interactions under this sequence. In the case of polycrystalline samples under the action of PAPS we considered only two internal

interactions namely, $\mathcal{H}_{\text{inhom}}$, $\mathcal{H}_{\text{tors}}$ and these have been shown to be averaged out. Under WAHUHA and MREV-8 sequences we have considered $\mathcal{H}_{\text{inhom}}$, $\mathcal{H}_{\text{tors}}$ only. It has been shown that, in the case of single crystals, these interactions do not average out under these sequences.

REFERENCES

- [1] U. Haeberlen, "High Resolution NMR in Solids: Selective Averaging," Supplement-1 to Advances in Magnetic Resonance, Ed. J.S. Waugh, Academic Press, N.Y. (1976).
- [2] M. Mehring, "Principles of High Resolution NMR in Solids," Springer-Verlag (1983).
- [3] E.D. Ostroff and J.S. Waugh, Phys. Rev. Lett., 16, 1097 (1966).
- [4] P. Mansfield and D. Ware, Phys. Lett., 22, 133 (1966).
- [5] R.A. Marino and S.M. Klainer, J. Chem. Phys., 67, 3388 (1977).
- [6] D. Ya. Osokin, Phys. Status Solidi (b), 102, 681 (1980).
- [7] D. Ya. Osokin, Phys. Status Solidi (b), 109, K7 (1982).
- [8] D. Ya. Osokin, J. Molec. Struct., 83, 243 (1982).
- [9] D. Ya. Osokin, Molec. Phys., 48, 283 (1983).
- [10] N.E. Ainbinder, G.B. Furman, G.E. Kibrik, A. Ya. Poljakov and I.G. Shaposhnikov, Z. Naturforsch., 41a, 366 (1986).
- [11] Narsimha Reddy and P.T. Narasimhan, Abstracts, 'Ninth International Symposium on Nuclear Quadrupole Resonance', Kanpur, India (1988), Abstract C1.
- [12] V.L. Ermakov and D. Ya. Osokin, Molec. Phys., 53, 1335 (1984).
- [13] J.S. Waugh, L.M. Huber and U. Haeberlen, Phys. Rev. Lett., 20, 180 (1968).
- [14] R.S. Cantor and J.S. Waugh, J. Chem. Phys., 73, 1054 (1980).

- [15] A.K. Hitrin, G.E. Karnaukh and B.N. Provotorov, J. Molec. Struct., 83, 269 (1982).
- [16] M. Matti Maricq, Phys. Rev., B33, 4501 (1986).
- [17] N.E. Ainbinder and G.B. Furman, Sov. Phys. (JETP), 58, 575 (1983).
- [18] N.E. Ainbinder, G.A. Volgina, A.N. Osipenko, G.B. Furman and I.G. Shaposhnikov, J. Molec. Struct., 111, 65 (1983).
- [19] N.N. Bogolyubov and Yu. A. Mitropolskii, "Analytic Methods in the Theory of Non-Linear Oscillations," Gordon and Breach (1964).
- [20] J.S. Waugh, C.H. Wang, L.M. Huber and R.L. Vold, J. Chem. Phys., 48, 662 (1968).
- [21] (a) S. Vega, J. Chem. Phys., 63, 3769 (1975).
(b) S. Vega and A. Pines, J. Chem. Phys., 66, 5624 (1977).
- [22] (a) A.R. Kessel and O.S. Zueva, Phys. Lett., 68, 347 (1978).
(b) O.S. Zueva and A.R. Kessel, Sov. Phys. Solid State, 21, 2037 (1979).
(c) O.S. Zueva, J. Molec. Struct., 83, 379 (1982).
(d) O.S. Zueva and A.R. Kessel, J. Molec. Struct., 83, 383 (1982).
- [23] Narsimha Reddy, Ph.D. Thesis, Indian Institute of Technology, Kanpur, India (1987).
- [24] M. Bloom, E.L. Hahn and B. Herzog, Phys. Rev., 97, 1699 (1955).
- [25] M.J. Weber, J. Phys. Chem. Solids, 17, 267 (1961).
- [26] M. Emshwiller, E.L. Hahn and D. Kaplan, Phys. Rev., 118, 414 (1960).

- [27] W.K. Rhim, D.D. Elleman and R.W. Vaughan, J. Chem. Phys., 58, 1772 (1973).
- [28] G.J. Bowden and W.D. Hutchison, J. Magn. Reson., 67, 403 (1986).
- [29] G.J. Bowden, W.D. Hutchison and J. Khachan, J. Magn. Reson., 67, 415 (1986).
- [30] G.J. Bowden and W.D. Hutchison, J. Magn. Reson., 70, 361 (1986).
- [31] G.J. Bowden and W.D. Hutchison, J. Magn. Reson., 72, 61 (1987).
- [32] W.D. Hutchison, Ph.D. Thesis, University of New South Wales, Australia (1987).
- [33] T.P. Das and E.L. Hahn, "Nuclear Quadrupole Resonance Spectroscopy," Solid State Physics, Supplement 1, Academic Press, New York (1958).
- [34] A. Abragam, "The Principles of Nuclear Magnetism," Clarendon Press, Oxford (1962).
- [35] B.C. Gerstein and C.R. Dybowski, "Transient Techniques in NMR of Solids. An Introduction to Theory and Practice," Academic Press (1985).
- [36] W. Magnus, Commun. Pure Appl. Matu., 7, 649 (1954).

CHAPTER V

STUDY OF MULTIPLE QUANTUM COHERENCES IN PURE NQR

In pulsed nuclear magnetic resonance (NMR) spectroscopy magnetic dipole-allowed transitions between the eigen states of the nuclear ensemble can be observed by perturbing the spin system with an r.f. pulse which brings the eigen states separated by $\Delta m = \pm 1$ into coherent superposition. Such transitions are referred to as the single quantum transitions or single quantum coherences. Because of the perturbing r.f. pulse the inherent time-dependence of each state, normally random in thermal equilibrium acquires a phase coherence across the ensemble. This coherence is known as transverse magnetization and it gives rise to the free induction signal. The rigorous definition of coherence is based on the elements of the density matrix σ [1,2] of the spin system. The diagonal element of the density matrix

$$\sigma_{rr} = \langle r | \sigma(t) | r \rangle = \overline{|C_r(t)|^2} \quad \dots (V.1)$$

is equal to the probability that the spin system is found in the eigen state $|r\rangle$, while the off-diagonal element

$$\sigma_{rs} = \langle r | \sigma(t) | s \rangle = \overline{C_r(t) C_s^*(t)} \quad \dots (V.2)$$

indicates a "coherent superposition" of eigen states $C_r(t) |r\rangle + C_s(t) |s\rangle$ in the state function $\Psi(t)$ of the ensemble, in the sense that the time dependence and the phase of the various members of the ensemble are correlated w.r.t. $|r\rangle$ and $|s\rangle$. Such a coherent superposition is known as "coherence". The

coherence σ_{rs} between two states with $\Delta m_{rs} = \pm 1$ leads to the observable transverse magnetization.

In general a matrix element σ_{rs} represents n quantum coherence which for $n \neq \pm 1$, does not lead to observable magnetization and can only be detected indirectly. In fact, any arbitrary coherence σ_{rs} can be made non-zero by preparing the spin system with appropriate r.f. pulses. This has been elegantly demonstrated in a number of experiments in the area of NMR [2].

The first experimental NMR detection of double quantum coherence was done by Hatanka et al. [3,4] using a multistep process. They carried out NMR experiment on ^{27}Al ($I = 5/2$) in a single crystal of Al_2O_3 which was oriented such that the efg axis is aligned with the external magnetic field. Out of six energy levels that are possible for spin $I = 5/2$ in high magnetic field (see Fig. V.1) they considered only three energy levels in their experiment. These levels are labelled as a, b and c in Fig. V.1. Hatanaka et al. have used a pulse sequence of the form $(\pi/2)_x(\omega_a)(\pi)_x(\omega_b)-\tau-(\pi)_x(\omega_a)$. Creation and detection of double quantum coherence in their experiment can be understood as follows.

A $(\pi/2)$ pulse applied to the (a, b) transition generates single-quantum coherence σ_{ab} . Immediately if one applies a π pulse to (b,c) transition, it not only interchanges the populations of levels b and c but also swaps the indices b and c. Thus, the π pulse establishes the coherence between a and c,

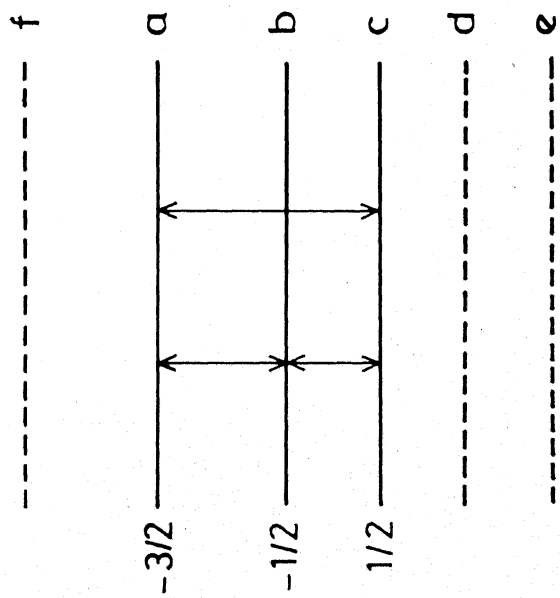


Fig.V.1 Energy level diagram of ^{27}Al ($I=5/2$) in Al_2O_3 in the presence of strong Zeeman field.

σ_{ac} which is a double quantum coherence. Since this double quantum coherence cannot be observed directly it has to be converted back into a single quantum coherence by a monitoring pulse. A second π pulse applied after a time τ , to b, c transition, converts this double quantum coherence into σ_{ab} . If the π pulse is applied to (a, b) transition then σ_{ac} coherence transfer into σ_{bc} . In either case, the observable magnetization appears in a transition which is not subjected to an r.f. pulse.

Since the first detection of double quantum coherence in NMR by Hatanaka et al. multiple quantum NMR spectroscopy has been developed and applied to the solution of problems in molecular structure and dynamics [2,5-8]. However, to our knowledge there has been no study of this phenomenon in the area of pure NQR spectroscopy.

Our interest in the study of multiple quantum coherences in NQR stems from the following considerations. As mentioned in Chapter I, the nuclei with $I \geq 2$ possess in addition to quadrupole moment, electric hexadecapole moment [9]. Since the hexadecapole coupling constant (HDCC) is very small of the order of few KHz, it is rather difficult to detect it directly. There have been several reports in the literature [9-11] where the HDCC has been determined by accurate measurements of the NQR frequencies. However, it is well known that the NQR frequencies are rather sensitive to slight temperature changes. Hence any error in the temperature measurement while measuring the NQR frequencies could lead to an error in the HDCC. Thus,

in order to measure HDCC accurately one needs to detect the two NQR frequencies simultaneously. It is in this context we thought of the possibility of the multiple quantum experiment in NQR. We have therefore undertaken the theoretical study of double quantum coherence in NQR of spin $I = 5/2$ nuclei in single crystals.

This chapter deals with the theoretical investigations of the creation and detection of double quantum coherence in pure NQR of nuclei with spin $I = 5/2$ in a single crystal. Our approach is based on the density matrix theory with the tensor operator formalism [12-16]. In the next section we present the details of the theoretical investigation.

V.A DOUBLE QUANTUM COHERENCE FOR SPIN $I = 5/2$ CASE IN PURE NQR

We consider the case of a non-interacting nuclear spin ensemble with axially symmetric field gradient. The energy levels for spin $I = 5/2$, and the pulse scheme considered for the double quantum coherence are shown in Fig. V.2. In all the calculations in this section we assume that the relaxation effects are not significant. We set $\hbar = 1$, and express energy values in radians per sec. The r.f. pulses are assumed to be applied along the principal x-axis of the efg tensor.

The net Hamiltonian, in the laboratory frame for a nuclear spin ensemble with quadrupole interaction in the presence of perturbing r.f. field can be written as

$$\mathcal{H}(t) = \mathcal{H}_Q + \mathcal{H}_{1a}(t) + \mathcal{H}_{1b}(t) \quad \dots \quad (V.3)$$

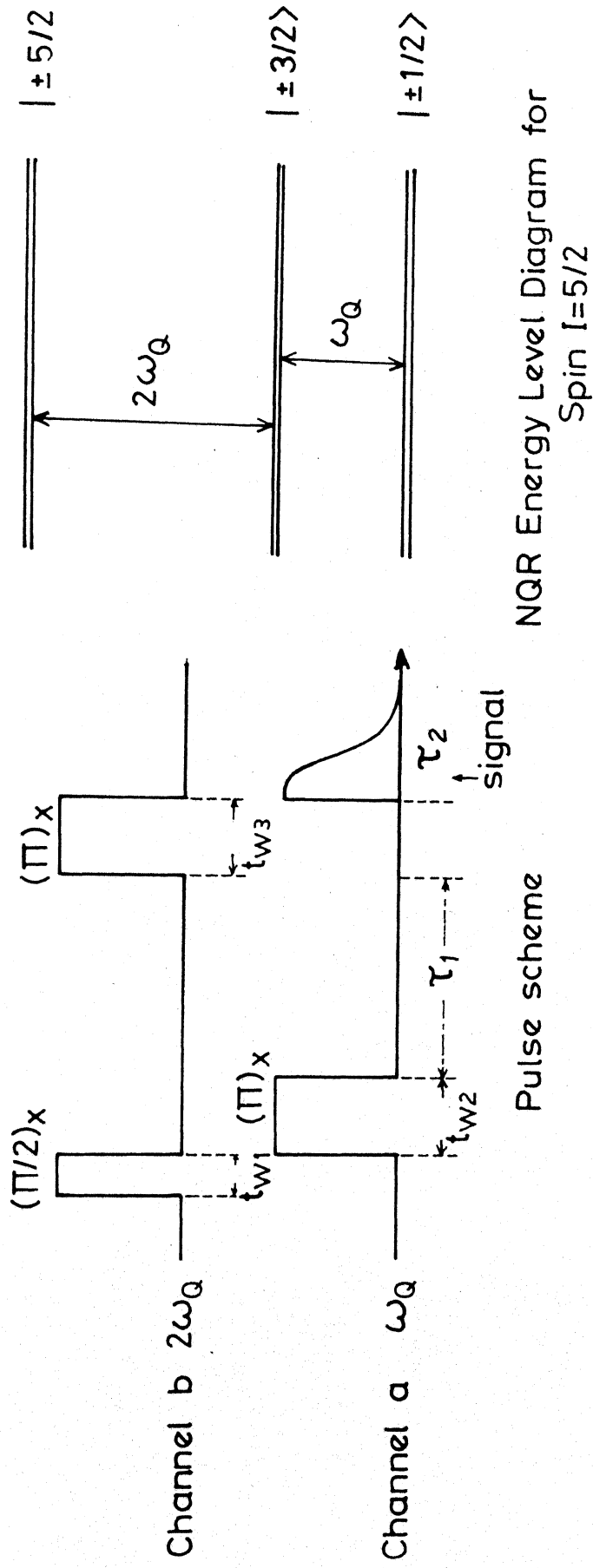


Fig.V.2 Energy level diagram for spin $I=5/2$ nuclear spin system with the axially symmetric electric field gradient. Pulse scheme for double quantum coherence is shown on the left.

where \mathcal{H}_Q is the quadrupolar Hamiltonian and for the axially symmetric efg case it is given by [17]

$$\mathcal{H}_Q = \frac{e^2 q Q}{4I(2I-1)} [3 \tilde{I}_z^2 - \tilde{I}^2] \quad \dots (V.4)$$

$\mathcal{H}_{1a}(t)$, $\mathcal{H}_{1b}(t)$ are the Hamiltonians which define the interaction between the nuclear spins and the applied r.f. pulses with frequencies ω_Q and $2\omega_Q$, respectively. These r.f. Hamiltonians can be written as

$$\mathcal{H}_{1a}(t) = -2\omega_{1a} \cos(\omega_Q t) \tilde{I}_x \quad \dots (V.5)$$

and

$$\mathcal{H}_{1b}(t) = -2\omega_{1b} \cos(2\omega_Q t) \tilde{I}_x \quad \dots (V.6)$$

where $\omega_{1a} = \gamma H_{1a}$ and $\omega_{1b} = \gamma H_{1b}$; γ is the gyromagnetic ratio of the nucleus, and \mathcal{H}_{1a} and \mathcal{H}_{1b} are the amplitudes of the applied r.f. pulses. It may be mentioned here that although in the total Hamiltonian we have given r.f. Hamiltonians corresponding to two different frequencies, for a given time only one of these Hamiltonians is active (see Fig. V.1).

Following Bowden et al. [12] the total Hamiltonian for spin $I = 5/2$ case can be written as

$$\mathcal{H}(t) = \frac{\omega_Q}{\sqrt{6}} \tilde{T}_0^2 + 2\omega_{1a} \cos(\omega_Q t) \tilde{T}_1^1(a) + 2\omega_{1b} \cos(2\omega_Q t) \tilde{T}_1^1(a) \quad \dots (V.7)$$

where $\omega_Q = \frac{3}{20} e^2 q Q$

As mentioned in the previous chapters, the response of the nuclear spin system to the r.f. pulse excitations can be calculated using the Liouville-von Neumann equation. Before the application of the r.f. pulses the spin system is assumed to be at thermal equilibrium under the influence of the pure quadrupolar Hamiltonian. In the high temperature approximation, the thermal equilibrium density matrix is given by [18]

$$\begin{aligned}
 \sigma(t \leq 0) &= \{ \text{Tr} [\exp(-\frac{\mathcal{H}_Q}{kT})] \}^{-1} \exp(-\frac{\mathcal{H}_Q}{kT}) \\
 &\simeq [\text{Tr}(\mathbb{1})]^{-1} (1 - \frac{\omega_Q}{\sqrt{6} kT} T_O^2) \\
 &\simeq [\text{Tr}(\mathbb{1})]^{-1} [1 - (\frac{1}{kT} \frac{\omega_Q}{\sqrt{6}}) \rho] \quad \dots (V.8)
 \end{aligned}$$

The first term on the right hand side of the above equation being a constant is not affected by any evolution of the spin system. Hence, we need to follow the evolution of the reduced density matrix

$$\rho(t \leq 0) = T_O^2 \quad \dots (V.9)$$

only.

In the quadrupolar interaction representation defined by the transformation operator

$$U = \exp [i \mathcal{H}_Q t] \quad \dots (V.10)$$

the total Hamiltonian is given by,

$$\tilde{\mathcal{H}} = U \mathcal{H}(t) U^{-1} = \tilde{\mathcal{H}}_{1a} + \tilde{\mathcal{H}}_{1b} \quad \dots (V.11)$$

$$\text{where } \tilde{\mathcal{H}}_{1a} = 2\omega_{1a} \cos(\omega_Q t) U T_1^1(a) U^{-1}$$

$$\approx \omega_{1a} \left[\frac{16}{35} T_1^1(a) - \frac{2}{9\sqrt{15}} T_1^3(a) - \frac{4}{3\sqrt{210}} T_1^5(a) \right] \quad \dots (V.12)$$

and

$$\tilde{\mathcal{H}}_{1b} = 2\omega_{1b} \cos(2\omega_Q t) U T_1^1(a) U^{-1}$$

$$\approx \omega_{1b} \left[\frac{2}{7} T_1^1(a) + \frac{5}{9\sqrt{15}} T_1^3(a) + \frac{1}{3\sqrt{210}} T_1^5(a) \right] \quad \dots (V.13)$$

In arriving at these equations we have made use of the evolution of the tensor operators under the influence of quadrupolar Hamiltonian \mathcal{H}_Q (see Table 12 of [13]) and the high frequency terms have been dropped as non-secular terms.

In order to follow the evolution of density matrix, in the interaction representation, following the r.f. pulses we need to know the evolution of tensor operators under the action of the Hamiltonians $\tilde{\mathcal{H}}_{1a}$ and $\tilde{\mathcal{H}}_{1b}$. The evolution of a few selected tensor operators under the influence of $\tilde{\mathcal{H}}_{1a}$ and $\tilde{\mathcal{H}}_{1b}$ can be obtained from Tables. II.5 and II.6, respectively.

V.A.1 General Expressions for the Density Matrix at Various Stages of the Pulse Sequence

From the NQR energy level diagram (see Fig.V.2) it is evident that double quantum coherence is possible between the states:

$$|+5/2\rangle \longleftrightarrow |+3/2\rangle$$

$$|-5/2\rangle \longleftrightarrow |-3/2\rangle$$

$$|+3/2\rangle \longleftrightarrow |-1/2\rangle$$

$$|-3/2\rangle \longleftrightarrow |+1/2\rangle$$

For spin $I = 5/2$ the operator set consists of 36 tensor operators [12]. Out of these, the operators that carry information about the double quantum coherence (i.e. $|\Delta m| = 2$) are

$$\tilde{T}_2^2(a,s), \tilde{T}_2^3(a,s), \tilde{T}_2^4(a,s) \text{ and } \tilde{T}_2^5(a,s)$$

In what follows, we give general expressions for the density matrix of the spin system at various stages of the pulse sequence. The thermal equilibrium reduced density matrix in the interaction representation is given by

$$\tilde{\rho}(0) = \tilde{T}_0^2 \quad \dots (V.14)$$

Immediately following the application of the r.f. pulse with frequency $2\omega_Q$ and width ' t_{w1} ' the density matrix is given by (see Table II.6):

$$\begin{aligned} \tilde{\rho}(t_{w1}) = & \frac{1}{7} \tilde{T}_0^2 [4+3 \cos(\varepsilon_1)] + \frac{2}{\sqrt{105}} \tilde{T}_0^4 (\cos(\varepsilon_1)-1) \\ & + i \frac{\sqrt{15}}{7} \tilde{T}_1^2(s) \sin(\varepsilon_1) + i \frac{2}{\sqrt{210}} \tilde{T}_1^4(s) \sin(\varepsilon_1) \end{aligned} \quad \dots (V.15)$$

where $\varepsilon_1 = \sqrt{5} \omega_{1b} t_{w1}$.

Immediately after this, if we apply an r.f. pulse with a frequency ω_Q and width ' t_{w2} ' then the density matrix just after the removal of the pulse is given by

$$\begin{aligned}\tilde{\rho}(t_{w1} + t_{w2}) = & \tilde{T}_0^2 B_1 + \tilde{T}_0^4 B_2 + \tilde{T}_1^2(s) B_3 + \tilde{T}_1^4(s) B_4 \\ & + \tilde{T}_2^2(s) B_5 + \tilde{T}_2^4(s) B_6 \quad \dots (V.16)\end{aligned}$$

In writing Eqn. V.16 we have made use of the results given in Table II.5. The expressions for the B's are given in Table V.1. Now, if we apply a $(\pi)_x$ pulse with a frequency $2\omega_Q$ and width ' t_{w3} ', then the density matrix immediately following the pulse is given by

$$\begin{aligned}\tilde{\rho}(t_{w1} + t_{w2} + t_{w3}) = & \tilde{T}_0^2 C_1 + \tilde{T}_0^4 C_2 + \tilde{T}_1^2(s) C_3 + \tilde{T}_1^4(s) C_4 \\ & + \tilde{T}_2^2(s) C_5 + \tilde{T}_2^4(s) C_6 + \tilde{T}_3^4(s) C_7 \quad \dots (V.17)\end{aligned}$$

Equation V.17 has been obtained in a manner similar to that of Eqn. V.15. The expressions for C's are given in Table V.2.

The magnetization operators at ω_Q and $2\omega_Q$ frequencies (90° out of phase with the r.f. pulses applied) in the laboratory frame are given, respectively by (in units of $\gamma\hbar$)

$$\begin{aligned}M_{xa} &= -\sin(\omega_Q t) T_1^1(a) \\ M_{xb} &= -\sin(2\omega_Q t) T_1^1(a) \quad \dots (V.18)\end{aligned}$$

Table V.1. Expressions for B's

$$\begin{aligned}
 B_1 &= A_1 \frac{1}{28} (25 + 3 \cos(\xi_2)) - A_2 \frac{15}{28} \frac{\sqrt{15}}{\sqrt{7}} (\cos(\xi_2) - 1) \\
 &\quad + i \sin(\xi_2) (A_3 \frac{\sqrt{3}}{7\sqrt{2}} - A_4 \frac{15}{14} \frac{\sqrt{3}}{\sqrt{7}}) \\
 B_2 &= A_1 \frac{5}{4\sqrt{105}} (\cos(\xi_2) - 1) A_2 \frac{1}{28} (3 + 25 \cos(\xi_2)) \\
 &\quad + i \sin(\xi_2) (A_3 \frac{5}{3\sqrt{70}} + A_4 \frac{25}{14\sqrt{5}}) \\
 B_3 &= i \sin(\xi_2) (A_1 \frac{\sqrt{3}}{7\sqrt{2}} - A_2 \frac{75}{7\sqrt{70}}) \\
 &\quad + A_3 \frac{1}{7} (2 \cos(\xi_2) + 5 \cos(\xi_2/2)) \\
 &\quad - A_4 \frac{30}{7\sqrt{14}} (\cos(\xi_2) - \cos(\xi_2/2)) \\
 B_4 &= i \sin(\xi_2) (-A_1 \frac{1}{2\sqrt{21}} + \frac{5\sqrt{15}}{14} A_2) \\
 &\quad - A_3 \frac{2}{3\sqrt{14}} (\cos(\xi_2) - \cos(\xi_2/2)) \\
 &\quad + A_4 \frac{1}{7} (5 \cos(\xi_2) + 2 \cos(\xi_2/2)) \\
 B_5 &= i \sin(\xi_2/2) (A_3 \frac{5}{7\sqrt{2}} + A_4 \frac{15}{7\sqrt{7}}) \\
 B_6 &= i \sin(\xi_2/2) (A_3 \frac{1}{\sqrt{14}} + \frac{3}{7} A_4)
 \end{aligned}$$

where

$$A_1 = \frac{1}{7} (4 + 3 \cos(\xi_1)), \quad A_2 = \frac{2}{\sqrt{105}} (\cos(\xi_1) - 1)$$

$$A_3 = i \sin(\xi_1) \frac{\sqrt{15}}{7}, \quad A_4 = i \sin(\xi_1) \frac{2}{\sqrt{210}}$$

$$\xi_1 = \sqrt{5} \omega_{1b} t_{w1}, \quad \xi_2 = \sqrt{8} \omega_{1a} t_{w2}$$

Table V.2. Expressions for C's

$$C_1 = B_1 \frac{1}{7} (4 + 3 \cos(\xi_3)) + B_2 \frac{90}{7\sqrt{105}} (\cos(\xi_3) - 1) \\ + i \sin(\xi_3) \left(\frac{\sqrt{15}}{7} B_3 + \frac{180}{7\sqrt{210}} B_4 \right)$$

$$C_2 = B_1 \frac{2}{\sqrt{105}} (\cos(\xi_3) - 1) + B_2 \frac{1}{7} (3 + 4 \cos(\xi_3)) \\ + i \sin(\xi_3) \left(\frac{2}{3\sqrt{7}} B_3 + \frac{4\sqrt{2}}{7} B_4 \right)$$

$$C_3 = i \sin(\xi_3) \left(B_1 \frac{\sqrt{15}}{7} + \frac{30}{7\sqrt{7}} B_2 \right) + B_3 \frac{1}{7} (2 \cos(\xi_3/2) + 5 \cos(\xi_3)) \\ + B_4 \frac{90}{21\sqrt{14}} (\cos(\xi_3) - \cos(\xi_3/2)) \\ - i \sin(\xi_3/2) \left(\frac{\sqrt{5}}{7} B_5 - \frac{45}{7\sqrt{35}} B_6 \right)$$

$$C_4 = i \sin(\xi_3) \left(B_1 \frac{2}{\sqrt{210}} + B_2 \frac{2\sqrt{2}}{7} \right) + B_3 \frac{2}{3\sqrt{14}} (\cos(\xi_3) - \cos(\xi_3/2)) \\ + B_4 \frac{1}{7} (5 \cos(\xi_3/2) + 2 \cos(\xi_3)) \\ + i \sin(\xi_3/2) \left(B_5 \frac{\sqrt{5}}{3\sqrt{14}} + \frac{15}{7\sqrt{10}} B_6 \right)$$

$$C_5 = i \sin(\xi_3/2) \left(-\frac{\sqrt{5}}{7} B_3 + \frac{75}{7\sqrt{70}} B_4 \right) + B_5 \cos(\xi_3/2)$$

$$C_6 = i \sin(\xi_3/2) \left(-\frac{1}{\sqrt{35}} B_3 + \frac{15}{7\sqrt{10}} B_4 \right) + B_6 \cos(\xi_3/2)$$

$$C_7 = i \sin(\xi_3/2) \left(\frac{1}{\sqrt{10}} B_5 + \frac{\sqrt{5}}{\sqrt{14}} B_6 \right)$$

$$\xi_3 = \sqrt{5} \omega_{1b} t_{w3}$$

In the interaction representation (see Eqn. V.10). These are given by

$$\begin{aligned}\tilde{M}_{xa} &\approx i \frac{1}{2} \left[-\frac{1}{7\sqrt{2}} T_1^2(s) + \frac{1}{6\sqrt{7}} T_1^4(s) \right] \\ \tilde{M}_{xb} &\approx -i \frac{1}{2} \left[\frac{5}{28\sqrt{2}} T_1^2(s) + \frac{1}{12\sqrt{7}} T_1^4(s) \right]\end{aligned}$$

the subscripts a and b refer to the ω_Q and $2\omega_Q$ frequencies.

The signal in the interaction representation is proportional to the expectation value of the magnetization operator

$$\langle \tilde{M}_{xi} \rangle \propto \text{Tr}[\tilde{\sigma} \cdot \tilde{M}_{xi}] \quad (i = a, b) \quad \dots (V.20)$$

V.A.2 Results

The status of the spin system at various stages of the pulse sequence can be summarized as follows. The first pulse with frequency $2\omega_Q$ is a $(\pi/2)_x$ pulse and hence we can set $\mathcal{E}_1 = \pi/2$ for this case. We can then obtain $\tilde{\rho}(t_{w1})$ using Eqn. (V.15). Immediately following the second pulse of width ' t_{w2} ' and frequency ω_Q , we have from Eqns. V.16, V.19 and V.20 and using the orthogonality property of the tensor operators

$$\langle \tilde{M}_{xa} \rangle = \frac{\omega_Q}{6 kT} \frac{\sqrt{8}}{2} \sin(\mathcal{E}_2) \quad \dots (V.21)$$

and

$$\langle \tilde{M}_{xb} \rangle = \frac{\omega_Q}{6 kT} \frac{\sqrt{5}}{2} \cos(\mathcal{E}_2/2) \quad \dots (V.22)$$

These results indicate that, when the flip angle of the second pulse of frequency ω_Q is different from (π) then we get free induction signals at both ω_Q and $2\omega_Q$, i.e., a and b channels. If we set $\xi_2 = \pi$, then from Eqn. V.21 and V.22 it is clear that there would not be any signal in either a or b channel. The density matrix Eqn. V.16 at this stage contains only the terms corresponding to quadrupolar and hexadecapole orders (T_{O}^2 and T_{O}^4) and $T_2^2(s)$, $T_2^4(s)$ multipolar states which carry information about double quantum coherence.

Let us now consider the situation following a $(\pi/2)$ pulse of frequency $2\omega_Q$ and a second pulse of ω_Q with a flip angle equal to (π) . If we now apply a third (π) pulse of frequency $2\omega_Q$ without any delay, i.e., $\tau_1 = 0$ (see Fig. V.2) then immediately following the pulse we have from Eqns. V.17, V.19 and V.20.

$$\langle \tilde{M}_{xa} \rangle = \frac{\omega_Q}{6 kT} \frac{\sqrt{8}}{2} \quad \dots (V.23)$$

$$\text{and } \langle \tilde{M}_{xb} \rangle = 0 \quad \dots (V.24)$$

Since the signal which is induced in channel 'a' following the pulse in channel b is, arising entirely from $T_2^2(s)$ and $T_2^4(s)$ multipolar states it corresponds to the double quantum coherence signal. This means that the invisible double quantum coherence which has been created by the first two r.f. pulses in the sequence has been converted into an observable single quantum coherence, in channel 'a' (detection frequency of ω_Q) by the second pulse in channel b.

We have also investigated the influence of resonance off-set on the double quantum coherence, in the particular case where the off-set of r.f. pulses in channel b is exactly twice to that of r.f. pulses in channel a. In this case using Tables II.5 and II.6 and Table 12 of [13] we have obtained for the signal, immediately following the last pulse in channel b (see Fig. V.2), the expressions

$$\langle \tilde{M}_{xa} \rangle = \frac{\omega_Q}{6 kT} \frac{\sqrt{8}}{2} \cos (3 \Delta\omega \tau_1) \quad \dots (V.25)$$

and

$$\langle \tilde{M}_{xb} \rangle = 0 \quad \dots (V.26)$$

where $\Delta\omega = (\omega_Q - \omega)$.

It may be noted here that the free precession frequency of the double quantum coherence is equal to three times the off-set, $\Delta\omega$, with respect to the r.f. carrier frequency, ω , of channel a in this case. If the spin system is allowed to evolve under $\frac{\Delta\omega}{\sqrt{6}} \tau_0^2$, during the period τ_2 , then we get,

$$\langle \tilde{M}_{xa} \rangle = \frac{\omega_Q}{6 kT} \frac{\sqrt{8}}{2} [\cos (3 \Delta\omega \tau_1 + \Delta\omega \tau_2)] \quad \dots (V.27)$$

$$\text{and } \langle \tilde{M}_{xb} \rangle = 0 \quad \dots (V.28)$$

In arriving at the Eqns. V.27 and V.28 again we have made use of the Tables II.5 and II.6 and Table 12 of [13].

From the above analysis it is evident that in principle, it should be possible to create and detect double quantum coherence in NQR of nuclear spin $I = 5/2$ in single crystals.

Encouraged by the above results, we have undertaken the experimental investigation of double quantum coherence in NQR. We have chosen ^{187}Re ($I = 5/2$) in KReO_4 ($\eta \approx 0$) for this purpose. Since the two quadrupolar frequencies of ^{187}Re are ($\nu_1 = 26.825$ MHz, $\nu_2 = 53.626$ MHz at 296 K) very widely separated, a pulsed NQR spectrometer equipped with a double resonance probe and two transmitters working at these frequencies is required to detect double quantum coherence. As all the pulses in the pulse scheme (see Fig. V.2) for the detection of double quantum coherence have to be applied along the x-axis of the crystal it is not possible to use a double resonance probe having two orthogonal coils, for this experiment. We have constructed a single-coil double resonance probe, based on the circuit of Kan et al. [19] and tuned it to the frequencies (ν_1 and ν_2) of ^{187}Re . We have made use of $\lambda/4$ cable (at ν_1) to couple the probe to transmitter and receiver. A diagram of experimental set-up, including the double resonance probe, is shown in Fig. V.3. Further work is in progress in our laboratory.

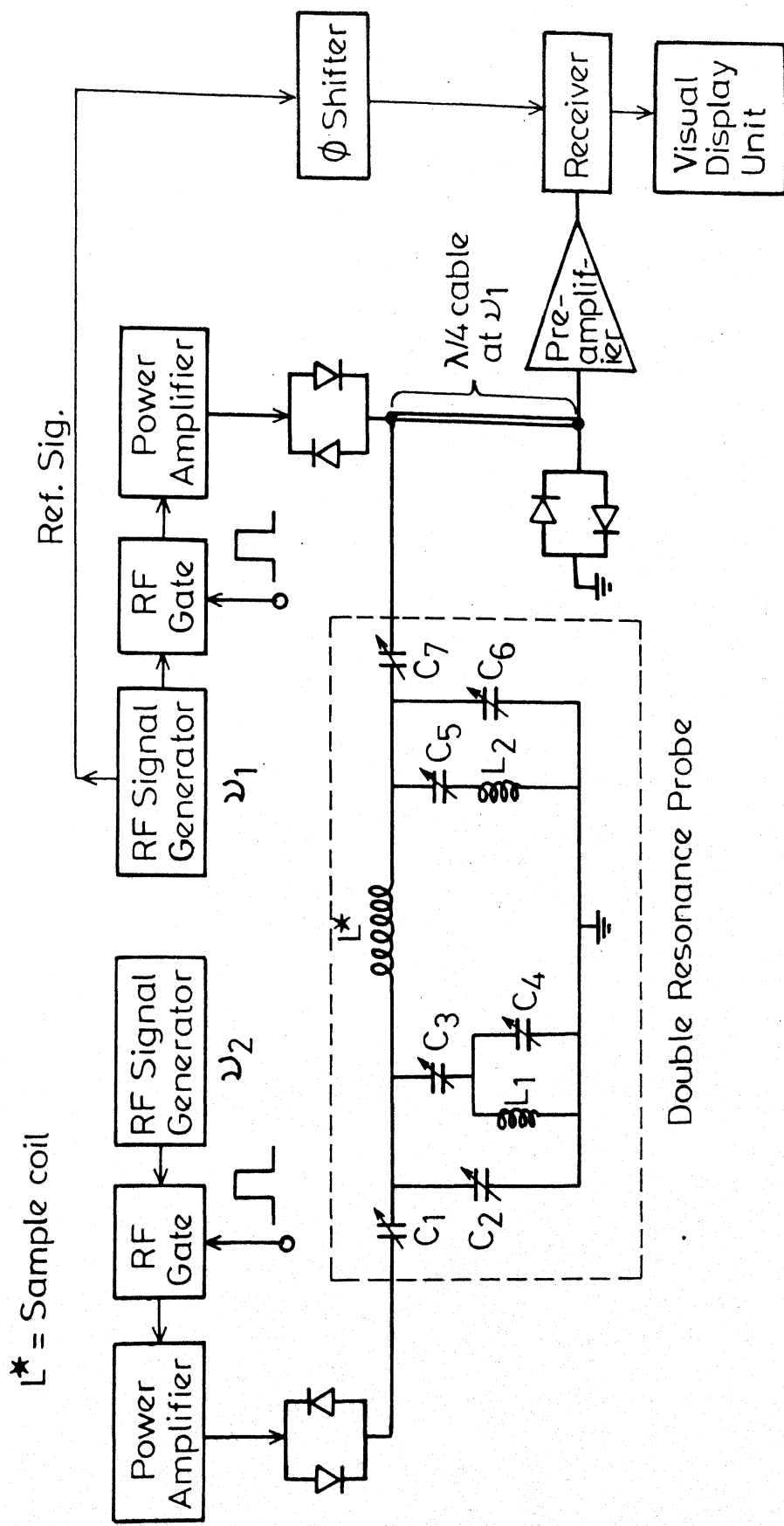


Fig.V.3 Experimental set-up for detecting double quantum coherence.

SUMMARY

Using tensor operator formalism theoretical investigation of double quantum coherence in NQR of spin $I = 5/2$ is presented. It has been shown that a pulse scheme of the form $(\pi/2)_x(2\omega_Q) - (\pi)_x(\omega_Q) - \tau - (\pi)_x(2\omega_Q)$ can be used to create and detect double quantum coherence.

REFERENCES

- [1] C.P. Slichter, "Principles of Magnetic Resonance," Springer-Verlag, Berlin (1980).
- [2] R.R. Ernst, G. Bodenhausen and A. Wokaun, "Principles of Nuclear Magnetic Resonance in one and two Dimensions," Clarendon Press, Oxford (1987).
- [3] H. Hatanaka, T. Terao, and T. Hashi, J. Phys. Soc. Japan, 39, 835 (1975).
- [4] H. Hatanaka and T. Hashi, J. Phys. Soc. Japan, 39, 1139 (1975).
- [5] G. Bodenhausen, Progr. NMR Spectrosc., 14, 137 (1981).
- [6] D.P. Weitekamp, Adv. Mag. Reson., 11, 111 (1983).
- [7] G. Drobny, Ann. Rev. Phys. Chem., 26, 451 (1985).
- [8] M. Munowitz and A. Pines, Adv. Chem. Phys., IXVI, 1 (1987).
- [9] T.J. Wang, Phys. Rev., 99, 566 (1955).
- [10] H. Gotou, J. Magn. Reson., 54, 36 (1983) and references therein.
- [11] T.J. Wang, J. Magn. Reson., 64, 194 (1985) and references therein.
- [12] G.J. Bowden and W.D. Hutchison, J. Magn. Reson., 67, 403 (1986).
- [13] G.J. Bowden, W.D. Hutchison and J. Khachan, J. Magn. Reson., 67, 415 (1986).
- [14] G.J. Bowden and W.D. Hutchison, J. Magn. Reson., 70, 361 (1986).

- [15] G.J. Bowden and W.D. Hutchison, J. Magn. Reson., 71, 61 (1987).
- [16] W.D. Hutchison, Ph.D. Thesis, University of New South Wales, Australia (1987).
- [17] T.F. Das and E.L. Hahn, "Nuclear Quadrupole Resonance Spectroscopy," Academic Press, New York and London (1958).
- [18] M. Goldman, "Spin Temperature and NMR in Solids," Oxford University Press, Oxford (1970).
- [19] S. Kan, M. Fan and J. Courtieu, Rev. Sci. Instrum., 51, 887 (1980).

CONCLUDING REMARKS

In this thesis tensor operator formalism has been extensively used in the description of pulsed NQR experiments in different situations. This formalism can be used with relative ease to describe the spin dynamics in the case of pure NQR also. However, the calculation of the time evolution of tensor operators under the action of the Zeeman Hamiltonian becomes rather cumbersome. Especially, for the case where the Zeeman field is oriented in a general (θ, ϕ) direction with respect to principal axes system of electric field gradient tensor, the calculation of time evolution of tensor operators is not possible either with the technique of "nested commutation relationship" or with "harmonics of the motion method". The tensor operator formalism is ideally suited for the study of multiple quantum coherences in NQR.